

Inaugural dissertation
for
obtaining the doctoral degree
of the
Combined Faculty of Mathematics, Engineering and Natural Sciences
of the
Ruprecht - Karls - University
Heidelberg

Presented by
M.Sc. Sarah Glenz
born in Regensburg
Oral examination: 07.07.2023

Structural and Functional Consequences of AAV Capsid Engineering

Referees: apl. Prof. Dr. Martin Müller

Prof. Dr. Dirk Jäger

For my Dad

*“The road is long
There are mountains in our way
But we climb a step every day”
- Joe Cocker -*

Abstract

The use of patients' own cells to fight cancer has become a focus of cancer research in recent years. The production of T cells with tumour-specific receptors, so-called chimeric antigen receptors (CARs), is a method to activate the patient's immune system by recognising the tumour. This type of treatment is already being used successfully, especially in the treatment of leukaemia and myeloma. Due to the simultaneous activation of many immune cells, many patients experience side effects such as Cytokine Release Syndrome (CRS), which manifests itself through sepsis-like symptoms. Currently, an anti-IL-6 receptor antibody is administered in such cases to reduce the symptoms of CRS. To make the treatment with CAR T cells safer, attempts are being made to control the activity of the cells, for example by modifications in the receptor or by adding antagonists.

In this project, AAV-based antagonists were generated for an anti-claudin-6 (CLDN6) CAR. For this purpose, an AAV-based screening method was used to identify the epitope of the CAR. This screening method should first be used to identify the anti-CD19 FMC63 antibody. When the CD19 protein was screened, it was found that the accumulation of aromatic amino acids, in the sequences displayed on the particles, prevented the formation of the viral capsids. Using capsid mutants, the production of epitope-bearing capsids could be improved, allowing the presentation of more complex structures and stronger charges. These improvements allowed the epitope of the anti-CD19 3B10 antibody and the anti-CLDN6 IMAB027 antibody to be validated. The epitope-bearing particles could then be used to demonstrate functional inhibition of the anti-CLDN6 CAR. In vitro, it was demonstrated that the simultaneous administration of the viral particles and the CAR T cells led to a temporarily reduced activation of the T cells. Furthermore, it could be shown that the cultivation of an anti-CLDN6 CAR Venus reporter cell line with the particles does not lead to an activation of the T cells, although the viral particles used presented the epitope of the CAR.

Zusammenfassung

Die Verwendung von Patienten eigenen Zellen zur Bekämpfung von Krebserkrankungen ist in den letzten Jahren ein Schwerpunkt in der Krebsforschung geworden. Die Herstellung von T Zellen mit tumorspezifischen Rezeptoren, sogenannten chimären Antigen Rezeptoren (CARs) ist eine Methode, um das Immunsystem des Patienten durch die Erkennung des Tumors zu aktivieren. Vor allem bei der Behandlung von Leukämien und Myelomen wird diese Art der Behandlung schon erfolgreich angewendet. Durch die gleichzeitige Aktivierung vieler Immunzellen kommt es in vielen Patienten zu Nebenwirkungen, wie dem Cytokine Release Syndrome (CRS), welches sich durch Sepsis-ähnliche Symptome äußert. Im Moment wird in solchen Fällen ein anti-IL-6 Rezeptor Antikörper verabreicht, um die Symptome des CRS zu verringern. Um die Behandlung mit CAR T Zellen sicherer zu machen, wird versucht die Aktivität der Zellen zu kontrollieren, zum Beispiel durch Modifikationen im Rezeptor oder durch die Zugabe von Antagonisten.

In diesem Projekt wurde für einen anti-Claudin-6 (CLDN6) CAR AAV-basierte Antagonisten generiert. Hierzu wurde eine AAV-basierte Screening Methode verwendet, um das Epitop des CARs zu identifizieren. Diese Screening Methode sollte zuerst für die Identifizierung des anti-CD19 FMC63 Antikörpers verwendet werden. Bei der Untersuchung des CD19 Proteins wurde festgestellt, dass die Anhäufung von aromatischen Aminosäuren, in den auf den Partikeln dargestellten Sequenzen die Formation der viralen Kapside verhindert. Mit Hilfe von Kapsid Mutanten konnte die Produktion von Epitop-tragenden Kapsiden verbessert werden und die Präsentation von komplexeren Strukturen und stärkeren Ladungen ermöglicht werden. Durch diese Verbesserungen konnten das Epitop des anti-CD19 3B10 Antikörpers und des anti-CLDN6 IMAB027 Antikörpers validiert werden. Die epitop-tragenden Partikel konnten dann verwendet werden, um die funktionale Inhibierung des anti-CLDN6 CARs zu zeigen. *In vitro* wurde demonstriert, dass die gleichzeitige Gabe der viralen Partikel und der CAR T Zellen zu einer temporär verringerten Aktivierung der T Zellen führt. Außerdem konnte gezeigt werden, dass die Kultivierung von einer anti-CLDN6 CAR Venus-Reporterzelllinie mit den Partikeln nicht zu einer Aktivierung der T Zellen führt, obwohl die verwendeten viralen Partikel das Epitop des CARs präsentierten.

Table of content

Abstract	1
Zusammenfassung	2
1 Introduction	6
1.1 Adeno-associated virus (AAV).....	6
1.1.1 Structure of Adeno-associated virus.....	6
1.1.2 Adeno-associated virus as gene therapy vector	8
1.2 Chimeric antigen receptors (CARs) for cancer immunotherapy	9
1.3 Management of CAR T side effects with engineered AAV-like particles (AAVLPs).10	
1.3.1 Screening for unknown epitopes with AAVLPs (AAViTOP).....	11
1.4 Aim of the project	12
2 Material	13
2.1 Equipment.....	13
2.2 Consumables	13
2.3 Standard Kits.....	14
2.4 Chemicals, media and additives	15
2.5 Antibodies	16
2.6 Enzymes	17
2.7 Plasmids	18
2.7.1 Lentiviral plasmids.....	18
2.7.2 Expression plasmids	18
2.7.3 Plasmids for AAV production.....	18
2.7.4 AAV capsid plasmids.....	19
2.8 Single-stranded Oligonucleotides	20
2.8.1 Insertions into VR-VIII loop.....	20
2.8.2 Insertions into VR-IV loop.....	45
2.8.3 Insertions into HI-loop	46
2.8.4 Insertions into β B	48
2.9 Primer	50
2.9.1 Primer for sequencing	50
2.9.2 Primer for site-directed mutagenesis	51
2.10 Cells.....	52
3 Methods	53
3.1 Cell Culture	53
3.1.1 Growth and maintenance	53
3.1.2 Isolation and cultivation of human T cells	53
3.1.3 Transfection of HEK293T cells	53

3.1.4	Co-transfection of HEK 293T cells for lentiviral particle production.....	54
3.1.5	Lentiviral transduction of Jurkat or human T cells.....	54
3.2	Molecular biology.....	55
3.2.1	Agarose gel electrophoresis.....	55
3.2.2	Bacterial cultures.....	55
3.2.3	Transformation of <i>E.coli</i> bacteria.....	55
3.2.4	Isolating Plasmid DNA.....	56
3.2.5	Analytical DNA digestion.....	56
3.2.6	Agarose Gel Purification.....	56
3.2.7	Oligo annealing and ligation into capsid backbones.....	56
3.2.8	Ligation of digested DNA fragments into target vectors.....	58
3.2.9	Gateway-cloning.....	58
3.2.10	Site-directed mutagenesis (SDM).....	58
3.3	Production of AAVLPs.....	59
3.3.1	Small-scale production of AAVLPs in crude lysates.....	59
3.3.2	Capsid assembly in the presence of proteasome inhibitor MG132.....	61
3.3.3	Large-scale production of purified AAVLPs.....	61
3.4	Enzyme-linked Immunosorbent Assays (ELISAs).....	63
3.4.1	Particle titration of AAVLP small-scale productions by A20 sandwich ELISA...63	63
3.4.2	Detection of Flag-tag insertion in intact AAVLPs by ELISA.....	63
3.4.3	Particle titration of AAVLP large-scale productions by ELISA.....	64
3.4.4	Human IFN γ ELISA.....	64
3.5	Western Blot – detection of AAV2 VP proteins.....	65
3.6	Flow cytometry analysis.....	66
3.6.1	Confirmation of a protein expressed on cell surfaces.....	66
3.6.2	A20-bead binding assay.....	66
3.7	<i>In vitro</i> experiments.....	67
3.7.1	Co-cultivation of CAR+ reporter cell line with AAVLPs.....	67
3.7.2	Inhibition assay - Co-cultivation of CAR+ T cells with AAVLPs.....	67
3.7.3	xCELLigence killing assay.....	68
3.7.4	Statistical analysis.....	68
4	Results.....	69
4.1	Insertions lead to disturbed capsid formation.....	69
4.1.1	Defining the assembly disturbing motifs.....	69
4.1.2	Premature degradation as a reason for non-existent particles.....	71
4.1.3	Verification of the crucial role of aromatic amino acids.....	73
4.1.4	Insertions in different parts of the AAVLP capsid.....	75
4.1.5	Backbone modifications – for a more tolerant environment.....	78

4.2	Screening efforts using the CD19 protein	81
4.2.1	CD19 – a delicate target.....	81
4.2.2	CD19 – detection of a linear epitope	84
4.2.3	Double insertions as an approach to identify a discontinuous epitope	87
4.3	Claudin-6 (CLDN-6) a new target for AAViTOP screening.....	89
4.3.1	Generating AAVLPs displaying CLDN6 sequence fragments	90
4.3.2	Screening for the IMAB027 epitope.....	93
4.3.3	Downregulation of the anti-CLDN6 CAR Expression	96
4.3.4	AAVLP-mediated internalization of the CAR without T cell activation	102
4.3.5	Short-term attenuation of CAR T cell efficacy	105
5	Discussion.....	109
5.1	Identification of assembly-disturbing motifs	109
5.2	Generating a tolerant capsid environment	112
5.2.1	Comparison of different insertion sites	112
5.2.2	Comparison of different point mutations in the capsid	114
5.3	The AAViTOP procedure as a tool for epitope mapping	116
5.3.1	Identifying epitopes in the CD19 protein sequence.....	116
5.3.2	Identifying epitopes in the CLDN6 sequence.....	119
5.3.3	Opportunities and challenges for the AAViTOP screening method	120
5.4	Using AAVLPs as CAR antagonists	120
6	References.....	124
7	Supplement.....	133
7.1	Row statistics	133
7.1.1	Alanine Scan CD19_42FL.....	133
7.1.2	Comparison alternative insertion sites.....	133
7.1.3	Backbone comparison.....	134
7.2	Abbreviations	139
7.3	List of figures.....	141
7.4	List of tables	141
8	Acknowledgments.....	143

1 Introduction

1.1 Adeno-associated virus (AAV)

Like many great discoveries, adeno-associated viruses (AAVs) were discovered by chance. In 1965, these non-autonomous viruses were discovered alongside adenoviruses. The location of the discovery and the fact that the particles only reproduce with the help of coinfection with adenovirus or herpes virus gave these small viruses their name¹⁻³.

1.1.1 Structure of Adeno-associated virus

Adeno-associated viruses are small, non-pathogenic parvoviruses. With a size of 25nm, they are one of the smallest DNA-containing known viruses. The simplicity of AAVs is also apparent in their genomic structure. The wildtype genome consists of only two genes (*rep* and *cap*) and exists as a single-stranded linear DNA genome (~4.7 kb)⁴. The *rep* and *cap* genes are flanked by two inverted terminal repeats (ITRs). Between these inverted terminal repeats, there is an associated open reading frame (ORF) for each gene. The *rep* gene encodes for four Rep proteins (Rep78, Rep68, Rep52, Rep40); these are responsible for transcription, packaging, and replication⁵. The *cap* gene encodes for the three viral capsid proteins (VPs) VP1, VP2 and VP3. These three proteins, which are controlled by the p40 promotor and differ in size due to alternative start codons, build up the viral capsid⁶. Due to the alternative start, VP1 (87 kDa), VP2 (73 kDa) and VP3 (62 kDa) only differ in their N-termini and possess the same stop codon^{7,8}. In addition, by using an alternative reading frame, the protein AAP (assembly activating protein) is translated from the *cap* gene, which helps in capsid formation⁹ (Figure 1.1.1, A).

The capsid proteins of all serotypes self-assemble into a 60-subunit icosahedral capsid in a ratio of 1:1:10¹⁰⁻¹² (Figure 1.1.1, B). The structure of the capsid is characterised by the three protrusions around the threefold axis and the pore around the fivefold axis. The peaks are formed from the VR-VIII and VR-IV loops with the help of neighbouring subunits and are assumed to be responsible for the interaction with host cell receptors⁸ (Figure 1.1.1, B, C). AAV2 uses heparan sulphate proteoglycan (HSPG) as its primary cell receptor and α V β 5 integrin and basic fibroblast growth factor as its secondary receptors¹³⁻¹⁵. Another well-known loop is the HI-loop, which forms a flexible part of the pore around the fivefold symmetry axis. This pore is particularly important for packaging DNA^{10,16,17}. Although the subunits of the capsid do not rigidly attach to each other but rather fit over and into each other, forming many and very tight bonds, the regions around the pore (Hi-loop) and the peaks (VR-IV, VR-VIII loop) of the capsid are used to introduce mutations or whole peptides into the capsid. Most of the modifications are intended to redirect the tropism to allow the AAV capsid to enter different cell types and act as a vehicle for gene therapies¹⁸⁻²².

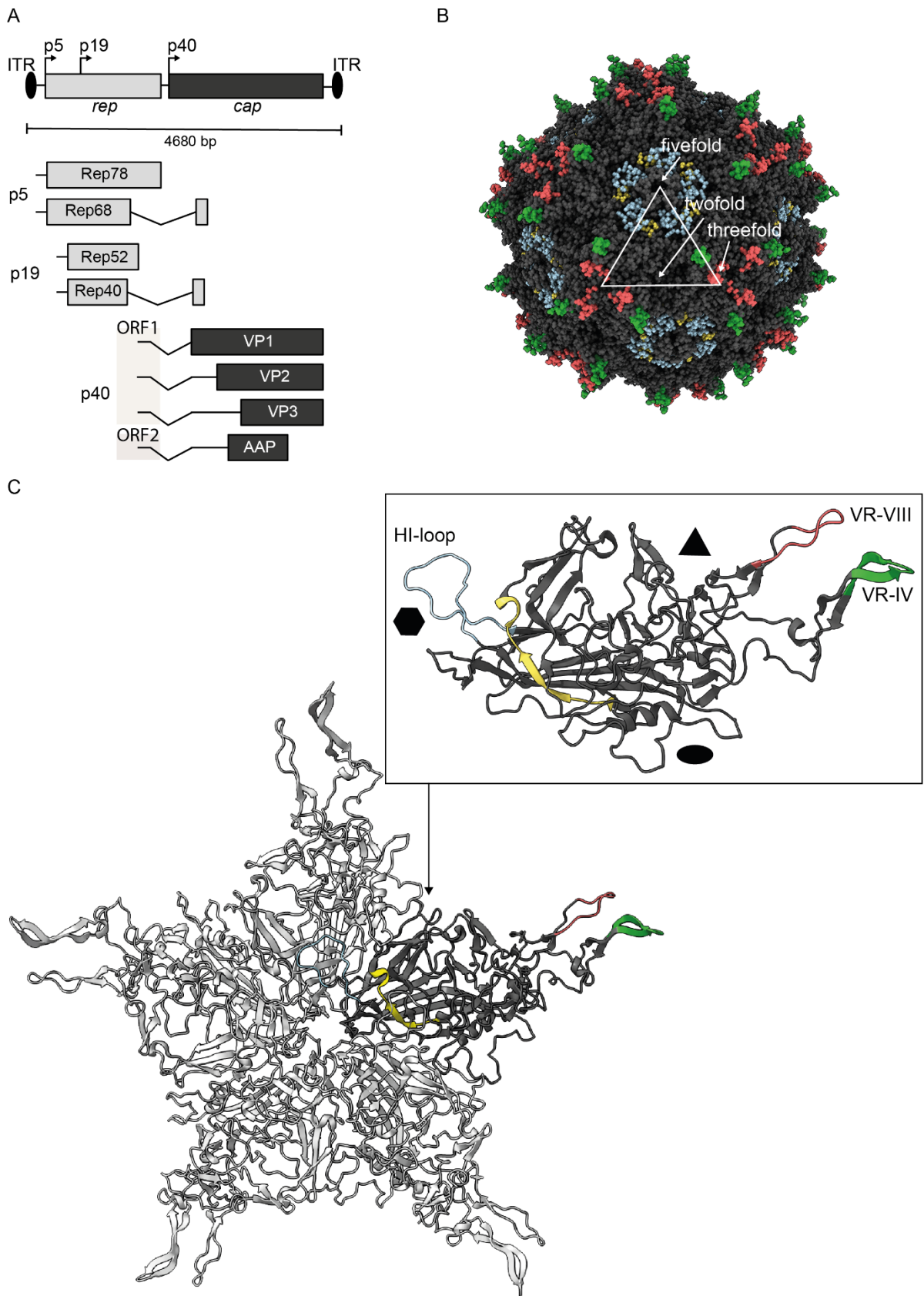


Figure 1.1.1: Genome and capsid structure of AAV2. A: Structure of the AAV wildtype genome. The genome consists of two genes (*rep* and *cap*), that are flanked by inverted terminal repeats (ITRs) (black ovals). The *rep* gene encodes four proteins (Rep78, Rep68, Rep52 and Rep40). The Rep proteins are expressed from two different promoters (p5, p19) and modified via alternative splicing. The *cap* gene encodes the three viral capsid proteins VP1, VP2 and VP3 via splicing and an assembly activating protein (AAP) by a second open reading frame (ORF2). B: Crystal structure of the AAV2 capsid (PDB:

6CBE, modified using ChimeraX²³). The viral capsid proteins form an icosahedral capsid by assembling in a 1:1:10 ratio. The coloured structures mark potential insertion sites. C: VP1 monomer in complex of five monomers. Enlarged: VP subunit with marked regions. Marked are regions where insertions were made during this work: HI-loop (blue), part of the beta-sheet (yellow), VR-IV (green) and VR-VIII (red). Figures modified from PDB entry 1lp3 using ChimeraX²³.

1.1.2 Adeno-associated virus as gene therapy vector

Adeno-associated viruses emerged early as a promising vector candidate for in vivo gene delivery. The AAV genome can be modified and used in recombinant vectors²⁴. For recombinant AAV vector production, the genes (*Rep*, *Cap*, *AAP*) between the inverted terminal repeats are transferred almost completely to a separate plasmid used in *trans*. The 145-bp ITRs must remain in *cis* for successful genome replication and packaging²⁵. Instead of the viral promoters and genes, a transgene cassette of choice can be inserted between the AAV ITRs which is used as transgene plasmid during vector production. Co-infection with adenovirus can be solved with the help of a recombinant vector (adenoviral helper plasmid) that contains the adenovirus genes encoding E1, E2A, E4 and virus-associated RNA, providing all the necessary helper factors for AAV replication²⁶.

In the absence of a helper virus, a latent AAV infection occurs within the cell. This can manifest itself through site-specific integration of the AAV genome into the host genome (*AAVS1* locus) or by remaining in episomal forms^{27–31}. However, infection with AAVs has been of little interest due to lack of pathogenicity, which has increased the potential of using these viruses as gene delivery vehicles^{26,32–34}. Hence, due to the lack of associated disease after infection, the permanent expression of transgenes without the need to integrate into the host genome, and the availability of different serotypes that can enter various cell types via different tropisms, the first gene therapies based on AAVs were developed³⁵. Five AAV-based therapies have yet been approved, for example most recently Hemgenix for the treatment of haemophilia type B³⁶. One of the biggest challenges for AAVs as a gene therapy tool is the cell-mediated immune response of the patient against the transduced cells and the humoral response producing neutralizing antibodies (NAbs) against the AAV particle itself^{37–39}. NAbs will not only be developed in many patients after the first administration of an AAV-based gene therapy but are already present in 30%- 60% (AAV serotype 2) of the population due to a past infection^{40–42}.

Another challenge is the specific uptake of the vectors into certain cells or organs. On the one hand, not all desired targets are covered by the natural tropisms of different AAV serotypes, on the other hand, the natural tropism can be too broad. Thus, capsid modifications became relevant, enabling the uptake into specific cells²¹. One method of redirecting AAVs is direct targeting, in which short peptides or ligands are integrated into the capsid. These insertions may neither disturb the correct assembly of the capsid during AAV vector packaging nor the uptake and intracellular processing of the vector particle in the target cell finally releasing the vector DNA for successful transduction^{43–45}. AAV capsid modifications have become

increasingly interesting for the design of gene therapy vectors in view of both above mentioned challenges, i.e., to prevent binding of neutralising antibodies and to ensure direct targeting and transduction of specific cell types^{18,21,46,47}.

1.2 Chimeric antigen receptors (CARs) for cancer immunotherapy

Chimeric antigen receptors (CARs) are synthetic cell surface receptors on genetically engineered immune cells that target proteins expressed on the surface of tumour cells (so called tumour antigens). With the help of CAR T cells, success has been achieved in the treatment of leukaemia, myeloma, and non-Hodgkin B-cell lymphoma^{48–54}. By arming patients' own T cells with the synthetic receptor, they can recognise a specific antigen independently of the T cell receptor and major histocompatibility complex (MHC)⁵⁵.

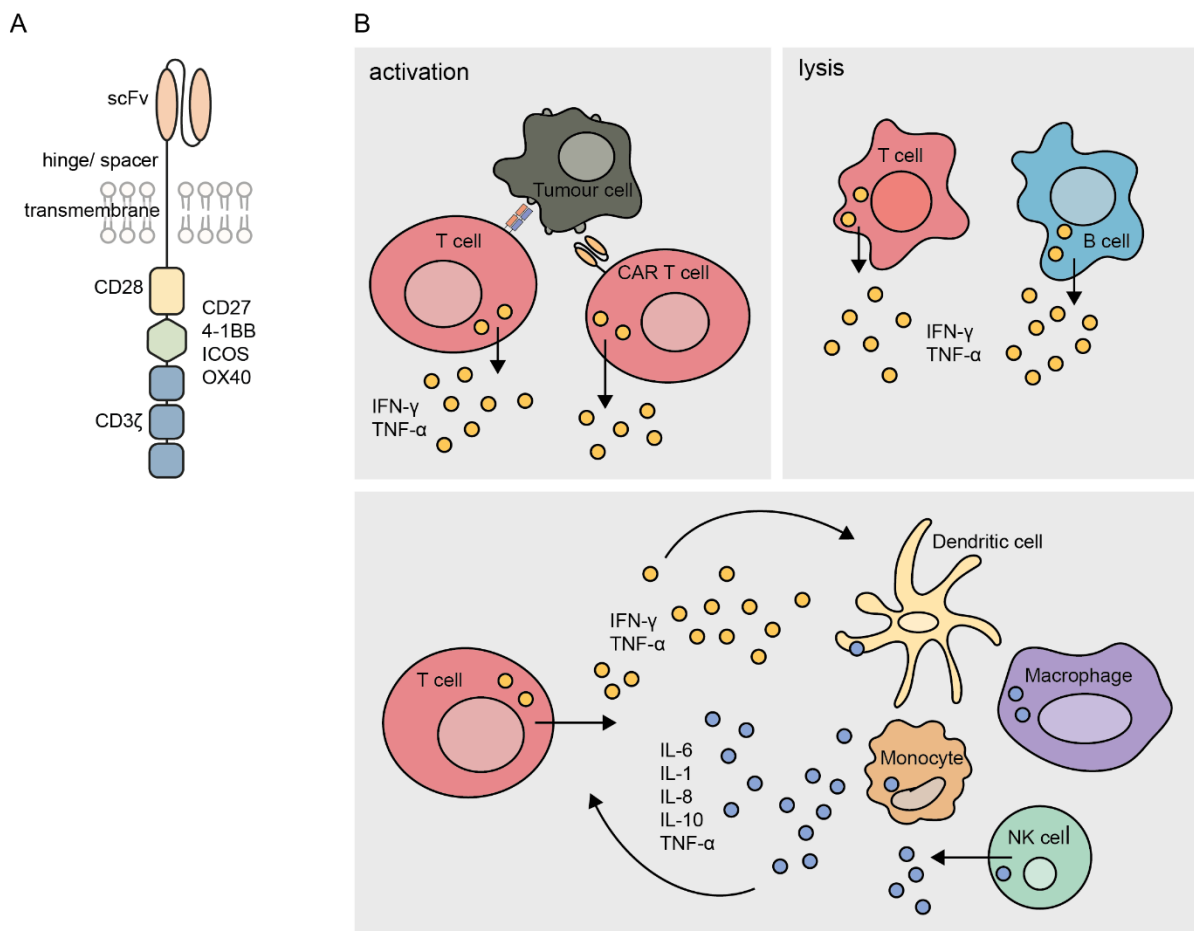


Figure 1.2.1: Chimeric antigen receptors for cancer treatment. A : Schematic figure of a chimeric antigen receptor. It consists of an extracellular domain: single chain variable fragment (scFv) and hinge, a transmembrane domain and an intracellular domain: one or more co-stimulatory domains (CD28, CD27, 4-1BB, ICOS, OX40) and a CD3 ζ signalling domain. B: Development of cytokine release syndrome. Activation of CAR- and bystander T cells or the lysis of other immune cells (e.g., B cells) leads to the release of cytokines such as interferon gamma (IFN- γ) and tumour necrosis factor alpha (TNF- α). The proinflammatory cytokines activate macrophages, dendritic cells and different other cells. The activated macrophages produce interleukins (IL-6, IL-1, IL-8, IL-10). IL-6 in turn activates T cells, which then release further cytokines. Figure was created according to the model of Shimabukuro-Vornhagen et al., 2018⁵⁸.

The ability to recognise a specific antigen on tumour cells depends on the single chain variable fragment (scFv), that is part of the extracellular part of the chimeric receptor and contains variable domains of heavy and light chains of an antibody with the specific binding properties for the target of interest. The scFv is fused to an intracellular signalling element by a flexible hinge and transmembrane domains. The intracellular part of a CAR often contains a part of CD28 as a co-stimulatory domain next to a CD3 ζ signalling domain. Depending on the generation of the CAR, additional co-stimulatory elements such as 4-1BB, OX40, or ICOS are possible^{56,57}.

However, treatment with CAR T cells is not only extremely expensive but can also have side effects⁵⁹. These side effects are directly related to the mode of action of the CAR T cells. After recognition of the antigen, the respective CAR T cell is activated with the help of the intracellular signalling elements. Cytokines and chemokines are then released to activate other components of the immune system and kill the recognised tumour cells. Since all CAR T cells recognise the same target at more or less the same time, the immune system is activated with enormous cumulative strength. This enormous release of cytokines and chemokines can lead to cytokine release syndrome (CRS), which manifests itself with sepsis-like symptoms and is the most common side effect of CAR T cell therapy^{58,60}. The gold standard treatment in these cases is an anti-IL-6 receptor antibody (tocilizumab), which does not affect the activity of the CAR T cells but minimises the symptoms of CRS⁶¹. Other severe side-effects that occurred during CAR T cell applications include neurotoxicity, allergy/anaphylaxis, cross-reactivity of CAR T cells with healthy tissues and insertional oncogenesis⁶².

In addition to the toxicity of the treatment, there are other challenges to the further development of CAR T cells. For example, solid tumours with their immunosuppressive environment, are difficult for CAR T cells to reach⁶³. Moreover, the identification of tumour-specific antigens is a challenge, because on-target/off-tumour effects are to be avoided⁶⁴. However, due to the promising successes of CAR T cell therapy, many potential strategies to overcome these challenges are being developed⁶⁵.

1.3 Management of CAR T side effects with engineered AAV-like particles (AAVLPs)

One way to reduce the toxicity of CAR T cells while maintaining treatment potential is the temporary, reversible reduction of chimeric antigen receptors on the cell surface, hence delaying the activation of CAR T cells. Exactly this reduction in CAR expression on the surface was successfully achieved in our research group with the help of AAVLPs and patented. The temporary internalisation of the CAR was demonstrated using an anti-NYBR1 CAR and its epitope-carrying AAVLP antagonist (WO2019043081)⁶⁶. Since the inhibition by AAVLPs has been shown to be non-activating, fast and reversible, it could be used as an emergency

medication for acute side effects or as a companion medication to control the dosage of CAR T cell activity.

1.3.1 Screening for unknown epitopes with AAVLPs (AAViTOP)

In order to generate AAVLP-based antagonists (= CARAAVs) for a given chimeric antigen receptor (CAR), it is necessary to know the epitope of the scFv that is used. Thus, an AAV-based epitope screening technology (AAViTOP, IP claimed by DKFZ and University Heidelberg (SVH)⁶⁷) has been developed in our group that allows screening and identification of ScFv/antibody epitopes displayed on AAVLPs in a systematic library approach (Figure 1.3.1). The innovative potential of our approach lies in the fact that the AAViTOP assay not only generates information of the identified epitope sequence but also delivers the blueprint of the “binder” CARAAV that can be directly translated to functional characterization *in vitro* and (pre-)clinical application as described in WO2019043081⁶⁶.

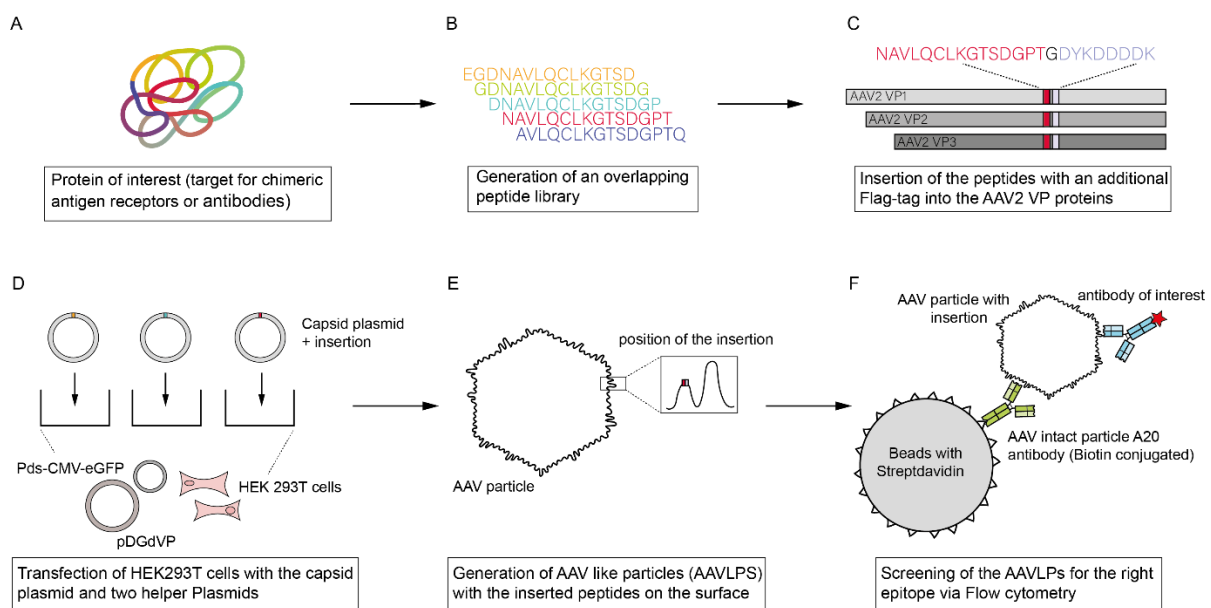


Figure 1.3.1: The AAViTOP screening procedure. A: The target protein (or part of the protein) of a chimeric antigen receptor or antibody is determined. B: An overlapping peptide library is generated. Each peptide has a length of 15 amino acids with an overlap to the next sequence of 14 amino acids. C: each sequence is extended by an additional Flag-tag and inserted into an AAV2 capsid backbone. D: HEK 293T cells are transfected with the capsid plasmid containing the insertion, the pds-CMV-eGFP and the pDGdVP plasmids. E The resulting AAVLPs contain the insertion 60 times on their surface. F: The generated particles are tested in a bead assay. The beads are coated with A20 antibody, which recognizes intact AAV particles. The antibody of interest binds only to particles that present the correct epitope on their surface. As control for the presence of particles the inserted Flag-tag can be detected by an anti-Flag-tag antibody. The entire construct is then analysed by flow cytometry.

The first step of the AAViTOP screening is to translate the protein sequence of interest into an overlapping peptide library (Figure 1.3.1, A-B). In the following work, these sequences will always have a length of 15 amino acids and an overlap with the next sequence of 14 amino acids. Thus, the consecutive sequences of the library always differ by two amino acids. Since

the beginning of this work, these sequences have been C-terminally extended by the Flag-tag sequence (DYKDDDDK) using glycine as a linker. Then, each peptide is reverse-translated and inserted into an AAV2 capsid backbone by molecular cloning. As yet, sequences have been inserted behind amino acid 588 of the VP1 protein, resulting in capsids displaying the insertion 60 times, but other insertion sites are possible (Figure 1.3.1, C). To produce AAVLPs with the respective insertion, the modified plasmid, along with a helper plasmid (pDGdVP) and a plasmid encoding GFP (Pds-CMV-eGFP) as transfection control, is transfected into HEK293T cells (Figure 1.3.1, D). This procedure is performed individually for each peptide insertion variant, resulting in a library of AAV-like particles that represents a continuous sequence. After transfection, crude lysates are prepared, which are then be used in the bead assay (Figure 1.3.1, F). In this assay, magnetic streptavidin beads are coupled with a biotinylated A20 antibody. Due to its conformational epitope, this antibody only binds intact particles in the lysates⁶⁸. The inserted epitopes are detected with the help of two further antibodies carrying different fluorescent dyes: first, with the antibody of interest whose epitope is to be identified, and secondly with an anti-Flag-tag antibody to normalize for the presence of assembled, epitope-displaying particles. The bead-AAVLP-antibody complexes can be analysed by flow cytometry. The AAVLPs identified as epitope-positive by this assay can then be produced in a larger format and used for further experiments and functional inhibition of the respective scFv/CAR.

1.4 Aim of the project

Adeno-associated viruses (AAVs) as vectors have become increasingly popular in human gene therapy. However, it is difficult to target the virus particles into specific cells because the ligands of receptors have to be displayed on the capsid, or natural tropisms have to be redirected. In addition, certain amino acid constellations show a negative effect on capsids. These effects were also visible in our AAViTOP screening technology used to identify the epitopes of chimeric antigen receptors (CARs) or antibodies. This project aimed to define the limitations of AAV capsid assembly more clearly and develop new strategies to overcome these limitations. Based on the results, the AAViTOP screening procedure should be optimized in order to identify as yet unknown CAR epitopes. Finally, the identified epitope-displaying particles (CARAAVs) should be functionally characterized regarding their potential to reduce CAR surface expression and inhibit CAR T cell-mediated killing of target cells in analogy to the findings of WO2019043081⁶⁶.

2 Material

2.1 Equipment

Equipment name	Manufacturer
2-Gel Tetra and Blotting Module	Bio-Rad
CellDrop Cell Counter	DeNovix
CKX31 Microscope	Olympus
CKX41 Microscope	Olympus
EG Präzisionswaage	Kern
Epoch Photometer	BioTek
FACSCanto™ II	BD Biosciences
HERAcell 240i	Thermo Scientific
HERAEUS Multifuge X1R	Thermo Scientific
Innova® 44 Incubator Shaker	New Brunswick
L8-70M Ultracentrifuge	Beckmann
Magnetic Stand -96	Invitrogen
Mini Vortex Mixer	Thermo Scientific
Mini-Protean Tetra System	Bio-Rad
NanoDrop ONE	Thermo Scientific
Power Pac 300	Bio-Rad
PowerPac HC	Bio-Rad
Quantum-ST4	Peqlab Biotechnologie GmbH
Sub Cell ® GT	Bio-Rad
T3000 Thermocycler	Biometra
Tube Sealer	Beckmann
Type 70 Ti Rotor	Beckmann
Ultra Rocker	Bio-Rad
WELLWASH	Thermo Scientific
xCelligence RTCA	OMNI LifeScience

2.2 Consumables

Product	Catalog Number	Manufacturer
14 ml PP Tube	187261	Greiner Bio-One
15 ml Conical Polypropylene Tube	188271	Greiner Bio-One
175 ml graduated Conical tube	352076	Falcon
50 ml Conical Polypropylene Tube	227261	Greiner Bio-One
96 well ELISA Plate	3690	Greiner Bio-One

Amicon Ultra-15, Centrifugal Filter, 50kDa	UFC905024	Merck
Cell Culture dishes (15 cm)	353025	Falcon
Cell Culture Flask (T175)	660175	Greiner Bio-One
Cell Culture Flask (T25)	690175	Greiner Bio-One
Cell Culture Flask (T75)	658175	Greiner Bio-One
Cell Culture Microplate (96 well, Flat-bottom)	655180	Greiner Bio-One
Cell Culture Microplate (96 well, U-bottom)	650185	Greiner Bio-One
Cell Culture Microplate (96 well, V-bottom)	651160	Greiner Bio-One
Cell Culture Multiwell Plate (48 well)	677180	Greiner Bio-One
Cell Culture Multiwell Plate (6 well)	657160	Greiner Bio-One
Centrifuge Tubes	342413	Beckman Coulter
Centricon® Plus-70	UFC703008	Merck Millipore
CryoTube™ Vials	377267	Thermo Scientific
E-Plate 96	5232368001	Agilent
Glasstic® Slide with 10 grids	87144	Kova International
Nalgene™ 250 mL conical PPCO tube	3143-0175	Thermo Scientific
Needle (20G x 0,90X40mm)	CH20112	Medoject
Pasteur Pipette	E327.1	Carl Roth
Sealing Mats	AB0674	Thermo Scientific
Syringe 1 mL	309628	BD
Whatman™ paper	3030-917	GE Healthcare

2.3 Standard Kits

Kit name	Catalog Number	Manufacturer
Biotinylation Kit, Lightning-Link®	ab201795	Abcam
Gateway™ LR clonase™ enzyme mix	11791019	Thermo Scientific
Monarch DNA Gel Extraction Kit	T1020	New England BioLabs® GmbH
Monarch Plasmid Miniprep Kit	T1010	New England BioLabs® GmbH
NucleoBond Xtra Maxi Kit	740414	Machery-Nagel
NucleoBond Xtra Midi Kit	740410	Machery-Nagel
Pan T cell isolation Kit human	130-096-535	Miltenyi Biotec
PE Phycoerythrin Fluorescence Quantitation Kit	340495	BD Biosciences
PE/R-Phycoerythrin Conjugation Kit, Lightning-Link®	ab102918	Abcam
PfuPlus! DNA Polymerase Kit	EK1118-02	Roboklon

Pierce™ BCA Protein Assay Kit	23225	Thermo Scientific
QIAquick PCR Purification Kit	28104	QIAGEN
qPCRBIO SyGreen Mix Hi-ROX	PB20.12	PCR Biosystems

2.4 Chemicals, media and additives

Product	Catalog number	Manufacturer
Acrylamide/ bisacrylamide 30% (37, 5:1)	3029	Carl Roth
Agar-Agar	1347.2	Carl Roth
Agarose	16500500	Thermo Scientific
Albumin Fraktion V (BSA)	T844.4	Carl Roth
Ammoniumperoxidisulfat (APS)	9592	Carl Roth
Bacto™ Agar	-	BD Biosciences
BD OptEIA (TMB)Substrate Reagent Set	555214	BD Biosciences
Carbenicillin disodium salt	6344.2	Carl Roth
CutSmart Buffer	B7204	New England Biolabs
D(+)-Sucrose p.A.	A4734	AppliChem
Dimethyl Sulfoxide (DMSO)	20385	Serva
DMEM + GlutaMAX™-I	61965-026	Thermo Scientific
DNA Ladder, 100 bp	N3231	New England Biolabs
DNA Ladder, 1kb	N3232	New England Biolabs
DPBS (1X)	14190-094	Thermo Scientific
Dynabeads™ M-270 Streptavidin	65305	Invitrogen
Ethanol	32221	Sigma-Aldrich
Ethidium Bromide	2218.1	Carl Roth
Ethylenediaminetetraacetic acid (EDTA)	E5134	Sigma-Aldrich
FCS	P40-47500	PAN-Biotech
Ficoll	17-1440-03	Thermo Scientific
Gel Loading Dye, Purple (6X)	B7024	New England Biolabs
Glycerol 87% BioChemica	A0970	AppliChem
Human IL-15	130-095-760	Miltenyi Biotec
Human IL-2	130-097-743	Miltenyi Biotec
Hydrogen chloride (HCl)	4625	Carl Roth
Isopropanol	33539	Sigma-Aldrich
Kanamycin	T832.1	Carl Roth
MG132 [10 nM/mL]	M1902	AbMole Bioscience
Milk powder	T145.2	Carl Roth
NEBuffer 2	B7002	New England Biolabs
NEBuffer 3.1	B7203	New England Biolabs

OptiMEM + GlutaMAX™-I	51985-026	Thermo Scientific
OptiPrep (Ioidixanol)	7820	Stemcell
PEG 8000	41600048-3	Biotrend
Pen/ Strep (Penicillin Streptomycin)	15070-063	Thermo Scientific
Phenol red	P0290	Sigma-Aldrich
Polyethylenimine (PEI)	23966-2	Sigma-Aldrich
Potassium chloride (KCl)	6781	Carl Roth
PureProteome™ Streptavidin Magnetiv Beads	LSKMAGT02	MerckMillipore
Puromycin	Anti-pr1	InvivoGen
RPMI 1640 + GlutaMAX™-I	61870-010	Thermo Scientific
Sodium chloride (NaCl)	3957	Carl Roth
Sodium dodecyl sulfate (SDS)	A7249	AppliChem
Strep-HRP	N100	Thermo Scientific
Sulfuric acid (H2SO4)	4623	Carl Roth
T cell Trans Act™ human	130-111-160	Miltenyi Biotec
T4 DNA Ligase Reaction Buffer	B0202	New England Biolabs
TEMED	2367	Carl Roth
TexMACS GMP	170-076-307	Miltenyi Biotec
Tris	4855	Carl Roth
Trypanblau	T8154	Sigma-Aldrich
Trypsin-EDTA	25300-054	Thermo Scientific
Tween20	P2287	Sigma-Aldrich
Western Lightning Plus-ECL	NEL103001EA	Perkin Elmer
Yeast extract	2363.3	Carl Roth

2.5 Antibodies

Antibody	Clone	Host	Catalog number	Manufacturer
AffiniPure F(ab') ₂ Fragment anti-hlgG, Fcy Fragment specific, APC conjugated	polyclonal	goat	109-136-098	Jackson Immuno Research
AffiniPure F(ab') ₂ Fragment anti-hlgG, Fcy Fragment specific, R-PE conjugated	polyclonal	goat	109-116-098	Jackson Immuno Research
anti-AAV2 (intact particle), biotin conjugated	A20	mouse	61555	PROGEN

anti-AAV2 (intact particle), hybridoma supernatant	A20	mouse	-	kindly provided by Martin Müller (DKFZ, Heidelberg)
anti-AAV VP B1 supernatant		mouse		Kindly provided by Oliver Müller (DKFZ, Heidelberg)
anti-Aktin (I-19)-R	polyclonal	rabbit	Sc-1616R	Santa Cruz
anti-CD19, R-PE conjugated	FMC63	mouse	MAB1794H	EMD Millipore Corp
anti-CD19, R-PE conjugated	OTI3B10		TA506236H M	OriGene
anti-Claudin-6 IMAB027	-		-	kindly provided by AG Jäger (DKFZ, Heidelberg)
anti-Flag-tag, APC conjugated	M2	mouse	ab72569	Abcam
anti-Flag-tag, HRP conjugated	M2	mouse	ab49763	Abcam
anti-Flag-tag, R-PE conjugated	M2	mouse	ab72469	Abcam
anti-human CD3, APC conjugated	-	mouse	555335	BD Pharmigen™
anti-mouse IgG - HRP	polyclonal	goat	115-035-003	Dianova
anti-rabbit IgG - HRP		donke y	Sc-2077	Santa Cruz
Streptavidin, R-PE conjugated	-	-	SAPE20	SL Biotech

2.6 Enzymes

Enzyme	Catalog number	Manufacturer
AccI	R0161	New England BioLabs
AgeI	R3552	New England BioLabs
Alkaline Phosphatase Calf Intestinal (CIP)	M0525	New England BioLabs
BamHI	R3136	New England BioLabs
Benzonase® Nuclease	70746-6	MerckMillipore
BmtI	R3658	New England BioLabs
DpnI	R0176	New England BioLabs
MfeI	R3589	New England BioLabs
NcoI	R0193	New England BioLabs
NheI	R3131	New England BioLabs
NotI	R3189	New England BioLabs
PfIMI	R0509	New England BioLabs
PmeI	R0560	New England BioLabs
Psil-v2	R0744	New England BioLabs

SfiI	R0123	New England BioLabs
SpeI	R3133	New England BioLabs
SphI	R0182	New England BioLabs
T4 DNA Ligase	M0202	New England BioLabs
XmaI	R0180	New England BioLabs

2.7 Plasmids

2.7.1 Lentiviral plasmids

pCMV-VSV-G	Lentiviral helper plasmid. Encodes envelope protein VSV-G
pCMV-dR874	Lentiviral helper plasmid. Encodes HIV-gag and HIB-pol protein.
pRRL-cPPT-hPGK-Lk- CLDN6scFv-hFc-hCD28tm- hCD3z-hOX40-IRES-puro-WPRE	Lentivirus transfer vector. Encodes Claudin-6 specific chimeric antigen receptor: CLDN6scFv-hFc-hCD28tm-hCD3z-hOX40. Contains puromycin resistance.

2.7.2 Expression plasmids

pcDNA- 21ABGGNP_Exon2_full_CD28tm	Mammalian expression vector. Encodes human CD19 Exon2 with an additional Flag-tag.
pcDNA- 21ABGGNP_Exon2_full_CD19Exo n3fus_CD28tm	Mammalian expression vector. Encodes human CD19 Exon2 and Exon3 with an additional Flag-tag.

2.7.3 Plasmids for AAV production

pds- CMV- eGFP	ITR-containing, self complementary transgene plasmid. Ampicillin resistance. Kindly provided by Oliver Müller (DKFZ, Heidelberg)
pDGΔVP	Adenoviral helper plasmid. Encoding helper genes (<i>VA</i> , <i>E3A</i> and <i>E4</i>) for AAV packaging. Kindly provided by Oliver Müller (DKFZ, Heidelberg)

2.7.4 AAV capsid plasmids

Insertion site (see table below) refers to the amino acid in the AAV2 wildtype VP1 sequence, behind which the peptide sequence including linkers is inserted. Wildtype sequence can slightly vary from wildtype sequence due to restriction site design.

Plasmid name	Description	Insertion site (AAV2 VP1 numbering)
pMT-AAV2wtRC	AAV <i>rep/cap</i> plasmid. Encodes AAV2 Rep and Cap proteins with wt sequence. Ampicillin resistance.	No insertion site
pMT-AAV2wtRC-HSPG-KO	AAV <i>rep/cap</i> plasmid. Encodes AAV2 Rep and Cap proteins with wt sequence but with destroyed HSPG binding site. Ampicillin resistance.	No insertion site
pMT-187-XX2	AAV2 <i>rep/cap</i> plasmid. Encodes AAV2 Rep and Cap proteins. Integrated insertion site in cap for the integration of peptides via Sfil after aa588. Ampicillin resistance. Kindly provided by Oliver Müller (DKFZ, Heidelberg)	R588
pMT-187-XX2-R585S-R588T	AAV2 <i>rep/cap</i> plasmid. Encodes AAV2 Rep and Cap proteins. Integrated insertion site in <i>cap</i> for the integration of peptides via Sfil behind aa588. Amino acid changes at the position R585 and R588. Ampicillin resistance	T588
pMT-187-XX2-Pos453mut-R585S-R588T	AAV2 <i>rep/cap</i> plasmid. Encodes AAV2 Rep and Cap proteins. Integrated insertion sites in cap for the integration of peptides via Sfil after aa588 and via Mfel and Spel after aa452. Amino acid changes at position 585 and 588. Ampicillin resistance.	I452, T588
pMT-AAV2wtRC-HSPG-KO-Pos453mut	AAV2 <i>rep/cap</i> plasmid. Encodes AAV2 Rep and Cap proteins. Destroyed HSPG binding site. Integrated insertion site in cap for the integration of peptides via Mfel and Spel after aa452. Ampicillin resistance.	I452

pMT-187-XX2_453mut	AAV2 <i>rep/cap</i> plasmid. Encodes AAV2 Rep and Cap proteins. Integrated insertion site in cap for the integration of peptides via NheI and SpeI after aa453. Ampicillin resistance. Kindly provides by Dr. Silke Uhrig-Schmidt.	G453
pMT-AAV2wtRC-HSPG-KO-HImut	AAV2 <i>rep/cap</i> plasmid. Encodes AAV2 Rep and Cap proteins. Destroyed HSPG binding site. Integrated insertion site in cap for the integration of peptides via AgeI and NheI after aa653. Ampicillin resistance.	V653
pMT-AAV2wtRC-HSPG-KO-Pos247mut	AAV2 <i>rep/cap</i> plasmid. Encodes AAV2 Rep and Cap proteins. Destroyed HSPG binding site. Integrated insertion site in cap for the integration of peptides via SphI and XmaI after aa245. Ampicillin resistance.	A245
pMT-AAV2wtRC-HSPG-KO-Pos259mut	AAV2 <i>rep/cap</i> plasmid. Encodes AAV2 Rep and Cap proteins. Destroyed HSPG binding site. Integrated insertion site in cap for the integration of peptides via SpeI and XmaI after aa245. Ampicillin resistance.	A245

2.8 Single-stranded Oligonucleotides

2.8.1 Insertions into VR-VIII loop

CD19_1FL_s	5'- AGGCGAAGGCGATAACGCGGTGCTGCAGTGCCTGAAAGGTACCAGCG ATGGCGATTATAAGGACGACGACGACAAGGCCAGG-3'
CD19_1FL_as	5'- GGGCCTTGTCGTCGTCGTCCTTATAATCGCCATCGCTGGTACCTTTCA GGCACTGCAGCACCGCGTTATCGCCTTCGCCTCTC-3'
CD19_2FL_s	5'- AGGCGGCGATAACGCGGTGCTGCAGTGCCTGAAAGGTACCAGCGATG GCGGCGATTATAAGGACGACGACGACAAGGCCAGG-3'
CD19_2FL_as	5'- GGGCCTTGTCGTCGTCGTCCTTATAATCGCCGCCATCGCTGGTACCTT TCAGGCACTGCAGCACCGCGTTATCGCCGCCTCTC-3'
CD19_3FL_s	5'- AGGCGATAACGCGGTGCTGCAGTGCCTGAAAGGTACCAGCGATGGCC CGGGCGATTATAAGGACGACGACGACAAGGCCAGG-3'

CD19_3FL_as	5'- GGGCCTTGTCGTCGTCGTCCTTATAATCGCCCCGGGCCATCGCTGGTA CCTTTCAGGCACTGCAGCACCGCGTTATCGCCTCTC-3'
CD19_4FL_s	5'- AGGCAACGCGGTGCTGCAGTGCCTGAAAGGTACCAGCGATGGCCCGA CCGGCGATTATAAGGACGACGACGACAAGGCCCAGG-3'
CD19_4FL_as	5'- GGGCCTTGTCGTCGTCGTCCTTATAATCGCCGGTCGGGCCATCGCTG GTACCTTTCAGGCACTGCAGCACCGCGTTGCCTCTC-3'
CD19_5FL_s	5'- AGGCGCGGTGCTGCAGTGCCTGAAAGGTACCAGCGATGGCCCGACC CAGGGCGATTATAAGGACGACGACGACAAGGCCCAGG-3'
CD19_5FL_as	5'- GGGCCTTGTCGTCGTCGTCCTTATAATCGCCCTGGGTCGGGCCATCG CTGGTACCTTTCAGGCACTGCAGCACCGCGCCTCTC-3'
CD19_6FL_s	5'- AGGCGTGCTGCAGTGCCTGAAAGGTACCAGCGATGGCCCGACCCAGC AGGGCGATTATAAGGACGACGACGACAAGGCCCAGG-3'
CD19_6FL_as	5'- GGGCCTTGTCGTCGTCGTCCTTATAATCGCCCTGCTGGGTCGGGCCA TCGCTGGTACCTTTCAGGCACTGCAGCACGCTCTC-3'
CD19_7FL_s	5'- AGGCCTGCAGTGCCTGAAAGGTACCAGCGATGGCCCGACCCAGCAGC TGGGCGATTATAAGGACGACGACGACAAGGCCCAGG-3'
CD19_7FL_as	5'- GGGCCTTGTCGTCGTCGTCCTTATAATCGCCCAGCTGCTGGGTCGGG CCATCGCTGGTACCTTTCAGGCACTGCAGGCCTCTC-3'
CD19_8FL_s	5'- AGGCCAGTGCCTGAAAGGTACCAGCGATGGCCCGACCCAGCAGCTGA CCGGCGATTATAAGGACGACGACGACAAGGCCCAGG-3'
CD19_8FL_as	5'- GGGCCTTGTCGTCGTCGTCCTTATAATCGCCGGTCAGCTGCTGGGTC GGGCCATCGCTGGTACCTTTCAGGCACTGGCCTCTC-3'
CD19_9FL_s	5'- AGGCTGCCTGAAAGGTACCAGCGATGGCCCGACCCAGCAGCTGACCT GGGGCGATTATAAGGACGACGACGACAAGGCCCAGG-3'
CD19_9FL_as	5'- GGGCCTTGTCGTCGTCGTCCTTATAATCGCCCCAGGTCAGCTGCTGG GTCGGGCCATCGCTGGTACCTTTCAGGCACTGGCCTCTC-3'
CD19_10FL_s	5'- AGGCCTGAAAGGTACCAGCGATGGCCCGACCCAGCAGCTGACCTGGA GCGGCGATTATAAGGACGACGACGACAAGGCCCAGG-3'
CD19_10FL_as	5'- GGGCCTTGTCGTCGTCGTCCTTATAATCGCCGCTCCAGGTCAGCTGCT GGGTCGGGCCATCGCTGGTACCTTTCAGGCCTCTC-3'
CD19_11FL_s	5'- AGGCAAAGGTACCAGCGATGGCCCGACCCAGCAGCTGACCTGGAGC CGCGGCGATTATAAGGACGACGACGACAAGGCCCAGG-3'
CD19_11FL_as	5'- GGGCCTTGTCGTCGTCGTCCTTATAATCGCCGCGGCTCCAGGTCAGC TGCTGGGTCGGGCCATCGCTGGTACCTTTCCTCTC-3'

CD19_12FL_s	5'- AGGCGGTACCAGCGATGGCCCCGACCCAGCAGCTGACCTGGAGCCGC GAAGGCGATTATAAGGACGACGACGACAAGGCCCAGG-3'
CD19_12FL_as	5'- GGGCCTTGTCGTCGTCGTCTTATAATCGCCTTCGCGGCTCCAGGTCA GCTGCTGGGTTCGGGCCATCGCTGGTACCGCCTCTC-3'
CD19_13FL_s	5'- AGGCACCAGCGATGGCCCCGACCCAGCAGTTAACCTGGAGCCGCGAAA GCGGCGATTATAAGGACGACGACGACAAGGCCCAGG-3'
CD19_13FL_as	5'- GGGCCTTGTCGTCGTCGTCTTATAATCGCCGCTTTCGCGGCTCCAG GTTAACTGCTGGGTTCGGGCCATCGCTGGTGCCTCTC-3'
CD19_14FL_s	5'- AGGCAGCGATGGCCCCGACCCAGCAGTTAACCTGGAGCCGCGAAAGC CCGGGCGATTATAAGGACGACGACGACAAGGCCCAGG-3'
CD19_14FL_as	5'- GGGCCTTGTCGTCGTCGTCTTATAATCGCCCCGGGCTTTCGCGGCTC CAGGTTAACTGCTGGGTTCGGGCCATCGCTGCCTCTC-3'
CD19_15FL_s	5'- AGGCGATGGCCCCGACCCAGCAGTTAACCTGGAGCCGCGAAAGCCCG CTGGGCGATTATAAGGACGACGACGACAAGGCCCAGG-3'
CD19_15FL_as	5'- GGGCCTTGTCGTCGTCGTCTTATAATCGCCCAGCGGGCTTTCGCGG CTCCAGGTTAACTGCTGGGTTCGGGCCATCGCCTCTC-3'
CD19_16FL_s	5'- AGGCGGCCCGACCCAGCAGTTAACCTGGAGCCGCGAAAGCCCGCTG AAAGGCGATTATAAGGACGACGACGACAAGGCCCAGG-3'
CD19_16FL_as	5'- GGGCCTTGTCGTCGTCGTCTTATAATCGCCTTTCAGCGGGCTTTCGC GGCTCCAGGTTAACTGCTGGGTTCGGGCCGCTCTC-3'
CD19_17FL_s	5'- AGGCCCGACCCAGCAGTTAACCTGGAGCCGCGAAAGCCCGCTGAAAC CGGGCGATTATAAGGACGACGACGACAAGGCCCAGG-3'
CD19_17FL_as	5'- GGGCCTTGTCGTCGTCGTCTTATAATCGCCCCGGTTCAGCGGGCTTT CGCGGCTCCAGGTTAACTGCTGGGTTCGGGCCCTCTC-3'
CD19_18FL_s	5'- AGGCACCCAGCAGTTAACCTGGAGCCGCGAAAGCCCGCTGAAACCGT TTGGCGATTATAAGGACGACGACGACAAGGCCCAGG-3'
CD19_18FL_as	5'- GGGCCTTGTCGTCGTCGTCTTATAATCGCCAAACGGTTCAGCGGGC TTTCGCGGCTCCAGGTTAACTGCTGGGTGCCTCTC-3'
CD19_19FL_s	5'- AGGCCAGCAGTTAACCTGGAGCCGCGAAAGCCCGCTGAAACCGTTTC TGGGCGATTATAAGGACGACGACGACAAGGCCCAGG-3'
CD19_19FL_as	5'- GGGCCTTGTCGTCGTCGTCTTATAATCGCCCAGAAACGGTTCAGCG GGCTTTCGCGGCTCCAGGTTAACTGCTGGCCTCTC-3'
CD19_20FL_s	5'- AGGCCAGTTAACCTGGAGCCGCGAAAGCCCGCTGAAACCGTTTCTGA AAGGCGATTATAAGGACGACGACGACAAGGCCCAGG-3'

CD19_20FL_as	5'- GGGCCTTGTCGTCGTCGTCCTTATAATCGCCTTTCAGAAACGGTTTCA GCGGGCTTTCGCGGCTCCAGGTTAACTGGCCTCTC-3'
CD19_21FL_s	5'- AGGCCTGACCTGGAGCCGCGAAAGCCCGCTTAAGCCGTTTCTTAAGC TGGGCGATTATAAGGACGACGACGACAAGGCCCAGG-3'
CD19_21FL_as	5'- GGGCCTTGTCGTCGTCGTCCTTATAATCGCCCAGCTTAAGAAACGGCT TAAGCGGGCTTTCGCGGCTCCAGGTCAGGCCTCTC-3'
CD19_22FL_s	5'- AGGCACCTGGAGCCGCGAAAGCCCGCTTAAGCCGTTTCTTAAGCTGA GCGGCGATTATAAGGACGACGACGACAAGGCCCAGG-3'
CD19_22FL_as	5'- GGGCCTTGTCGTCGTCGTCCTTATAATCGCCGCTCAGCTTAAGAAACG GCTTAAGCGGGCTTTCGCGGCTCCAGGTGCCTCTC-3'
CD19_23FL_s	5'- AGGCTGGAGCCGCGAAAGCCCGCTTAAGCCGTTTCTTAAGCTGAGCC TGGGCGATTATAAGGACGACGACGACAAGGCCCAGG-3'
CD19_23FL_as	5'- GGGCCTTGTCGTCGTCGTCCTTATAATCGCCCAGGCTCAGCTTAAGAA ACGGCTTAAGCGGGCTTTCGCGGCTCCAGCCTCTC-3'
CD19_24FL_s	5'- AGGCAGCCGCGAAAGCCCGCTTAAGCCGTTTCTTAAGCTGAGCCTGG GCGGCGATTATAAGGACGACGACGACAAGGCCCAGG-3'
CD19_24FL_as	5'- GGGCCTTGTCGTCGTCGTCCTTATAATCGCCGCCAGGCTCAGCTTAA GAAACGGCTTAAGCGGGCTTTCGCGGCTGCCTCTC-3'
CD19_25FL_s	5'- AGGCCGCGAAAGCCCGCTTAAGCCGTTTCTTAAGCTGAGCCTGGGCC TGGGCGATTATAAGGACGACGACGACAAGGCCCAGG-3'
CD19_25FL_as	5'- GGGCCTTGTCGTCGTCGTCCTTATAATCGCCCAGGCCCAGGCTCAGC TTAAGAAACGGCTTAAGCGGGCTTTCGCGGCTCTC-3'
CD19_26FL_s	5'- AGGCGAAAGCCCGCTTAAGCCGTTTCTTAAGCTGAGCCTGGGCCTGC CGGGCGATTATAAGGACGACGACGACAAGGCCCAGG-3'
CD19_26FL_as	5'- GGGCCTTGTCGTCGTCGTCCTTATAATCGCCCCGGCAGGCCCAGGCTC AGCTTAAGAAACGGCTTAAGCGGGCTTTCGCCTCTC-3'
CD19_27FL_s	5'- AGGCAGCCCGCTTAAGCCGTTTCTTAAGCTGAGCCTGGGCCTGCCGG GCGGCGATTATAAGGACGACGACGACAAGGCCCAGG-3'
CD19_27FL_as	5'- GGGCCTTGTCGTCGTCGTCCTTATAATCGCCGCCCGGCAGGCCCAGG CTCAGCTTAAGAAACGGCTTAAGCGGGCTGCCTCTC-3'
CD19_28FL_s	5'- AGGCCCGCTTAAGCCGTTTCTTAAGCTGAGCCTGGGCCTGCCGGGCC TGGGCGATTATAAGGACGACGACGACAAGGCCCAGG-3'
CD19_28FL_as	5'- GGGCCTTGTCGTCGTCGTCCTTATAATCGCCCAGGCCCGGCAGGCC AGGCTCAGCTTAAGAAACGGCTTAAGCGGGCTCTC-3'

CD19_29FL_s	5'- AGGCCTTAAGCCGTTTCTTAAGCTGAGCCTGGGCCTGCCGGGCCTGG GCGGCGATTATAAGGACGACGACGACAAGGCCCAGG-3'
CD19_29FL_as	5'- GGGCCTTGTCGTCGTCGTCCTTATAATCGCCGCCAGGCCCGGCAGG CCCAGGCTCAGCTTAAGAAACGGCTTAAGGCCTCTC-3'
CD19_30FL_s	5'- AGGCAAACCGTTTCTTAAGCTGAGCCTGGGCCTGCCGGGCCTGGGCA TTGGCGATTATAAGGACGACGACGACAAGGCCCAGG-3'
CD19_30FL_as	5'- GGGCCTTGTCGTCGTCGTCCTTATAATCGCCAATGCCCAGGCCCGGC AGGCCCAGGCTCAGCTTAAGAAACGGTTTGCCTCTC-3'
CD19_31FL_s	5'- AGGCCCGTTTCTTAAGCTGAGCCTGGGCCTGCCGGGCCTGGGCATTC ATGGCGATTATAAGGACGACGACGACAAGGCCCAGG-3'
CD19_31FL_as	5'- GGGCCTTGTCGTCGTCGTCCTTATAATCGCCATGAATGCCCAGGCC GGCAGGCCCAGGCTCAGCTTAAGAAACGGGCCTCTC-3'
CD19_32FL_s	5'- AGGCTTCCTTAAGCTGAGCCTGGGCCTGCCCGGCCTGGGCATCCACA TGGGCGATTATAAGGACGACGACGACAAGGCCCAGG-3'
CD19_32FL_as	5'- GGGCCTTGTCGTCGTCGTCCTTATAATCGCCCATGTGGATGCCCAGG CCGGGCAGGCCCAGGCTCAGCTTAAGGAAGCCTCTC-3'
CD19_33FL_s	5'- AGGCCTTAAGCTGAGCCTGGGCCTGCCCGGCCTGGGCATCCACATGA GAGGCGATTATAAGGACGACGACGACAAGGCCCAGG-3'
CD19_33FL_as	5'- GGGCCTTGTCGTCGTCGTCCTTATAATCGCCTCTCATGTGGATGCCCA GGCCGGCAGGCCCAGGCTCAGCTTAAGGCCTCTC-3'
CD19_34FL_s	5'- AGGCAAGCTGAGCCTGGGCCTGCCCGGCCTGGGGATCCACATGAGA CCCGGCGATTATAAGGACGACGACGACAAGGCCCAGG-3'
CD19_34FL_as	5'- GGGCCTTGTCGTCGTCGTCCTTATAATCGCCGGGTCTCATGTGGATCC CCAGGCCGGGCAGGCCCAGGCTCAGCTTGCCTCTC-3'
CD19_35FL_s	5'- AGGCCTGAGCCTGGGCCTGCCCGGCCTGGGGATCCACATGAGACCC CTGGGCGATTATAAGGACGACGACGACAAGGCCCAGG-3'
CD19_35FL_as	5'- GGGCCTTGTCGTCGTCGTCCTTATAATCGCCCAGGGGTCTCATGTGGA TCCCAGGCCGGGCAGGCCCAGGCTCAGGCCTCTC-3'
CD19_36FL_s	5'- AGGCAGCCTGGGCCTGCCCGGCCTGGGGATCCACATGAGACCCCTG GCCGCGATTATAAGGACGACGACGACAAGGCCCAGG-3'
CD19_36FL_as	5'- GGGCCTTGTCGTCGTCGTCCTTATAATCGCCGGCCAGGGGTCTCATG TGGATCCCCAGGCCGGGCAGGCCCAGGCTGCCTCTC-3'
CD19_37FL_s	5'- AGGCCTGGGCCTGCCCGGCCTGGGGATCCACATGAGACCCCTGGCC ATCGGCGATTATAAGGACGACGACGACAAGGCCCAGG-3'

CD19_37FL_as	5'- GGGCCTTGTTCGTCGTCGTCCTTATAATCGCCGATGGCCAGGGGTCTC ATGTGGATCCCCAGGCCGGGCAGGCCAGGCCTCTC-3'
CD19_38FL_s	5'- AGGCGGCCTGCCCGGCCTGGGGATCCACATGAGACCCCTGGCCATCT GGGGCGATTATAAAGGACGACGACGACAAGGCCCAGG-3'
CD19_38FL_as	5'- GGGCCTTGTTCGTCGTCGTCCTTATAATCGCCCCAGATGGCCAGGGGT CTCATGTGGATCCCCAGGCCGGGCAGGCCGCCTCTC-3'
CD19_39FL_s	5'- AGGCCTGCCCGGCCTGGGGATCCACATGAGACCCCTGGCCATCTGGC TGGGCGATTATAAAGGACGACGACGACAAGGCCCAGG-3'
CD19_39FL_as	5'- GGGCCTTGTTCGTCGTCGTCCTTATAATCGCCCAGCCAGATGGCCAGG GGTCTCATGTGGATCCCCAGGCCGGGCAGGCCTCTC-3'
CD19_40FL_s	5'- AGGCCCCGGCCTGGGGATCCACATGAGACCCCTGGCCATCTGGCTGT TCGGCGATTATAAAGGACGACGACGACAAGGCCCAGG-3'
CD19_40FL_as	5'- GGGCCTTGTTCGTCGTCGTCCTTATAATCGCCGAACAGCCAGATGGCC AGGGGTCTCATGTGGATCCCCAGGCCGGGGCCTCTC-3'
CD19_41FL_s	5'- AGGCGGCCTGGGGATCCACATGAGACCCCTGGCCATCTGGCTGTTCA TCGGCGATTATAAAGGACGACGACGACAAGGCCCAGG-3'
CD19_41FL_as	5'- GGGCCTTGTTCGTCGTCGTCCTTATAATCGCCGATGAACAGCCAGATGG CCAGGGGTCTCATGTGGATCCCCAGGCCGCCTCTC-3'
CD19_42FL_s	5'- AGGCCTGGGGATCCACATGAGACCCCTGGCCATCTGGCTGTTTCATCTT CGGCGATTATAAAGGACGACGACGACAAGGCCCAGG-3'
CD19_42FL_as	5'- GGGCCTTGTTCGTCGTCGTCCTTATAATCGCCGAAGATGAACAGCCAGA TGGCCAGGGGTCTCATGTGGATCCCCAGGCCTCTC-3'
CD19_43FL_s	5'- AGGCGGGATCCACATGAGACCCCTGGCCATCTGGCTGTTTCATCTTCAA CGGCGATTATAAAGGACGACGACGACAAGGCCCAGG-3'
CD19_43FL_as	5'- GGGCCTTGTTCGTCGTCGTCCTTATAATCGCCGTTGAAGATGAACAGCC AGATGGCCAGGGGTCTCATGTGGATCCCCGCCTCTC-3'
CD19_44FL_s	5'- AGGCATCCACATGAGACCCCTGGCCATATGGCTGTTTCATCTTCAACGT GGGCGATTATAAAGGACGACGACGACAAGGCCCAGG-3'
CD19_44FL_as	5'- GGGCCTTGTTCGTCGTCGTCCTTATAATCGCCCACGTTGAAGATGAACA GCCATATGGCCAGGGGTCTCATGTGGATGCCTCTC-3'
CD19_45FL_s	5'- AGGCCACATGAGACCCCTGGCCATATGGCTGTTTCATCTTCAACGTGAG CGGCGATTATAAAGGACGACGACGACAAGGCCCAGG-3'
CD19_45FL_as	5'- GGGCCTTGTTCGTCGTCGTCCTTATAATCGCCGCTCACGTTGAAGATGA ACAGCCATATGGCCAGGGGTCTCATGTGGCCTCTC-3'

CD19_46FL_s	5'- AGGCATGAGACCCCTGGCCATATGGCTGTTTCATCTTCAACGTGAGCCA GGGCGATTATAAGGACGACGACGACAAGGCCCAGG-3'
CD19_46FL_as	5'- GGGCCTTGTCGTCGTCGTCCTTATAATCGCCCTGGCTCACGTTGAAGA TGAACAGCCATATGGCCAGGGGTCTCATGCCTCTC-3'
CD19_47FL_s	5'- AGGCAGACCCCTGGCCATATGGCTGTTTCATCTTCAACGTGAGCCAGCA GGGCGATTATAAGGACGACGACGACAAGGCCCAGG-3'
CD19_47FL_as	5'- GGGCCTTGTCGTCGTCGTCCTTATAATCGCCCTGCTGGCTCACGTTGA AGATGAACAGCCATATGGCCAGGGGTCTGCCTCTC-3'
CD19_48FL_s	5'- AGGCCCCCTGGCCATATGGCTGTTTCATCTTCAACGTGAGCCAGCAGAT GGGCGATTATAAGGACGACGACGACAAGGCCCAGG-3'
CD19_48FL_as	5'- GGGCCTTGTCGTCGTCGTCCTTATAATCGCCCATCTGCTGGCTCACGT TGAAGATGAACAGCCATATGGCCAGGGGGCCTCTC-3'
CD19_49FL_s	5'- AGGCCTGGCCATATGGCTGTTTCATCTTCAACGTGAGCCAGCAGATGG GCGGCGATTATAAGGACGACGACGACAAGGCCCAGG-3'
CD19_49FL_as	5'- GGGCCTTGTCGTCGTCGTCCTTATAATCGCCGCCATCTGCTGGCTCA CGTTGAAGATGAACAGCCATATGGCCAGGCCTCTC-3'
CD19_50FL_s	5'- AGGCGCCATATGGCTGTTTCATCTTCAACGTGAGCCAGCAGATGGGCG GCGGCGATTATAAGGACGACGACGACAAGGCCCAGG-3'
CD19_50FL_as	5'- GGGCCTTGTCGTCGTCGTCCTTATAATCGCCGCCGCCATCTGCTGG CTCACGTTGAAGATGAACAGCCATATGGCGCCTCTC-3'
CD19_51FL_s	5'- AGGCATCTGGCTGTTTCATCTTCAACGTGAGCCAGCAGATGGGCGGCT TCGGCGATTATAAGGACGACGACGACAAGGCCCAGG-3'
CD19_51FL_as	5'- GGGCCTTGTCGTCGTCGTCCTTATAATCGCCGAAGCCGCCATCTGCT GGCTCACGTTGAAGATGAACAGCCAGATGCCTCTC-3'
CD19_52FL_s	5'- AGGCTGGCTGTTTCATCTTCAACGTGAGCCAGCAGATGGGCGGCTTCT ACGGCGATTATAAGGACGACGACGACAAGGCCCAGG-3'
CD19_52FL_as	5'- GGGCCTTGTCGTCGTCGTCCTTATAATCGCCGTAGAAGCCGCCATCT GCTGGCTCACGTTGAAGATGAACAGCCAGCCTCTC-3'
CD19_53FL_s	5'- AGGCCTGTTTCATCTTCAACGTGAGCCAGCAGATGGGCGGCTTCTACCT GGGCGATTATAAGGACGACGACGACAAGGCCCAGG-3'
CD19_53FL_as	5'- GGGCCTTGTCGTCGTCGTCCTTATAATCGCCCAGGTAGAAGCCGCC ATCTGCTGGCTCACGTTGAAGATGAACAGGCCTCTC-3'
CD19_54FL_s	5'- AGGCTTCATCTTCAACGTGAGCCAGCAGATGGGCGGCTTCTACCTGTG CGGCGATTATAAGGACGACGACGACAAGGCCCAGG-3'

CD19_54FL_as	5'- GGGCCTTGTCGTCGTCGTCCTTATAATCGCCGCACAGGTAGAAGCCG CCCATCTGCTGGCTCACGTTGAAGATGAAGCCTCTC-3'
CD19_55FL_s	5'- AGGCATCTTCAACGTGAGCCAGCAGATGGGCGGCTTCTACCTGTGCC AGGGCGATTATAAGGACGACGACGACAAGGCCCAGG-3'
CD19_55FL_as	5'- GGGCCTTGTCGTCGTCGTCCTTATAATCGCCCTGGCACAGGTAGAAG CCGCCATCTGCTGGCTCACGTTGAAGATGCCTCTC-3'
CD19_56FL_s	5'- AGGCTTCAACGTGAGCCAGCAGATGGGCGGCTTCTACCTGTGCCAGC CCGGCGATTATAAGGACGACGACGACAAGGCCCAGG-3'
CD19_56FL_as	5'- GGGCCTTGTCGTCGTCGTCCTTATAATCGCCGGGCTGGCACAGGTAG AAGCCGCCATCTGCTGGCTCACGTTGAAGCCTCTC-3'
CD19_57FL_s	5'- AGGCAACGTGAGCCAGCAGATGGGCGGCTTCTACCTGTGCCAGCCCG GCGGCGATTATAAGGACGACGACGACAAGGCCCAGG-3'
CD19_57FL_as	5'- GGGCCTTGTCGTCGTCGTCCTTATAATCGCCCCGGGCTGGCACAGG TAGAAGCCGCCATCTGCTGGCTCACGTTGCCTCTC-3'
CD19_58FL_s	5'- AGGCGTGAGCCAGCAGATGGGCGGCTTCTACCTGTGCCAGCCCGGC CCCGGCGATTATAAGGACGACGACGACAAGGCCCAGG-3'
CD19_58FL_as	5'- GGGCCTTGTCGTCGTCGTCCTTATAATCGCCGGGCCCGGGCTGGCAC AGGTAGAAGCCGCCATCTGCTGGCTCACGCCTCTC-3'
CD19_59FL_s	5'- AGGCAGCCAGCAGATGGGCGGCTTCTACCTGTGCCAGCCCGGCCCC CCCGGCGATTATAAGGACGACGACGACAAGGCCCAGG-3'
CD19_59FL_as	5'- GGGCCTTGTCGTCGTCGTCCTTATAATCGCCGGGGGGGCCCGGGCTGG CACAGGTAGAAGCCGCCATCTGCTGGCTGCCTCTC-3'
CD19_60FL_s	5'- AGGCCAGCAGATGGGCGGCTTCTACCTGTGCCAGCCCGGCCCCCCCC AGCGGCGATTATAAGGACGACGACGACAAGGCCCAGG-3'
CD19_60FL_as	5'- GGGCCTTGTCGTCGTCGTCCTTATAATCGCCGCTGGGGGGGCCGGGC TGGCACAGGTAGAAGCCGCCATCTGCTGGCCTCTC-3'
CD19_61FL_s	5'- AGGCCAGATGGGCGGCTTCTACCTGTGCCAGCCCGGCCCCCCCCAGC GAGGGCGATTATAAGGACGACGACGACAAGGCCCAGG-3'
CD19_61FL_as	5'- GGGCCTTGTCGTCGTCGTCCTTATAATCGCCCTCGCTGGGGGGCCCG GGCTGGCACAGGTAGAAGCCGCCATCTGGCCTCTC-3'
CD19_62FL_s	5'- AGGCATGGGCGGCTTCTACCTGTGCCAGCCCGGCCCCCCCCAGCGAG AAGGGCGATTATAAGGACGACGACGACAAGGCCCAGG-3'
CD19_62FL_as	5'- GGGCCTTGTCGTCGTCGTCCTTATAATCGCCCTTCTCGCTGGGGGGC CCGGGCTGGCACAGGTAGAAGCCGCCATGCCTCTC-3'

CD19_63FL_s	5'- AGGCGGCGGCTTCTACCTGTGCCAGCCCGGCCCCCCCAGCGAGAAG GCCGCGATTATAAGGACGACGACGACAAGGCCCAGG-3'
CD19_63FL_as	5'- GGGCCTTGTCTCGTCGTCTCCTTATAATCGCCGGCCTTCTCGCTGGGG GGCCCGGGCTGGCACAGGTAGAAGCCGCGCCTCTC-3'
CD19_64FL_s	5'- AGGCGGCTTCTACCTGTGCCAGCCCGGCCCCCCCAGCGAGAAGGCC TGGGGCGATTATAAGGACGACGACGACAAGGCCCAGG-3'
CD19_64FL_as	5'- GGGCCTTGTCTCGTCGTCTCCTTATAATCGCCCCAGGCCTTCTCGCTGG GGGGCCCGGGCTGGCACAGGTAGAAGCCGCTCTC-3'
CD19_65FL_s	5'- AGGCTTCTACCTGTGCCAGCCCGGCCCCCCCAGCGAGAAGGCCTGG CAGGGCGATTATAAGGACGACGACGACAAGGCCCAGG-3'
CD19_65FL_as	5'- GGGCCTTGTCTCGTCGTCTCCTTATAATCGCCCTGCCAGGCCTTCTCGC TGGGGGGCCCGGGCTGGCACAGGTAGAAGCCTCTC-3'
CD19_66FL_s	5'- AGGCTACCTGTGCCAGCCCGGCCCCCCCAGCGAGAAGGCCTGGCAG CCCGGCGATTATAAGGACGACGACGACAAGGCCCAGG-3'
CD19_66FL_as	5'- GGGCCTTGTCTCGTCGTCTCCTTATAATCGCCGGGCTGCCAGGCCTTC TCGCTGGGGGGCCCGGGCTGGCACAGGTAGCCTCTC-3'
CD19_67FL_s	5'- AGGCCTGTGCCAGCCCGGCCCCCCCAGCGAGAAGGCCTGGCAGCCC GGCGGCGATTATAAGGACGACGACGACAAGGCCCAGG-3'
CD19_67FL_as	5'- GGGCCTTGTCTCGTCGTCTCCTTATAATCGCCGCCGGGCTGCCAGGCC TTCTCGCTGGGGGGCCCGGGCTGGCACAGGCCTCTC-3'
CD19_68FL_s	5'- AGGCTGCCAGCCCGGCCCCCCCAGCGAGAAGGCCTGGCAGCCCGGC TGGGGCGATTATAAGGACGACGACGACAAGGCCCAGG-3'
CD19_68FL_as	5'- GGGCCTTGTCTCGTCGTCTCCTTATAATCGCCCCAGCCGGGCTGCCAG GCCTTCTCGCTGGGGGGCCCGGGCTGGCAGCCTCTC-3'
CD19_69FL_s	5'- AGGCCAGCCCGGCCCCCCCAGCGAGAAGGCCTGGCAGCCCGGCTGG ACCGGCGATTATAAGGACGACGACGACAAGGCCCAGG-3'
CD19_69FL_as	5'- GGGCCTTGTCTCGTCGTCTCCTTATAATCGCCGGTCCAGCCGGGCTGC CAGGCCTTCTCGCTGGGGGGCCCGGGCTGGCCTCTC-3'
CD19_70FL_s	5'- AGGCCCGGCCCCCCCAGCGAGAAGGCCTGGCAGCCCGGCTGGACC GTGGGCGATTATAAGGACGACGACGACAAGGCCCAGG-3'
CD19_70FL_as	5'- GGGCCTTGTCTCGTCGTCTCCTTATAATCGCCCACGGTCCAGCCGGGC TGCCAGGCCTTCTCGCTGGGGGGCCCGGGCCTCTC-3'
CD19_71FL_s	5'- AGGCGGCCCCCCCAGCGAGAAGGCCTGGCAGCCCGGCTGGACCGTG AACGGCGATTATAAGGACGACGACGACAAGGCCCAGG-3'

CD19_71FL_as	5'- GGGCCTTGTCGTCGTCGTCCTTATAATCGCCGTTACGGTCCACCCG GGTGCCAGGCCTTCTCGCTGGGGGGGCCGCTCTC-3'
CD19_72FL_s	5'- AGGCCCCCCCAGCGAGAAGGCCTGGCAGCCCGGCTGGACCGTGAAC GTGGGCGATTATAAGGACGACGACGACAAGGCCCAGG-3'
CD19_72FL_as	5'- GGGCCTTGTCGTCGTCGTCCTTATAATCGCCCACGTTACGGTCCACC CGGGCTGCCAGGCCTTCTCGCTGGGGGGCCTCTC-3'
CD19_73FL_s	5'- AGGCCCCAGCGAGAAGGCCTGGCAGCCCGGCTGGACCGTGAACGTG GAGGGCGATTATAAGGACGACGACGACAAGGCCCAGG-3'
CD19_73FL_as	5'- GGGCCTTGTCGTCGTCGTCCTTATAATCGCCCTCCACGTTACGGTCC ACCCGGGCTGCCAGGCCTTCTCGCTGGGGCCTCTC-3'
CD19_74FL_s	5'- AGGCAGCGAGAAGGCCTGGCAGCCCGGCTGGACCGTGAACGTGGAG GGCGGCGATTATAAGGACGACGACGACAAGGCCCAGG-3'
CD19_74FL_as	5'- GGGCCTTGTCGTCGTCGTCCTTATAATCGCCGCCCTCCACGTTACGG TCCACCCGGGCTGCCAGGCCTTCTCGCTGCCTCTC-3'
CD19_75FL_s	5'- AGGCGAGAAGGCCTGGCAGCCCGGCTGGACCGTGAACGTGGAGGGC AGCGGCGATTATAAGGACGACGACGACAAGGCCCAGG-3'
CD19_75FL_as	5'- GGGCCTTGTCGTCGTCGTCCTTATAATCGCCGCTGCCCTCCACGTTCA CGGTCCACCCGGGCTGCCAGGCCTTCTCGCCTCTC-3'
CD19_6FL2_s	5'- AGGCGACGACGACGACAAGGGCGTGCTGCAGTGCCTGAAAGGTACCA GCGATGGCCCGACCCAGCAGGGCGATTATAAGGACGACGACGACAAG GCCCAGG-3'
CD19_6FL2_as	5'- GGGCCTTGTCGTCGTCGTCCTTATAATCGCCCTGCTGGGTCCGGCCA TCGCTGGTACCTTTCAGGCACTGCAGCACGCCCTTGTCGTCGTCGTC GCCTCTC-3'
CD19_23FL2_s	5'- AGGCGACGACGACGACAAGGGCTGGAGCCGCGAAAGCCCGCTTAAG CCGTTTCTTAAGCTGAGCCTGGGCGATTATAAGGACGACGACGACAAG GCCCAGG-3'
CD19_23FL2_as	5'- GGGCCTTGTCGTCGTCGTCCTTATAATCGCCCAGGCTCAGCTTAAGAA ACGGCTTAAGCGGGCTTTCGCGGCTCCAGCCCTTGTCGTCGTCGTCG CCTCTC-3'
CD19_33FL2_s	5'- AGGCGACGACGACGACAAGGGCCTTAAGCTGAGCCTGGGCCTGCC GGCCTGGGCATCCACATGAGAGGCGATTATAAGGACGACGACGACAA GGCCAGG-3'
CD19_33FL2_as	5'- GGGCCTTGTCGTCGTCGTCCTTATAATCGCCTCTCATGTGGATGCCCA GGCCGGGCAGGCCAGGCTCAGCTTAAGGCCCTTGTCGTCGTCGTCG CCTCTC-3'
CD19_42FL2_s	5'- AGGCGACGACGACGACAAGGGCCTGGGGATCCACATGAGACCCCTG

	GCCATCTGGCTGTTTCATCTTCGGCGATTATAAGGACGACGACGACAAG GCCCAGG-3'
CD19_42FL2_as	5'- GGGCCTTGTCTGTCGTCGTCCTTATAATCGCCGAAGATGAACAGCCAGA TGGCCAGGGGTCTCATGTGGATCCCCAGGCCCTTGTCTGTCGTCGTCG CCTCTC-3'
CD19_51FL2_s	5'- AGGCGACGACGACGACAAGGGCATCTGGCTGTTTCATCTTCAACGTGA GCCAGCAGATGGGCGGCTTCGGCGATTATAAGGACGACGACGACAAG GCCCAGG-3'
CD19_51FL2_as	5'- GGGCCTTGTCTGTCGTCGTCCTTATAATCGCCGAAGCCGCCATCTGCT GGCTCACGTTGAAGATGAACAGCCAGATGCCCTTGTCTGTCGTCGTCG CCTCTC-3'
CD19_55FL2_s	5'- AGGCGACGACGACGACAAGGGCATCTTCAACGTGAGCCAGCAGATGG GCGGCTTCTACCTGTGCCAGGGCGATTATAAGGACGACGACGACAAG GCCCAGG-3'
CD19_55FL2_as	5'- GGGCCTTGTCTGTCGTCGTCCTTATAATCGCCCTGGCACAGGTAGAAG CCGCCATCTGCTGGCTCACGTTGAAGATGCCCTTGTCTGTCGTCGTC GCCTCTC-3'
NYBR1C2_FL2s	5'- AGGCGACGACGACGACAAGGGCCTGAAAAACGAACAGACCTTAAGAG CGGATCAGATGTTTGGCGATTATAAGGACGACGACGACAAGGCCAG G-3'
NYBR1C2_FL2_as	5'- GGGCCTTGTCTGTCGTCGTCCTTATAATCGCCTCTCATGTGGATGCCCA GGCCGGCAGGCCAGGCTCAGCTTAAGGCCCTTGTCTGTCGTCGTCG CCTCTC-3'
CD19_6FL_R588T_a s	5'- GGGCCTTGTCTGTCGTCGTCCTTATAATCGCCCTGCTGGGTCTGGCCA TCGCTGGTACCTTTCAGGCACTGCAGCACGCCTGTC-3'
CD19_23FL_R588T_ as	5'- GGGCCTTGTCTGTCGTCGTCCTTATAATCGCCCAGGCTCAGCTTAAGAA ACGGCTTAAGCGGGCTTTCGCGGCTCCAGCCTGTC-3'
CD19_33FL_R588T_ as	5'- GGGCCTTGTCTGTCGTCGTCCTTATAATCGCCTCTCATGTGGATGCCCA GGCCGGCAGGCCAGGCTCAGCTTAAGGCCCTGTC-3'
CD19_42FL_R588T_ as	5'- GGGCCTTGTCTGTCGTCGTCCTTATAATCGCCGAAGATGAACAGCCAGA TGGCCAGGGGTCTCATGTGGATCCCCAGGCCTGTC-3'
CD19_51FL_R588T_ as	5'- GGGCCTTGTCTGTCGTCGTCCTTATAATCGCCGAAGCCGCCATCTGCT GGCTCACGTTGAAGATGAACAGCCAGATGCCTGTC-3'
CD19_55FL_R588T_ as	5'- GGGCCTTGTCTGTCGTCGTCCTTATAATCGCCCTGGCACAGGTAGAAG CCGCCATCTGCTGGCTCACGTTGAAGATGCCTGTC-3'
NYBR1C2_FL_R588 T_as	5'- GGGCCTTGTCTGTCGTCGTCCTTATAATCGCCAAACATCTGATCCGCTC TTAAGGTCTGTTTCGTTTTTCAGGCCTGTC-3'

CD19_6FL_A593T_s	5'- AGGCGTGCTGCAGTGCCTGAAAGGTACCAGCGATGGCCCCACCCAGC AGGGCGATTATAAGGACGACGACGACAAGGCCAAGA-3'
CD19_23FL_A593T_s	5'- AGGCTGGAGCCGCGAAAGCCCGCTTAAGCCGTTTCTTAAGCTGAGCC TGGGCGATTATAAGGACGACGACGACAAGGCCAAGA-3'
CD19_33FL_A593T_s	5'- AGGCCTTAAGCTGAGCCTGGGCCTGCCGGCCTGGGCATCCACATGA GAGGCGATTATAAGGACGACGACGACAAGGCCAAGA-3'
CD19_42FL_A593T_s	5'- AGGCCTGGGGATCCACATGAGACCCCTGGCCATCTGGCTGTTTCATCTT CGGCGATTATAAGGACGACGACGACAAGGCCAAGA-3'
CD19_51FL_A593T_s	5'- AGGCATCTGGCTGTTTCATCTTCAACGTGAGCCAGCAGATGGGCGGCT TCGGCGATTATAAGGACGACGACGACAAGGCCAAGA-3'
CD19_55FL_A593T_s	5'- AGGCATCTTCAACGTGAGCCAGCAGATGGGCGGCTTCTACCTGTGCC AGGGCGATTATAAGGACGACGACGACAAGGCCAAGA-3'
NYBR1C2FL_A593T_s	5'- AGGCCTGAAAAACGAACAGACCTTAAGAGCGGATCAGATGTTTGGCGA TTATAAGGACGACGACGACAAGGCCAAGA-3'
A1_CD19_42FL_s	5'- AGGCGCCGGCATCCACATGAGACCCCTGGCCATCTGGCTGTTTCATCT TCGGCGATTATAAGGACGACGACGACAAGGCCAAGG-3'
A1_CD19_42FL_as	5'- GGGCCTTGTCGTCGTCGTCCCTTATAATCGCCGAAGATGAACAGCCAGA TGGCCAGGGGTCTCATGTGGATGCCGGCGCCTCTC-3'
A2_CD19_42FL_s	5'- AGGCCTGGCCATCCACATGAGACCCCTGGCCATCTGGCTGTTTCATCTT CGGCGATTATAAGGACGACGACGACAAGGCCAAGG-3'
A2_CD19_42FL_as	5'- GGGCCTTGTCGTCGTCGTCCCTTATAATCGCCGAAGATGAACAGCCAGA TGGCCAGGGGTCTCATGTGGATGCCAGGCCTCTC-3'
A3_CD19_42FL_s	5'- AGGCCTGGGCGCCACATGAGACCCCTGGCCATCTGGCTGTTTCATCT TCGGCGATTATAAGGACGACGACGACAAGGCCAAGG-3'
A3_CD19_42FL_as	5'- GGGCCTTGTCGTCGTCGTCCCTTATAATCGCCGAAGATGAACAGCCAGA TGGCCAGGGGTCTCATGTGGGCGCCAGGCCTCTC-3'
A4_CD19_42FL_s	5'- AGGCCTGGGCATCGCCATGAGACCCCTGGCCATCTGGCTGTTTCATCT TCGGCGATTATAAGGACGACGACGACAAGGCCAAGG-3'
A4_CD19_42FL_as	5'- GGGCCTTGTCGTCGTCGTCCCTTATAATCGCCGAAGATGAACAGCCAGA TGGCCAGGGGTCTCATGGCGATGCCAGGCCTCTC-3'
A5_CD19_42FL_s	5'- AGGCCTGGGCATCCACGCCAGACCCCTGGCCATCTGGCTGTTTCATCT TCGGCGATTATAAGGACGACGACGACAAGGCCAAGG-3'
A5_CD19_42FL_as	5'- GGGCCTTGTCGTCGTCGTCCCTTATAATCGCCGAAGATGAACAGCCAGA TGGCCAGGGGTCTGGCGTGGATGCCAGGCCTCTC-3'

A6_CD19_42FL_s	5'- AGGCCTGGGCATCCACATGGCCCCCTGGCCATCTGGCTGTTTCATCT TCGGCGATTATAAGGACGACGACGACAAGGCCCAGG-3'
A6_CD19_42FL_as	5'- GGGCCTTGTCGTCGTCGTCCTTATAATCGCCGAAGATGAACAGCCAGA TGGCCAGGGGGGCCATGTGGATGCCCAGGCCTCTC-3'
A7_CD19_42FL_s	5'- AGGCCTGGGCATCCACATGAGAGCCCTGGCCATCTGGCTGTTTCATCTT CGGCGATTATAAGGACGACGACGACAAGGCCCAGG-3'
A7_CD19_42FL_as	5'- GGGCCTTGTCGTCGTCGTCCTTATAATCGCCGAAGATGAACAGCCAGA TGGCCAGGGCTCTCATGTGGATGCCCAGGCCTCTC-3'
A8_CD19_42FL_s	5'- AGGCCTGGGCATCCACATGAGACCCGCGCCATCTGGCTGTTTCATCT TCGGCGATTATAAGGACGACGACGACAAGGCCCAGG-3'
A8_CD19_42FL_as	5'- GGGCCTTGTCGTCGTCGTCCTTATAATCGCCGAAGATGAACAGCCAGA TGGCGGCGGGTCTCATGTGGATGCCCAGGCCTCTC-3'
A10_CD19_42FL_s	5'- AGGCCTGGGCATCCACATGAGACCCCTGGCCGCCTGGCTGTTTCATCT TCGGCGATTATAAGGACGACGACGACAAGGCCCAGG-3'
A10_CD19_42FL_as	5'- GGGCCTTGTCGTCGTCGTCCTTATAATCGCCGAAGATGAACAGCCAG GCGGCCAGGGGTCTCATGTGGATGCCCAGGCCTCTC-3'
A11_CD19_42FL_s	5'- AGGCCTGGGCATCCACATGAGACCCCTGGCCATCGCCCTGTTTCATCTT CGGCGATTATAAGGACGACGACGACAAGGCCCAGG-3'
A11_CD19_42FL_as	5'- GGGCCTTGTCGTCGTCGTCCTTATAATCGCCGAAGATGAACAGGGCG ATGGCCAGGGGTCTCATGTGGATGCCCAGGCCTCTC-3'
A12_CD19_42FL_s	5'- AGGCCTGGGCATCCACATGAGACCCCTGGCCATCTGGGCCTTCATCT TCGGCGATTATAAGGACGACGACGACAAGGCCCAGG-3'
A12_CD19_42FL_as	5'- GGGCCTTGTCGTCGTCGTCCTTATAATCGCCGAAGATGAAGGCCCAG ATGGCCAGGGGTCTCATGTGGATGCCCAGGCCTCTC-3'
A13_CD19_42FL_s	5'- AGGCCTGGGCATCCACATGAGACCCCTGGCCATCTGGCTGGCCATCT TCGGCGATTATAAGGACGACGACGACAAGGCCCAGG-3'
A13_CD19_42FL_as	5'- GGGCCTTGTCGTCGTCGTCCTTATAATCGCCGAAGATGGCCAGCCAG ATGGCCAGGGGTCTCATGTGGATGCCCAGGCCTCTC-3'
A14_CD19_42FL_s	5'- AGGCCTGGGCATCCACATGAGACCCCTGGCCATCTGGCTGTTTCGCT TCGGCGATTATAAGGACGACGACGACAAGGCCCAGG-3'
A14_CD19_42FL_as	5'- GGGCCTTGTCGTCGTCGTCCTTATAATCGCCGAAGGCGAACAGCCAG ATGGCCAGGGGTCTCATGTGGATGCCCAGGCCTCTC-3'
A15_CD19_42FL_s	5'- AGGCCTGGGCATCCACATGAGACCCCTGGCCATCTGGCTGTTTCATCG CCGGCGATTATAAGGACGACGACGACAAGGCCCAGG-3'

A15_CD19_42FL_as	5'- GGGCCTTGTCGTCGTCGTCCTTATAATCGCCGGCGATGAACAGCCAG ATGGCCAGGGGTCTCATGTGGATGCCAGGCCTCTC-3'
A16_CD19_42FL_s	5'- AGGCCTGGGCATCCACATGAGACCCCTGGCCATCTGGCTGTTTCATCG CCGGCGATTATAAGGACGACGACGACAAGGCCAGG-3'
A16_CD19_42FL_as	5'- GGGCCTTGTCGTCGTCGTCCTTATAATCGCCGAAGATGGCCAGGGCG ATGGCCAGGGGTCTCATGTGGATGCCAGGCCTCTC-3'
A17_CD19_42FL_s	5'- AGGCCTGGGCATCCACATGAGACCCCTGGCCATCGCCCTGGCCATCT TCGGCGATTATAAGGACGACGACGACAAGGCCAGG-3'
A17_CD19_42FL_as	5'- GGGCCTTGTCGTCGTCGTCCTTATAATCGCCGGCGATGGCCAGCCAG ATGGCCAGGGGTCTCATGTGGATGCCAGGCCTCTC-3'
A18_CD19_42FL_s	5'- AGGCCTGGGCATCCACATGAGACCCCTGGCCATCTGGCTGGCCATCG CCGGCGATTATAAGGACGACGACGACAAGGCCAGG-3'
A18_CD19_42FL_as	5'- GGGCCTTGTCGTCGTCGTCCTTATAATCGCCGGCGATGAACAGGGCG ATGGCCAGGGGTCTCATGTGGATGCCAGGCCTCTC-3'
A19_CD19_42FL_s	5'- AGGCCTGGGCATCCACATGAGACCCCTGGCCATCGCCCTGTTTCATCG CCGGCGATTATAAGGACGACGACGACAAGGCCAGG-3'
A19_CD19_42FL_as	5'- GGGCCTTGTCGTCGTCGTCCTTATAATCGCCGGCGATGGCCAGGGCG ATGGCCAGGGGTCTCATGTGGATGCCAGGCCTCTC-3'
A20_CD19_42FL_s	5'- AGGCCTGGGCATCCACATGAGACCCCTGGCCATCGCCCTGGCCATCG CCGGCGATTATAAGGACGACGACGACAAGGCCAGG-3'
A20_CD19_42FL_as	5'- GGGCCTTGTCGTCGTCGTCCTTATAATCGCCGGCGATGAACAGCCAG ATGGCGGCGGGTCTCATGTGGATGCCAGGCCTCTC-3'
A21_CD19_42FL_s	5'- AGGCCTGGGCATCCACATGAGACCCGCGCCATCTGGCTGTTTCATCG CCGGCGATTATAAGGACGACGACGACAAGGCCAGG-3'
A21_CD19_42FL_as	5'- GGGCCTTGTCGTCGTCGTCCTTATAATCGCCGAAGATGAACAGCCAG GCGGCGGCGGGCCTCATGTGGATGCCAGGCCTCTC-3'
A22_CD19_42FL_s	5'- AGGCCTGGGCATCCACATGAGGCCCGCCGCCATCTGGCTGTTTCGCT TCGGCGATTATAAGGACGACGACGACAAGGCCAGG-3'
A22_CD19_42FL_as	5'- GGGCCTTGTCGTCGTCGTCCTTATAATCGCCGAAGGCGAACAGCCAG ATGGCGGCGGGCCTCATGTGGATGCCAGGCCTCTC-3'
A23_CD19_42FL_s	5'- AGGCCTGGGCATCCACATGAGGCCCGCCGCCATCTGGGCCTTCATCT TCGGCGATTATAAGGACGACGACGACAAGGCCAGG-3'
A23_CD19_42FL_as	5'- GGGCCTTGTCGTCGTCGTCCTTATAATCGCCGAAGATGAAGGCCAG ATGGCGGCGGGCCTCATGTGGATGCCAGGCCTCTC-3'

A24_CD19_42FL_s	5'- AGGCCTGGGCATCCACATGAGGCCCTGGCCATCTGGCTGGCCGCT TCGGCGATTATAAGGACGACGACGACAAGGCCAGG-3'
A24_CD19_42FL_as	5'- GGGCCTTGTCTCGTCGTCTTATAATCGCCGAAGGCGGCCAGCCAG ATGGCCAGGGGCCTCATGTGGATGCCAGGCCTCTC-3'
A25_CD19_42FL_s	5'- AGGCCTGGGCATCCACATGAGGCCCTGGCCATCTGGCTGGCCGCC GCCGCGATTATAAGGACGACGACGACAAGGCCAGG-3'
A25_CD19_42FL_as	5'- GGGCCTTGTCTCGTCGTCTTATAATCGCCGGCGGCCAGCCAG ATGGCCAGGGGCCTCATGTGGATGCCAGGCCTCTC-3'
A1_CD19_51_s	5'- AGGCGCCTGGCTGTTTCATCTTCAACGTGAGCCAGCAGATGGGCGGCT TCGGCGATTATAAGGACGACGACGACAAGGCCAGG-3'
A1_CD19_51_as	5'- GGGCCTTGTCTCGTCGTCTTATAATCGCCGAAGCCGCCATCTGCT GGCTCACGTTGAAGATGAACAGCCAGGCGCCTCTC-3'
A2_CD19_51_s	5'- AGGCATCGCCCTGTTTCATCTTCAACGTGAGCCAGCAGATGGGCGGCT TCGGCGATTATAAGGACGACGACGACAAGGCCAGG-3'
A2_CD19_51_as	5'- GGGCCTTGTCTCGTCGTCTTATAATCGCCGAAGCCGCCATCTGCT GGCTCACGTTGAAGATGAACAGGGCGATGCCTCTC-3'
A3_CD19_51_s	5'- AGGCATCTGGCTGGCCATCTTCAACGTGAGCCAGCAGATGGGCGGCT TCGGCGATTATAAGGACGACGACGACAAGGCCAGG-3'
A3_CD19_51_as	5'- GGGCCTTGTCTCGTCGTCTTATAATCGCCGAAGCCGCCATCTGCT GGCTCACGTTGAAGATGGCCAGCCAGATGCCTCTC-3'
A4_CD19_51_s	5'- AGGCATCTGGCTGTTTCGCTTCAACGTGAGCCAGCAGATGGGCGGCT TCGGCGATTATAAGGACGACGACGACAAGGCCAGG-3'
A4_CD19_51_as	5'- GGGCCTTGTCTCGTCGTCTTATAATCGCCGAAGCCGCCATCTGCT GGCTCACGTTGAAGGCGAACAGCCAGATGCCTCTC-3'
A5_CD19_51_s	5'- AGGCATCTGGCTGTTTCATCGCCAACGTGAGCCAGCAGATGGGCGGCT TCGGCGATTATAAGGACGACGACGACAAGGCCAGG-3'
A5_CD19_51_as	5'- GGGCCTTGTCTCGTCGTCTTATAATCGCCGAAGCCGCCATCTGCT GGCTCACGTTGGCGATGAACAGCCAGATGCCTCTC-3'
A6_CD19_51_s	5'- AGGCATCGCCCTGGCCATCTTCAACGTGAGCCAGCAGATGGGCGGCT TCGGCGATTATAAGGACGACGACGACAAGGCCAGG-3'
A6_CD19_51_as	5'- GGGCCTTGTCTCGTCGTCTTATAATCGCCGAAGCCGCCATCTGCT GGCTCACGTTGAAGATGGCCAGGGCGATGCCTCTC-3'
A7_CD19_51_s	5'- AGGCATCTGGCTGGCCATCGCCAACGTGAGCCAGCAGATGGGCGGCT TCGGCGATTATAAGGACGACGACGACAAGGCCAGG-3'

A7_CD19_51_as	5'- GGGCCTTGTCGTCGTCGTCCTTATAATCGCCGAAGCCGCCCATCTGCT GGCTCACGTTGGCGATGGCCAGCCAGATGCCTCTC-3'
A8_CD19_51_s	5'- AGGCATCGCCCTGTTTCATCGCCAACGTGAGCCAGCAGATGGGCGGCT TCGGCGATTATAAGGACGACGACGACAAGGCCCAGG-3'
A8_CD19_51_as	5'- GGGCCTTGTCGTCGTCGTCCTTATAATCGCCGAAGCCGCCCATCTGCT GGCTCACGTTGGCGATGAACAGGGCGATGCCTCTC-3'
A9_CD19_51_s	5'- AGGCATCGCCCTGGCCATCGCCAACGTGAGCCAGCAGATGGGCGGC TTCGGCGATTATAAGGACGACGACGACAAGGCCCAGG-3'
A9_CD19_51_as	5'- GGGCCTTGTCGTCGTCGTCCTTATAATCGCCGAAGCCGCCCATCTGCT GGCTCACGTTGGCGATGGCCAGGGCGATGCCTCTC-3'
3rd_loop_588_1_s	5'- AGGCAGCAGGGGCCCCCTGAGCTGGACCCACGTGCACCCCAAGGGC CCCGGCGATTATAAGGACGACGACGACAAGGCCCAGG-3'
3rd_loop_588_1_as	5'- GGGCCTTGTCGTCGTCGTCCTTATAATCGCCGGGGCCCTTGGGGTGC ACGTGGGTCCAGCTCAGGGGGGCCCTGCTGCCTGTC-3'
3rd_loop_588_2_s	5'- AGGCAGGGGCCCCCTGAGCTGGACCCACGTGCACCCCAAGGGCCCC AAGGGCGATTATAAGGACGACGACGACAAGGCCCAGG-3'
3rd_loop_588_2_as	5'- GGGCCTTGTCGTCGTCGTCCTTATAATCGCCCTTGGGGCCCTTGGGG TGCACGTGGGTCCAGCTCAGGGGGGCCCTGCCTGTC-3'
3rd_loop_588_3_s	5'- AGGCGGCCCCCTGAGCTGGACCCACGTGCACCCCAAGGGCCCCAAG AGCGGCGATTATAAGGACGACGACGACAAGGCCCAGG-3'
3rd_loop_588_3_as	5'- GGGCCTTGTCGTCGTCGTCCTTATAATCGCCGCTCTTGGGGCCCTTG GGGTGCACGTGGGTCCAGCTCAGGGGGGCCCTGTC-3'
3rd_loop_588_4_s	5'- AGGCCCCCTGAGCTGGACCCACGTGCACCCCAAGGGCCCCAAGAGC CTGGGCGATTATAAGGACGACGACGACAAGGCCCAGG-3'
3rd_loop_588_4_as	5'- GGGCCTTGTCGTCGTCGTCCTTATAATCGCCCAGGCTCTTGGGGCCC TTGGGGTGCACGTGGGTCCAGCTCAGGGGGCCTGTC-3'
3rd_loop_588_5_s	5'- AGGCCTGAGCTGGACCCACGTGCACCCCAAGGGCCCCAAGAGCCTG CTGGGCGATTATAAGGACGACGACGACAAGGCCCAGG-3'
3rd_loop_588_5_as	5'- GGGCCTTGTCGTCGTCGTCCTTATAATCGCCCAGCAGGCTCTTGGGG CCCTTGGGGTGCACGTGGGTCCAGCTCAGGCCTGTC-3'
3rd_loop_588_6_s	5'- AGGCAGCTGGACCCACGTGCACCCCAAGGGCCCCAAGAGCCTGCTG AGCGGCGATTATAAGGACGACGACGACAAGGCCCAGG-3'
3rd_loop_588_6_as	5'- GGGCCTTGTCGTCGTCGTCCTTATAATCGCCGCTCAGCAGGCTCTTGG GGCCCTTGGGGTGCACGTGGGTCCAGCTGCCTGTC-3'

3B10_-4_s	5'- AGGCCCCAGCGGCAAGCTGATGAGCCCCAAGCTGTACGTGTGGGCCA AGGGCGATTATAAGGACGACGACGACAAGGGCGCCCAGG-3'
3B10_-4_as	5'- GGGCGCCCTTGTCTCGTCGTCCTTATAATCGCCCTTGGCCCACACGT ACAGCTTGGGGCTCATCAGCTTGCCGCTGGGGCCTGTC-3'
3B10_-3_s	5'- AGGCAGCGGCAAGCTGATGAGCCCCAAGCTGTACGTGTGGGCCAAG GACGGCGATTATAAGGACGACGACGACAAGGGCGCCCAGG-3'
3B10_-3_as	5'- GGGCGCCCTTGTCTCGTCGTCCTTATAATCGCCGTCCTTGGCCCACA CGTACAGCTTGGGGCTCATCAGCTTGCCGCTGCCTGTC-3'
3B10_-2_s	5'- AGGCGGCAAGCTGATGAGCCCCAAGCTGTACGTGTGGGCCAAGGACA GGGGCGATTATAAGGACGACGACGACAAGGGCGCCCAGG-3'
3B10_-2_as	5'- GGGCGCCCTTGTCTCGTCGTCCTTATAATCGCCCCTGTCCTTGGCCC ACACGTACAGCTTGGGGCTCATCAGCTTGCCGCTGTC-3'
3B10_-1_s	5'- AGGCAAGCTGATGAGCCCCAAGCTGTACGTGTGGGCCAAGGACAGGC CCGGCGATTATAAGGACGACGACGACAAGGGCGCCCAGG-3'
3B10_-1_as	5'- GGGCGCCCTTGTCTCGTCGTCCTTATAATCGCCGGGCCTGTCCTTG GCCACACGTACAGCTTGGGGCTCATCAGCTTGCCCTGTC-3'
3B10_0_s	5'- AGGCCTGATGAGCCCCAAGCTGTACGTGTGGGCCAAGGACAGGCC GAGGGCGATTATAAGGACGACGACGACAAGGGCGCCCAGG-3'
3B10_0_as	5'- GGGCGCCCTTGTCTCGTCGTCCTTATAATCGCCCTCGGGCCTGTCC TTGGCCCACACGTACAGCTTGGGGCTCATCAGGCCTGTC-3'
3B10_1_s	5'- AGGCATGAGCCCCAAGCTGTACGTGTGGGCCAAGGACAGGCCCGAG ATCGGCGATTATAAGGACGACGACGACAAGGGCGCCCAGG-3'
3B10_1_as	5'- GGGCGCCCTTGTCTCGTCGTCCTTATAATCGCCGATCTCGGGCCTG TCCTTGGCCCACACGTACAGCTTGGGGCTCATGCCTGTC-3'
3B10_2_s	5'- AGGCAGCCCCAAGCTGTACGTGTGGGCCAAGGACAGGCCCGAGATCT GGGGCGATTATAAGGACGACGACGACAAGGGCGCCCAGG-3'
3B10_2_as	5'- GGGCGCCCTTGTCTCGTCGTCCTTATAATCGCCCCAGATCTCGGGC CTGTCCTTGGCCCACACGTACAGCTTGGGGCTGCCTGTC-3'
3B10_3_s	5'- AGGCCCAAGCTGTACGTGTGGGCCAAGGACAGGCCCGAGATCTGG GAGGGCGATTATAAGGACGACGACGACAAGGGCGCCCAGG-3'
3B10_3_as	5'- GGGCGCCCTTGTCTCGTCGTCCTTATAATCGCCCTCCCAGATCTCGG GCCTGTCCTTGGCCCACACGTACAGCTTGGGGCCTGTC-3'
3B10_4_s	5'- AGGCAAGCTGTACGTGTGGGCCAAGGACAGGCCCGAGATCTGGGAG GGCGGCGATTATAAGGACGACGACGACAAGGGCGCCCAGG-3'

3B10_4_as	5'- GGGCGCCCTTGTCTCGTCGTCCTTATAATCGCCGCCCTCCCAGATCT CGGGCCTGTCCTTGGCCCACACGTACAGCTTGCCTGTC-3'
3B10_5_s	5'- AGGCCTGTACGTGTGGGCCAAGGACAGGCCCGAGATCTGGGAGGGC GAGGGCGATTATAAGGACGACGACGACAAGGGCGCCCAGG-3'
3B10_5_as	5'- GGGCGCCCTTGTCTCGTCGTCCTTATAATCGCCCTCGCCCTCCCAG ATCTCGGGCCTGTCCTTGGCCCACACGTACAGGCCTGTC-3'
3B10_6_s	5'- AGGCTACGTGTGGGCCAAGGACAGGCCCGAGATCTGGGAGGGCGAG CCCGGCGATTATAAGGACGACGACGACAAGGGCGCCCAGG-3'
3B10_6_as	5'- GGGCGCCCTTGTCTCGTCGTCCTTATAATCGCCGGGCTCGCCCTCC CAGATCTCGGGCCTGTCCTTGGCCCACACGTAGCCTGTC-3'
3B10_7_S	5'- AGGCGTGTGGGCCAAGGACAGGCCCGAGATCTGGGAGGGCGAGCCC CCCGGCGATTATAAGGACGACGACGACAAGGGCGCCCAGG-3'
3B10_7_as	5'- GGGCGCCCTTGTCTCGTCGTCCTTATAATCGCCGGGGGGCTCGCC TCCCAGATCTCGGGCCTGTCCTTGGCCCACACGCCTGTC-3'
3B10_8_s	5'- AGGCTGGGCCAAGGACAGGCCCGAGATCTGGGAGGGCGAGCCCCC TGCGGCGATTATAAGGACGACGACGACAAGGGCGCCCAGG-3'
3B10_8_as	5'- GGGCGCCCTTGTCTCGTCGTCCTTATAATCGCCGCAGGGGGGCTCG CCCTCCCAGATCTCGGGCCTGTCCTTGGCCCAGCCTGTC-3'
3B10_9_s	5'- AGGCGCCAAGGACAGGCCCGAGATCTGGGAGGGCGAGCCCCCTGC CTGGGCGATTATAAGGACGACGACGACAAGGGCGCCCAGG-3'
3B10_9_as	5'- GGGCGCCCTTGTCTCGTCGTCCTTATAATCGCCCAGGCAGGGGGC TCGCCCTCCCAGATCTCGGGCCTGTCCTTGGCGCCTGTC-3'
3B10_10_s	5'- AGGCAAGGACAGGCCCGAGATCTGGGAGGGCGAGCCCCCTGCCTG CCCGGCGATTATAAGGACGACGACGACAAGGGCGCCCAGG-3'
3B10_10_as	5'- GGGCGCCCTTGTCTCGTCGTCCTTATAATCGCCGGGCAGGCAGGGG GGCTCGCCCTCCCAGATCTCGGGCCTGTCCTTGCCTGTC-3'
3B10_11_s	5'- AGGCGACAGGCCCGAGATCTGGGAGGGCGAGCCCCCTGCCTGCC CCCGGCGATTATAAGGACGACGACGACAAGGGCGCCCAGG-3'
3B10_11_as	5'- GGGCGCCCTTGTCTCGTCGTCCTTATAATCGCCGGGGGGCAGGCAG GGGGGCTCGCCCTCCCAGATCTCGGGCCTGTCGCTGTC-3'
3B10_12_s	5'- AGGCAGGCCCGAGATCTGGGAGGGCGAGCCCCCTGCCTGCCCCCC AGGGGCGATTATAAGGACGACGACGACAAGGGCGCCCAGG-3'
3B10_12_as	5'- GGGCGCCCTTGTCTCGTCGTCCTTATAATCGCCCTGGGGGGCAGG CAGGGGGGCTCGCCCTCCCAGATCTCGGGCCTGCCTGTC-3'

3B10_13_s	5'- AGGCCCGAGATCTGGGAGGGCGAGCCCCCTGCCTGCCCCCAGG GACGGCGATTATAAGGACGACGACGACAAGGGCGCCCAGG-3'
3B10_13_as	5'- GGGCGCCCTTGTCTCGTCGTCTCCTTATAATCGCCGTCCCTGGGGGGC AGGCAGGGGGGCTCGCCCTCCAGATCTCGGGGCCTGTC-3'
3B10_14_s	5'- AGGCGAGATCTGGGAGGGCGAGCCCCCTGCCTGCCCCCAGGGAC AGCGGCGATTATAAGGACGACGACGACAAGGGCGCCCAGG-3'
3B10_14_as	5'- GGGCGCCCTTGTCTCGTCGTCTCCTTATAATCGCCGTGTCCCTGGGG GGCAGGCAGGGGGGCTCGCCCTCCAGATCTCGCCTGTC-3'
3B10_3_A1_s	5'- AGGCCCAAGCTGTACGTGTGGGCCAAGGACAGGCCGAGATCGCC GAGGGCGATTATAAGGACGACGACGACAAGGGCGCCCAGG-3'
3B10_3_A1_as	5'- GGGCGCCCTTGTCTCGTCGTCTCCTTATAATCGCCCTCGGCGATCTCG GGCCTGTCCTTGGCCACACGTACAGCTTGGGGCCTGTC-3'
3B10_3_A2_s	5'- AGGCCCAAGCTGTACGTGTGGGCCGCGACAGGCCGAGATCTGG GAGGGCGATTATAAGGACGACGACGACAAGGGCGCCCAGG-3'
3B10_3_A2_as	5'- GGGCGCCCTTGTCTCGTCGTCTCCTTATAATCGCCCTCCAGATCTCGG GCCTGTCGGCGGCCACACGTACAGCTTGGGGCCTGTC-3'
3B10_3_A3_s	5'- AGGCCCAAGCTGTACGTGTGGGCCAAGGACAGGCCGAGATCTGG GCCGGCGATTATAAGGACGACGACGACAAGGGCGCCCAGG-3'
3B10_3_A3_as	5'- GGGCGCCCTTGTCTCGTCGTCTCCTTATAATCGCCGGCCAGATCTCG GGCCTGTCCTTGGCCACACGTACAGCTTGGGGCCTGTC-3'
3B10_10_A1_s	5'- AGGCAAGGACAGGCCCGAGATCGCCGAGGGCGAGCCCCCTGCCTG CCCGGCGATTATAAGGACGACGACGACAAGGGCGCCCAGG-3'
3B10_10_A1_as	5'- GGGCGCCCTTGTCTCGTCGTCTCCTTATAATCGCCGGGCAGGCAGGGG GGCTCGCCCTCGGCGATCTCGGGCCTGTCCTTGCCTGTC-3'
3B10_10_A2_s	5'- AGGCAAGGACAGGCCCGAGATCTGGGAGGGCGAGCCCCCTGCCTG GCCGGCGATTATAAGGACGACGACGACAAGGGCGCCCAGG-3'
3B10_10_A2_as	5'- GGGCGCCCTTGTCTCGTCGTCTCCTTATAATCGCCGGCCAGGCAGGGG GGCTCGCCCTCCAGATCTCGGGCCTGTCCTTGCCTGTC-3'
3B10_10_A3_s	5'- AGGCGCCGACAGGCCCGAGATCTGGGAGGGCGAGCCCCCTGCCTG CCCGGCGATTATAAGGACGACGACGACAAGGGCGCCCAGG-3'
3B10_10_A3_as	5'- GGGCGCCCTTGTCTCGTCGTCTCCTTATAATCGCCGGGCAGGCAGGGG GGCTCGCCCTCCAGATCTCGGGCCTGTCGGCGCCTGTC-3'
3B10_10_A4_s	5'- AGGCAAGGACAGGCCCGAGATCTGGGCCGCGAGCCCCCTGCCTG CCCGGCGATTATAAGGACGACGACGACAAGGGCGCCCAGG-3'

3B10_10_A4_as	5'- GGGCGCCCTTGTCTCGTCGTCCTTATAATCGCCGGGCAGGCAGGGG GGCTCGCCGGCCCAGATCTCGGGCCTGTCCTTGCTGTC-3'
CLDN6_1FL_s	5'- AGGCATGTGGAAGGTGACCGCCTTCATCGGCAACAGCATCGTGGTGG CCGGCGATTATAAGGACGACGACGACAAGGGCGCCCAGG-3'
CLDN6_1FL_as	5'- GGGCGCCCTTGTCTCGTCGTCCTTATAATCGCCGGCCACCACGATG CTGTTGCCGATGAAGGCGGTACCTTCCACATGCCTGTC-3'
CLDN6_2FL_s	5'- AGGCTGGAAGGTGACCGCCTTCATCGGCAACAGCATCGTGGTGGCCC AGGGCGATTATAAGGACGACGACGACAAGGGCGCCCAGG-3'
CLDN6_2FL_as	5'- GGGCGCCCTTGTCTCGTCGTCCTTATAATCGCCCTGGGCCACCACG ATGCTGTTGCCGATGAAGGCGGTACCTTCCAGCCTGTC-3'
CLDN6_3FL_s	5'- AGGCAAGGTGACCGCCTTCATCGGCAACAGCATCGTGGTGGCCCAGG TGGGCGATTATAAGGACGACGACGACAAGGGCGCCCAGG-3'
CLDN6_3FL_as	5'- GGGCGCCCTTGTCTCGTCGTCCTTATAATCGCCCACCTGGGCCACC ACGATGCTGTTGCCGATGAAGGCGGTACCTTGCCTGTC-3'
CLDN6_4FL_s	5'- AGGCGTGACCGCCTTCATCGGCAACAGCATCGTGGTGGCCCAGGTGG TGGGCGATTATAAGGACGACGACGACAAGGGCGCCCAGG-3'
CLDN6_4FL_as	5'- GGGCGCCCTTGTCTCGTCGTCCTTATAATCGCCCACCACCTGGGCC ACCACGATGCTGTTGCCGATGAAGGCGGTACGCCTGTC-3'
CLDN6_5FL_s	5'- AGGCACCGCCTTCATCGGCAACAGCATCGTGGTGGCCCAGGTGGTGT GGGGCGATTATAAGGACGACGACGACAAGGGCGCCCAGG-3'
CLDN6_5FL_as	5'- GGGCGCCCTTGTCTCGTCGTCCTTATAATCGCCCCACACCACCTGG GCCACCACGATGCTGTTGCCGATGAAGGCGGTGCCTGTC-3'
CLDN6_6FL_s	5'- AGGCGCCTTCATCGGCAACAGCATCGTGGTGGCCCAGGTGGTGTGGG AGGGCGATTATAAGGACGACGACGACAAGGGCGCCCAGG-3'
CLDN6_6FL_as	5'- GGGCGCCCTTGTCTCGTCGTCCTTATAATCGCCCTCCCACACCACCT GGGCCACCACGATGCTGTTGCCGATGAAGGCGCCTGTC-3'
CLDN6_7FL_s	5'- AGGCTTCATCGGCAACAGCATCGTGGTGGCCCAGGTGGTGTGGGAGG GCGGCGATTATAAGGACGACGACGACAAGGGCGCCCAGG-3'
CLDN6_7FL_as	5'- GGGCGCCCTTGTCTCGTCGTCCTTATAATCGCCGCCCTCCCACACC ACCTGGGCCACCACGATGCTGTTGCCGATGAAGCCTGTC-3'
CLDN6_8FL_s	5'- AGGCATCGGCAACAGCATCGTGGTGGCCCAGGTGGTGTGGGAGGGC CTGGGCGATTATAAGGACGACGACGACAAGGGCGCCCAGG-3'
CLDN6_8FL_as	5'- GGGCGCCCTTGTCTCGTCGTCCTTATAATCGCCCAGGCCCTCCCAC ACCACCTGGGCCACCACGATGCTGTTGCCGATGCCTGTC-3'

CLDN6_9FL_s	5'- AGGCGGCAACAGCATCGTGGTGGCCCAGGTGGTGTGGGAGGGCCTG TGGGGCGATTATAAGGACGACGACGACAAGGGCGCCCAGG-3'
CLDN6_9FL_as	5'- GGGCGCCCTTGTCTCGTCGTCCTTATAATCGCCCCACAGGCCCTCC CACACCACCTGGGCCACCACGATGCTGTTGCCGCTGTC-3'
CLDN6_10FL_s	5'- AGGCAACAGCATCGTGGTGGCCCAGGTGGTGTGGGAGGGCCTGTGG ATGGGCGATTATAAGGACGACGACGACAAGGGCGCCCAGG-3'
CLDN6_10FL_as	5'- GGGCGCCCTTGTCTCGTCGTCCTTATAATCGCCCATCCACAGGCCCT CCCACACCACCTGGGCCACCACGATGCTGTTGCCTGTC-3'
CLDN6_11FL_s	5'- AGGCAGCATCGTGGTGGCCCAGGTGGTGTGGGAGGGCCTGTGGATG AGCGGCGATTATAAGGACGACGACGACAAGGGCGCCCAGG-3'
CLDN6_11FL_as	5'- GGGCGCCCTTGTCTCGTCGTCCTTATAATCGCCGCTCATCCACAGG CCCTCCCACACCACCTGGGCCACCACGATGCTGCCTGTC-3'
CLDN6_12FL_s	5'- AGGCATCGTGGTGGCCCAGGTGGTGTGGGAGGGCCTGTGGATGAGC TGCGGCGATTATAAGGACGACGACGACAAGGGCGCCCAGG-3'
CLDN6_12FL_as	5'- GGGCGCCCTTGTCTCGTCGTCCTTATAATCGCCGAGCTCATCCACA GGCCCTCCCACACCACCTGGGCCACCACGATGCCTGTC-3'
CLDN6_13FL_s	5'- AGGCGTGGTGGCCCAGGTGGTGTGGGAGGGCCTGTGGATGAGCTGC GTGGGCGATTATAAGGACGACGACGACAAGGGCGCCCAGG-3'
CLDN6_13FL_as	5'- GGGCGCCCTTGTCTCGTCGTCCTTATAATCGCCCACGCAGCTCATCC ACAGGCCCTCCCACACCACCTGGGCCACCACGCCTGTC-3'
CLDN6_14FL_s	5'- AGGCGTGGCCCAGGTGGTGTGGGAGGGCCTGTGGATGAGCTGCGTG GTGGGCGATTATAAGGACGACGACGACAAGGGCGCCCAGG-3'
CLDN6_14FL_as	5'- GGGCGCCCTTGTCTCGTCGTCCTTATAATCGCCCACCACGCAGCTC ATCCACAGGCCCTCCCACACCACCTGGGCCACGCCTGTC-3'
CLDN6_15FL_s	5'- AGGCGCCCAGGTGGTGTGGGAGGGCCTGTGGATGAGCTGCGTGGTG CAGGGCGATTATAAGGACGACGACGACAAGGGCGCCCAGG-3'
CLDN6_15FL_as	5'- GGGCGCCCTTGTCTCGTCGTCCTTATAATCGCCCTGCACCACGCAG CTCATCCACAGGCCCTCCCACACCACCTGGGCGCCTGTC-3'
CLDN6_16FL_s	5'- AGGCCAGGTGGTGTGGGAGGGCCTGTGGATGAGCTGCGTGGTGCAG AGCGGCGATTATAAGGACGACGACGACAAGGGCGCCCAGG-3'
CLDN6_16FL_as	5'- GGGCGCCCTTGTCTCGTCGTCCTTATAATCGCCGCTCTGCACCACG CAGCTCATCCACAGGCCCTCCCACACCACCTGGCCTGTC-3'
CLDN6_17FL_s	5'- AGGCGTGGTGTGGGAGGGCCTGTGGATGAGCTGCGTGGTGCAGAGC ACCGGCGATTATAAGGACGACGACGACAAGGGCGCCCAGG-3'

CLDN6_17FL_as	5'- GGGCGCCCTTGTCTCGTCGTCCTTATAATCGCCGGTGTCTCTGCACC ACGCAGCTCATCCACAGGCCCTCCCACACCACGCCTGTC-3'
CLDN6_18FL_s	5'- AGGCGTGTGGGAGGGCCTGTGGATGAGCTGCGTGGTGCAGAGCACC GGCGGCGATTATAAGGACGACGACGACAAGGGCGCCCAGG-3'
CLDN6_18FL_as	5'- GGGCGCCCTTGTCTCGTCGTCCTTATAATCGCCGCCGGTGTCTCTGC ACCACGCAGCTCATCCACAGGCCCTCCCACACGCCTGTC-3'
CLDN6_19FL_s	5'- AGGCTGGGAGGGCCTGTGGATGAGCTGCGTGGTGCAGAGCACCGGC CAGGGCGATTATAAGGACGACGACGACAAGGGCGCCCAGG-3'
CLDN6_19FL_as	5'- GGGCGCCCTTGTCTCGTCGTCCTTATAATCGCCCTGGCCGGTGTCTC TGCACCACGCAGCTCATCCACAGGCCCTCCCAGCCTGTC-3'
CLDN6_20FL_s	5'- AGGCGAGGGCCTGTGGATGAGCTGCGTGGTGCAGAGCACCGGCCAG ATGGGCGATTATAAGGACGACGACGACAAGGGCGCCCAGG-3'
CLDN6_20FL_as	5'- GGGCGCCCTTGTCTCGTCGTCCTTATAATCGCCCATCTGGCCGGTG CTCTGCACCACGCAGCTCATCCACAGGCCCTCGCCTGTC-3'
CLDN6_21FL_s	5'- AGGCGGCCTGTGGATGAGCTGCGTGGTGCAGAGCACCGGCCAGATG CAGGGCGATTATAAGGACGACGACGACAAGGGCGCCCAGG-3'
CLDN6_21FL_as	5'- GGGCGCCCTTGTCTCGTCGTCCTTATAATCGCCCTGCATCTGGCCG GTGCTCTGCACCACGCAGCTCATCCACAGGCCCGCCTGTC-3'
CLDN6_22FL_s	5'- AGGCCTGTGGATGAGCTGCGTGGTGCAGAGCACCGGCCAGATGCAGT GCGGCGATTATAAGGACGACGACGACAAGGGCGCCCAGG-3'
CLDN6_22FL_as	5'- GGGCGCCCTTGTCTCGTCGTCCTTATAATCGCCGCACTGCATCTGG CCGGTGTCTCTGCACCACGCAGCTCATCCACAGGCCCTGTC-3'
CLDN6_23FL_s	5'- AGGCTGGATGAGCTGCGTGGTGCAGAGCACCGGCCAGATGCAGTGC AAGGGCGATTATAAGGACGACGACGACAAGGGCGCCCAGG-3'
CLDN6_23FL_as	5'- GGGCGCCCTTGTCTCGTCGTCCTTATAATCGCCCTTGCATCTGCACT GGCCGGTGTCTCTGCACCACGCAGCTCATCCAGCCTGTC-3'
CLDN6_24FL_s	5'- AGGCATGAGCTGCGTGGTGCAGAGCACCGGCCAGATGCAGTGCAAG GTGGGCGATTATAAGGACGACGACGACAAGGGCGCCCAGG-3'
CLDN6_24FL_as	5'- GGGCGCCCTTGTCTCGTCGTCCTTATAATCGCCACCTTGCATCTGCA TCTGGCCGGTGTCTCTGCACCACGCAGCTCATGCCTGTC-3'
CLDN6_25FL_s	5'- AGGCAGCTGCGTGGTGCAGAGCACCGGCCAGATGCAGTGCAAGGTG TACGGCGATTATAAGGACGACGACGACAAGGGCGCCCAGG-3'
CLDN6_25FL_as	5'- GGGCGCCCTTGTCTCGTCGTCCTTATAATCGCCGTACACCTTGCAT GCATCTGGCCGGTGTCTCTGCACCACGCAGCTGCCTGTC-3'

CLDN6_26FL_s	5'- AGGCTGCGTGGTGCAGAGCACCGGCCAGATGCAGTGCAAGGTGTAC GACGGCGATTATAAGGACGACGACGACAAGGGCGCCCAGG-3'
CLDN6_26FL_as	5'- GGGCGCCCTTGTTCGTCGTCGTCCTTATAATCGCCGTCGTACACCTTGC ACTGCATCTGGCCGGTGCTCTGCACCACGCAGCCTGTC-3'
CLDN6_27FL_s	5'- AGGCGTGGTGCAGAGCACCGGCCAGATGCAGTGCAAGGTGTACGACA GCGGGCGATTATAAGGACGACGACGACAAGGGCGCCCAGG-3'
CLDN6_27FL_as	5'- GGGCGCCCTTGTTCGTCGTCGTCCTTATAATCGCCGCTGTCGTACACCT TGCACTGCATCTGGCCGGTGCTCTGCACCACGCCTGTC-3'
CLDN6_28FL_s	5'- AGGCGTGCAGAGCACCGGCCAGATGCAGTGCAAGGTGTACGACAGC CTGGGCGATTATAAGGACGACGACGACAAGGGCGCCCAGG-3'
CLDN6_28FL_as	5'- GGGCGCCCTTGTTCGTCGTCGTCCTTATAATCGCCCAGGCTGTCGTACA CCTTGCACTGCATCTGGCCGGTGCTCTGCACGCCTGTC-3'
CLDN6_29FL_s	5'- AGGCCAGAGCACCGGCCAGATGCAGTGCAAGGTGTACGACAGCCTGC TGGGCGATTATAAGGACGACGACGACAAGGGCGCCCAGG-3'
CLDN6_29FL_as	5'- GGGCGCCCTTGTTCGTCGTCGTCCTTATAATCGCCCAGCAGGCTGTCC TACACCTTGCACTGCATCTGGCCGGTGCTCTGGCCTGTC-3'
CLDN6_30FL_s	5'- AGGCAGCACCGGCCAGATGCAGTGCAAGGTGTACGACAGCCTGCTGG CCGGCGATTATAAGGACGACGACGACAAGGGCGCCCAGG-3'
CLDN6_30FL_as	5'- GGGCGCCCTTGTTCGTCGTCGTCCTTATAATCGCCGGCCAGCAGGCTG TCGTACACCTTGCACTGCATCTGGCCGGTGCTGCCTGTC-3'
CLDN6_31FL_s	5'- AGGCACCGGCCAGATGCAGTGCAAGGTGTACGACAGCCTGCTGGCCC TGGGCGATTATAAGGACGACGACGACAAGGGCGCCCAGG-3'
CLDN6_31FL_as	5'- GGGCGCCCTTGTTCGTCGTCGTCCTTATAATCGCCCAGGGCCAGCAGG CTGTTCGTACACCTTGCACTGCATCTGGCCGGTGCTGCCTGTC-3'
CLDN6_32FL_s	5'- AGGCGGCCAGATGCAGTGCAAGGTGTACGACAGCCTGCTGGCCCTGC CCGGCGATTATAAGGACGACGACGACAAGGGCGCCCAGG-3'
CLDN6_32FL_as	5'- GGGCGCCCTTGTTCGTCGTCGTCCTTATAATCGCCGGGCAGGGCCAGC AGGCTGTTCGTACACCTTGCACTGCATCTGGCCGCCTGTC-3'
CLDN6_33FL_s	5'- AGGCCAGATGCAGTGCAAGGTGTACGACAGCCTGCTGGCCCTGCCCC AGGGCGATTATAAGGACGACGACGACAAGGGCGCCCAGG-3'
CLDN6_33FL_as	5'- GGGCGCCCTTGTTCGTCGTCGTCCTTATAATCGCCCTGGGGCAGGGCC AGCAGGCTGTTCGTACACCTTGCACTGCATCTGGCCTGTC-3'
CLDN6_34FL_s	5'- AGGCATGCAGTGCAAGGTGTACGACAGCCTGCTGGCCCTGCCCCAGG ACGGCGATTATAAGGACGACGACGACAAGGGCGCCCAGG-3'

CLDN6_34FL_as	5'- GGGCGCCCTTGTCTCGTCGTCCTTATAATCGCCGTCCTGGGGCAGG GCCAGCAGGCTGTCTACACCTTGCACTGCATGCCTGTC-3'
CLDN6_35FL_s	5'- AGGCCAGTGCAAGGTGTACGACAGCCTGCTGGCCCTGCCCCAGGACC TGGGCGATTATAAGGACGACGACGACAAGGGCGCCCAGG-3'
CLDN6_35FL_as	5'- GGGCGCCCTTGTCTCGTCGTCCTTATAATCGCCCAGGTCCTGGGGC AGGGCCAGCAGGCTGTCTACACCTTGCACTGGCCTGTC-3'
CLDN6_36FL_s	5'- AGGCTGCAAGGTGTACGACAGCCTGCTGGCCCTGCCCCAGGACCTGC AGGGCGATTATAAGGACGACGACGACAAGGGCGCCCAGG-3'
CLDN6_36FL_as	5'- GGGCGCCCTTGTCTCGTCGTCCTTATAATCGCCCTGCAGGTCCTGG GGCAGGGCCAGCAGGCTGTCTACACCTTGCACTGCCTGTC-3'
CLDN6_37FL_s	5'- AGGCAAGGTGTACGACAGCCTGCTGGCCCTGCCCCAGGACCTGCAG GCCGCGATTATAAGGACGACGACGACAAGGGCGCCCAGG-3'
CLDN6_37FL_as	5'- GGGCGCCCTTGTCTCGTCGTCCTTATAATCGCCGGCCTGCAGGTCC TGGGGCAGGGCCAGCAGGCTGTCTACACCTTGCTGTC-3'
CLDN6_38FL_s	5'- AGGCGTGTACGACAGCCTGCTGGCCCTGCCCCAGGACCTGCAGGCC GCCGCGATTATAAGGACGACGACGACAAGGGCGCCCAGG-3'
CLDN6_38FL_as	5'- GGGCGCCCTTGTCTCGTCGTCCTTATAATCGCCGGCGGCCTGCAGG TCCTGGGGCAGGGCCAGCAGGCTGTCTACACGCTGTC-3'
CLDN6_39FL_s	5'- AGGCTACGACAGCCTGCTGGCCCTGCCCCAGGACCTGCAGGCCGCC AGGGGCGATTATAAGGACGACGACGACAAGGGCGCCCAGG-3'
CLDN6_39FL_as	5'- GGGCGCCCTTGTCTCGTCGTCCTTATAATCGCCCCTGGCGGCCTGC AGGTCCTGGGGCAGGGCCAGCAGGCTGTCTAGCCTGTC-3'
CLDN6_40FL_s	5'- AGGCTGGACCGCCACGCCATCATCAGGGACTTCTACAACCCCTGG TGGGCGATTATAAGGACGACGACGACAAGGGCGCCCAGG-3'
CLDN6_40FL_as	5'- GGGCGCCCTTGTCTCGTCGTCCTTATAATCGCCCACCAGGGGGTTG TAGAAGTCCCTGATGATGGCGTGGGCGGTCCAGCCTGTC-3'
CLDN6_41FL_s	5'- AGGCACCGCCACGCCATCATCAGGGACTTCTACAACCCCTGGTGG CCGGCGATTATAAGGACGACGACGACAAGGGCGCCCAGG-3'
CLDN6_41FL_as	5'- GGGCGCCCTTGTCTCGTCGTCCTTATAATCGCCGGCCACCAGGGGG TTGTAGAAGTCCCTGATGATGGCGTGGGCGGTGCCTGTC-3'
CLDN6_42FL_s	5'- AGGCGCCACGCCATCATCAGGGACTTCTACAACCCCTGGTGGCCG AGGGCGATTATAAGGACGACGACGACAAGGGCGCCCAGG-3'
CLDN6_42FL_as	5'- GGGCGCCCTTGTCTCGTCGTCCTTATAATCGCCCTCGGCCACCAGG GGGTTGTAGAAGTCCCTGATGATGGCGTGGGCGCCTGTC-3'

CLDN6_43FL_s	5'- AGGCCACGCCATCATCAGGGACTTCTACAACCCCCTGGTGGCCGAGG CCGGCGATTATAAGGACGACGACGACAAGGGCGCCCAGG-3'
CLDN6_43FL_as	5'- GGGCGCCCTTGTCTCGTCGTCTCCTTATAATCGCCGGCCTCGGCCACC AGGGGGTTGTAGAAGTCCCTGATGATGGCGTGGCCTGTC-3'
CLDN6_44FL_s	5'- AGGCGCCATCATCAGGGACTTCTACAACCCCCTGGTGGCCGAGGCC AGGGCGATTATAAGGACGACGACGACAAGGGCGCCCAGG-3'
CLDN6_44FL_as	5'- GGGCGCCCTTGTCTCGTCGTCTCCTTATAATCGCCCTGGGCCTCGGCC ACCAGGGGGTTGTAGAAGTCCCTGATGATGGCGCCTGTC-3'
CLDN6_45FL_s	5'- AGGCATCATCAGGGACTTCTACAACCCCCTGGTGGCCGAGGCCCAGA AGGGCGATTATAAGGACGACGACGACAAGGGCGCCCAGG-3'
CLDN6_45FL_as	5'- GGGCGCCCTTGTCTCGTCGTCTCCTTATAATCGCCCTTCTGGGCCTCG GCCACCAGGGGGTTGTAGAAGTCCCTGATGATGCCTGTC-3'
CLDN6_46FL_s	5'- AGGCATCAGGGACTTCTACAACCCCCTGGTGGCCGAGGCCCAGAAGA GGGGCGATTATAAGGACGACGACGACAAGGGCGCCCAGG-3'
CLDN6_46FL_as	5'- GGGCGCCCTTGTCTCGTCGTCTCCTTATAATCGCCCTTCTTCTGGGCCT CGGCCACCAGGGGGTTGTAGAAGTCCCTGATGCCTGTC-3'
CLDN6_47FL_s	5'- AGGCAGGGACTTCTACAACCCCCTGGTGGCCGAGGCCCAGAAGAGG GAGGGCGATTATAAGGACGACGACGACAAGGGCGCCCAGG-3'
CLDN6_47FL_as	5'- GGGCGCCCTTGTCTCGTCGTCTCCTTATAATCGCCCTCCCTCTTCTGGG CCTCGGCCACCAGGGGGTTGTAGAAGTCCCTGCCTGTC-3'
CLDN6_48FL_s	5'- AGGCGACTTCTACAACCCCCTGGTGGCCGAGGCCCAGAAGAGGGAG CTGGGCGATTATAAGGACGACGACGACAAGGGCGCCCAGG-3'
CLDN6_48FL_as	5'- GGGCGCCCTTGTCTCGTCGTCTCCTTATAATCGCCAGCTCCCTCTTCT GGCCTCGGCCACCAGGGGGTTGTAGAAGTGCCTGTC-3'
CLDN6_1FL_A1_s	5'- AGGCATGGCCAAGGTGACCGCCTTCATCGGCAACAGCATCGTGGTGG CCGGCGATTATAAGGACGACGACGACAAGGGCGCCCAGG-3'
CLDN6_1FL_A1_as	5'- GGGCGCCCTTGTCTCGTCGTCTCCTTATAATCGCCGGCCACCACGATG CTGTTGCCGATGAAGGCGGTACCTTGGCCATGCCTGTC-3'
CLDN6_2FL_A1_s	5'- AGGCGCCAAGGTGACCGCCTTCATCGGCAACAGCATCGTGGTGGCCC AGGGCGATTATAAGGACGACGACGACAAGGGCGCCCAGG-3'
CLDN6_2FL_A1_as	5'- GGGCGCCCTTGTCTCGTCGTCTCCTTATAATCGCCCTGGGCCACCACG ATGCTGTTGCCGATGAAGGCGGTACCTTGGCGCCTGTC-3'
CLDN6_5FL_A1_s	5'- AGGCACCGCCTTCATCGGCAACAGCATCGTGGTGGCCCAGGTGGTGG CCGGCGATTATAAGGACGACGACGACAAGGGCGCCCAGG-3'

CLDN6_5FL_A1_as	5'- GGGCGCCCTTGTCTCGTCGTCCTTATAATCGCCGGCCACCACCTGG GCCACCACGATGCTGTTGCCGATGAAGGCGGTGCCTGTC-3'
-----------------	---

2.8.2 Insertions into VR-IV loop

CD19_72_453 _s	5'- AATTGGACCCCCAGCGAGAAGGCCTGGCAGCCCGGCTGGACCGTGAACGT GGGCGATTATAAGGACGACGACGACAAGA-3'
CD19_72_453 _as	5'- CTAGTCTTGTCTCGTCGTCCTTATAATCGCCACGTTACGGTCCAGCCGG GCTGCCAGGCCTTCTCGCTGGGGGTCC-3'
3rd_loop_453 _1_s	5'- AATTGGAAGCAGGGGCCCTGAGCTGGACCCACGTGCACCCCAAGGGCCC CGGCGATTATAAGGACGACGACGACAAGA-3'
3rd_loop_453 _1_as	5'- CTAGTCTTGTCTCGTCGTCCTTATAATCGCCGGGGCCCTTGGGGTGCACGT GGGTCCAGCTCAGGGGGCCCTGCTTCC-3'
3rd_loop_453 _2_s	5'- AATTGGAAGGGGCCCTGAGCTGGACCCACGTGCACCCCAAGGGCCCCAA GGGCGATTATAAGGACGACGACGACAAGA-3'
3rd_loop_453 _2_as	5'- CTAGTCTTGTCTCGTCGTCCTTATAATCGCCCTTGGGGCCCTTGGGGTGCA CGTGGGTCCAGCTCAGGGGGCCCTTCC-3'
3rd_loop_453 _3_s	5'- AATTGGAGGCCCTGAGCTGGACCCACGTGCACCCCAAGGGCCCCAAGAG CGGCGATTATAAGGACGACGACGACAAGA-3'
3rd_loop_453 _3_as	5'- CTAGTCTTGTCTCGTCGTCCTTATAATCGCCGCTCTTGGGGCCCTTGGGGT GCACGTGGGTCCAGCTCAGGGGGCCCTCC-3'
3rd_loop_453 _4_s	5'- AATTGGACCCCTGAGCTGGACCCACGTGCACCCCAAGGGCCCCAAGAGCCT GGGCGATTATAAGGACGACGACGACAAGA-3'
3rd_loop_453 _4_as	5'- CTAGTCTTGTCTCGTCGTCCTTATAATCGCCAGGCTCTTGGGGCCCTTGG GGTGCACGTGGGTCCAGCTCAGGGGTCC-3'
3rd_loop_453 _5_s	5'- AATTGGACTGAGCTGGACCCACGTGCACCCCAAGGGCCCCAAGAGCCTGCT GGGCGATTATAAGGACGACGACGACAAGA-3'
3rd_loop_453 _5_as	5'- CTAGTCTTGTCTCGTCGTCCTTATAATCGCCAGCAGGCTCTTGGGGCCCT TGGGGTGCACGTGGGTCCAGCTCAGTCC-3'
3rd_loop_453 _6_s	5'- AATTGGAAGCTGGACCCACGTGCACCCCAAGGGCCCCAAGAGCCTGCTGAG CGGCGATTATAAGGACGACGACGACAAGA-3'
3rd_loop_453 _6_as	5'- CTAGTCTTGTCTCGTCGTCCTTATAATCGCCGCTCAGCAGGCTCTTGGGGC CCTTGGGGTGCACGTGGGTCCAGCTTCC-3'
CD19_6FL_45 3_s	5'- AATTGGAGTGCTGCAGTGCCTGAAAGGTACCAGCGATGGCCCGACCCAGCA GGGCGATTATAAGGACGACGACGACAAGA-3'

CD19_6FL_45_3_as	5'- CTAGTCTTGTGTCGTCGTCGTCCTTATAATCGCCCTGCTGGGTGCGGCCATCGC TGGTACCTTTCAGGCACTGCAGCACTCC-3'
CD19_23FL_453_s	5'- AATTGGATGGAGCCGCGAAAGCCCGCTTAAGCCGTTTCTTAAGCTGAGCCTG GGCGATTATAAGGACGACGACGACAAGA-3'
CD19_23FL_453_as	5'- CTAGTCTTGTGTCGTCGTCGTCCTTATAATCGCCCAGGCTCAGCTTAAGAAACGG CTTAAGCGGGCTTTCGCGGCTCCATCC-3'
CD19_33FL_453_s	5'- AATTGGACTTAAGCTGAGCCTGGGCCTGCCCGGCCTGGGCATCCACATGAG AGGCGATTATAAGGACGACGACGACAAGA-3'
CD19_33FL_453_as	5'- CTAGTCTTGTGTCGTCGTCGTCCTTATAATCGCCTCTCATGTGGATGCCAGGCC GGGCAGGCCAGGCTCAGCTTAAGTCC-3'
CD19_42FL_453_s	5'- AATTGGACTGGGGATCCACATGAGACCCCTGGCCATCTGGCTGTTTCATCTTC GGCGATTATAAGGACGACGACGACAAGA-3'
CD19_42FL_453_as	5'- CTAGTCTTGTGTCGTCGTCGTCCTTATAATCGCCGAAGATGAACAGCCAGATGG CCAGGGGTCTCATGTGGATCCCCAGTCC-3'
CD19_51FL_453_s	5'- AATTGGAATCTGGCTGTTTCATCTTCAACGTGAGCCAGCAGATGGGCGGCTTC GGCGATTATAAGGACGACGACGACAAGA-3'
CD19_51FL_453_as	5'- CTAGTCTTGTGTCGTCGTCGTCCTTATAATCGCCGAAGCCGCCATCTGCTGGC TCACGTTGAAGATGAACAGCCAGATTCC-3'
CD19_55FL_453_s	5'- AATTGGAATCTTCAACGTGAGCCAGCAGATGGGCGGCTTCTACCTGTGCCAG GGCGATTATAAGGACGACGACGACAAGA-3'
CD19_55FL_453_as	5'- CTAGTCTTGTGTCGTCGTCGTCCTTATAATCGCCCTGGCACAGGTAGAAGCCGC CCATCTGCTGGCTCACGTTGAAGATTCC-3'
NYBR1C2_FL_453_s	5'- AATTGGACTGAAAAACGAACAGACCTTAAGAGCGGATCAGATGTTTGCGATT ATAAGGACGACGACGACAAGA-3'
NYBR1C2_FL_453_as	5'- CTAGTCTTGTGTCGTCGTCGTCCTTATAATCGCCAAACATCTGATCCGCTCTTAA GGTCTGTTGTTTTTTCAGTCC-3'

2.8.3 Insertions into HI-loop

NYBR1C2_HI_s	5'- CCGGTACTGAAAAACGAACAGACCTTAAGAGCGGATCAGATGTTT G-3'
NYBR1C2_HI_as	5'- CTAGCAAACATCTGATCCGCTCTTAAGGTCTGTTTCGTTTTTTCAGTA -3'
FL_HI_s	5'-CCGGTAGGCGATTATAAGGACGACGACGACAAGGGCG-3'
FL_HI_as	5'-CTAGCGCCCTTGTGTCGTCGTCGTCCTTATAATCGCCTA-3'

NYBR1C2_FL_HI_s	5'- CCGGTACTGAAAAACGAACAGACCTTAAGAGCGGATCAGATGTTT GGCGATTATAAGGACGACGACGACAAGG-3'
NYBR1C2_FL_HI_as	5'- CTAGCCTTGTCTGTCGTCGTCCTTATAATCGCCAAACATCTGATCC GCTCTTAAGGTCTGTTCGTTTTTCAGTA-3'
CD19_42FL_HI_s	5'- CCGGTACTGGGGATCCACATGAGACCCCTGGCCATCTGGCTGTT CATCTTCGGCGATTATAAGGACGACGACGACAAGG-3'
CD19_42FL_HI_as	5'- CTAGCCTTGTCTGTCGTCGTCCTTATAATCGCCGAAGATGAACAGC CAGATGGCCAGGGGTCTCATGTGGATCCCCAGTA-3'
NYBR1C2_HI_PK_s	5'- CCGGTACCTCTGAAAAACGAACAGACCTTAAGAGCGGATCAGATG TTTAAGTTTG-3'
NYBR1C2_HI_PK_as	5'- CTAGCAAACCTTAAACATCTGATCCGCTCTTAAGGTCTGTTCGTTTT TCAGAGGTA-3'
FL_HI_PK_s	5'- CCGGTACCTGGCGATTATAAGGACGACGACGACAAGGGCAAGTT TG-3'
FL_HI_PK_as	5'- CTAGCAAACCTTGCCCTTGTCTGTCGTCGTCCTTATAATCGCCAGGT A-3'
NYBR1C2_FL_HI_PK_s	5'- CCGGTACCTCTGAAAAACGAACAGACCTTAAGAGCGGATCAGATG TTTGCGGATTATAAGGACGACGACGACAAGAAGTTTG-3'
NYBR1C2_FL_HI_PK_as	5'- CTAGCAAACCTTCTTGTCTGTCGTCGTCCTTATAATCGCCAAACATCT GATCCGCTCTTAAGGTCTGTTCGTTTTTCAGAGGTA-3'
NYBR1C2_HI_FS_s	5'- CCGGTACTGAAAAACGAACAGACCTTAAGAGCGGATCAGATGTTT TTCAGTGCGGCAAAGTTTG-3'
NYBR1C2_HI_FS_as	5'- CTAGCAAACCTTTGCCGCACTGAAAAACATCTGATCCGCTCTTAAG GTCTGTTCGTTTTTCAGTA-3'
FL_HI_FS_s	5'- CCGGTAGGCGATTATAAGGACGACGACGACAAGGGCTTCAGTGC GGCAAAGTTTG-3
FL_HI_FS_as	5'- CTAGCAAACCTTTGCCGCACTGAAGCCCTTGTCTGTCGTCGTCCTTA TAATCGCCTA-3'
NYBR1C2_FL_HI_FS_s	5'- CCGGTACTGAAAAACGAACAGACCTTAAGAGCGGATCAGATGTTT GGCGATTATAAGGACGACGACGACAAGTTCAGTGCGGCAAAGTTT G-3'
NYBR1C2_FL_HI_FS_as	5'- CTAGCAAACCTTTGCCGCACTGAACTTGTCTGTCGTCGTCCTTATAAT CGCCAAACATCTGATCCGCTCTTAAGGTCTGTTCGTTTTTCAGTA- 3'
FL_HI_ANP_s	5'- CCGGTACCTGCGAATCCTGGCGATTATAAGGACGACGACGACAA GGGCG-3'

FL_HI_ANP_as	5'- CTAGCGCCCTTGTCTCGTCGTCCTTATAATCGCCAGGATTCGCA GGTA-3'
CD19_42FL_HI_ANP_s	5'- CCGGTACCTGCGAATCCTCTGGGGATCCACATGAGACCCCTGGC CATCTGGCTGTTTCATCTTCGGCGATTATAAAGGACGACGACGACAA GG-3'
CD19_42FL_HI_ANP_as	5'- CTAGCCTTGTCTCGTCGTCGTCCTTATAATCGCCGAAGATGAACAGC CAGATGGCCAGGGGTCTCATGTGGATCCCCAGAGGATTCGCGAG TA-3'
CD19_6FL_HI_s	5'- CCGGTAGTGTCTGAGTGCCTGAAAGGTACCAGCGATGGCCCGAC CCAGCAGGGCGATTATAAAGGACGACGACGACAAGG-3'
CD19_6FL_HI_as	5'- CTAGCCTTGTCTCGTCGTCGTCCTTATAATCGCCCTGCTGGGTCTGGG CCATCGCTGGTACCTTTCAGGCACTGCAGCACTA-3'
CD19_23FL_HI_s	5'- CCGGTATGGAGCCGCGAAAGCCCGCTTAAGCCGTTTCTTAAGCT GAGCCTGGGCGATTATAAAGGACGACGACGACAAGG-3'
CD19_23FL_HI_as	5'- CTAGCCTTGTCTCGTCGTCGTCCTTATAATCGCCCAGGCTCAGCTTA AGAAACGGCTTAAGCGGGCTTTCGCGGCTCCATA-3'
CD19_33FL_HI_s	5'- CCGGTACTTAAGCTGAGCCTGGGCCTGCCCGGCCTGGGCATCCA CATGAGAGGCGATTATAAAGGACGACGACGACAAGG-3'
CD19_33FL_HI_as	5'- CTAGCCTTGTCTCGTCGTCGTCCTTATAATCGCCTCTCATGTGGATG CCCAGGCCGGGCAGGCCAGGCTCAGCTTAAGTA-3'
CD19_51FL_HI_s	5'- CCGGTAATCTGGCTGTTTCATCTTCAACGTGAGCCAGCAGATGGGC GGCTTCGGCGATTATAAAGGACGACGACGACAAGG-3'
CD19_51FL_HI_as	5'- CTAGCCTTGTCTCGTCGTCGTCCTTATAATCGCCGAAGCCGCCATC TGCTGGCTCACGTTGAAGATGAACAGCCAGATTA-3'
CD19_55FL_HI_s	5'- CGGTAATCTTCAACGTGAGCCAGCAGATGGGCGGCTTCTACCTGT GCCAGGGCGATTATAAAGGACGACGACGACAAGG-3'
CD19_55FL_HI_as	5'- CTAGCCTTGTCTCGTCGTCGTCCTTATAATCGCCCTGGCACAGGTAG AAGCCGCCCATCTGCTGGCTCACGTTGAAGATTA-3'

2.8.4 Insertions into β B

NYBR1C2_245 _Spel_s	5'-CCGGGCCCTGAAAAACGAACAGACCTTAAGAGCGGATCAGATGTTTAAA- 3'
NYBR1C2_245 _Spel_as	5'-CTAGTTTAAACATCTGATCCGCTCTTAAGGTCTGTTCGTTTTTCAGGGC-3'
FL_245_Spel_s	5'-CCGGGCCGGCGATTATAAAGGACGACGACGACAAGGGCAAA-3'
FL_245_Spel_a s	5'-CTAGTTTGGCCTTGTCTCGTCGTCCTTATAATCGCCGGC-3'

NYBR1C2_FL_245_Spel_s	5'- CCGGGCCCTGAAAAACGAACAGACCTTAAGAGCGGATCAGATGTTTGGCGA TTATAAGGACGACGACGACAAGAAA-3'
NYBR1C2_FL_245_Spel_as	5'- CTAGTTTCTTGTCGTCGTCGTCCTTATAATCGCCAAACATCTGATCCGCTCT TAAGGTCTGTTTCGTTTTTCAGGGC-3'
CD19_42FL_245_Spel_s	5'- CCGGGCCCTGGGGATCCACATGAGACCCCTGGCCATCTGGCTGTTTCATCTT CGGCGATTATAAGGACGACGACGACAAGAAA-3'
CD19_42FL_245_Spel_as	5'- CTAGTTTCTTGTCGTCGTCGTCCTTATAATCGCCGAAGATGAACAGCCAGAT GGCCAGGGGTCTCATGTGGATCCCCAGGGC-3'
CD19_6FL_245_Spel_s	5'- CCGGGCCGTGCTGCAGTGCCTGAAAGGTACCAGCGATGGCCCGACCCAGC AGGGCGATTATAAGGACGACGACGACAAGAAA-3'
CD19_6FL_245_Spel_as	5'- CTAGTTTCTTGTCGTCGTCGTCCTTATAATCGCCCTGCTGGGTCTGGGCCAT CGCTGGTACCTTTCAGGCACTGCAGCACGGC-3'
CD19_23FL_245_Spel_s	5'- CCGGGCCTGGAGCCGCGAAAGCCCGCTTAAGCCGTTTCTTAAGCTGAGCC TGGGCGATTATAAGGACGACGACGACAAGAAA-3'
CD19_23FL_245_Spel_as	5'- CTAGTTTCTTGTCGTCGTCGTCCTTATAATCGCCCAGGCTCAGCTTAAGAAA CGGCTTAAGCGGGCTTTCGCGGCTCCAGGC-3'
CD19_33FL_245_Spel_s	5'- CCGGGCCCTTAAGCTGAGCCTGGGCCTGCCCGGCCTGGGCATCCACATGA GAGGCGATTATAAGGACGACGACGACAAGAAA-3'
CD19_33FL_245_Spel_as	5'- CTAGTTTCTTGTCGTCGTCGTCCTTATAATCGCCTCTCATGTGGATGCCAG GCCGGCAGGCCAGGCTCAGCTTAAGGGC-3'
CD19_51FL_245_Spel_s	5'- CCGGGCCATCTGGCTGTTTCATCTTCAACGTGAGCCAGCAGATGGGCGGCT TCGGCGATTATAAGGACGACGACGACAAGAAA-3'
CD19_51FL_245_Spel_as	5'- CTAGTTTCTTGTCGTCGTCGTCCTTATAATCGCCGAAGCCGCCATCTGCTG GCTCACGTTGAAGATGAACAGCCAGATGGC-3'
CD19_55FL_245_Spel_s	5'- CCGGGCCATCTTCAACGTGAGCCAGCAGATGGGCGGCTTCTACCTGTGCC AGGGCGATTATAAGGACGACGACGACAAGAAA-3'
CD19_55FL_245_Spel_as	5'- CTAGTTTCTTGTCGTCGTCGTCCTTATAATCGCCCTGGCACAGGTAGAAGC CGCCCATCTGCTGGCTCACGTTGAAGATGGC-3'
NYBR1C2_245_Sphl_s	5'- CCGGGCCCTGAAAAACGAACAGACCTTAAGAGCGGATCAGATGTTTGGCAT G-3'
NYBR1C2_245_Sphl_as	5'-CCAAACATCTGATCCGCTCTTAAGGTCTGTTTCGTTTTTCAGGGC-3'
FL_245_Sphl_s	5'-CCGGGCCGGCGATTATAAGGACGACGACGACAAGGGCGGCATG-3'
FL_245_Sphl_as	5'-CCGCCCTTGTCGTCGTCGTCCTTATAATCGCCGGC-3'

NYBR1C2_FL_245_Sphl_s	5'- CCGGGCCCTGAAAAACGAACAGACCTTAAGAGCGGATCAGATGTTTGGCGA TTATAAGGACGACGACGACAAGGGCATG-3'
NYBR1C2_FL_245_Sphl_as	5'- CCCTTGTGTCGTCGTCCTTATAATCGCCAAACATCTGATCCGCTCTTAAGG TCTGTTCGTTTTTCAGGGC-3'
CD19_42FL_245_Sphl_s	5'- CCGGGCCCTGGGGATCCACATGAGACCCCTGGCCATCTGGCTGTTTCATCTT CGGCGATTATAAGGACGACGACGACAAGGGCATG-3'
CD19_42FL_245_Sphl_as	5'- CCCTTGTGTCGTCGTCCTTATAATCGCCGAAGATGAACAGCCAGATGGCC AGGGGTCTCATGTGGATCCCCAGGGC-3'
CD19_6FL_245_Sphl_s	5'- CCGGGCCGTGCTGCAGTGCCTGAAAGGTACCAGCGATGGCCCGACCCAGC AGGGCGATTATAAGGACGACGACGACAAGGGCATG-3'
CD19_6FL_245_Sphl_as	5'- CCCTTGTGTCGTCGTCCTTATAATCGCCCTGCTGGGTCCGGCCATCGCTG GTACCTTTCAGGCACTGCAGCACGGC-3'
CD19_23FL_245_Sphl_s	5'- CCGGGCCTGGAGCCGCGAAAGCCCGCTTAAGCCGTTTCTTAAGCTGAGCC TGGGCGATTATAAGGACGACGACGACAAGGGCATG-3'
CD19_23FL_245_Sphl_as	5'- CCCTTGTGTCGTCGTCCTTATAATCGCCCAGGCTCAGCTTAAGAAACGGC TTAAGCGGGCTTTCGCGGCTCCAGGC-3'
CD19_33FL_245_Sphl_s	5'- CCGGGCCCTTAAGCTGAGCCTGGGCCTGCCCGCCTGGGCATCCACATGA GAGGCGATTATAAGGACGACGACGACAAGGGCATG-3'
CD19_33FL_245_Sphl_as	5'- CCCTTGTGTCGTCGTCCTTATAATCGCCTCTCATGTGGATGCCCAGGCCG GGCAGGCCCAGGCTCAGCTTAAGGGC-3'
CD19_51FL_245_Sphl_s	5'- CCGGGCCATCTGGCTGTTTCATCTTCAACGTGAGCCAGCAGATGGGCGGCT TCGGCGATTATAAGGACGACGACGACAAGGGCATG-3'
CD19_51FL_245_Sphl_as	5'- CCCTTGTGTCGTCGTCCTTATAATCGCCGAAGCCGCCATCTGCTGGCTC ACGTTGAAGATGAACAGCCAGATGGC-3'
CD19_55FL_245_Sphl_s	5'- CCGGGCCATCTTCAACGTGAGCCAGCAGATGGGCGGCTTCTACCTGTGCC AGGGCGATTATAAGGACGACGACGACAAGGGCATG-3'
CD19_55FL_245_Sphl_as	5'- CCCTTGTGTCGTCGTCCTTATAATCGCCCTGGCACAGGTAGAAGCCGCC ATCTGCTGGCTCACGTTGAAGATGGC-3'

2.9 Primer

2.9.1 Primer for sequencing

AAV2-sey-mid2-fwd	5'-AAGGCGTATCAGAACTGTG-3'
AAV2-cap-fwd	5'-AGAGTCATCACCACCAGCAC-3'
AAV2-cap-rev	5'-TTACAGATTACGAGTCAGGT-3'

2.9.2 Primer for site-directed mutagenesis

Name	Sequence	Annealing Temp (°C)
AAV2-HSPG-KO-fwd	5'- GTATCTACCAACCTCCAGGCAGGCAACGCACAAGC AGCTACCGCAGA-3'	68
AAV2-HSPG-KO-rev	5'- TCTGCGGTAGCTGCTTGTGCGTTGCCTGCCTGGAG GTTGGTAGATAC-3'	68
AAV2-R585S-R588T-fwd	5'- ATCTACCAACCTCCAGAGCGGCCAGACAGGCCAAG GCCAGGCGG-3'	60
AAV2-R585S-R588T-rev	5'- CCGCCTGGGCCTTGGCCTGTCTGGCCGCTCTGGAG GTTGGTAGAT-3'	60
AAV2-E499D-fwd	5'- GGATAACAACAACAGTGACTACTCGTGGACTGGAG CT-3'	56
AAV2-E499D-rev	5'- AGCTCCAGTCCACGAGTAGTCACTGTTGTTGTTATC C-3'	56
AAV2-AgeI-fwd	5'-CTCATCAAGAACACACCGGTACCTGCG-3'	68
AAV2-AgeI-rev	5'-CGCAGGTACCGGTGTGTTCTTGATGAG-3'	68
AAV2-NheI-fwd	5'- GCGGCAAAGTTTGCTAGCTTCATCACACAGTACTCC -3'	68
AAV2-NheI-rev	5'- GGAGTACTGTGTGATGAAGCTAGCAAACCTTTGCCGC -3'	68
AAV2-A593T-fwd	5'-ACAGGCCAAGGCCAGACGGCCACCGCAGA-3'	68
AAV2-A593T-rev	5'-TCTGCGGTGGCCGTCTGGGCCTTGGCCTGT-3'	68
AAV2-XmaI-fwd	5'-ACCAGCACCCGGGCCTGGGCCCTGCCACC-3'	68
AAV2-XmaI-rev	5'-GGTGGGCAGGGCCAGGCCCGGGTGCTGGT-3'	68
AAV2-SpeI-fwd	5'- AACCACCTCTACAACTAGTTTCCAGCCAATCAGGA- 3'	61
AAV2-SpeI-rev	5'- TCCTGATTGGCTGGAACTAGTTTGTAGAGGTGGTT -3'	61
AAV2-SphI-fwd	5'-ACCCGGGCCTGGGGCATGCCACCTA-3'	61
AAV2-SphI-rev	5'-TAGGTGGGCATGCCCCAGGCCCGGGT-3'	61
AAV2-MfeI-fwd	5'-AACAAACACTCCAATTGGAACCACCACGCA-3'	54
AAV2-MfeI-rev	5'-TGCCTGGTGGTTCCAATTGGAGTGTGTT-3'	54
AAV2-SpeI-fwd	5'-AACCACCACGCACTAGTCAGCTTCCAGTT-3'	56
AAV2-SpeI-rev	5'-AACTGAAGCTGACTAGTGCCTGGTGGTT-3'	56
AAV2-T450A-fwd	5'-GAGCAGAACAACGCTCCAAGTGAACCACCA-3'	58
AAV2-T450A-rev	5'-TGGTGGTTCCACTTGGAGCGTTTGTCTGCTC-3'	58

AAV2-R447K-588-fwd	5'-TACCTGTATTACTTGAGCAAAACAAACTCCAA-3'	53
AAV2-R447K-588-fwd	5'-TTGGAGTGTGTTTGTGTTGCTCAAGTAATACAGGTA-3'	53
AAV2-Q457M_fwd	5'-GAGCAGAACAACGCTCCAAGTGAACCACCA-3'	56
AAV2-Q457M_rev	5'-TGGTGGTTCCACTTGGAGCGTTTGTCTGCTC-3'	56
AAV2-E548G-fwd	5'-AAGCAAGGCTCAGGGAAAACAATGTGGA-3'	55
AAV2-E548G-rev	5'-TCCACATTTGTTTTCCCTGAGCCTTGCTT-3'	55
AAV2-G546D-wt-fwd	5'-ATCTTTGGGAAGCAAGACTCAGAGAAAACA-3'	54
AAV2-G546D-wt-rev	5'-TGTTTTCTCTGAGTCTTGCTTCCCAAAGAT-3'	54
AAV2-G546D-mut-fwd	5'-TCTTTGGGAAGCAAGACTCAGGGAAAACA-3'	56
AAV2-G546D-mut-rev	5'-TTGTTTTCCCTGAGTCTTGCTTCCCAAAGA-3'	56
AAV2-V151A-fwd	5'-AGAGCACTCTCCTGCGGAGCCAGACTCCT-3'	61
AAV2-V151A-re	5'-AGGAGTCTGGCTCCGCAGGAGAGTGCTCT-3'	61
AAV2-K39Q-fwd	5'-AGAGCGGCATCAGGACGACAGCAGGGGT-3'	61
AAV2-K39Q-rev	5'-ACCCCTGCTGTGCTCCTGATGCCGCTCT-3'	61
AAV2-F533Y-fw	5'-AAGGACGATGAAGAAAAGTATTTTCCTCAGA-3'	51
AAV2-F533Y-rev	5'-TCTGAGGAAAATACTTTTCTTCATCGTCCTT-3'	51
AAV2-S492A-fw	5'-AGTATCAAAGACAGCTGCGGATAACAACAA-3'	51
AAV2-S492A-rev	5'-TTGTTGTTATCCGCAGCTGTCTTTGATACT-3'	51

2.10 Cells

Cell line	DSMZ No.	Medium	Provider
HEK293T	ACC 635	DMEM + 10% FCS + 1% Pen/Strep	AG Jäger
Jurkat	ACC 282	RPMI + 10% FCS + 1% Pen/Strep	AG Jäger
Jurkat-Venus		RPMI + 10% FCS + 1% Pen/Strep	Kindly provided by Eren Boga (DKFZ, Heidelberg)
Jurkat-Venus-CLDN6-CAR		RPMI + 10% FCS + 1% Pen/Strep	Generated in this study
Jurkat-CLDN6-CAR		RPMI + 10% FCS + 1% Pen/Strep	Generated in this study
HepG2		RPMI + 10% FCS + 1% Pen/Strep	kindly provided by AG Köhler (NCT, Heidelberg)
NIH-OvCar3		RPMI + 20% FCS + 1% Pen/Strep	kindly provided by Joshua Malapit (DKFZ, Heidelberg)

3 Methods

3.1 Cell Culture

3.1.1 Growth and maintenance

All cell lines mentioned above were cultured in humidified incubators at 37 °C and 5% CO₂. After removing the culture medium, adherent cells were detached using a trypsin-EDTA solution (0.05%) and resuspended in complete culture medium. Cells were counted (CellDrop, DeNovix) and seeded at the required density. For long term storage, cells were resuspended in fetal calf serum (FCS) containing 10% Dimethylsulfoxide (DMSO) and were frozen at -150 °C.

3.1.2 Isolation and cultivation of human T cells

For the isolation of human T cells, Peripheral Blood Mononuclear Cells (PBMCs) were isolated from human blood using density gradient centrifugation. For this purpose, blood was diluted with phosphate-buffered saline (PBS) (up to 35 mL) and added to a 15 mL Ficoll layer. Next, tubes were centrifuged at 2200 rpm for 20 min at room temperature (RT) without break. The interphase was transferred into a new 50 mL tube. Cells were washed twice with PBS (1800 rpm, 10 min) and counted. Isolation of human T cells was carried out using the Pan T cell Isolation Kit (Miltenyi Biotec) according to the manufacturer's instructions. Finally, isolated T cells were transferred to TexMACS medium (Miltenyi Biotec) (max. 2 x 10⁶ cells per mL) supplemented with TransAct™ (Miltenyi Biotec) (diluted 1:100), IL-7 (5 ng/mL) and IL-15 (5 ng/mL).

3.1.3 Transfection of HEK293T cells

To generate HEK293T cells that express a particular protein, HEK293T cells were transfected with the respective expression plasmid (2.7.2). Transfection was performed in 6-well cell culture plates by dropwise addition of transfection mix (Table 3.1.1). 3.1 x 10⁶ HEK293T cells were seeded in 3mL culture medium per well 24 h before the transfection mix was added dropwise. After 24 h transgene expression was analysed by flow cytometry (3.5.1)

Table 3.1.1: Transfection mix per 6-well

Component	Volume (µL)
OptiMEM	300
Esxpression Plasmid [1 µg/µL]	3
PEI [1 mg/mL]	12

3.1.4 Co-transfection of HEK 293T cells for lentiviral particle production

Lentiviral particles were produced by co-transfecting HEK 293T cells with two helper plasmids (VSVG - envelope plasmid (pCMV_VSV_G); *HIV Gag-Pol* - packaging plasmid (pCMVR8.74)) and the lentiviral (transfer) plasmid. 48 h prior to transfection, 6×10^6 HEK 293T cells were plated into cell culture dishes (15 cm) in 22.5 mL culture medium (2.10). For transfection, the appropriate amounts (Table 3.1.3) of the lentiviral transfer plasmid and two helper plasmids were mixed in OptiMEM. The resulting DNA/ OptiMEM master mix was mixed with polyethyleneimine (PEI (1 mg/mL)) by vortexing for 10 seconds. After an incubation time of 10 min at RT, the transfection mix was added dropwise to the cell culture medium. 24 h later, the cell culture medium was replaced by 14 mL fresh DMEM (without phenol red) which is supplemented with 1% P/S. 24 h post transfection, the supernatant was collected and centrifuged at 1800 rpm for 5 min in order to pellet the detached HEK 293T cells. Afterwards, the supernatant was filtered by using membrane filters (0.45 μ m pore size), transferred to Centricon® centrifugal filters, and centrifuged at 3500 g for 30 min. An additional centrifugation step with inverted Centricon® centrifugal filters at 1000 g for 2 min was carried out to concentrate the virus in the supernatant. These centrifugation steps were repeated until the viral supernatant was concentrated to 400 - 800 μ L. Finally, concentrated viral supernatants were stored at -80 °C. Transduction of Jurkat cells was carried out to determine the lentiviral particle titer. One day before transduction, Jurkat cells (1×10^5 / well) were seeded in 24 well plates and incubated in 1 mL RPMI supplemented with 10% FCS and 1% P/S. For lentiviral transduction, different volumes of concentrated viral supernatant were added. The transduction efficiency was determined by flow cytometric analysis 72 h post-transduction.

Table 3.1.2: Transfection mix for co-transfection of HEK293T cells for lentiviral particle production

Component	Volume (μ L)
OptiMEM	1500
Transfer vector [1 μ g/ μ L]	22.5
Packaging vector [1 μ g/ μ L]	14.6
Envelope vector [1 μ g/ μ L]	7.9
PEI [1 mg/mL]	132

3.1.5 Lentiviral transduction of Jurkat or human T cells

For transduction of Jurkat cells or human T cells, thawed lentiviral supernatant of co-transfected HEK 293T cells (3.1.4) was added to a pre-determined number of cells (MOI 3 to 5) cultivated in RPMI medium (with 10% FCS and 1% P/S). The success of transduction was evaluated by flow cytometry analysis after 48 h (3.6).

3.2 Molecular biology

3.2.1 Agarose gel electrophoresis

DNA samples were separated by size using agarose gel electrophoresis. DNA samples were mixed with Gel loading Dye and loaded on 1% or 1.5% agarose gels in Tris-acetate EDTA (TAE) buffer (Table 3.2.1) containing 0.0001% ethidium bromide. The separation process was performed at 100 V in the TAE buffer.

Table 3.2.1: Tris-acetate EDTA (TAE) buffer

Component	Concentration
Tris	40 mM
EDTA	1 mM
Acetic acid	20 mM
H ₂ O	

3.2.2 Bacterial cultures

Bacteria were grown at 37 °C in lysogeny broth (LB) medium (Table 3.2.2) containing antibiotics Carbenicillin (100 µg/mL). To obtain single clones, bacteria were streaked and grown on plates of 15 g/L agar-agar in LB medium. Liquid bacterial cultures of 3 mL (small-scale; Miniprep), 100 mL (mid-scale; Midiprep), or 400 mL (large-scale; Maxiprep) LB medium was inoculated with a single bacterial colony from an agar plate and grown shaking at 37 °C. For long-term storage of bacterial cultures at -80 °C, glycerol was added to bacterial suspensions at a final concentration of 30%.

Table 3.2.2: Lysogeny broth (LB) medium

Component	Concentration
Tryptone	10 g/L
Sodium chloride	10 g/L
Yeast extract	5 g/L
H ₂ O	

3.2.3 Transformation of *E.coli* bacteria

Heat-competent *Escherichia coli* (*E.coli*) bacteria of the XL-1 strain or the K12 (dam⁻/dcm⁻) were thawed and mixed with 25 ng plasmid DNA. After resting on ice for 15 min, a heat shock was performed for 45 sec at 42 °C, followed by cooling down the bacteria on ice for 2 min. The mixture was supplemented with 300 µL LB medium and incubated, shaking at 37 °C for 1 h. Transformed bacteria were plated on antibiotic-containing LB agar plates and incubated over night at 37 °C.

3.2.4 Isolating Plasmid DNA

Single clones of transformed bacteria were selected and grown in small-scale liquid bacterial cultures (3 mL), followed by plasmid purification using the Monarch® Plasmid Miniprep Kit (New England BioLabs) according to the manufacturer's instructions. Correct plasmid sequences were confirmed by control digest (3.2.5) and/ or sequencing (GENEWIZ from Azenta, Leipzig, Germany).

To expand plasmid DNA, LB medium (100 mL (Midi)/ 400 mL (Maxi)) containing the respective antibiotic was inoculated with transformed bacteria from small-scale liquid bacterial cultures or from frozen glycerol stocks. The culture was incubated overnight at 37 °C, before harvesting the bacteria by centrifugation at 5000 x g for 15 min. The plasmid DNA was isolated using the NucleoBond Xtra Midi kit/ NucleoBond Xtra Maxi kit (MACHEREY-NAGEL) according to the manufacturer's instructions.

3.2.5 Analytical DNA digestion

To check the accuracy of isolated plasmid DNA, analytical digestions were carried out. 100 – 200 ng of isolated plasmid DNA (3.2.4) was incubated with 1 µL of each appropriate restriction enzyme. Moreover, 2 µL of 10 x digestion buffer and H₂O were added to a total volume to 20 µL. The reaction mix was incubated for 1 h at the enzyme-specific temperature and the digested plasmid DNA was analysed by gel electrophoresis (3.2.1).

3.2.6 Agarose Gel Purification

To obtain DNA fragments for molecular cloning, the desired fragments were cut from the gel under UV light after size separation using gel electrophoresis. DNA was isolated from the gel using the Monarch® DNA Gel Extraction Kit (New England BioLabs) as described by the manufacturer's instructions.

3.2.7 Oligo annealing and ligation into capsid backbones

To generate AAVLP capsid sequences (based on AAV serotype 2) with inserted peptides, the peptide sequences were reverse translated into DNA sequences using the "reverse translate"-tool⁶⁹. For each insertion, two complementary oligo-nucleotides (ssDNA) were designed, consisting of the desired sequence and the respective matching overhangs for the restriction site used (Table 3.2.3).

Table 3.2.3: Restriction sites of the different capsid backbones

Position of the insertion	Plasmid	Restriction sites
βB-aa245	pMT-AAV2wtRC-HSPG-KO-Pos247mut	XmaI + SphI
	pMT-AAV2wtRC-HSPG-KO-Pos259mut	XmaI + SpeI
VR-IV-aa452/ aa453	pMT-AAV2wtRC-HSPG-KO-Pos453mut	MfeI + SpeI
	pMT-187-XX2_453mut	NheI + SpeI
VR-VIII-aa588	pMT-187-XX2	SfiI
HI-loop-aa653	pMT-AAV2wtRC-HSPG-KO-Himut	AgeI + NheI

3.2.7.1 Oligo annealing

To obtain double-stranded DNA with single-stranded overhangs, the matching sense and anti-sense oligonucleotides were annealed. For this purpose, the ssDNAs were mixed as shown in Table 3.2.4, and heated to 95 °C for 3 min, and then cooled slowly to RT.

Table 3.2.4: Annealing of DNA oligonucleotides

Component	Volume (μL)
ssDNA oligonucleotide s [100 μM]	2.5
ssDNA oligonucleotide as [100 μM]	2.5
NEBuffer 2 (10x)	5
H ₂ O	40

3.2.7.2 Linearization of the target vector

The target vectors were linearized by restriction enzyme digest according to Table 3.2.5. The digestion mix was incubated at 37°C (exception: restriction digest with SfiI at = 50 °C) for 1 h. Post incubation, the restriction mix was separated using gel electrophoresis (3.2.1), and the linearized vector was isolated (3.2.6).

Table 3.2.5: Linearization of capsid plasmids

Component	Volume (μL)
Vector DNA [1 μg/μL]	5
Enzyme 1	1
Enzyme 2 (if necessary)	1
CutSmart Buffer (10x)	5
H ₂ O	

3.2.7.3 Ligation of dsDNA oligonucleotides into target vectors

Annealed dsDNA oligonucleotides were inserted into the linearized vector using T4 DNA Ligase, as shown in Table 3.2.6. The ligation was incubated either at 1 h at RT or overnight at 4 °C and then used for transformation into XL-1 bacteria. Correct clones were selected as described in section 3.2.3.

Table 3.2.6: Ligation of annealed DNA oligonucleotides into linearized vector DNA

Component	Volume (μL)
dsDNA oligonucleotides (1:100)	1
Linearized vector DNA [50 ng/ μL]	1
T4 DNA Ligase	1
T4 DNA Ligase Buffer (10x)	2
H ₂ O	15

3.2.8 Ligation of digested DNA fragments into target vectors

Ligation of inserts (e.g. digested DNA fragments) into a linearized plasmid DNA (3.2.7.2) was usually performed at a molar ratio of 3:1 or 5:1. The insert DNA mass was calculated using the online tool NEBBioCalculator⁷⁰. Then, DNA fragments were inserted into the linearized vector using T4 DNA Ligase as shown in Table 3.2.7.

Table 3.2.7: Ligation of digested DNA fragments into linearized vector DNA

Component	Volume (μL)
Insert	calculated for 3:1 or 5:1
Linearized vector DNA [50 ng/ μL]	1
T4 DNA Ligase	1
T4 DNA Ligase Buffer (10x)	2
H ₂ O	filled up to 20

3.2.9 Gateway-cloning

The Gateway cloning technology (Invitrogen) allows the transfer of DNA fragments by recombination reactions. The entry vector encodes the gene of interest flanked by attL sites, whereas the destination vector harbours the ccdB gene flanked by attR sites. To perform cloning, a reaction mix was prepared as shown in Table 3.2.8, incubated at 25 °C for 1 h and stopped by adding 0.5 μL proteinase K [2 mg/mL]. After an additional incubation period of 10 min at 37 °C, the transformation was performed as described in section 3.2.3.

Table 3.2.8: LR- reaction mix

Component	Volume
Entry vector	200 ng
Destination vector	200 ng
LR clonase enzyme mix	1 μL

3.2.10 Site-directed mutagenesis (SDM)

Some AAVLP capsids were modified by mutating single amino acids. To induce the mutation by SDM, complementary polymerase chain reaction (PCR) primers were designed (2.9.2), spanning the target site, and changing single nucleotides in the original sequence. The reaction mix was prepared according to Table 3.2.9 and processed in a T3000 Thermocycler

(Biometra) using PCR cycles as indicated in Table 3.2.10. The PCR product was purified using the QIAquick PCR Purification Kit (QIAGEN) in accordance with the manufacturer's instructions. Purified DNA was transformed into XL-1 bacteria as described previously (section 3.2.3). Successful mutation was confirmed by sequencing (GENEWIZ from Azenta, Leipzig, Germany). Plasmids intended for SfiI digestion were subsequently transformed into K12 (dam⁻/dcm⁻) bacteria.

Table 3.2.9: PCR mix for site-directed mutagenesis

Component	Volume (µL)
Plasmid template [25 ng/µl]	1
Fwd primer [10 µM]	1
Rev primer [10 µM]	1
dNTP mix [5 mM each]	2.5
Pfu Buffer (10 x)	5
PfuPlus! DNA Polymerase [5U/µl]	0.5
H ₂ O	39

Table 3.2.10: PCR cycles for site-directed mutagenesis

Step	Cycles	Temperature	Time
Initial Denaturation	1	95 °C	2 min
Denaturation	40	95 °C	0.5 min
Annealing		According to 2.9.2	1 min
Extension		68 °C	9 min
Final Extension	1	68 °C	7 min

3.3 Production of AAVLPs

AAVLP production was performed in two scales: From small-scale production in 6-well plates, 48-well plates, or 96-well plates, particles were used in the form of crude lysates in following experiments. Large-scale productions in several 15 cm cell culture dishes were carried out if a high number of purified particles was needed. For AAVLP production, HEK293T the cells were transfected with the adenoviral helper plasmid pDGdVP, the ITR containing, self-complementary transgene plasmid pds-CMV-GFP and an AAV2 plasmid encoding Rep and Cap proteins^{71,72}. Plasmid pds-CMV-GFP encoded a green fluorescent protein (GFP) transgene and was included as a reporter gene to confirm transfection efficiency⁷³.

3.3.1 Small-scale production of AAVLPs in crude lysates

24 h prior to transfection, cells were seeded into 96-, 48- or 6-well cell culture plates. The cell number was determined according to the plate format (Table 3.3.1). Then the cells were incubated for 24 h under standard cell culture conditions (3.1.1) and transfected according to Table 3.3.2 with a capsid plasmid, pds-CMV-GFP and pDGdVP. The resulting DNA/ OptiMEM

master mix was mixed with polyethylenimine (PEI (1 mg/ mL)) at a DNA/PEI ratio of 1:3 by vortexing for 10 seconds. After an incubation time of 10 min at RT, the transfection mix was added dropwise to the cell culture medium.

Table 3.3.1: Cells per well for transfection of HEK293T cells for AAVLP small-scale production

Plate format	Cells per well	Volume per well (µL)
96-well	3×10^4	100
48-well	7.5×10^4	250
6-well	3.1×10^5	1500

Table 3.3.2: Transfection mix for AAVLP small-scale transfection in different cell culture plates

Component	96-well volume (µL)	48-well volume (µL)	6-well volume (µL)
Capsid plasmid ~8500 bp [100 ng/µl]	0.6	1.5	6.3
GFP transgene plasmid 5800 bp [100 ng/µl]	0.4	1.04	4.3
Ad helper plasmid ~21000 bp [100 ng/µl]	1.48	3.7	15.4
OptiMEM	12.5	21.75	170
PEI [1 mg/mL]	0.75	1.88	7.8

48-72 h post transfection, first, transfection efficiency was analysed by detecting the fluorescence of the cotransfected GFP. Then, cells were detached by resuspension in the culture medium. The cells were pelleted by centrifugation (400g, 5 min, 4 °C) and the supernatant was discarded. After centrifugation at 400 g for 5 min and washing in phosphate-buffered saline (PBS), cell pellets were resuspended in an appropriate amount of PBS (Table 3.3.3). The resuspended cells were lysed in three consecutive freeze-thaw cycles of shock freezing in liquid nitrogen and thawing at 37 °C. The suspension was centrifugated to separate the AAVLPs from the cell debris (14000rpm, 10 min, RT). The AAVLP-containing supernatant was stored at -80 °C.

Table 3.3.3: Final volume of crude lysates depending on the transfection plate format

Transfection plate format	Crude lysate volume (µl)
96-well	60
48-well	80
6-well	200

3.3.2 Capsid assembly in the presence of proteasome inhibitor MG132

For studying capsid assembly in the presence of a proteasome inhibitor, transfection of HEK293T cells to produce AAVLP crude lysates was performed as described in 3.3.1. 24 h post the transfection, MG132 was added to the cells via medium exchange with culture medium containing 1 μ M to 5 μ M MG132. After 24 h incubation, crude lysate production and quantification were performed as described in 3.3.1.

3.3.3 Large-scale production of purified AAVLPs

5.0×10^6 HEK293T cells (per 15 cm dish) were seeded in 22mL medium and incubated for 48 h under standard cell culture conditions (3.1.1). A transfection mix was prepared in OptiMEM with the capsid plasmid (pMT_187_XX2), pdsCMV-GFP, and pDGdVP, as described in Table 3.3.4. First, PEI was added to the DNA/OptiMEM mix in a ratio of 1:4 and incubated for 10 min at RT. Then the mix was added dropwise to the cells.

Table 3.3.4: Transfection mix for AAVLP large-scale production in 15 cm cell culture dish

Component	Volume (μ L)
Capsid plasmid ~8500 bp [1 μ g/ μ l]	10.6
GFP plasmid 5800 bp [1 μ g/ μ l]	7.3
Ad helper plasmid ~21000 bp [1 μ g/ μ l]	26.1
OptiMEM	2500
PEI [1 mg/mL]	176

72 h post-transfection, cells were collected and centrifuged at 400 x g for 20 min. Next, the cell culture supernatant was collected for optional precipitation using polyethylene glycol (PEG). For precipitation, 40% PEG 8000 solution (Table 3.3.5) was added to the collected supernatant until a concentration of 8% was reached. The PEG/AAVLP supernatant mix was then stirred at 4 °C for 1 h and incubated overnight at 4 °C. The mix was centrifuged (2800 x g, 15 min, 4 °C) and the resulting pellet was resuspended in AAVLP lysis buffer (2.5 mL per 20 dishes) (Table 3.3.6).

For the processing of AAVLP-containing cells, the generated cell pellet was washed with PBS and resuspended in AAVLP lysis buffer (10 mL per 20 dishes) (Table 3.3.6). Subsequently, the resuspended pellets were shock-frozen in liquid nitrogen and thawed at 37 °C for three times, before adding the PEG precipitate of the supernatant. 50 U Benzonase per mL lysate was added to eliminate DNA/RNA impurities and the mixture was incubated for 30 min at 37°C.

To remove cellular debris, the lysate was centrifuged (3800 x g, 20 min, RT) before being purified using an iodixanol gradient. The lysate from twenty plates was filled up to 15 mL using AAV lysis buffer and then transferred to an ultracentrifuge tube. Afterwards, the lysate was sub-layered with four iodixanol phases of 15% (9mL), 25% (6 mL), 40% (5 mL) and 60% (4 mL) (Table 3.3.7). The tubes were sealed and the gradients were centrifuged at 55000 rpm for 3 h at 4 °C (L8-70M Ultracentrifuge, Beckman). After centrifugation, the 40 % phase was harvested. Depending on the demands of further use, the purified particles were subsequently re-buffered and concentrated. For this, the particles were first diluted to 15 mL (1:4) in AAVLP concentration buffer (Table 3.3.8) and then concentrated to 1 mL using Amicon Ultra-15 (50 kDa) filters by centrifugation (2300 x g, RT). The concentrate was diluted with AAVLP concentration buffer to a volume of 15 mL and then centrifuged again (1150 x g, RT) until the particles were concentrated in 200-300 µL. Final AAVLP preparations were stored at -80 °C.

Table 3.3.5: PEG solution

Component	Concentration (%)
PEG 8000	40
NaCl	2.4
H ₂ O	
pH 7.4	

Table 3.3.6: AAVLP lysis buffer

Component	Concentration [nM]
Tris/HCl	50
MgCl ₂	2
NaCl	150
H ₂ O	
pH 8.5	

Table 3.3.7: Iodixanol solutions

Component	15%	25%	40%	60%
PBS (10 x)	5 mL	5 mL	5 mL	-
MgCl ₂ [1 M]	50 µL	50 µL	50 µL	50 µL
KCl [1 M]	50 µL	50 µL	50 µL	50 µL
NaCl [2.5 M]	10 mL	-	-	-
Iodixanol (60 %)	12.5 mL	20 mL	33.3 mL	50 mL
Pheolred (0.5 %)	-	75 µL	-	50 µL
H ₂ O	22.4 mL	24.8 mL	11.6 mL	-

Table 3.3.8: AAVLP concentration buffer

Component	Concentration
Sodium citrate	100 mM
Tris/HCl	10 mM
Pluronic F68	0.001 %
H ₂ O	
pH 8.0	

3.4 Enzyme-linked Immunosorbent Assays (ELISAs)

3.4.1 Particle titration of AAVLP small-scale productions by A20 sandwich ELISA

The A20 sandwich ELISA was used to determine the titer of intact AAV particles in the produced crude lysates (3.3.1). At first, a 96-well plate (high-binding) was coated with A20 hybridoma supernatant (30 μ L per well). After overnight incubation at 4 °C, the coated wells were washed three times with 150 μ L washing buffer (PBS containing 0.05% Tween20) and blocked with 100 μ L blocking buffer (washing buffer containing 3% BSA and 5% Sucrose) for 1 h at RT. Subsequently, the supernatant was discarded, and the samples and the standard dilutions of AAV2 WT capsids (starting concentration 5×10^{10} caps/mL serially diluted 1:2) were added. The samples were incubated for 1 h at RT, followed by three washing steps and the subsequent addition of a biotin-labelled A20 antibody (diluted 1:150 in blocking buffer). After 1 h incubation at RT, the antibody was discarded, and the wells were washed three times. Next, 50 μ L of Streptavidin-HRP (diluted 1:1000 in blocking buffer) was added and incubated for 1 h at RT. The wells were washed three times with washing buffer and two times with H₂O. For final detection, 50 μ L Tetramethylbenzidine (TMB) substrate was added. The reaction was stopped after 4 min by adding 2N H₂SO₄ and quantified at 450 nm with background subtraction at 650 nm using a spectrophotometer (Epoch, BioTek). The AAVLP titer was determined using the standard AAVLP-WT concentration curve. Samples within the linear range of the standard curve were used to calculate the titer.

3.4.2 Detection of Flag-tag insertion in intact AAVLPs by ELISA

This ELISA was used to analyse successful insertions into intact AAV particles by detecting both intact particles and the inserted Flag-tag. At first, a 96-well plate (high-binding) was coated with the A20 hybridoma supernatant (30 μ L per well). After overnight incubation at 4°C, the coated wells were washed three times with 150 μ L washing buffer (PBS containing 0.05% Tween20). Afterwards, the prepared wells were filled with 100 μ L blocking buffer (washing buffer containing 3% BSA and 5% Sucrose) per well and incubated for 1 h at RT. The supernatants were discarded, and the samples (20 μ L crude lysate with 10 μ L blocking buffer) were added, followed by 1h incubation at RT. The wells were washed thrice, and 50 μ L of anti-Flag-tag-HRP conjugate (diluted 1:2000 in blocking buffer) was added per well. After 1 h at

RT, the wells were washed three times with washing buffer and two times with H₂O. The reaction was stopped after 15 min by adding 2N H₂SO₄ and quantified at 450 nm with background subtraction at 650 nm using a spectrophotometer (Epoch, BioTek).

3.4.3 Particle titration of AAVLP large-scale productions by ELISA

To determine the titer of the purified AAVLPs, a 96-well ELISA plate was coated with the prepared particles. For this purpose, the viral samples were diluted 1:2 serially with a starting dilution of 1:120 in PBS. AAV2 WT particles with a known concentration were used as a standard and applied to the plate in a serial dilution of 1:2 with a starting concentration of 5.0E+10 capsids/mL. The coated plate was incubated at 4 °C overnight.

The coated wells were washed three times with 150 µL washing buffer (PBS containing 0.05% Tween20) and blocked with 100 µL blocking buffer (washing buffer containing 3% BSA and 5% Sucrose) for 1 h at RT. A20 hybridoma supernatant was added at a dilution of 1:10 in blocking buffer and incubated for 1 h at RT. Next, wells were washed, and HRP-coupled anti-mouse immunoglobulin G (IgG) (1:2000 in blocking buffer) was added. After 1 h incubation at RT, wells were washed three times with washing buffer and twice with H₂O, before adding 100 µL TMB substrate solution. The color reaction was stopped after 5 min using 50 µL 2N H₂SO₄ and quantified at 450 nm with background subtraction at 650 nm using a spectrophotometer (BioTek Epoch). The AAVLP titer was determined using the standard AAV2 WT concentration curve.

3.4.4 Human IFN γ ELISA

The human ELISA set from BD Pharmigen was used for this ELISA. A 96-well ELISA plate was coated with 30 µL of human capture antibody diluted 1:250 in coating buffer (Table 3.4.1) overnight at 4 °C. Following five washing steps with washing buffer (PBS with 0.05 % Tween20), the coated wells were blocked by adding 150 µL of assay diluent (PBS with 10% FCS) per well at RT for 1 h. After five wash steps, 30µL of the cell culture supernatants being tested was added to the plate. A known concentration series of human IFN γ , provided by BD, was prepared according to the manufacturer's instructions. After an incubation period of 2 h at 37 °C, wells were washed five times with washing buffer, and 30 µL / well of the working detector (diluted 1:250 in assay diluent) were added and incubated for 1 h at RT. Afterwards wells were washed seven times with washing buffer (with 1 min soaks) and samples were incubated with 50 µL / well of the TMB substrate solution (BD OptEIA) for 30 min at RT in the dark. The color reaction was stopped using 25 µL 2N H₂SO₄ and the absorbance was determined at 450 nm within 30 min with a reference wavelength of 570 nm using the spectrophotometer (BioTek Epoch). The quantitative evaluation was carried out by a regression line created from the human IFN γ standards.

Table 3.4.1: Coating buffer for IFN γ ELISA

Component	
Sodium carbonate	0.1 M
NaHCO ₃	7.13 g
Na ₂ CO ₃	1.59 g
H ₂ O	1 L
pH 9.5 (with 10 N NaOH)	

3.5 Western Blot – detection of AAV2 VP proteins

50 μ g of AAVLP crude lysate samples with 5 x Laemmli buffer (593.3.1) were separated on an 8% polyacrylamide gel (Table 3.5.1) with a 5% collection gel (80 V, 10 min; 130 V, 60-90 min) followed by wet-blot transfer (90 V, 2h) in 1x transfer buffer (Table 3.5.3) to nitrocellulose membrane. Before adding the antibody, the membrane was blocked with a blocking solution (5% milk powder in PBST (0.1%)) for 1 h at RT. Then, the blocking solution was removed and the mouse B1 supernatant (1:10 dilution in blocking solution) was added to the membrane to detect the three VP proteins. The membrane was incubated overnight at 4 °C. After the incubation, the membrane was washed three times for 5 min with PBST (0.1%). The secondary antibody (goat anti-mouse IgG-HRP, 1:10000 dilution in blocking solution) was added, and the membrane was incubated for 1 h in the dark at RT. Following incubation, the detection was achieved using Western Lightning Plus-ECL substrate (Perkin Elmer). β - actin staining was performed with the same membrane afterwards: The membrane was washed again and incubated with anti-Actin(I-19)-R (1:500 dilution) overnight at 4 °C. The next day, the membrane was washed, and the secondary antibody (donkey anti-rabbit IgG-HRP, 1:5000) was added to the membrane for 1 h in the dark, at RT. The detection process was performed as described above the B1 staining.

Table 3.5.1: 8% Polyacrylamide gel

Component	
H ₂ O	3.25 mL
Tris-HCl [1.5 M] pH 8.8	1.35 mL
SDS solution (10%)	68 μ L
Acrylamide/Bis (30%)	1.8 mL
Ammonium persulfate (APS) (10%)	45 μ L
TEMED	5 μ L

Table 3.5.2: 5 % Collection gel

Component	
H ₂ O	1.7 mL
Tris-HCl [0.5 M] pH 6.8	0.6 mL
SDS solution (10 %)	30 µL
Acrylamide/Bis (30 %)	0.5 mL
Ammonium persulfate (APS) (10 %)	30 µL
TEMED	5 µL

Table 3.5.3: 1x Transferbuffer (1 Liter)

Component	Volume (mL)
10x Transferbuffer (25 mM Tris-Base, 190 mM Glycin)	100
Methanol	200
H ₂ O	700

3.6 Flow cytometry analysis

3.6.1 Confirmation of a protein expressed on cell surfaces

For staining of extracellular cell markers approximately 2×10^5 cells were transferred into flow cytometry tubes. The tubes were made up to 3mL with PBS and centrifuged at 1400 rpm for 4 min at RT. The supernatant was discarded, and cells were stained with fluorochrome-conjugated mAbs or with non-conjugated primary antibodies (with the manufacturer's concentration specifications) in 100 µL PBS for 30 min at 4 °C in the dark. After the incubation period, cells were washed twice with 3 mL PBS. If secondary antibodies were added, a second staining step was performed as previously described, followed by two washing steps. After the final washing step, 1 µL DAPI (3 µM) was added to distinguish between dead and live cells, and the cells were resuspended in 200 µL PBS. Unstained cells or stained cells without the searched features served as negative controls.

3.6.2 A20-bead binding assay

The produced AAVLP-containing crude lysates, can only be examined by FACS analysis after binding to A20-coupled beads. PureProteome beads ($\sim 4 \times 10^4$ / µL) were coupled with biotinylated A20 antibody. The desired amount of beads was transferred to a tube and filled up with 500 µL PBS. The liquid was separated from the beads using a magnet and removed. The washed beads were resuspended in 1 x PBS and 0.5 µg of A20-biotin per µL beads was added and incubated in PBS for 30 min using gentle rotation at RT. To separate the antibody-coated beads, the tube was placed on a magnet and washed 2-3 times with PBS. The washed beads were then resuspended in PBS to a final concentration of 2.5×10^4 beads per 10 µL.

The AAVLP containing crude lysates were thawed on ice for the bead assay. 50 μ L PBS with 0.1% BSA was filled into each well of a V-bottom 96-well plate. Next, 10 μ L of the A20-coupled magnetic beads were added, followed by the addition of 20 μ L AAVLP lysate. The mixture was resuspended carefully and incubated for 30-45 min on a rotating device (RT, 150 rpm). For washing, the plate was placed on a magnet and the supernatant was removed and the beads were washed with PBS + BSA (0.1%). To target the unknown epitope a PE-conjugated antibody (anti-CD19 (FMC63/3B10)-PE / IMAB027-PE) was used. In a double-staining approach an anti-Flag-tag APC antibody was utilised for the detection of the assembled particle. The antibodies were diluted to a final concentration of 5 μ g/mL, and a total amount of 100 μ L of the dilution was added to the beads. After the antibody had been added, the plate was wrapped in aluminium foil and placed on a rotating device (45 min, RT, 150 rpm). Then, the beads were washed two times with PBS + BSA 0.1%, as described above. Finally, the beads were resuspended in 350 μ L PBS and transferred into FACS tubes.

3.7 *In vitro* experiments

3.7.1 Co-cultivation of CAR⁺ reporter cell line with AAVLPs

A reporter cell line was used to analyse whether epitope-carrying AAVLPs can activate CAR⁺ cells. For this reason, the Jurkat Venus cell line (kindly provided by Eren Boga) was lentiviral transduced with a CAR expression plasmid (543.1.5). The expression of the CAR was confirmed after 48 h by Flow Cytometry (3.6.1). For the co-cultivation, 5 x 10⁴ target-positive adherent cells were seeded as a positive control for activation in a volume of 1 mL in a 24-well cell culture plate and incubated under normal growth conditions (3.1.1). 24 h later, the medium of the target cells was removed and the CAR⁺ 7I-Jurkat cells (8 x 10⁴ per well) were added to the target cells and were co-cultured with the epitope-carrying AAVLPs (5x10⁶ AAVLPs per CAR⁺ cell) in 1 mL cell culture medium and incubated at 37°C. After 24 h, the cells were analysed by fluorescence microscopy and flow cytometry (3.6.1) for GFP signal and CAR expression.

3.7.2 Inhibition assay - Co-cultivation of CAR⁺ T cells with AAVLPs

To investigate the effect of AAVLPs on CAR expression, primary CAR T cells or a CAR bearing Jurkat cell line were co-cultured with AAVLPs, and then CAR expression was determined by flow cytometry (3.6.1). For this purpose, primary T cells were isolated (3.1.3) and lentivirally transduced (3.1.5). CAR⁺ T cells and untransduced mock cells were then washed, counted, and resuspended in RPMI medium. 9 x 10⁴ CAR-bearing cells were co-incubated with 1 x 10⁷ AAVLPs in 1 mL volume at normal cultivation conditions (3.1.1). After 24 h, cells were collected

and stained with anti-hIgG-PE (1:100 dilution) to detect the CAR expression and anti-Flag-tag-APC (1:20 dilution) to detect cell-bound AAVLPs by flow cytometry (3.6.1).

To investigate the full binding capacity of the AAVLPs to the CARs at the cell surface, the same assay was performed at 4 °C instead of 37 °C to inhibit endocytosis and the co-incubation time was shortened to 4 h instead of 24 h.

3.7.3 xCELLigence killing assay

To investigate the influence of AAVLPs on the killing activity of CAR T cells, a method based on changes in the proliferation and attachment of target cells was applied. Cellular impedance was measured in real-time using the xCelligence RTCA instrument (ACEA Biosciences). Adherent target cells were resuspended in RPMI medium and seeded into the 96-well microtiter plate (2.5×10^4 cells / well) in a total volume of 100 μ L. After 24 h the CAR+ T cells (ratio 1:2) and AAVLPs were added in a total volume of 100 μ L. Every condition was tested in triplicates. The measurement occurred for at least two days. To calculate the viability of the target cells, an untreated control was used. The cell indices were normalized to the time point of treatment addition, i.e. application of CAR T cells and/or AAVLPs to target cells. In addition, the normalized values were evaluated in relation to the untreated control group. The concentration of IFN γ in the cell culture supernatants was determined by IFN γ ELISA (3.4.4).

3.7.4 Statistical analysis

Data was visualised and the statistical analysis were performed using GraphPad Prism 8.0.2 (GraphPad Software Inc, USA). To determine significant differences between more than three normally distributed groups a One-way ANOVA was performed, followed by a Tukey's multiple comparison test. To compare the values of many time points of two groups with each other multiple t-tests were performed, followed by Holm-Sidak's multiple comparison test.

4 Results

4.1 Insertions lead to disturbed capsid formation

In my master thesis, the screening method AAViTOP (1.3.1) was used for an attempt to identify the epitope of the anti-CD19 clone FMC63 antibody⁷⁴. The scFv of this antibody serves as binding unit of the CAR of the approved CAR T cell products Kymriah and Yescarta⁷⁵. During my master thesis, I generated AAVLPs, presenting short sequence fragments of the sequence of CD19 exon 2 on the capsid surface. Due to previous studies finding a connection between mutations or even the absence of exon 2 and resistance to treatment with CAR T cells, the FMC63 epitope was suspected to be located in exon 2^{76,77}. The results of my master thesis showed that not all sequence fragments of the exon 2 could be presented on the AAV capsid, as in many cases no intact particles were detectable. By C-terminally adding the Flag-tag sequence to the insert sequence and by forming chimeric particles without any insertion, the production of some specific particles could be realized⁷⁴. Based on these findings, I now attempted to verify and improve the screening procedure independently of the target protein, as it is necessary to close the gap in production success for a robust screening technology.

4.1.1 Defining the assembly disturbing motifs

In this work, the objective was to present the entire CD19 exon 2 peptide library on the AAVLP surface. This is an extension to my preceding master thesis, for which only half of the sequences were utilized⁷⁴. Based on my previous results, first, the whole overlapping peptide library of CD19 exon 2 was extended by a Flag-tag (2.8.1) at the C-terminal end of the sequence with one glycine between insert and Flag-tag sequence. This change elongate the inserted sequences from 15 to 25 amino acids. I inserted the 75 extended sequences into the capsid backbone (pMT-187-XX2) via the SfiI insertion site (3.2.6). The correct clones were identified by a control digestion (3.2.1) with the enzyme PstI-v2, which cuts in the Flag-tag sequence and was used as a control for any further cloning that includes a Flag-tag sequence. After cloning, the plasmids were used for small-scale production of AAVLPs (3.3.1). To be able to use all plasmids simultaneously for transfection, I used the 96-well format in this case. The subsequently generated crude lysates were then quantified in the A20 sandwich ELISA (3.4.1). This process from cloning to quantification is going to be repeated later in this work when different capsid backbones are tested (Figure 4.1.1, A). I repeated the whole process up to quantification several times (n = 3).

After quantification, I observed large differences between the individual titers. For example, the lowest mean value (CD19_31) is 1.68×10^4 and the highest mean value (CD19_67) is 1.09×10^6 . Compared to the results of my master thesis, 34% more sequence fragments can be presented, but there is a sequence region that still does not seem to be presentable⁷⁴. This gap includes the insertions CD19_41 to CD19_51 with the exception of CD19_48 (Figure 3.2.1,

B + C). After I analysed the sequences, it was striking that most aromatic amino acids can be found within the sequences in this region. Furthermore, no acidic sequences are found in this area (Figure 4.1.1, B).

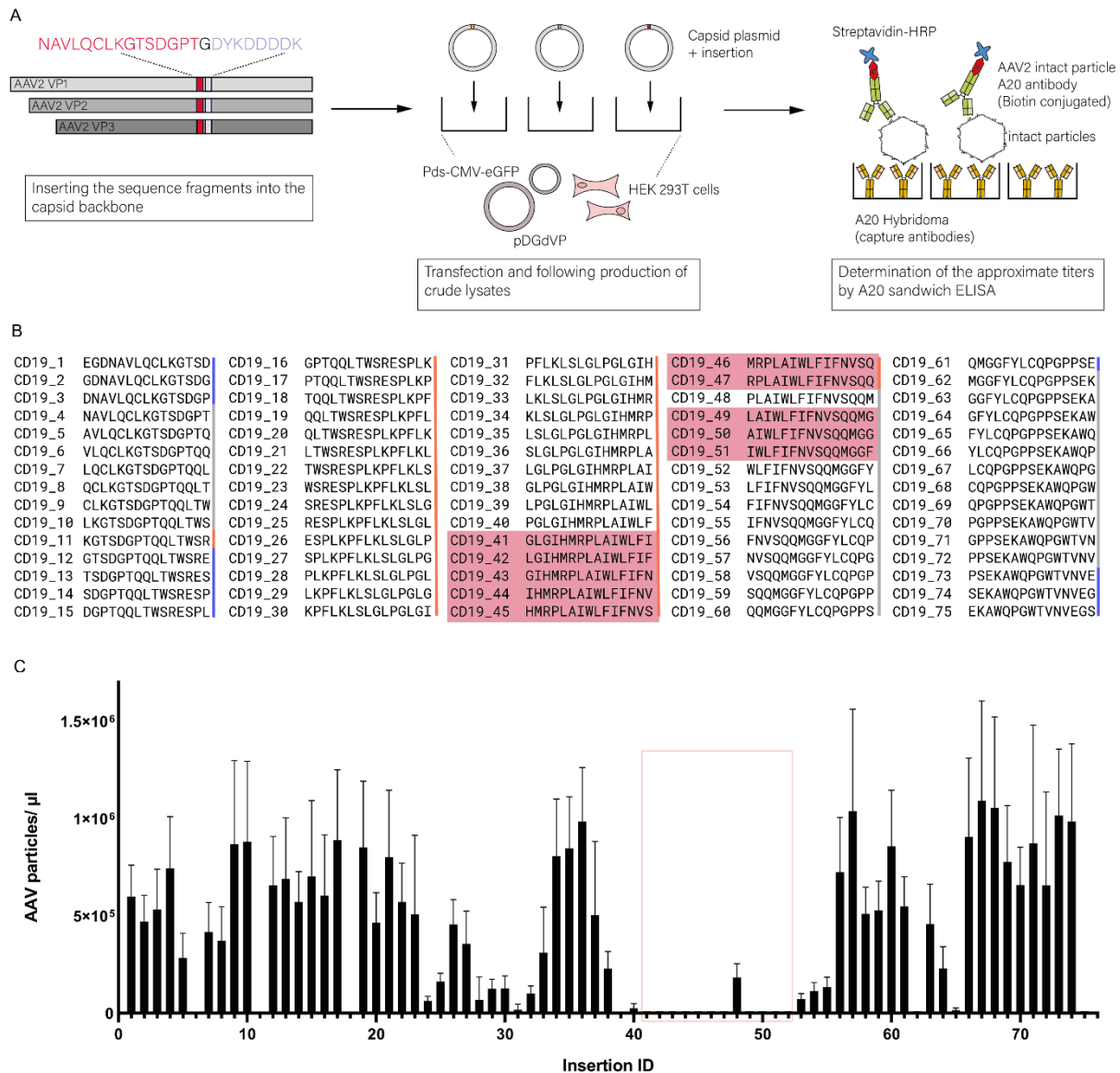


Figure 4.1.1: Overlapping sequence library of CD19 exon 2 as basis for further improvements.

A: To analyse the impact of the additional Flag-tag all CD19 exon 2 sequences were C-terminally extended by a Flag-tag and inserted into the capsid plasmid. The capsid plasmid was used with two helper plasmids for the transfection of HEK293T cells. The particle titers of the produced crude lysates were determined by an A20 sandwich ELISA. **B:** the overlapping peptide library of CD19 exon 2 consists of 75 sequences (here shown without the Flag-tag), every sequence was named CD19 followed by the number of the peptide. The net charge of the amino acid sequence is visualised by a coloured line next to the sequence: blue = negatively charged (acidic), grey = neutral, orange = positively charged (basic). The sequences marked in red do not lead to virus assembly. **C:** The entire library was produced and quantified by ELISA multiple times ($n = 3$). The mean value was calculated from the results and presented as a bar with the standard error of mean (SEM) as line.

The sequences CD19_6, _11, _18, _39, _62 and _65 also showed no assembled particles, but I was able to proof that in these cases a frameshift occurred during cloning, due to the

insertion of an additional base. This error prevented the formation of capsids. After I repeated the cloning, I was able to detect intact particles by A20 sandwich ELISA (data not shown). Due to the positive effect on the particle titers and the facilitated cloning control through a uniform restriction site (P_{sil-v2}), the Flag tag was included in all experiments and marked by the abbreviation FL. This library was also the basis for the following experiments. To test different changes in the capsid, I used sequences with different properties from this library.

4.1.2 Premature degradation as a reason for non-existent particles

The capsid of AAV2 consists of 60 subunits, which are arranged to form the capsid⁸. However, if the inserted sequences lead to e.g., ubiquitination and degradation of the proteins, intact particles cannot be formed. Thus, I performed a western blot with crude lysates of untreated samples of the CD19 library to compare the protein level with the particle titers I have detected before (Figure 4.1.2, A). I selected five CD19 library sequences with different characteristics, such as the charge (CD19_23FL, CD19_33FL positive charged), and the number of aromatic amino acids (CD19_55FL contains 4 aromatic amino acids). All particles were produced in a small-scale production in 6-well cell culture plates. To be able to use a total protein amount of 50 µg for the blot, I have taken up the lysates in only 50 µL PBS. The VP 1-3 proteins were detectable in every CD19 library sample with the additional Flag-tag. Interestingly, the crude lysates with no intact particles (CD19_42FL, CD19_51FL) showed slightly darker bands than the sample CD19_33FL, which can build up a small quantity of intact particles as shown in Figure 4.1.1, C. I used crude lysates as additional controls with the AAV-wt particles and AAVLPs, which present a sequence fragment of the NYBR1 protein (C2FL) on the surface. The NYBR1 sequence was well tolerated, and the capsid formation was not disturbed, as will be shown later (4.1.4).

To test whether particle titers can be increased by inhibiting the proteasome, I cultured the transfected cells with the proteasome inhibitor MG132. MG132 is a reversible inhibitor of calpain proteases and disturb the proteasome-regulated degradation of intracellular proteins⁷⁸. I examined the crude lysates both via A20 ELISA (3.4.1) to see whether the number of intact particles can be increased and by western blot (3.5) to assess whether differences in protein levels of the free VP capsid proteins can be detected (Figure 4.1.2, B-C). I performed the MG132 treatment with sample CD19_33 (without Flag-tag), which like CD19_42 is a capsid disturbing sequence, but the capsid formation was rescued by adding the Flag-tag and generating chimeric particles⁷⁴. These chimeric particles were formed with fewer insertions on the surface by using not only the plasmid with the inserted sequence during transfection, but a second plasmid (HSPGKO) corresponding to the wild-type sequence with point-mutated HSPG binding site lacking any insertion. Here, a 1:1 ratio of the two plasmids was used for transfection. The formation of chimeric particles is not possible with the CD19_42FL and

CD19_51FL insertions. Only HSPGKO proteins are used to construct the capsids and the CD19_42FL/ CD19_51FL sequences are not integrated. I tested different MG132 concentrations because it has been shown that MG132 can reduce the activity of those enzymes required for degradation in a range from a molarity of 0.5 μM ⁷⁹.

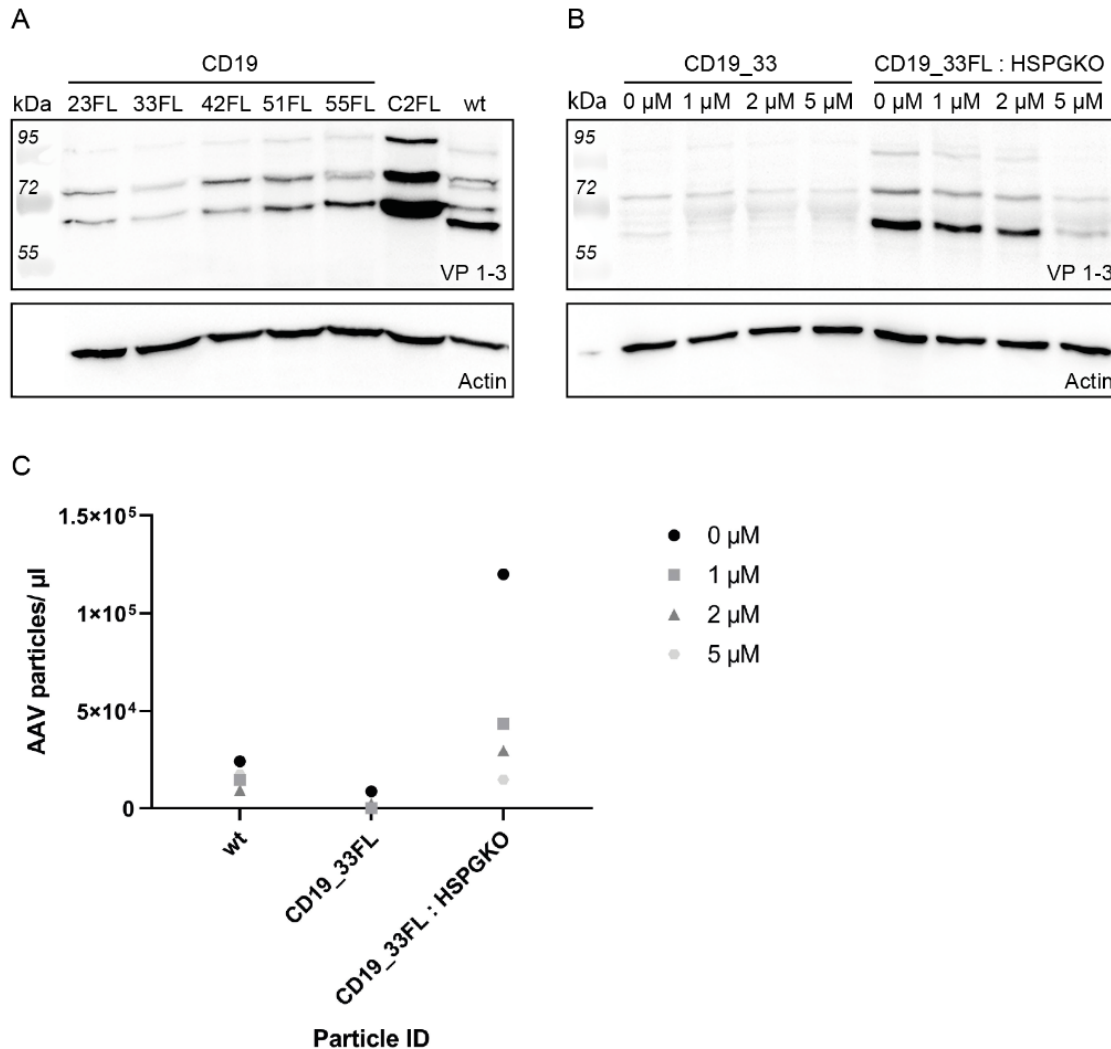


Figure 4.1.2: Inhibiting the proteasome as an attempt to promote capsid assembly. Western blot analysis of AAV capsid proteins VP1 (87kDa), VP2 (72 kDa) and VP3 (62 kDa) in HEK293T cell crude lysates. Equal total protein amounts were separated and analysed with the anti-AAV capsid mouse B1 supernatant. A: samples of the CD19 exon 2 library with additional Flag-tag were compared to the wt capsid proteins (wt) and a capsid with a NYBR1 insertion (C2FL). B: The samples show the capsid proteins (VP1-VP3) after treatment with the proteasome inhibitor MG132 (1 μM - 5 μM). The capsids with the CD19_33FL insertion and the chimeric form were compared, in which a wt-like plasmid (HSPGKO) was added 1:1 with the capsid backbone during transfection. C: the generated particles in the crude lysates were quantified by an A20 sandwich ELISA and the number of intact particles were determined in particles/ μL .

Interestingly, after MG132 treatment, a reduction in the protein amount of VP1-3 was detected in the chimeric particles while no change was detected in the β -actin loading control. This reduction was also detectable in the particle amount. Here, the particles per μL decreased concentration-dependently (Figure 4.1.2, C). Protein detection after MG132 treatment was

difficult for the CD19_33 samples, as the bands were already very weak before treatment, although according to the actin control the total protein amounts were very similar (Figure 4.1.2., B).

The inhibition of the proteasome showed a negative effect on protein formation and thus on the capsid titers of the tested samples. I was able to confirm this result after a further repetition, which is why this type of treatment was not pursued further as a method for improved capsid assembly or for further investigations about the degradation of the capsid proteins.

4.1.3 Verification of the crucial role of aromatic amino acids

To better understand what may prevent capsid formation, I looked more closely at the sequences from the CD19 exon 2 overlapping library, particularly the CD19_41 to CD19_51 sequences. This part of the sequence comprises several aromatic amino acids. Aromatic amino acids are very large due to their ring structures. Each ring can also form further bonds with other aromatics and with side chains in the surrounding⁸⁰. Thus, an accumulation of aromatic amino acids in a construct such as the AAVLP could possibly lead to interactions that negatively affect capsid assembly. In my previous experiments I already showed that the VP proteins are detectable for these sequences (Figure 4.1.2, A) but the assembly of subunits to form the complete capsid did not take place. To find out if the aromatic amino acids were the cause of this observation, I performed an alanine scan with two exemplary fragments of the respective sequence of CD19 exon 2. In sequence 42, each amino acid was replaced by alanine first individually and later in different combinations (Figure 4.1.3, A). In sequence 51, only the amino acids that are also present in sequence 42 were replaced by alanine (Figure 4.1.3, B). I ordered the modified sequences with the respective overhangs for the cloning strategy and inserted the fragments into the capsid backbone (pMT-187-XX2) via SfiI restriction sites.

The two sequences share an identical area (yellow background) but at different positions. In the CD19_42FL sequence, this area is located at the end of the CD19 sequence and thus directly in front of the Flag-tag sequence. In the CD19_51FL sequence, this region forms the N-terminal end of the insertion and links directly to the capsid sequence.

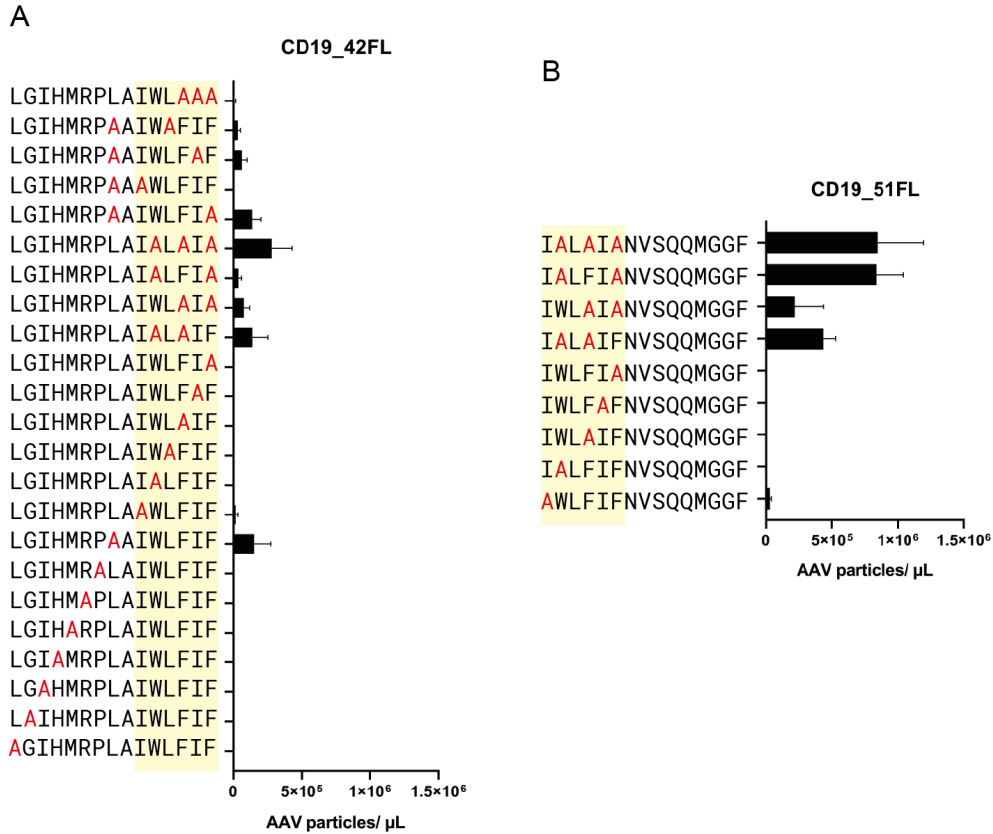


Figure 4.1.3: Comparison of the impact of the same aromatic amino acids in different positions in short sequence fragments. The sequences CD19_42FL (A) and 51FL (B) of the CD19 exon 2 epitope screening were compared. Oligos with single or multiple amino acid exchanges and the additional C-terminal Flag-tag sequence were cloned into the pMT-187-XX2 plasmid. The plasmids were used for the transfection of HEK293T cells (48-well format). Crude cell lysates were produced, and the number of particles was quantified by A20 sandwich ELISA (Figure 4.1.1). The alanine scan was produced and quantified multiple times (CD19_42FL $n =$ see appendix (7.1.1); CD19_51FL $n = 2$). The mean value was calculated from the results and presented as a bar with the standard deviation (SD) as line. The exchanged amino acids in the sequence are marked in red. Identical sequence areas are marked yellow.

An improvement in assembly became apparent in sequence 42FL when either the leucine located in the middle was replaced or at least two aromatic amino acids were exchanged. The most intact particles were determined when all 3 aromatic amino acids were exchanged. In sequence 51, the leucine from the middle of sequence 42 was no longer contained. The replacement of the individual aromatic amino acids does not have a positive effect on particle assembly. In this case, only the replacement of several aromatic amino acids leads to a higher number of particles. In these two sequences, it was not an individual aromatic amino acid that seemed to prevent the assembly of the capsids, but rather the accumulation of aromatics. Leucine appears to be able to have a negative effect even when occurring individually. This was indicated in sequence CD19_42FL. In sequence 51FL the shared leucine has not been investigated since no effect for this leucine was observed when mutated individually in CD19_42FL. In both sequences, replacing tryptophan (W) and phenylalanine (F) resulted in higher titers than replacing the two phenylalanines in the sequence that both insertions share.

Interestingly, the titers of the particles with the modified CD19_51FL sequences are higher than those of CD19_42FL. Thus, replacing the three aromatic amino acids in the CD19_42FL sequence yields an average of 2.79×10^5 particles/ μL and replacing the same amino acids in the CD19_51FL sequence yields an average of 8.45×10^5 particles/ μL .

The replacement of critical amino acids leads to the production of intact particles, this principle was also applied in the further course of this work to ensure capsid formation or to identify amino acids, that are relevant for antibody binding.

4.1.4 Insertions in different parts of the AAVLP capsid

In the previous experiments (4.1.1, 4.1.2, 4.1.3), the insertion was always placed in the VR-III loop downstream of amino acid 588 (Figure 4.1.4, A, red). The loop is thus extended. Since the aromatic amino acids are a particular problem and may hinder the assembly of the capsid through interactions with their environment, I tried to insert the individual sequences at other locations in the capsid. I used for the insertion in the VR-VIII loop aa588 (pMT-187-XX2) and VR-IV loop aa453 (pMT-187-XX2_453mut) (Figure 4.1.4, A, green) backbones that already existed with insertion sites at the specific positions. The HI-loop insertion site (HI-loop-aa653) (Figure 4.1.4, A, blue) was inserted into a wildtype capsid backbone with destroyed HSPG tropism using published primers (AAV2-NheI, AAV2-AgeI) by SDM (3.2.9) and resulted in the capsid backbone pMT-AAV2wtRC-HSPG-KO-HImut¹⁰. I also created an insertion site in the β -sheet (βB) with two different insertion strategies by SDM (3.2.9). For this, I created a common primer to insert the first restriction site (AAV2-XmaI) and a respective primer for starting strategy A (AAV2-SphI) or B (AAV2-SpeI). The insertion in βB -aa245A (pMT-AAV2wtRC-HSPG-KO-Pos247mut) results in an extension of this area. The insertion into βB -aa245B (pMT-AAV2wtRC-HSPG-KO-Pos259mut) results in a greater loss of the original sequence and thus results in a smaller extension of the region (Figure 4.1.4, A, yellow/ light orange).

To test the four different insertion sites, I inserted seven different sequences. The inserts were inserted into the respective backbones (3.2.7) and the fabricated plasmids were used to produce AAVLPs in small scale format (3.3.1). I used six sequences from the CD19 exon 2 library with different characteristics with the additional Flag-tag, five of them were used in the previous experiments. These samples have a total length of 25 amino acids (CD19 sequence = 15 amino acids + Flag-tag = 10 amino acids). The seventh sample is a part of the NYBR1 protein (C2) with the additional Flag-tag and is a shorter sample in the experiments with a total length of 23 amino acids. AAVLPs with the neutrally charged insertion CD19_6FL can be formed if the insertion is located downstream of amino acid 588 or downstream of 245(A) (Figure 4.1.4,B). Whether it is possible to present this insertion in the VR-IV loop is not known, since this construct has not been established. Whereas the number of intact particles differed remarkably between the two insertion sites. On average, three times more particles were able

to assemble when the CD19_6FL was integrated into the VR-VIII loop. The two positive charged inserted sequences (CD19_23FL and CD19_33FL) can be presented in the VR-VIII and in the VR-IV loop. In both cases, more particles are assembled when the inserted sequence was located in the VR-IV loop. The two sequences containing aromatic amino acids in a cluster (CD19_42FL and CD19_51FL) could only be detected in very small quantities. Most of the intact particles with these insertions could be detected when the sequences were inserted in the β -sheet (A). The number of intact particles (CD19_42FL = 2.37×10^5 ; CD19_51FL = 2.88×10^5) reached almost the same values as CD19_23FL (3.3×10^5) inserted in the VR-VIII loop. The sequence with four aromatic amino acids (CD19_55FL) but not in near proximity of each other lead to no intact particles in the β -sheet.

However, AAVLPs were detectable (except of CD19_42FL and CD19_51FL) when the sequences were inserted in the VR-VIII or the VR-IV loop but the individual productions with insertions in the VR-IV loop showed the greatest differences among each other. In contrast, it was not possible to detect any intact particles with insertions in the β -sheet in variant B and only very low particle titers were detectable for the HI-loop insertions (Figure 4.1.4, B). Interestingly, in both the β -sheet variant B and the HI-loop insertion strategies, inserting the desired sequence results in a rather great loss of the original wildtype capsid sequence.

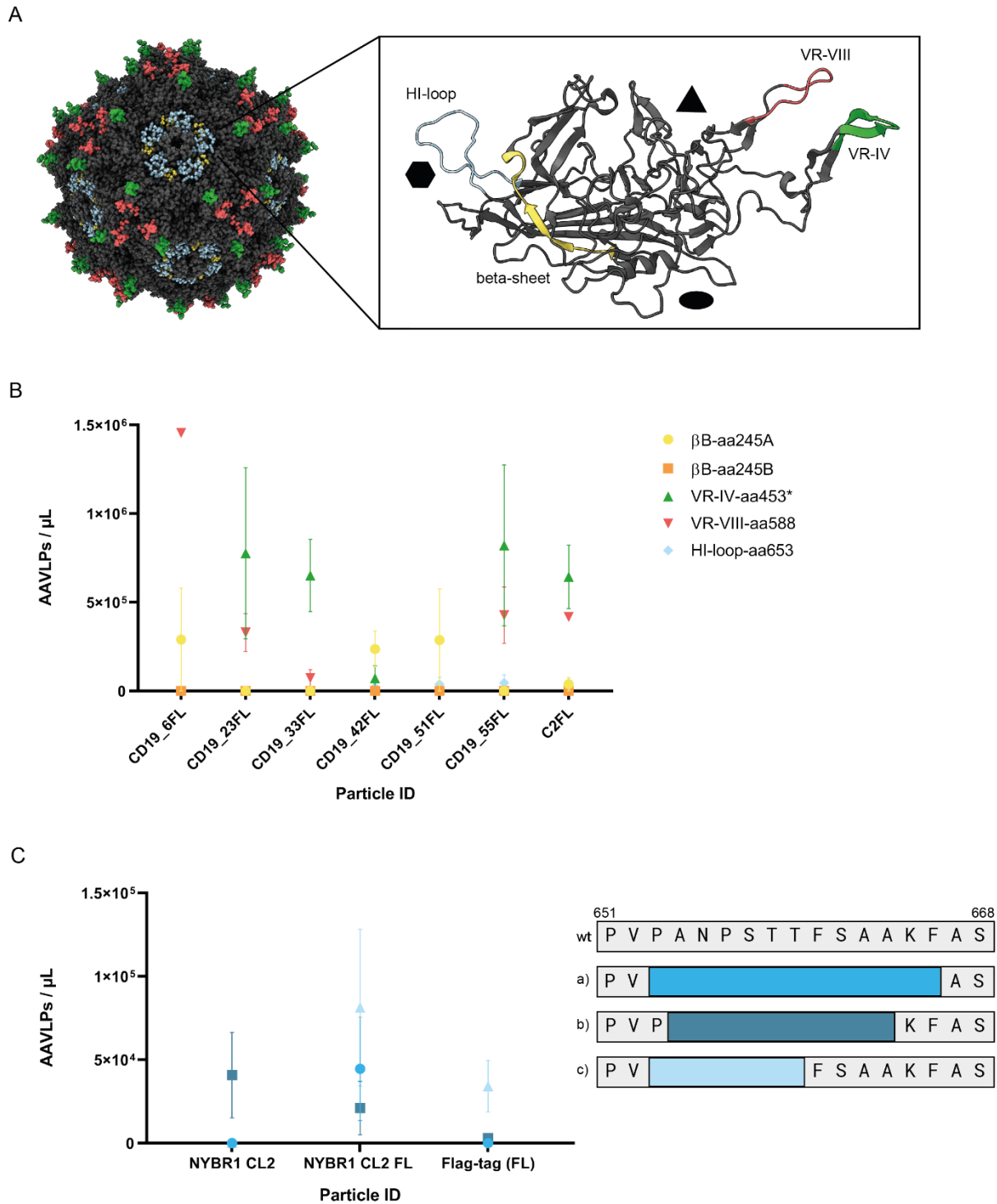


Figure 4.1.4: Comparison of alternative insertion sites in the AAVLP capsid. A: To display the peptides on the surface of the capsid, they are inserted at different positions of the VP1 protein. The four insertion regions are coloured: insertion site VR-IV-aa453 (green), VR-VIII-aa588 (red), HI-loop-aa654 (blue) and β B-aa245A/B (yellow/light orange). Figures modified from PDB entry 1lp3 and 6CBE using ChimeraX²³. B: Seven different Oligos were inserted into the five different insertions sites. The plasmids were used for the transfection of HEK293T cells (48-well format). Crude cell lysates were produced, and the number of particles was quantified by A20 sandwich ELISA (Figure 4.1.1). The different particles were produced and quantified multiple times. The mean value was calculated from the results and presented as a symbol in different colours with the standard error of mean (SEM) as line. C: Three slightly different sequences (NYBR1 CL2, NYBR1 CL2 FL, Flag-tag) were inserted between position 652 and 667 of the HI-loop (blue) via *AgeI* and *NheI* restriction sites. Three different insertion strategies were used: a) the sequences of interest were inserted directly between the restriction sites.

b) K665 is highly conserved in many serotypes and forms a salt bridge to another subunit, the K665 was preserved. c) it was assumed that the F661 interacts with a conserved proline in another loop and is critical for the capsid stability. For that reason, the F661 was preserved. The produced particles of different small-scale productions were quantified by A20 sandwich ELISA. The symbols (different blue shades) in the graph show the mean of several productions. The bars represent the standard error of the mean (SEM). The n for each construct can be found in the appendix (7.1.2).

To find out if assembly is less disrupted by insertion in the HI-loop as in the β -sheet when the loop is enlarged rather than partially replaced, I extended the inserted sequence to preserve amino acids of the original sequence¹⁶. In this regard, three different insertion strategies were tested by using three different peptides. First the NYBR1 protein fragment (CL2), second the NYBR1 protein fragment with additional Flag-tag and the last insertion was the Flag-tag (length = 9 amino acids) alone. Like in the comparison before, the sequences of interest were inserted directly between the restriction sites and 13 amino acids of the original wildtype capsid sequence were exchanged by the inserted sequences (Figure 4.1.4, C, a)). The second approach was to preserve the proline (P653) and the lysine (Figure 4.1.4, C, b)) because the K665 is highly conserved in many serotypes and forms a salt bridge to another subunit of the viral capsid¹⁰. The third strategy was to preserve, additionally to the proline and lysine of the approach before, the valine at position 654 (V654) and the phenylalanine (F661) (Figure 4.1.4, C, c)). It was assumed that the F661 interacts with a conserved proline in another loop and is critical for the capsid stability¹⁰. To preserve the F661 at the right position every amino acid between 661 and K665 was preserved. In this insertion strategy only 6 amino acids were exchanged by the inserted peptides. This means that in this case the loop was enlarged the most.

The NYBR1 protein fragment without Flag-tag (CL2) only yielded assembled capsids using insertion strategy b). The same fragment with the Flag-tag extension resulted in fewer detectable intact particles using the same strategy. Most particles, but with large differences in individual productions, could be obtained when most amino acids of the original sequence were retained (c)). The Flag-tag sequence could also be integrated into the HI-loop and allow the formation of capsids if strategy c) was used. However, all values obtained are at very low levels and in no case more than 1×10^5 capsids/ μL could be formed.

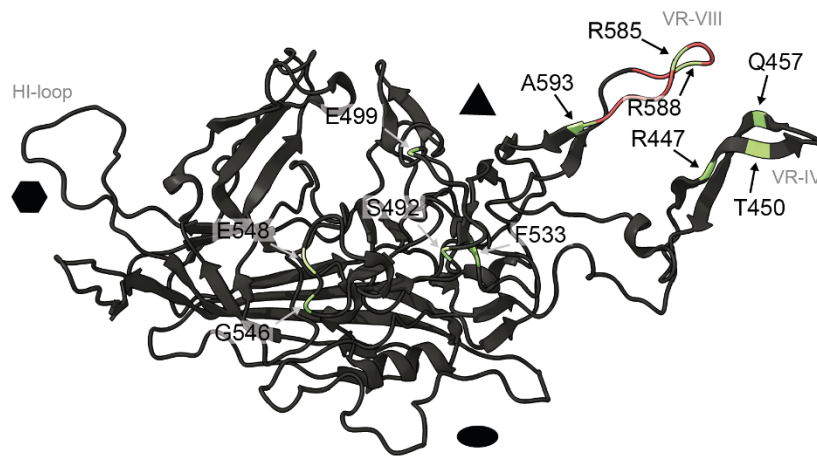
Based on these results, I decided against further work with the insertion sites in the HI-loop and β -sheet areas. The insertion in the VR-IV loop was not reliable at this point due to large differences in the production yields, so I performed the next experiments with insertions in the VR-VIII loop.

4.1.5 Backbone modifications – for a more tolerant environment

During this work, different strategies were developed to overcome the limitations of capsid assembly i.e., by adding the additional Flag-tag, the replacement of aromatic amino acids or inserting the sequences of interest in different regions in the capsid. However, the overall aim

for a screening procedure would be to display every sequence independently of the amino acid composition.

A



B

Position	AAV2	AAVv66
39	K	Q
151	V	A
447	R	K
450	T	A
457	Q	M
492	S	A
499	E	D
533	F	Y
546	G	D
548	E	G
585	R	S
588	R	T
593	A	T

C

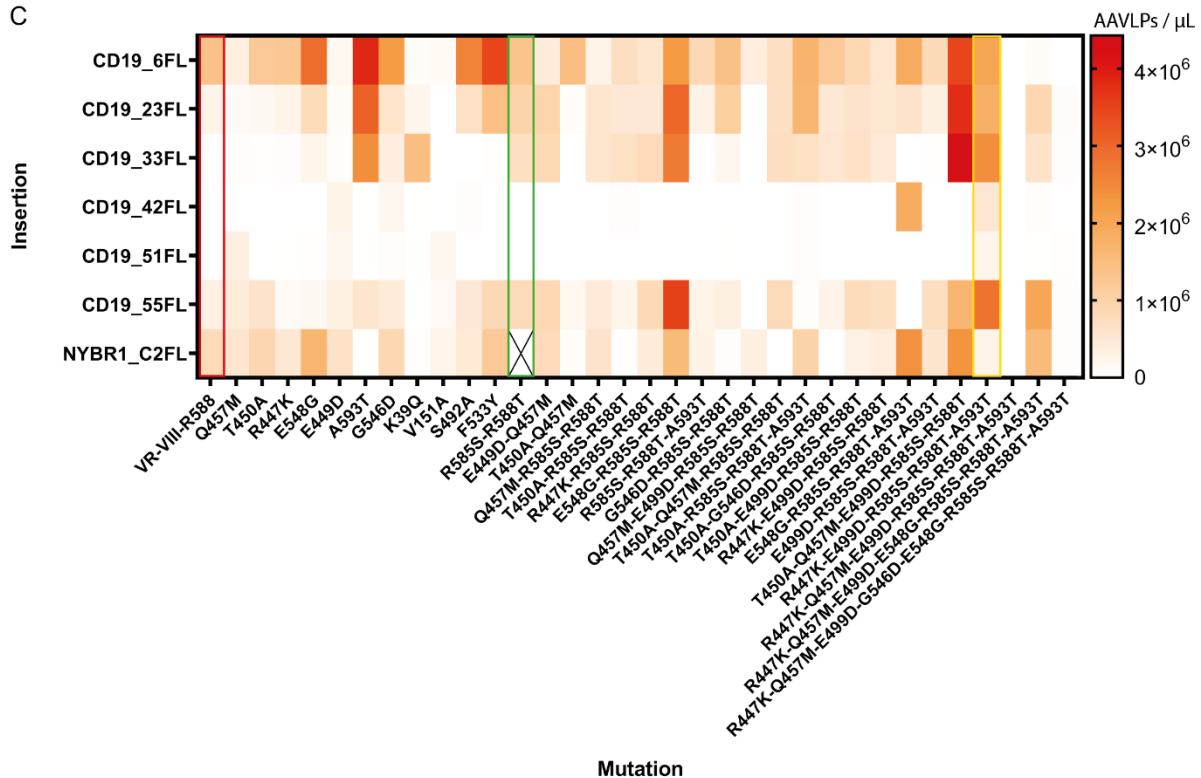


Figure 4.1.5: Sequence changes in the backbone plasmid can improve capsid assembly. A: The VP1 protein of AAV2 with amino acids marked in green. The region in the VR-VIII loop that will be extended by the insertions is marked in red. Figure modified from PDB entry using ChimeraX²³. B: Amino acid differences between the capsid of AAV2 and AAV-v66⁸¹. C: Heat map of AAVLPs per μL . Six sequences of CD19 exon 2 or the NYBR1 clone 2 epitope with a C-terminal additional Flag-tag (short: FL) (rows) were inserted into the different backbone plasmids with single or combined mutations (columns). Particles were quantified by A20 sandwich ELISA and titers (particles/ μL) are shown as colours indicated by the bar on the right. The standard capsid plasmid before modifications is marked with a red box. An improved version of the standard plasmid, that is used in further experiments is marked with a green box. An improved version of the standard plasmid that needed further validation is marked with a yellow box. Missing values are marked with a X in the heat map. The results in the heatmap show the mean of several productions (n and SEM for each plasmid can be found in the appendix (7.1.3)).

For this reason, I started to modify the plasmid backbone (Figure 4.1.5, C, VR-VIII-R588, red box), that was used for the first screening approaches. The modifications are based on the newly discovered capsid AAV-v66, which showed higher production yields and virion stability compared to AAV2⁸¹. AAV-v66 differs from AAV2 in only 13 amino acids (Figure 4.1.5, B). Thus, I generated capsid backbones by site-directed mutagenesis (3.2.10) that each represent one of these altered amino acids. I also combined different amino acid changes. In the new backbone constructs, peptides can be inserted after amino acid position 588. The backbones were then compared, based on the assembled particle titers with different insertions after transfection of HEK293T in 48-well cell culture plates. The insertions were sequence fragments from the CD19 exon 2 screen and represent different characteristics as mentioned before. When comparing the single mutations, most insertions on the capsid surface were observed when glycine at position 546 was replaced by aspartic acid (Figure 4.1.5, C). In this backbone, all CD19 sequences except CD19_51FL can be displayed, although this mutation is not located in close proximity to the inserted sequence. In addition, the titers are similar or higher than with the previous standard backbone (Figure 4.1.5,C, red outline). The fewest insertions resulted in intact capsids when I replaced the lysine at position 39 (K39Q) or the valine at position 151 (V151A). When I replaced the two arginine (R585S, R588T) around the insertion site, this modified backbone tolerated all insertions, except for the sequences CD19_42FL and CD19_51FL with the clustered aromatic amino acids. Furthermore, the titers of the produced particles with the different insertions were very similar and higher than in the previous standard backbone. For this reason, I carried out all further screening experiments in this plasmid (Figure 4.1.5, C, green outline), while several other mutations still had to be tested.

When I combined different mutations, I achieved very high particle counts with two combinations. These include the combination of three mutations at positions 548, 585 and 588; as before, the change of glutamic acid to a glycine (E548G) is located further away from the inserted sequence. The second combination consists of five mutations at position 450, 457, 499, 585 and 588. In this combination, four out of five mutations are in the variable loops of the protein. With the help of this plasmid backbone, I was able to achieve even higher titers for the insertions CD19_6FL, CD19_23FL and CD19_33FL. However, with the help of neither of these plasmids, I was able to display the sequences CD19_42FL or CD19_51FL. These two sequences were detectable on the surface of some modified capsids, but usually in very small amounts ($< 1 \times 10^6$ particle/ μ L) or with the loss of presentability of another tested sequence. Only one combination of five mutations (R447K-E499D-R585S-R588T-A593T (Figure 4.1.5, C, yellow box)) has been able to tolerate each of the insertions tested. However, this combination has only been produced and quantified twice so far.

Because of this comparative experiment, I was able to improve the productivity of the already assembling capsids. In addition, more capsid plasmid backbones were generated that tolerate

the accumulation of aromatic amino acids more than the previously used plasmid. In the following experiments, I mainly used plasmid pMT-187-XX2-R585S-R588T, as it was one of the first plasmids to show improved capsid assembly. All subsequently discovered plasmids were only tested in this setup and not yet used for other experiments.

4.2 Screening efforts using the CD19 protein

The B-cell signalling surface protein CD19 is a common target for approved CAR T cell therapy⁸²⁻⁸⁴. Most of these approved therapies are based on the antigen binding properties of anti-CD19 antibody clone FMC63⁷⁵. In the past, it was assumed that patients who did not respond to therapy carried an isoform that no longer contained the epitope of the receptor⁷⁶. More recently, the structure of CD19 has been largely elucidated and shows a very specific folding⁸⁵. Even small deviations in the sequence lead to a change in the 3D structure and result in the epitope no longer being accessible^{86,87}. As a consequence of these new findings, the epitope of FMC63 was no longer assumed to be located only in exon 2 but distributed across three loops of the protein⁸⁸. For identifying the FMC63 epitope, this meant that one was no longer looking for a linear epitope, but for a discontinuous one, which constituted a different challenge for the developed AAViTOP assay.

4.2.1 CD19 – a delicate target

In my master thesis, I demonstrated that various sequences interfere with capsid assembly, while I was nevertheless able to carry out the bead assay (3.6.2) with the assembled particles. The particles with the sequence fragment CD19_72 (PPSEKAWQPGWTV) showed the greatest binding with the anti-CD19 (FMC63) antibody⁷⁴. However, I could not reproduce these results, so I assumed that binding should be visible in the context of the complete exon 2. Once I would have verified the binding to the exon 2, it would have been possible to change individual amino acids by site-directed mutagenesis in the CD19_72 sequence to prove that the binding was taking place there. To this end, a fusion protein was designed to be transiently expressed on the cell surface of HEK293T. The protein consisted of the complete CD19 exon 2 and an N-terminal Flag-tag (Figure 4.2.1, B) to detect cell surface expression independent of anti-CD19 (FMC63) binding. The sequence for the fusion protein was inserted into a human expression vector by restriction digestion (3.2.7.2) and ligation (3.2.8). I transfected HEK293T cells with the cloned plasmid (pcDNA-21ABGGNP_Exon2_full_CD28tm) (3.1.3). After transfection, I was able to detect the expression of the fusion protein with the help of the integrated Flag-tag (53.6%) via flow cytometry (3.6.1). However, no binding of the anti-CD19 (FMC63) antibody (0.22%) was detectable (Figure 4.2.1, B). The fusion protein was then extended by exon 3 to allow a more natural folding and to possibly represent yet another part of the epitope of the FMC63 clone (Figure 4.2.1, C). The sequence of CD19 exon 3 was

ordered with appropriate overhangs to be inserted downstream of exon 2 via restriction digestion and ligation, as was done for the previous protein. This extension also included a binding site for another CD19 antibody. It is suspected that a linear sequence within exon 3 is recognised by the anti-CD19 antibody clone 3B10. This should serve as an additional control to investigate whether it is at all possible to detect this incomplete version of the CD19 protein⁸⁸. HEK293T cells were transfected with the modified plasmid (pcDNA- 21ABGGNP_Exon2_full_CD19Exon3fus_CD28tm) containing the extended version of the fusion protein. I confirmed the presence of the fusion protein on the cell surface by detecting the Flag-tag (27.9%). However, neither clone FMC63 (0.73 %) nor 3B10 (3.68 %) showed binding to the fusion protein (Figure 4.2.1, C).

Because it was not possible to detect a linear epitope within this fusion protein, it was assumed that the folding of the protein did not correspond to that of the wild-type protein. Further tests with this construct would not have been reliable. However, this experiment brought the anti-CD19 clone 3B10 antibody to my attention, whose linear epitope could be used to validate the AAViTOP method.

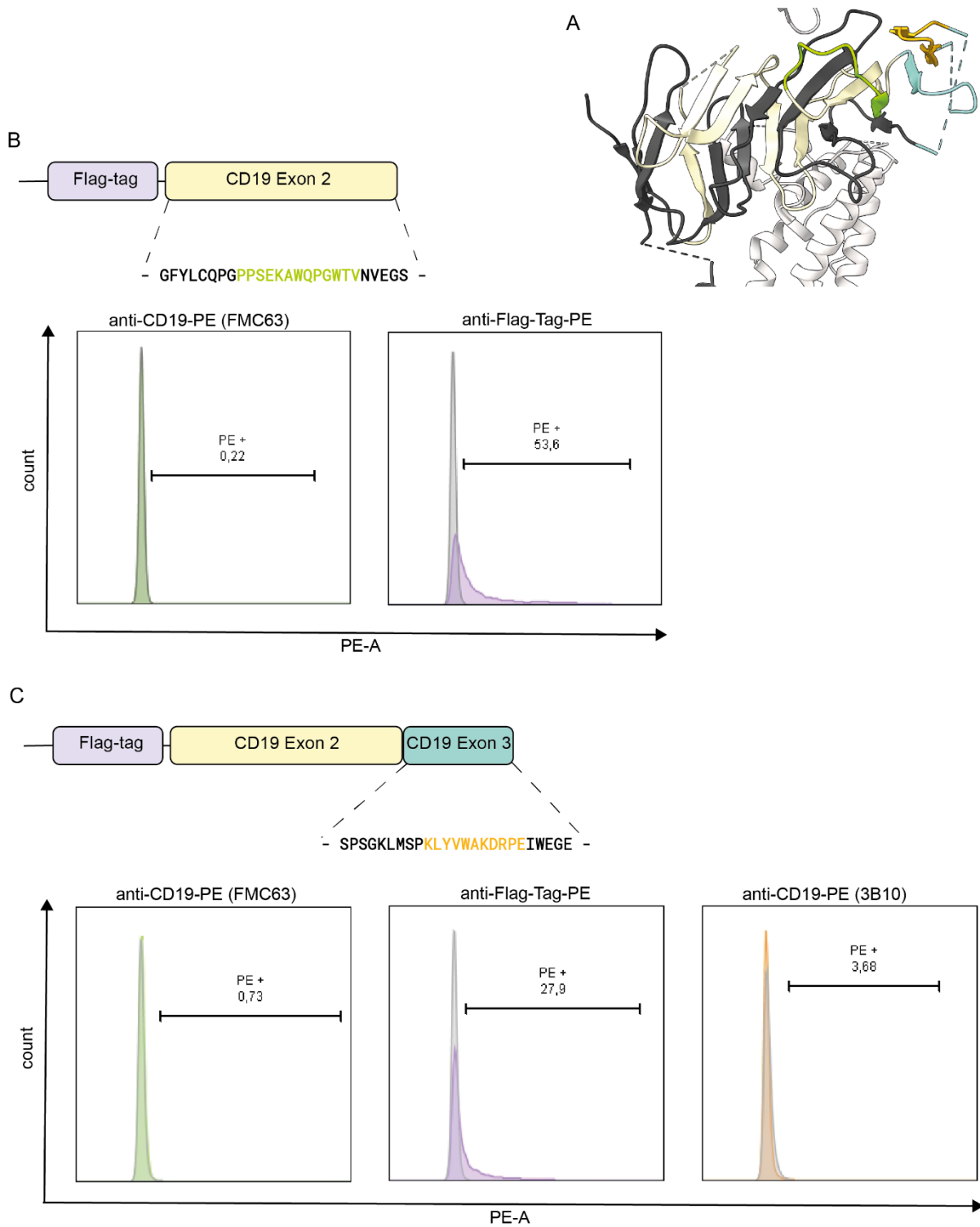


Figure 4.2.1: An attempt to generate a CD19 fusion protein. A: Structure of the CD19 protein (black) here in complex with the human CD81 co-receptor (white). Exon 2 is coloured in yellow with the CD19₇₂ sequence (PPSEKAWQPGWTV) in green. Exon 3 is coloured in turquoise and the linear epitope of clone 3B10 located within it is coloured orange. The colours have been retained throughout the illustration. Figure modified from PDB entry 7JIC using ChimeraX²³. B: Schematic illustration of the CD19 fusion protein. The part of the protein expressed on the surface consists of the Flag-tag (purple) and the complete exon 2 of the CD19 protein. The transfected cells were stained with an anti-CD19-PE (FMC63) antibody investigating the binding to exon 2 or with an anti-Flag-tag-PE antibody investigating the surface expression of the protein and analysed by flow cytometry. C: Schematic illustration of the extended CD19 fusion protein. The surface expressed part is identical to the fusion protein in B but was extended by Exon3 (dark green). The transfected cells were stained with an anti-CD19-PE (FMC63),

anti-Flag-tag-PE or with the anti-CD19-PE (3B10) investigating the binding to a linear epitope within the fusion protein. The cells were analysed by flow cytometry.

4.2.2 CD19 – detection of a linear epitope

The epitope of the anti-CD19 clone 3B10 antibody was only narrowed down in one publication so far⁸⁸. In this publication, the epitope was investigated by single mutations in the CD19 protein and the resulting changes in the binding of the antibody. Furthermore, it was shown that the binding was also accessible for the antibody, when the CD19 protein was denatured. The published epitope was reduced to this linear amino acid sequence: KLYVWAKDRPEIWEGEPP^{87,88}.

In the previous experiment, using a fusion protein expressed on the cell surface, I could not detect any binding of the antibody in the predicted area (4.2.1). To find out whether the binding was disturbed by the folding of the CD19 fusion protein, or whether the AAViTOP application reaches its limits with the CD19 protein, I created an overlapping peptide library with 19 peptides extending beyond the predicted epitope and an additional Flag-tag. These peptides were inserted into the capsid plasmid (pMT-187-XX2_R585S_R588T) and the generated plasmids were used for small-scale AAVLP production. All sequences were able to be displayed on the capsid surface.

The particles possessing the putative 3B10 epitope and the Flag-tag provided two different types of information in one readout by flow cytometry: in addition to the assessment of 3B10 binding, using the Flag-tag antibody it is possible to both check if particles containing the insert have been formed and to normalize quantitative differences between the lysates. For screening with the anti-CD19 (3B10) antibody, I used a double staining and stained the lysates simultaneously with anti-CD19 (3B10)-PE and anti-Flag-APC. As a negative control for both staining, I used crude lysates with particles without insertion (w/o). As positive control for the anti-Flag-tag staining I used crude lysates containing particles presenting only the Flag-tag sequence. These particles serve as an additional negative control for anti-CD19 (3B10) staining (Figure 4.2.2, A). The screening was performed several times with different crude lysate productions. Afterwards, I calculated the ratio of epitope-positive events per Flag-tag-positive events (E/F ratio) to achieve a result that is independent of fluctuations in the production of the particles and the associated change in positive events (Figure 4.2.2, B).

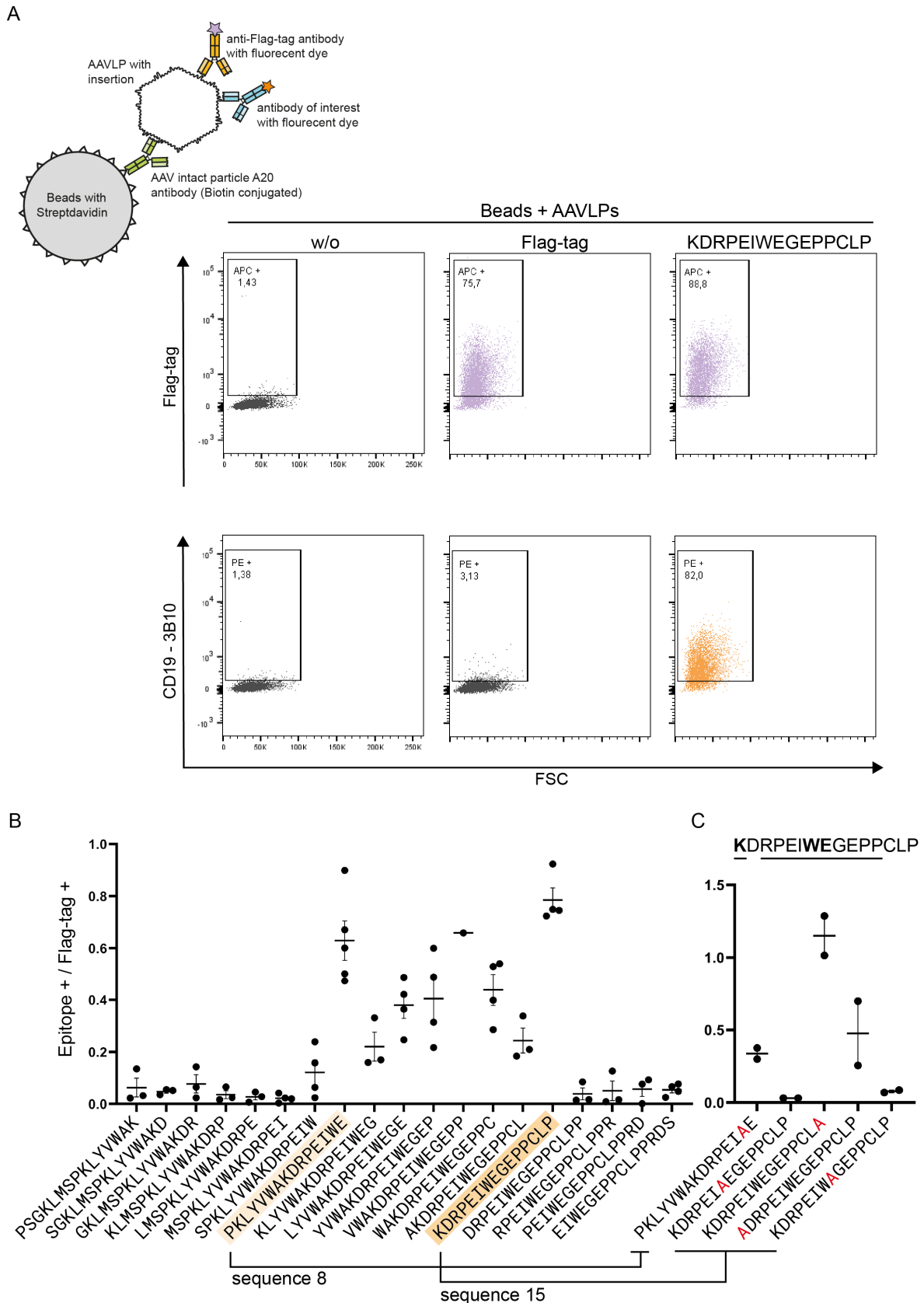


Figure 4.2.2: Using the AAViTOP procedure to verify a linear epitope within the CD19 protein. To determine the epitope of the anti-CD19 clone 3B10 antibody an overlapping peptide library of 19 sequences was generated including the published epitope KLYVWAKDRPEIWEGEPP. The CD19 sequences were extended with a C-terminally Flag-tag and inserted into the capsid plasmid via *Sfi*I restriction sites. **A:** Crude lysates containing the CD19 sequence-bearing AAVLPs were used for a

double-staining bead assay. In this, magnetic beads coupled with an A20-biotin antibody are used to bind the intact AAVLPs from the crude lysate, to screen them for insertion using a Flag-tag APC antibody (purple), and to screen for the epitope of the antibody using the anti-CD19 (3B10)-PE antibody (orange). AAVLPs without insertion (w/o) served as negative control (black) for anti-Flag-tag staining and AAVLPs with integrated Flag-tag served as positive control. Both AAVLPs served as negative controls for anti-CD19 staining. B: The ratio of epitope-positive events to Flag-tag-positive events (E/F ratio) were calculated after several measurements with different crude lysates (black dots). The axis shows the presented amino acid sequence on the capsid surface (without the Flag-tag). The mean value was calculated from the results and presented as a horizontal bar with the standard error of mean (SEM). Significant differences between the groups were determined using a One-way ANOVA with a Tukey's multiple comparison test. No group showed significant differences to all other groups. C: Sequence 8 and Sequence 15 from B were used for alanine replacements (red A's). AAVLPs with the modified sequences were tested for changed binding to the anti-CD19 (3B10) antibody by performing a double-staining bead assay. The E/F ratio were calculated, and the mean value is indicated by a horizontal bar with the standard error of mean (SEM).

The first six and the last three inserted sequences were not bound by the antibody (mean E/F ratio < 0.1). Only with the appearance of the tryptophan (W) in the seventh sequence (SPKLYVWAKDRPEIW) could I detect slightly increased values (mean E/F ratio = 0.121). A strong increase took place with sequence 8 (PKLYVWAKDRPEIWE) and the appearance of glutamic acid (E). This sequence also showed the second highest mean E/F ratio of 0.629. But the values of the individual measurements also showed greater variability. The following sequences first showed a strong decrease in E/F ratios, which then increase again to almost similar values as sequence 8 (particles with the sequence VWAKDRPEIWEGEPP were only tested once (N=1) due to technical limitations in the lab). From sequence 12 to 14, the epitope detection decreased again to a mean E/F ratio of 0.244. Sequence 15 (KDRPEIWEGEPPCLP) is characterised by the fact that a lysine (K) now forms the N-terminal end of the sequence, and a proline (P) forms the C-terminal end of the CD19 sequence before the Flag-tag sequence starts. The particles carrying this sequence yielded the highest E/F ratio of 0.785 (Figure 4.2.2, B).

Since I was able to detect binding of the anti-CD19 (3B10) antibody to the AAVLPs and this region also matches the previously published epitope, I wanted not only to determine the epitope but also to verify the amino acids considered critical for binding. To do this, I replaced individual amino acids in the CD19 sequence with an alanine. The newly generated insertions were inserted into the same capsid backbone plasmid and the crude lysates produced were tested for binding of the antibody using the bead assay (Figure 4.2.2, C). Three amino acids within the linear sequence were found to be essential, as mutation at these sites did not result in binding of the antibody. These include lysine (K), tryptophan (W) and glutamic acid (E) (Figure 4.2.2, C, bold)⁸⁸. Compared to the unchanged sequence, the E/F ratio decreased due to the replacement of lysine in sequence 15. By replacing the glutamic acid (E) or the tryptophan (W) in sequence 15, almost no epitope positive events could be recorded in two measurements. Interestingly, the replacement of the tryptophan by alanine in sequence 8 did not completely prevent the binding of the antibody but only strongly reduced it to a mean E/F ratio of 0.338. In addition to the completely mutation intolerant amino acids, other amino acids

were described as relatively mutation intolerant (Figure 4.2.2, C, underlined). This category includes proline (P) at the C-terminal end of sequence 15. Replacing this amino acid at this position with an alanine does not lead to any reduction in binding. Interestingly, the individual measurements lied above the measurement points of the original sequence.

In summary, I was able to identify the amino acid sequence between sequences 8 and 15 (PKLYVWAKDRPEIWEGEPPCLP) as a linear binding motif for clone 3B10 and I showed that shorter regions within this motif are sufficient to enable binding (i.e., sequence 8 and 15). In addition, I was able to verify important amino acids with the help of the alanine-modified particles.

4.2.3 Double insertions as an approach to identify a discontinuous epitope

A discontinuous epitope consists of sequences that are not present as a contiguous sequence but are recognised by the antibody through their three-dimensional arrangement. The current assumption is, that the anti-CD19 clone FMC63 epitope is shared partially with other anti-CD19 mAbs (i.e., 4G7 and B43). The binding of the B43 antibody to CD19 was investigated in more detail and it was found that three loops are involved in the interaction⁸⁵. Two of these loops have already been addressed in this study. The first loop (97 - 107) contains the epitope that was identified in my master thesis, which was attempted to be validated with the help of the fusion protein. The second loop (155 - 166) contains the linear epitope of the anti-CD19 clone 3B10 antibody. And then there is the third loop (199 - 205), whose sequence has not yet been used in this work. However, in the meanwhile, important amino acids were also defined in this loop for binding to the antibody FMC63 (Figure 4.2.3, A)⁸⁸. By their arrangement, these three loops may all be responsible for binding to different anti-CD19 antibodies. In a daring attempt, I decided to try to recreate this arrangement on the surface of the AAVLPs. First, I determined the distances between the CD19 loops involved in antibody binding and between the two highest peaks on the capsid surface with the help of the ribbon structures (Figure 4.2.3, A-B). Depending on the origin point of the measurement, the two AAV2 peaks are about 20 – 24 Å apart. This distance is similar to the distance between the first and third loop (20.81 Å) of CD19. Since my previous experiments indicated that both peaks tolerate insertions well, I decided to generate a capsid plasmid with two insertion sites, to represent at least two of the three loops. I performed site-directed mutagenesis (3.2.10) to insert the restriction sites for the enzymes MfeI and SpeI with the appropriate primers. As a template, I used the pMT-187-XX2-R585S-R588T plasmid, which already had the SfiI sites for insertion behind amino acid 588. After successful sequence modification, this plasmid (pMT-187-XX2-Pos453mut-R585S-R588T) can be used to insert a sequence of interest downstream of isoleucine at position 452 in addition to the insertion downstream of amino acid 588.

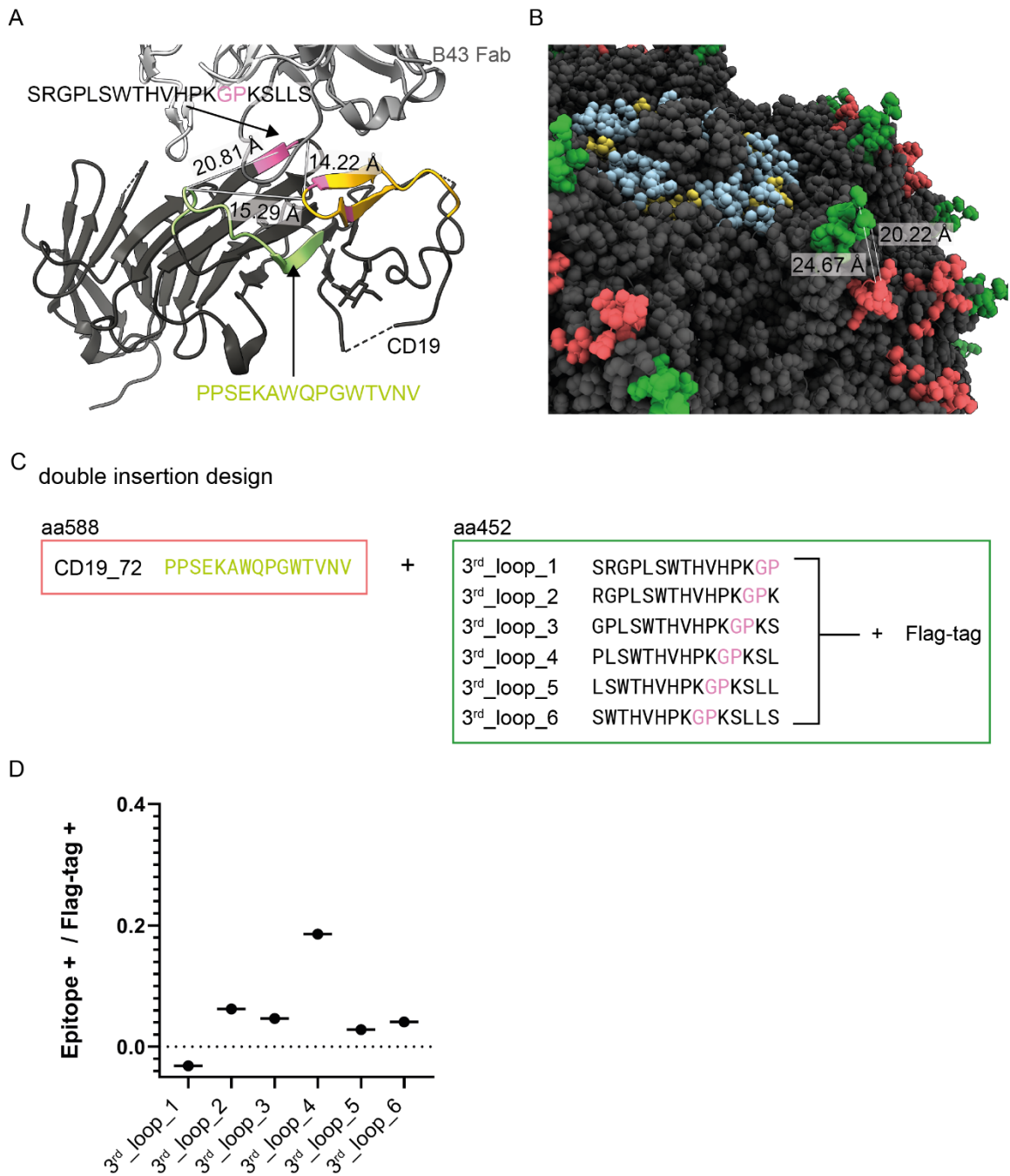


Figure 4.2.3: Recreating discontinuous epitopes on the AAVLP surface. A: Ribbon presentation of the complex of the CD19 extracellular domain and the anti-CD19 Fab B43. The linear epitope of the anti-CD19 antibody clone 3B10 is coloured in orange. The CD19₇₂ sequence is coloured in green with the respective sequence below. Amino acids later identified as important for binding the FMC63 antibody are marked in pink⁸⁸. The distances (Å) between the different regions are visualised by a connecting white line. B: Detail of the capsid surface. The distances between the insertion sites after amino acid 588 (red) and behind amino acid 452 (green) are visualised by a white line. Figure modified from PDB entries 6a15 and 1lp3 using ChimeraX²³. C: schematic overview of the double insertion design. Sequence CD19₇₂ was inserted behind aa588 (red) and six different 3rd_loop fragments were inserted with an additional Flag-tag after aa452 (green). D: A bead assay was performed with the AAVLPs. The E/F ratio (epitope-positive events per Flag-tag-positive events) were calculated after one measurement (black dots). The axis shows the name of the presented amino acid sequence on the capsid surface (without Flag-tag).

I created a small overlapping peptide library with the sequence of the third loop. Six Sequence fragments (3rd_loop_1 – 3rd_loop_6) were designed with the additional Flag-tag for the insertion in the highest peak (aa 452) on the capsid surface. The sequence of the first loop was limited to the sequence CD19_72 from the initial CD19 screening Flag-tag and inserted into the second highest peak (aa 588). The individual AAVLPs therefore only differ within the one peak. After the successful small-scale production of the particles in 6-well format, I checked the crude lysates for the presence of the Flag-tag and for the binding of the CD19 FMC63 antibody using the bead assay, as I had done previously with the linear epitope of 3B10. I used the same positive and negative controls. The initial and only measurement so far showed an increased E/F value (0.186) for the particles with the 3rd_loop_4 insertion. This value is relatively high compared to all other samples, however, due to as yet missing repetitions, the binding must be validated.

4.3 Claudin-6 (CLDN-6) a new target for AAViTOP screening

Identification of the epitope of anti-CD19 (FMC63) using AAVLPs for epitope mapping proved to be difficult, due to the impact of specific sequences on the assembly of the capsids and of the discontinuous nature of the epitope. However, the successful verification of the linear epitope of the anti-CD19 (3B10) antibody showed that the AAViTOP screening method was superior in detecting antibody binding compared to an attempt with a cell-surface expressed fusion protein. However, there is no chimeric antigen receptor (CAR) with the binding properties of the 3B10 clone, so I was not able to demonstrate the inhibitory function of the identified particles in this example. For this reason, a new antibody with corresponding CAR had to be searched and targeted in order to broaden the patent application and reach one of my thesis aims.

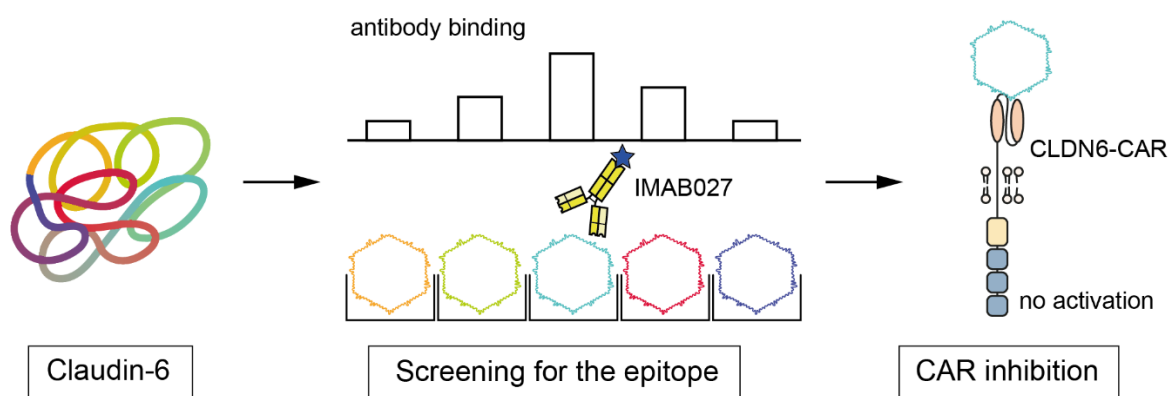


Figure 4.3.1: Claudin-6 as a new target for the epitope screening and application beyond the AAViTOP procedure. The extracellular domains of CLDN6 protein are presented as a peptide library on individual AAVLPs. These are then screened for the epitope of the antibody IMAB027. Since the binding properties of the antibody match those of an anti-CLDN6 CAR, the identified particles can be used to inhibit CAR function.

Claudin-6 (CLDN6) was selected as a new target protein for further epitope screening. Claudin-6, like the other members of the claudin family, belongs to the tight-junction membrane proteins and is mainly expressed in embryonic tissue and is not found in healthy adult tissues^{89,90}. However, high CLDN6 transcript levels have been found in several solid cancers (testicular, ovarian, uterine and lung adenocarcinoma)⁹¹⁻⁹³. Therefore, CLDN6 will now be the target of a CAR, which is already being tested in a clinical trial (NCT04503278).

For the following experiments, a CAR construct was cloned based on the CAR published by Reinhard et al., 2020⁹¹. As described, the CLDN6-specific single chain variable fragment (scFv) of the CAR was taken from IMAB206-C46S (WO2012156018). This sequence was ordered in a pEX-A128 plasmid. Using the existing restriction sites NcoI and NotI, the scFv sequence could be inserted into a plasmid that already existing in our group contains the required domains for a CAR flanked by attL1 and attL2 sites. In contrast to Reinhard et al., 2020⁹¹, I used the CAR composition that is routinely used in our laboratory: the scFv was inserted in front of a human Fc spacer, followed by the transmembrane region of CD28 and the intracellular CD3 ζ endodomain. OX40 is used as co-stimulatory domain. Using an LR cloning reaction, the CAR construct could be inserted into a lentiviral transfer vector resulting in the plasmid pRRL-cPPT-hPGK-Lk-CLDN6scFv-hFc-hCD28tm-hCD3z-hOX40-IRES-puro-WPRE, which could then be used for production of lentiviral particles. For the epitope screening, the antibody IMAB027 (WO2015014870) was used, because the sequence of the heavy chain, according to the patent, matches that of IMAB206 and should have the same binding properties⁹⁴.

4.3.1 Generating AAVLPs displaying CLDN6 sequence fragments

Claudin-6 has two extracellular domains EC1 (aa 27-81) and EC2 (aa 137-161) both of which may contain possible binding sites for antibodies⁹⁵. Therefore, I created an overlapping peptide library of these two domains. This library contains 48 sequence fragments. The sequences were reverse-translated and inserted into the pMT-187-XX2-R585S-R588T plasmid. For the scFv of the CAR, which I used, potentially important amino acids for binding were determined by high-resolution epitope mapping in the associated patent and are also published. These amino acids include a phenylalanine (F35), a glycine (G37), a serine (S39) and possibly the threonine at position 33 (T33)⁹⁴. For this reason, I focused on the first sequences of the first extracellular domain (sequence 1-8) at the start. After the first small-scale productions of AAVLPs with the corresponding sequences, I could see that it was not possible to obtain assembled capsids with every insertion similar to some sequence fragments of CD19 exon 2. Three sequences out of eight were not producing intact particles. Sequence CLDN6_1, CLDN6_2 and CLDN6_5. The sequence CLDN6_6 showed lower numbers of intact particles than the other producing sequences (data not shown). However, with the knowledge I obtained

during the work with CD19, I was able to try two different strategies to overcome this assembly issue. First, I attempted to assemble chimeric particles and decrease the number of insertions by mixing the capsid backbone with the insertion with the HSPGKO plasmid in a ratio of 1:2 during the transfection. For this experiment, I used only the first four sequences of the CLDN6 library (CLDN6_1_FL – CLDN6_4_FL). I then calculated the approximate number of intact particles in the lysates using the measured absorbances of the A20 sandwich ELISA and a linear regression (3.4.1). All samples showed particle amounts above 1×10^6 AAVLPs per μL (Figure 4.3.2, A). The samples CLDN6_1_FL (1.08×10^6) and CLDN6_2_FL (1.27×10^6) showed the lowest titres. However, the A20 ELISA alone does not provide information on whether subunits carrying the insertion have been incorporated into the capsid. Therefore, I performed another A20 Flag-tag ELISA (3.4.2) with the same lysates. With this ELISA, no quantification takes place afterwards, but one can assess the differences based on the measured absorbance of the controls. Here, the HSPGKO particles served as a negative control (0.049), since no Flag-tag is contained, and the particles with only the Flag-tag insertion served as a positive control (0.351). The particles with the insertion CLDN6_3FL (0.375) and CLDN6_4FL (0.49) showed absorbances similar to the positive control or even higher. For the particles with the insertions CLDN6_1_FL (0.087) and CLDN6_2_FL (0.096), only values slightly above the negative control were obtained (Figure 4.3.2., A).

Since I could hardly detect Flag-tag, which is directly linked to the insertion, I had to assume that the capsids formed consist mainly of the wild-type-like sequence of the HSPGKO plasmid. For this reason, I ruled out further work with the chimeric particles and tried to make the inserted sequence more compatible by an alanine exchange and thus enable the assembly of the capsids. In the attempt to present CD19 exon 2 within the capsid structure, I was able to show with the help of the alanine scan that the aromatic amino acids present a challenge in the assembly of the capsids from the free subunits (4.1.3). For this reason, I replaced one aromatic amino acid in the sequence of CLDN6 with alanine. In this case, I decided to exchange tryptophan (W), which is at the N-terminal end of the sequence CLDN6_1 and CLDN6_2 and does not appear in the well-producing sequences CDLN6_3 and CLDN6_4. Another tryptophan then appears in CLDN6_5 at the C-terminal end of the sequence, which I have also replaced by an alanine. Since sequence CLDN6_6 has the lowest titre, I also replaced the tryptophan in this sequence (Figure 4.3.2, B). The modified sequences were ordered as DNA single-strands with the C-terminal Flag-tag extension and integrated into the capsid backbone as before. After transfection, crude lysates were checked for the presence of intact particles using the A20 sandwich ELISA (3.4.1).

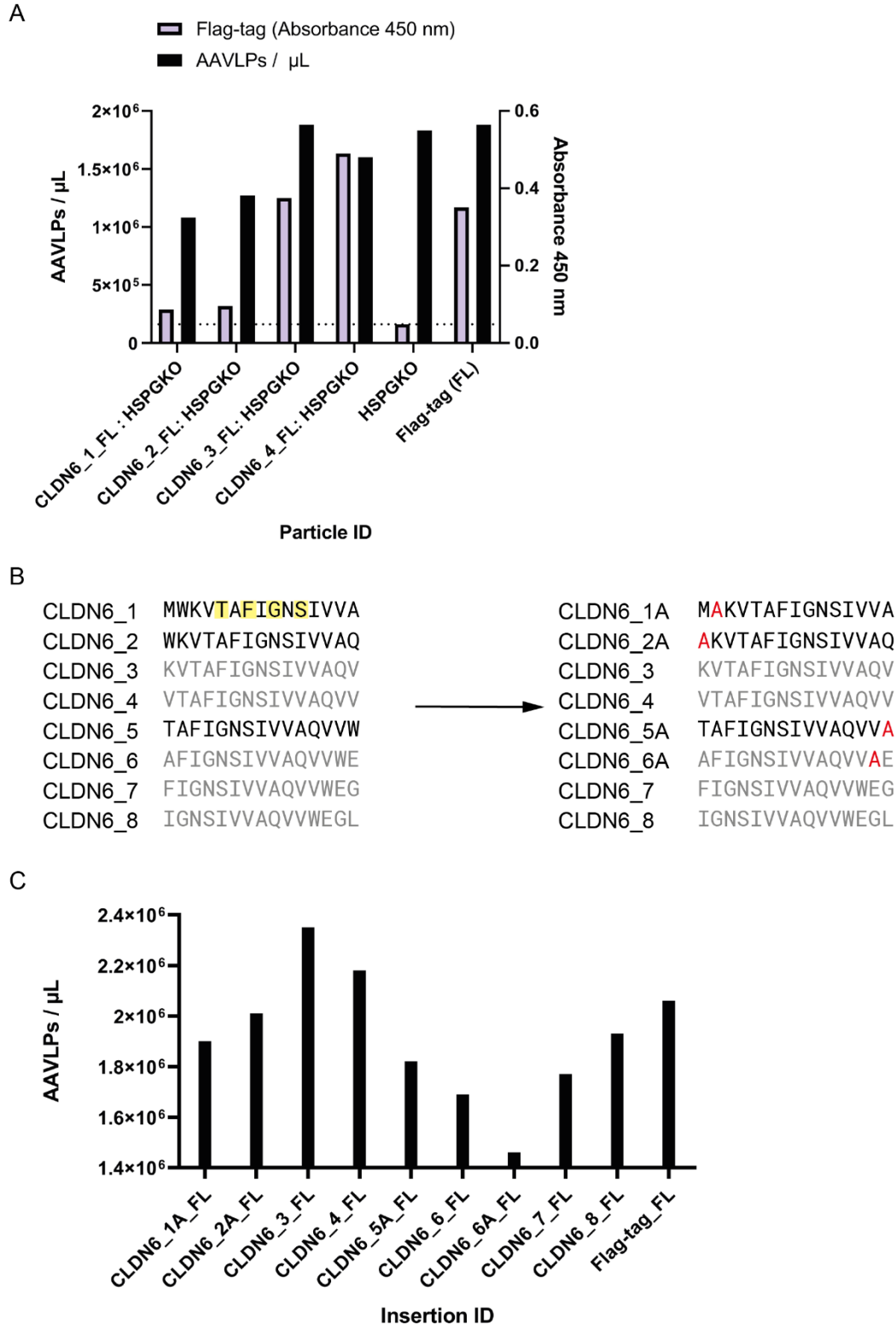


Figure 4.3.2: Generation of assembled AAVLPs with CLDN6 sequence insertion. A: Generation of AAVLPs with reduced insertions. By the additional addition of the HSPGKO plasmid during transfection in a ratio of 1:2, chimeric particles can be formed. The particles are quantified using the A20 sandwich ELISA (black bars) in AAVLP capsids per μL . The presence of Flag-tag on the capsid surface was checked using an A20 Flag-tag ELISA (purple bars) with the help of the measured absorbance at 450 nm. **B: The first eight sequences of the overlapping peptide library of the extracellular domains of the CLDN6 protein (left) with published amino acids relevant for IMAB027 antibody binding highlighted in yellow.** Sequences that do not lead to intact Particles are written in black. Sequences that do not affect the assembly of AAVLPs are written in grey. Sequences in which a tryptophan has been replaced

are indicated with an A at the end of their ID. The replaced alanine is marked in red in the sequence. C: Quantification of AAVLPs of a production following an A20 sandwich ELISA. The number of intact particles is marked by black bars.

All sequences resulted in intact particles. In this particular production the particles with the modified sequences CLDN6_1A_FL (1.9×10^6), CLDN6_2A_FL (2.01×10^6) and CLDN6_5A_FL (1.82×10^6) showed higher particle numbers than the unmodified sequences CLDN6_6_FL (1.69×10^6) and CLDN6_7_FL (1.77×10^6). The alanine exchange in sequence CLDN6_6A did not increase the particle titer in this production (Figure 4.3.2, C). Since the binding-relevant amino acids are published, it can be assumed that the exchange of the tryptophan does not influence the binding to the antibody used in the screening. Therefore, I worked with the modified sequences for the screening procedure.

4.3.2 Screening for the IMAB027 epitope

The epitope screening for the anti-CLDN6 CAR was performed with the IMAB027 antibody. Before I started the screening of the AAVLP containing crude lysates, I performed a functional test of the antibody with different cell lines. I tested five different tumour cell lines for CLDN6 expression: HEK293T, HepG2, NIH-OvCar3, HT29 and Panc02. The IMAB027 antibody was provided as an unconjugated antibody. To reduce incubation steps during the bead assay I conjugated the antibody with the help of the PE / R-Phycoerythrin Conjugation Kit – Lightning-Link®. Therefore, the testing of the cell lines served on the one hand to test the conjugated complex and on the other hand to identify CLDN6 positive target cells for later experiments. Two cell lines showed clear CLDN6 expression unstained cells served as negative controls. 92.9 % of the living HepG2 cells showed CLDN6 expression on the surface. The NIH-OvCar3 cells showed less CLDN6 expression with 48.5 % positive events. The other cell lines showed only very low or no CLDN6 expression on the cell surface with a maximum of 15.6 % positive events (HEK293T) (Figure 4.3.3, A). These results were consistent with the previously identified expression pattern of CLDN6 in tumours, so it could be assumed that the antibody successfully bound to CLDN6^{91,96}. Thus, the cell lines HepG2 and NIH-OvCar3 are going to be used in following killing assays as target cells for the anti-CLDN6 CAR.

After testing the antibody, I performed the first bead assays with the CLDN6 sequence carrying AAVLPs. At the beginning of these first measurements, only the unmodified particles were available for the bead assay. The capsids with the alanine exchange were not produced yet. The first binding assays showed most positive events for the AAVLPs with the insertions CLDN6_3FL and CLDN6_4FL. Overall, the measured values for these two insertions show high deviations. CLDN6_3 reaches a mean E/F ratio of 0.240 (SEM = 0.139) and CLDN6_4 reaches a mean E/F ratio of 0.294 (SEM = 0.150) (Figure 4.3.3, C). After I was able to test the capsids with the alanine exchange for the binding of the antibody using the bead assay, the

AAVLPs with the CLDN6_5AFL showed the highest mean E/F ratio with a mean value of 0.292 (SEM = 0.051) and less variation between separate experiments (Figure 4.3.3, B).

Due to the fact that I obtained the hits with CLDN6_3 and CLDN6_4 prior to knowing that CLDN6_5A was even superior, I performed the following functional experiments with the particles CLDN6_3 and CLDN6_4.

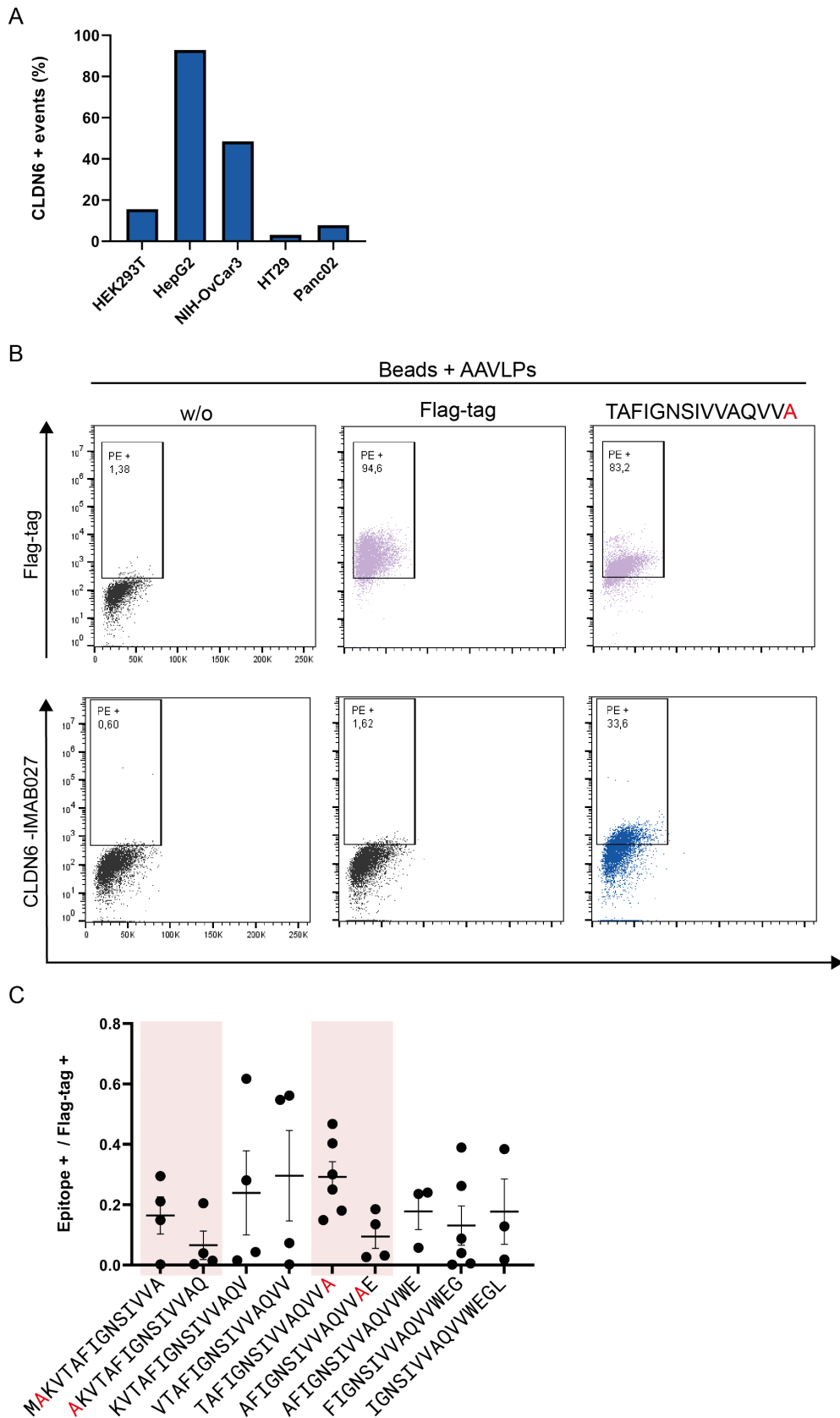


Figure 4.3.3: Using the IMAB027 antibody to screen for the epitope of a anti-CLDN6 CAR. A: Verification of the specificity of the IMAB02-PE antibody. After labelling the unconjugated antibody with PE. Different cell lines (HEK293T, HepG2, NIH-OvCar3, HT29 and Panc02) were stained and analysed by flow cytometry for CLDN6 surface expression. B: Crude lysates containing the CLDN6 sequence-bearing AAVLPs were used for two separate bead assays, to screen them for insertion using a Flag-tag PE antibody (purple), and to screen for the epitope of the antibody using the IMAB027-PE antibody

(blue). AAVLPs without insertion (w/o) served as negative control (black) for anti-Flag-tag staining and AAVLPs with integrated Flag-tag served as positive control. Both AAVLPs served as negative controls for anti-CLDN6 staining. C: The E/F ratio of epitope-positive events to Flag-tag-positive events were calculated after several measurements with different crude lysates (black dots). The axis shows the presented amino acid sequence on the capsid surface (without the Flag-tag). The mean value was calculated from the results and presented as a horizontal bar with the standard error of mean (SEM). Significant differences between the groups were determined using a One-way ANOVA with a Tukey's multiple comparison test. No group showed significant differences to all other groups. The results with red background show the results using the modified sequences.

4.3.3 Downregulation of the anti-CLDN6 CAR Expression

The screening procedure with AAVLPs should not only identify the epitope of IMAB027 and verify crucial amino acids for antibody binding but also identify particles that are able to interfere with the appropriate chimeric antigen receptor (CAR). This specific kind of interference, resulting in a temporary internalisation of the receptor was as yet only described for the NYBR1 clone 2 CAR (WO2019043081 A1). When the first particles with integrated CLDN6 sequence could be screened for the epitope, especially CLDN6_3FL and CLDN6_4FL showed the most epitope positive events (Figure 4.3.3). Therefore, I decided to produce these two AVVs (now described as AAV CLDN6_3 and AAV CLDN6_4) in large format and to purify them by iodixanol gradients (3.3.3). PEG participation, concentration and re-buffering did not take place at that time.

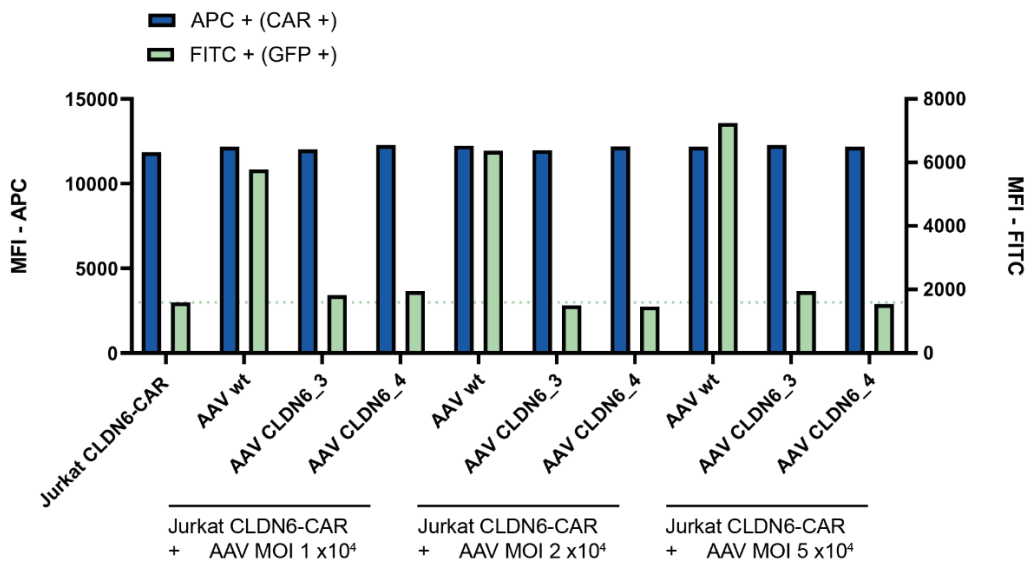


Figure 4.3.4: Low MOI does not lead to down-regulation of CAR expression and CLDN6 presenting AAVLPs do not enter the cells. CLDN6-CAR+ Jurkat cells were co-cultivated with AAV wt, AAV CLDN6_3 or AAV CLDN6_4 to determine the multiplicity of infection needed to decrease CAR surface expression (CAR +). Three different MOIs were tested: 1×10^4 , 2×10^4 and 5×10^4 . 24 h post transduction the cells were analysed by flow cytometry. The CAR expression was determined by an anti-hIgG-APC staining shown here as the mean fluorescence intensity (MFI) (blue bars, left y-axis)). The GFP signal, which is induced by the expression of the transgene contained in the AAVLPs, was detected via FITC and plotted as MFI in the graph (green bars, right y-axis). The level of the FITC background signal is shown as a green line.

I also established a stable CLDN6-CAR-positive Jurkat cell line (Jurkat CLDN6-CAR). To generate this cell line, first HEK293T cells were transfected with the previously cloned lentiviral transfer vector, that contains the CLDN6 CAR construct pRRL-cPPT-hPGK-Lk-CLDN6scFv-hFc-hCD28tm-hCD3z-hOX40-IRES-puro-WPRE to produce lentiviral particles (performed by Alexandra Tuch) (3.1.4). I then used these lentiviral particles to transduce Jurkat wildtype cells to achieve sustained CAR expression (3.1.5).

With the help of the first experiment, I tried to find out which of multiplicity of infection (MOI) would be needed to detect a reduction in CAR surface expression. As a benchmark, I used 5×10^4 per cell, as this amount of epitope carrying AAVLPs had led to a significant downregulation in the NYBR1 CAR clone 2 (WO2019043081 A1). For this reason, I co-cultured the Jurkat CLDN6-CAR cells with three different MOIs (1×10^4 , 2×10^4 , 5×10^4 per cell) of CLDN6 AAVLPs. I did not only use the CLDN6-bearing AAVLPs, but also wildtype AAVLPs (AAV wt) to exclude non-specific effects. After 24 h incubation, I was able to examine the cells via flow cytometry for CAR expression (anti-IgG-APC) and for AAVLP-mediated transgene expression (GFP) as an indicator of successful transduction. Compared to the untreated control, neither a specific MOI nor a specific AAVLP construct shows any effect on CAR expression, as can be seen from the consistent APC mean fluorescence intensity (MFI) around 12000. Compared to the modified AAVLPs, the Jurkat CLDN6-CAR cells co-cultured with AAV wt show a GFP signal after 24h. The FITC MFI also increases with higher AAV wt MOI (Figure 4.3.3). The experiment has shown that the expression of this CAR cannot be downregulated with the amounts of AAVLPs tested here. For this reason, higher MOIs were used in the next experiments. Furthermore, I have shown that after 24 h there is no significant AAVLP-mediated GFP expression from CLDN6-insertion variants taking place, therefore staining with a PE-labelled antibody is possible without overlapping with a GFP signal of the cells.

In the course of the experiment, I decided to observe the expression of the CLDN6 CAR not only on the surface of the generated Jurkat cell line, but also on primary T cells. For this purpose, T cells from a blood donation were isolated (performed by Alexandra Tuch) (3.1.2) and lentivirally transduced (3.1.5). The CAR positive primary T cells of donor RNK97 and the Jurkat CLDN6-CAR cell line were co-cultured for 24 h with a mix of AAV CLDN6_3 and AAV CLDN6_4 (ratio 1:1) at a MOI of 1×10^6 particles per cell. This represents a twenty-fold increase compared to the first experiment. After 24 h incubation, cells were stained with anti-IgG to investigate CAR expression by flow cytometry. Non-transduced cells (mock) or unstained cells (unstained) served as negative controls. CAR expression was compared with untreated CAR positive cells of the same type. After FACS analysis, several differences were observed. As in the previous experiment, the Jurkat CLDN6-CAR cell line showed no change in CAR expression after co-cultivation with the AAVLPs (MFI-APC: 4676 vs. 4649) (Figure 4.3.4, B). However, the MFI values obtained in the measurements of the cell line samples were

four times higher than those of the primary cells (MFI-APC =1044) (Figure 4.3.4, A). This indicates an overall lower CAR expression in the primary T cells. In addition, a slight reduction in CAR expression (MFI-APC = 973) could be seen compared to the untreated RNK97 sample.

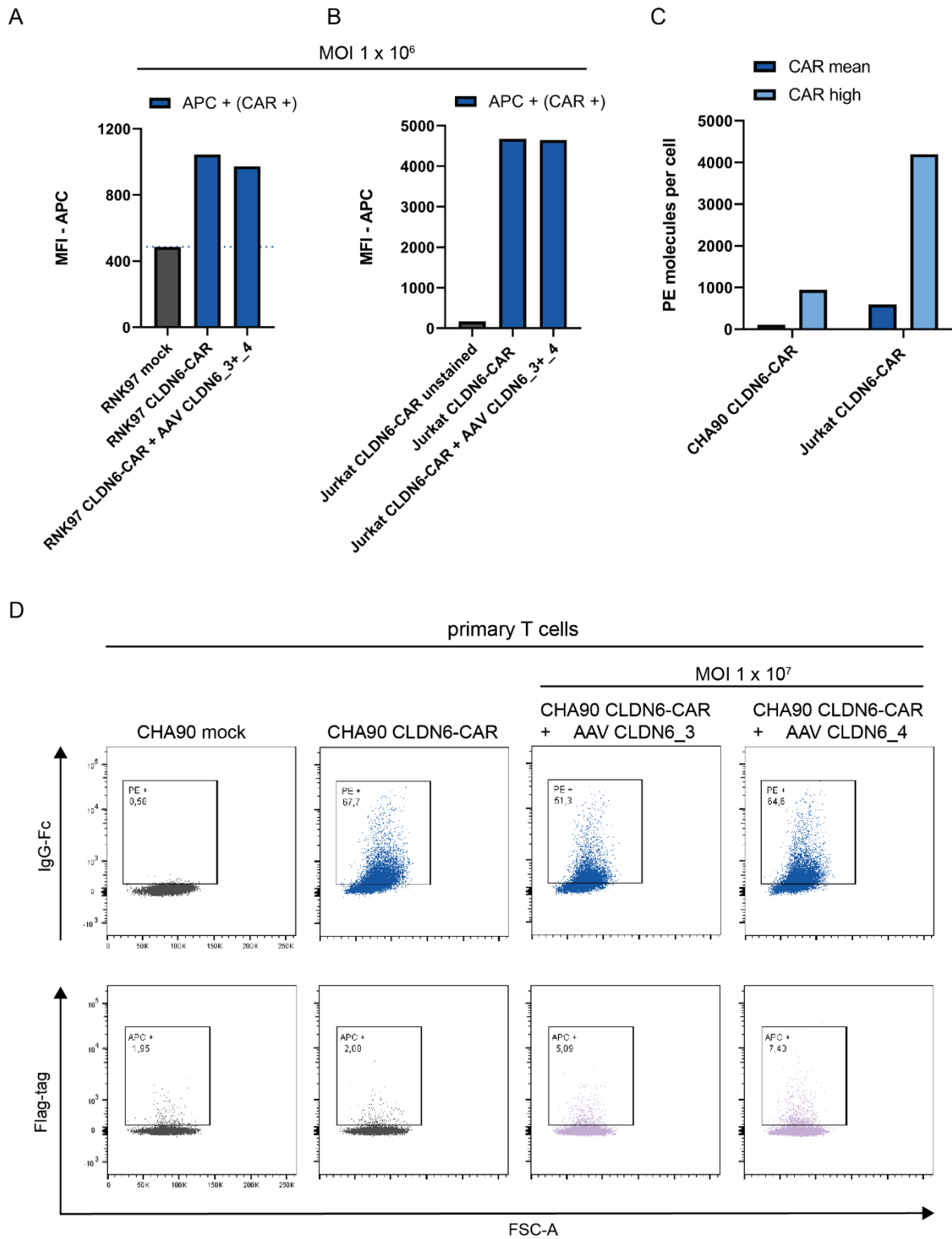


Figure 4.3.5: At an MOI of 1×10^6 particles and above, a reduction in CLDN6 CAR expression on primary T cells can be observed. A: lentivirally transduced CAR positive primary T cells (RNK97) were co-cultured for 24 hours with a mix of AAV CLDN6_3 and AAV CLDN6_4 particles (MOI 1×10^6). Subsequently, the cells were analysed for CAR expression (anti-IgG-APC) via flow cytometry. Untransduced cells (mock) were used as negative control for the staining (black bar). The mean of

fluorescence intensity was calculated and is shown as bars. B: A stable CAR expressing Jurkat cell line (Jurkat CLDN6-CAR) was also co-cultured with the same amount of AAVLPs and examined in the same way. Unstained cells were used as negative control for the staining. C: lentivirally CAR positive primary T cells (CHA90) and the cell line Jurkat CLDN6-CAR were stained with an anti-hlgG-PE to quantify the amount of CAR molecules on the cell surface with the help of the BD Quantibrite™ Beads. On the one hand, the mean value of the entire CAR positive cell population was determined (CAR mean, blue) and, on the other hand, the mean value of PE molecules on the cells with very high expression (CAR high, light blue). The calculation is based on an assumed antibody to PE molecule ratio of 1:1. D: lentivirally transduced CAR positive T cells (CHA90) were co-cultured for 24 h with purified AAV CLDN6_3 or AAV CLDN6_4 (MOI 1×10^7). Post incubation, the cells were stained with anti-Flag-tag-APC for AAVLP detection (lower row, purple) and with anti-hlgG-PE for CAR detection (upper row, blue). Untransduced T cells were used as negative control for the staining.

To understand why there are these distinct differences between the Jurkat CLDN6-CAR cell line and the primary T cells, I performed a quantification of PE molecules per cell. For this purpose, T cells were isolated from a blood donation (CHA90) and transduced lentivirally so that CLDN6 CAR expression takes place. These cells and the Jurkat CLDN6-CAR cells were stained with an anti-hlgG-PE antibody to detect the CAR via flow cytometry. The measured geometric mean of the population was used and converted to PE molecules per cell using BD Quantibrite™ beads and linear regression. It is assumed that the ratio of PE to antibody is 1:1. I calculated the average number of PE molecules per cell of the entire CAR positive population (CAR mean). I have also calculated the number of PE molecules per cell for the part of the population with very high expression (CAR high). The average CAR positive CHA90 T cell carries 106.18 PE molecules, assuming that each antibody detects a CAR, that is 106.18 CAR constructs. In comparison, an average cell of the Jurkat CLDN6-CAR cell line carries 594.31 CAR constructs on its cell surface. When considering the cells that show a high expression, the primary cells come to 943.17 CARs per cell and the cell line to 4198.28 CARs. As seen from the much higher MFI values, it can be assumed that this cell line has more than four times as many CARs per cell as the primary T cells.

To exclude the possibility that the CARs are no longer accessible in these experiments due to AAVLP binding, but are internalised, I repeated the co-cultivation of CAR positive primary T cells (CHA90) and AAVLPs with an MOI of 1×10^7 . AAV CLDN6_3 and AAV CLDN6_4 were tested separately. After incubation, cells were analysed for CAR expression (Figure 4.3.5, D, upper panel) with anti-hlgG-PE and for bound AAVLPs on the cell surface with anti-Flag-tag APC (Figure 4.3.4, D, lower panel). This staining is possible in this case because the AAVLPs do not successfully express their GFP transgene. After cocultivation with the AAV CLDN6_3 particles, a reduction in CAR detection of 24.2% was observed compared to the untreated control. The CAR expression after cocultivation with AAV CLDN6_4 particles decreased by only 4.6%. Interestingly, an increased Flag-tag detection was observed in both cases. In the cells with AAV CLDN6_4 (7.43%) even more than in the cells with AAV CLDN6_3 (5.09%). Taken together, these data show that the downregulation of CAR expression for this specific CLDN6 CAR is evident from an MOI of 10^6 and increases with the addition of significantly more

particles. The AAV CLDN6_3 and AAV CLDN6_4 particles both mediate a reduction in CAR expression to different degrees. At the same time, the binding, which was already shown in the bead assay, could be demonstrated again, as small amounts of the particles were detectable on the cell surface with the help of the Flag-tag.

4.3.3.1 Binding and internalisation of the CAR are a matter of temperature

In the previous experiment (4.3.3), I was able to show that there is a slight decrease in CAR expression when the specific AAVLPs are added to the primary CAR positive T cells. To a small extent, I was also able to detect bound particles by their Flag-tag. In another approach, I wanted to demonstrate this bound state again. For this reason, I again performed a cocultivation of the Jurkat-CLDN6-CAR cell line with the AAV CLDN6_3 particles. For 4 hours the cells were incubated either at 4 °C or at 37 °C. At 37 °C the metabolism of a cell functions rapidly and processes such as degradation and internalisation can take place. At a temperature of 4 °C, these processes no longer take place or are greatly slowed down⁹⁷. As a control, I also performed this experiment with an anti-NYBR1 CAR-positive cell line (Jurkat NYBR1-CAR) and the corresponding epitope-bearing AAV particles (AAV NYBR1). Like the CLDN6 AAVLPs, these particles carry a Flag-tag downstream of the epitope. For this experiment, AAVLP particles were again produced in large scale and purified, in order to lose less particles in the cell culture medium supernatant, a PEG precipitation was also performed (performed by Master student Katharina von Werthern) (3.3.3). As a further control to exclude non-specific binding, I used AAVLPs that only present the Flag-tag in their capsid, as these would also be detectable with the Flag-tag antibody and were already available in the lab. After the incubation I analysed the cells by flow cytometry for binding AAVLPs (anti-Flag-tag-APC) and for the CAR expression (anti-hlgG-PE).

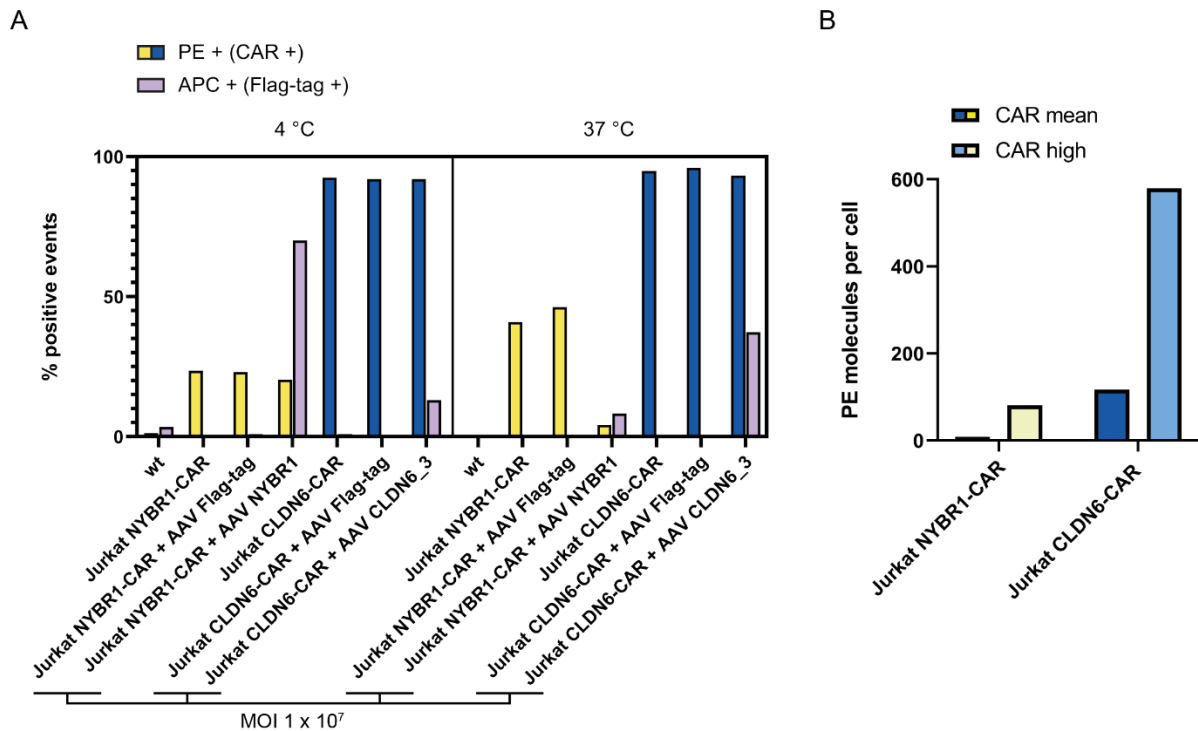


Figure 4.3.6: Internalisation can be prevented by co-incubation at 4 °C. A: The two different CAR expressing cell lines Jurkat NYBR1-CAR and Jurkat CLDN6-CAR were co-incubated with AAVLPs (AAV Flag-tag/ AAV NYBR1/ AAV CLDN6_3) at 4 °C and at 37 °C. After 3 h incubation time the CAR expression was observed by staining with an anti-hlgG-PE antibody (yellow = NYBR1 CAR, blue = CLDN6 CAR) and the presence of any AAVLPs (purple) was observed by staining with anti-Flag-tag-APC antibody. Jurkat wt cells were used as negative staining control. The samples were analysed by flow cytometry. B: the cell line Jurkat NYBR1-CAR (yellow bars) and the cell line Jurkat CLDN6-CAR (blue bars) were stained with an anti-hlgG-PE to quantify the amount of CAR molecules on the cell surface with the help of the BD Quantibrite™ Beads. On the one hand, the mean value of the entire CAR positive cell population was determined (CAR mean, dark blue/ yellow) and, on the other hand, the mean value of PE molecules on the cells with very high CAR expression (CAR high, light blue/ yellow). The calculation is based on an assumed antibody to PE molecule ratio of 1:1.

The first conspicuity that is noticeable is the different CAR expression of the two different cell lines Jurkat NYBR1-CAR and Jurkat CLDN6-CAR. At 4 °C, 23.5% PE positive events were measured in the untreated Jurkat NYBR1-CAR cells. Since I determined CAR expression of the cell line before the experiment, four times more Jurkat NYBR1-CAR cells were used in this experiment in order to obtain similar numbers of CAR-positive cells in both sets of experiments. In the untreated Jurkat CLDN6-CAR cells, I was able to detect 92.5 % PE positive events. The addition of Flag-tag bearing particles had no effect on any cell line: neither at 4 °C nor at 37 °C a change in CAR expression was detected, nor was binding to the receptors shown. Addition of AAV NYBR1 to Jurkat NYBR1-CAR cells decreases CAR expression only very slightly (23.5% to 20.3%) when incubated at 4 °C. But it is possible to detect AAVLPs on the surface of the cells: 70% APC-positive events were measured. At 37°C, a different picture can be seen with the same components. CAR expression is only detectable with 4.19% PE-positive events in the presence of AAV NYBR1 and the presence of AAVLPs on the cell surface also

decreases significantly to 8.26% residual APC signal. When Jurkat CLDN6-CAR cells are co-cultured with the AAV CLDN6 AAVLPs at 4 °C, CAR expression does not change (92%). And, as with the NYBR1 components, binding of the particles on the surface was observed, but to a lower degree (13%). After the incubation at 37 °C the CAR expression of the co-cultured Jurkat CLDN6-CAR cells was with 93.2% PE-positive events slightly reduced to the untreated control (94.9%) and unexpectedly more Flag-tag positive events (37.3%) were measured compared to the 4 °C incubation sample (Figure 4.3.6, A).

As in the previous experiments with the Jurkat CLDN6-CAR cell line, there is no clear reduction in CAR expression on the surface. But the binding of the particles to the CAR could be demonstrated again. As described before, I again used the BD Quantibrite™ Quantification beads to calculate the amount of PE molecules per cell with the help of the geometric mean of the CAR positive cell population. As with the primary T cells, there is a big difference in the amount of expressed CARs on the cell surface between the Jurkat NYBR1-CAR cell line (CAR mean = 8.74 PE molecules per cell) and the Jurkat CLDN6-CAR cell line (CAR mean = 116,5 PE molecules per cell). This difference was even higher when I observed the high expressing CAR positive cells (Figure 4.3.6, B).

4.3.4 AAVLP-mediated internalization of the CAR without T cell activation

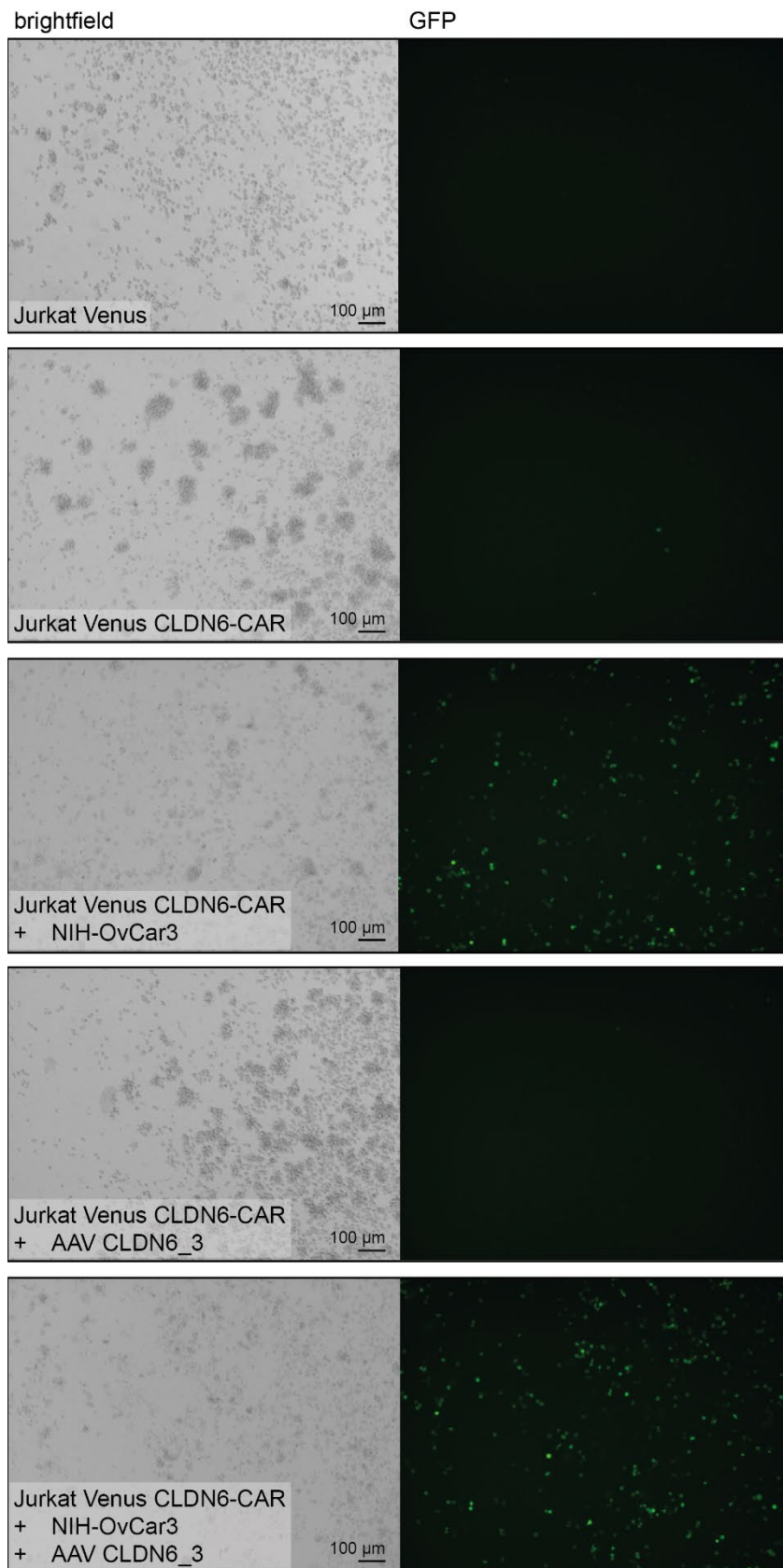
In the previous experiments, I successfully demonstrated binding to the anti-CLDN6 CAR using the AAVLPs AAV CLDN6_3 and AAV CLDN6_4, and the reduction in CAR expression was also seen, especially in primary T cells. In order to use these AAVLPs as CAR antagonists, the binding of the CAR to the epitope on the viral particle should not be followed by activation of the T cells. To find out whether the binding of the epitope leads to an activation of the cells, I used a reporter cell line (Jurkat Venus) that was generated in our laboratory. This cell line is based on a single clone and contains a reporter construct consisting of 12 NFAT binding sites upstream of an IL-2 minimal promoter that drives the expression of Venus. NFAT is a key transcription factor in CAR T cell activation⁹⁸. Venus is a variant of the green fluorescent protein GFP⁹⁹. To make the cell line usable for my purposes, I stably transduced the Jurkat Venus cell line using the previously used lentiviral particles. The resulting CAR positive cell line will be referred to as Jurkat Venus CLDN6-CAR. To test whether the generated cell line is activated by the presence and binding of the purified AAVLPs, the cells were cultured together with the AAVLPs (MOI 5 x 10⁶) for 24 hours. Because AAV CLDN6_3 showed the greater effect in reducing CAR expression in primary T cells, I used only AAV CLDN6_3 particles here. As a control, the cells were also cultured with the CLDN6 positive cell line NIH-OvCar3⁹¹. In addition, it was tested whether the AAVLPs could compete for the CAR-binding with the tumour cell line in this quantity. The expression of the Venus reporter gene could be determined by

fluorescence microscopy (GFP) (Figure 4.3.7, A) and flow cytometry (Figure 4.3.7, B), where CAR expression could also be investigated by anti-hlgG-APC staining.

The Jurkat Venus CLDN6-CAR cell line shows low perceptible Venus expression without stimulation. This is at an MFI-FITC value of 8030. The CAR expression leads to an MFI-APC value of 1674. Visible were isolated fluorescent cells. When the CAR positive cells are cultured with CLDN6-positive cells, Venus expression was clearly visible in the microscope and was confirmed by FACS analysis with an MFI-FITC of 35916. CAR expression was slightly decreased (MFI-APC =1414). After culturing the Jurkat Venus CLDN6-CAR cells with AAV CLDN6_3 particles, the Venus expression was visible just in isolated cells similar to the picture of the untreated Jurkat Venus CLDN6-CAR cells. I was able to confirm this impression by flow cytometry (MFI-FITC = 7692). Also, the CAR expression was similar to the untreated control (MFI-APC =1624). When the AAV CLDN6_3 AAVLPs and the NIH-OVCar3 cells were cultured simultaneously with the CAR positive cells, the AAVLPs appear to be outcompeted. Under the microscope, the cells appear similar to those exposed only to the CLDN6-positive target cells. FACS analysis also revealed high Venus expression with an MFI-FITC of 34405. CAR expression was lowest in this approach with an MFI-APC of 1214.

In summary, cocultivation and the presumed binding of AAVLPs does not lead to activation of Jurkat Venus CLDN6-CAR positive cells. However, they cannot prevent activation in this number and setting if a CLDN6 positive tumour cell line is present at the same time.

A



B

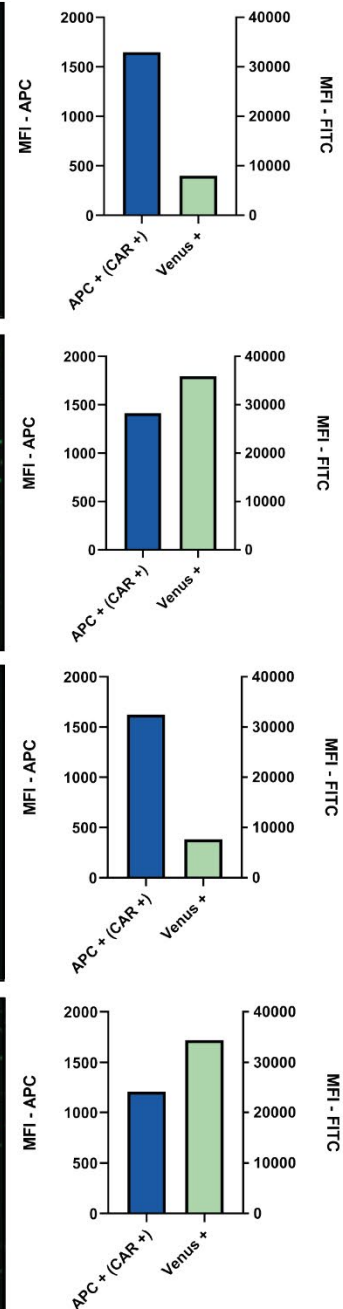


Figure 4.3.7: The presence of epitope-carrying AAVLPs does not lead to activation of Jurkat Venus reporter cell line. The Venus expressing cell line Jurkat Venus CLDN6-CAR (8×10^4) was co-cultivated with CLDN6 positive cells (NIH-OvCar3, 5×10^4), purified AAV CLDN6_3 AAVLPs (MOI 5×10^6) or with both components simultaneously for 24 h. Afterwards the Venus expression as a CAR-

mediated activation was observed by fluorescence microscopy (A) and by flow cytometry (B). Additionally, the cells were stained with an anti-hlgG-APC antibody to investigate CAR expression. The mean of fluorescence intensity (MFI) was calculated and plotted as bars (APC + = blue, Venus + = green).

4.3.5 Short-term attenuation of CAR T cell efficacy

I was able to show in isolated experiments that the AAVLPs I identified, AAV CLDN6_3 and CLDN6_4, bind to the specific anti-CLDN6 CAR and downregulate the expression of the CAR. Furthermore, binding of the epitope-presenting capsids did not lead to cell activation. However, none of these experiments considered the actual function of the CAR T cells, yet. To find out whether the AAVLPs can also slow down the killing of tumour cells, the viability of the corresponding target cells was monitored with the help of the xCelligence RTCA platform by measuring the cell impedance in real time (3.7.3). For the first experiment (Figure 4.3.8, A), I used AAVLPs that were not yet re-buffered but formulated in 40% iodixanol. In addition, I used the cell line HepG2 (human liver cancer cells), which had already been tested positive for CLDN6, as a target cell line. The anti-CLDN6-CAR positive T cells (Donor: RNK97) were co cultured with the HepG2 cells in three approaches (AAV CLDN6_3, AAV CLDN6_4, AAV CLDN6_3 + AAV CLDN6_4). The T cells were added to the target cells with the AAVLPs simultaneously. For this first attempt, I was again guided by the experiments with the NYBR1 clone2 antagonist (WO2019043081)⁶⁶. Therefore, the AAVLPs were used individually with an MOI of 4×10^4 and once in combination with a total MOI of 8×10^4 . As shown in Figure 4.3.8, A, the AAVLPs were indeed able to reduce CAR T cell activity for over ten hours (3-12 hours after T cell addition), which is indicated by a higher viability of the target cells. Significant differences in viability were achieved in all three approaches, although of different lengths. In a following experiment (Figure 4.3.8, B), the amounts of AAVLPs were to be increased, as more particles were also needed for the internalisation of the CARs in the previous experiments. Up to 5×10^6 AAVLPs per CAR-positive cell were used. In addition, a control containing only AAVLPs, and no CAR T cells was included to find out whether the iodixanol still contained could have a negative effect on the target cells. However, after the addition of mock T cells, a reduction in the viability of the target cells, compared to the untreated cells, was detected. Therefore, no conclusion could be drawn about the success of the treatment. Furthermore, it became apparent that the addition of particles without T cells also reduced the viability to a certain point, although it does not lead to a complete death of the cells.

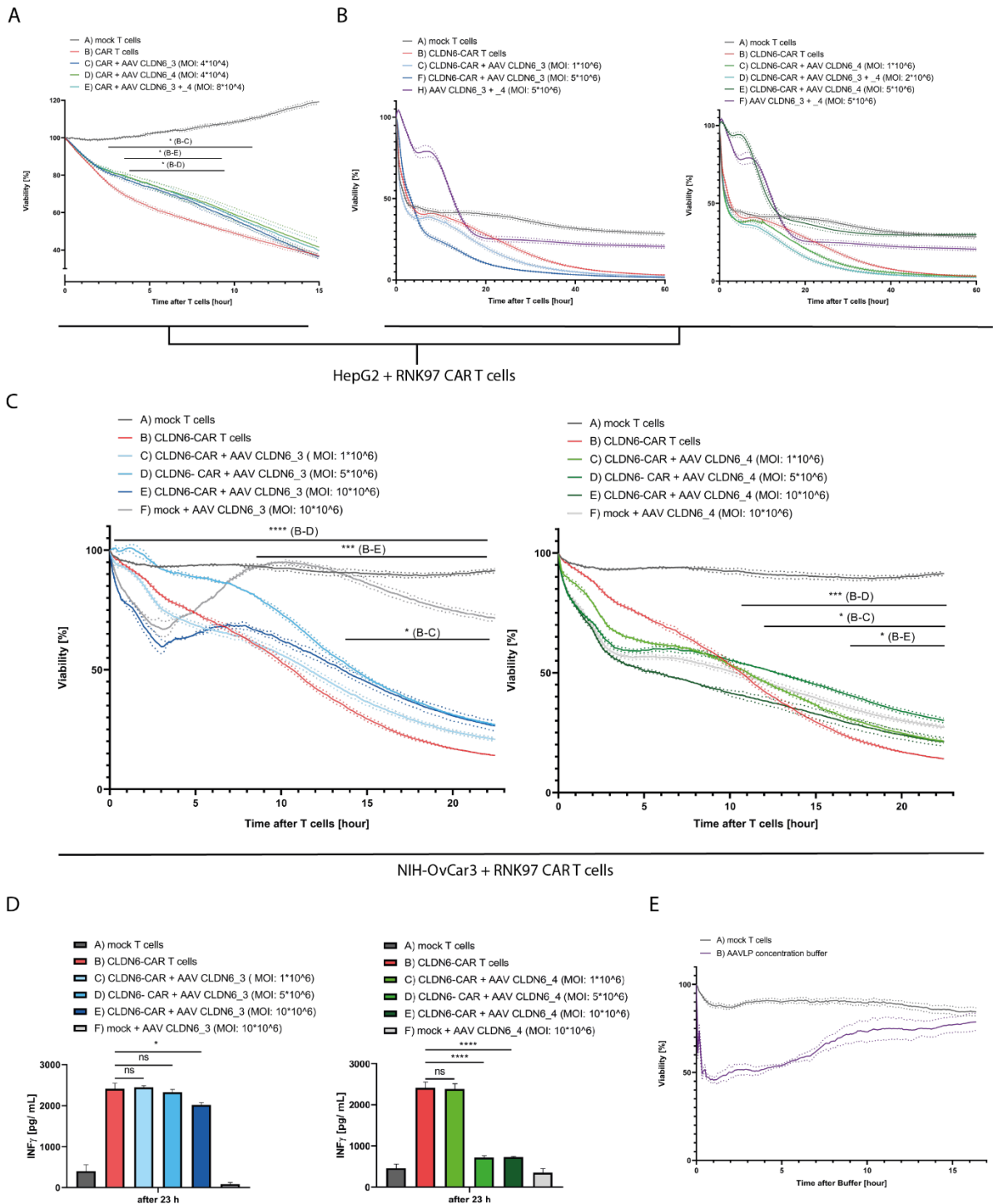


Figure 4.3.8: Temporarily reduced killing of target cells (HepG2/ NIH-OvCar3). Anti-CLDN6-CAR + primary T cells (RNK97) and AAV CLDN6_3/ AAV CLDN6_4 particles were co-cultivated with target cells at a ratio 1:2 in a 96 electronic microtiter plate. Untransduced T cells (mock) were used as controls. The AAVLPs were incubated together with the T cells for 5 min before being added to the target cells. A: HepG2 tumor cells were co-cultivated with RNK97 CAR + T cells and with AAVLPs in three approaches: AAV CLDN6_3 (MOI 4×10^4), AAV CLDN6_4 (MOI 4×10^4), AAV CLDN6_3 + _4 (MOI 8×10^4). B: HepG2 tumor cells were co-cultivated with RNK97 CAR + T cells and with AAVLPs in five approaches: AAV CLDN6_3 (MOI 1×10^6), AAV CLDN6_3 (MOI 5×10^6), AAV CLDN6_4 (MOI 1×10^6), AAV CLDN6_4 (MOI 5×10^6), AAV CLDN6_3 + _4 (MOI 2×10^2). As additional control AAVLPs (AAV CLDN6_3 + _4, MOI 5×10^6 (compared to the T cells)) were added to the HepG2 cells. C: NIH-OvCar3 target cells were co-cultivated with anti-CLDN6-CAR T cells and AAV CLDN6_3/ CLDN6_4 particles in three different MOI (1×10^6 , 5×10^6 and 1×10^7). As additional control, mock T cells were co-cultivated with the highest MOI of the respective particle. All experiments were performed in

triplicates. The standard error of mean (SEM) is visualised as dotted lines. Significant (, $p < 0.05$; ***, $p < 0.001$; **** $p < 0.0001$; multiple t-tests followed Holm-Sidak's multiple comparison test) difference marked with a timeline. D: The cell culture supernatants of the experiment described in C, were used for evaluation of T cell activity by determination of the $IFN\gamma$ concentration by $IFN\gamma$ ELISA. The mean of each approach is visualised as coloured bar with the specific SEM. The significant differences between the approaches were determined by one-way ANOVA followed by Holm-Sidak's multiple comparison test. E: NIH-OvCar3 cells were co-cultivated with mock T cells or 10 μ L of the AAVLP concentration buffer.*

To prevent the untransduced T cells (mock) from being directed against the target cells again, the cell line HepG2 was replaced by the tumour cell line NIH-OvCar3 for further experiments. In addition, for the next experiments, as in some experiments before, I used particles that were concentrated and therefore should contain less iodixanol. By concentrating the particles, less volume must be used in order to minimise the side effects of the buffer. In this way, the required volume could be reduced by a factor of ten. The different experimental approaches are similar to the previous experiment. I tested again a MOI of 1×10^6 , 5×10^6 and even increased the particle number to a MOI of 1×10^7 . I also changed the additional control. As an additional control, I now used mock T cells with the highest MOI of the individual particle in order to compare the same components in the respective amount on the target cells (Figure 4.3.8, C). All approaches achieved a significant difference in the viability of the target cells compared to the CAR T cells for different durations. For both AAV CLDN6_3 and _4, the MOI 5×10^6 seems to be the most effective in this case. However, it is noticeable that immediately after the addition of the components to the target cells, there is a strong reduction in viability. In the case of AAV CLDN6_3, this effect is only noticeable at an MOI of 1×10^7 , which makes this curve very similar to the control curve (mock T cells + AAV CLDN6_3). With AAV CLDN6_4, this effect is already clearly noticeable from an MOI of 5×10^6 . Comparably, there is a strong similarity between the curves with CAR T cells and the control curve (mock T cells + AAV CLDN6_4). These differences correlate with the required volumes of the particles. In order to obtain the same number of particles, twice as much volume of AAV CLDN6_4 was needed. Despite this side effect, the particles were able to slow down the killing of the target cells. To show that the negative effect immediately after the addition of the particles does not come from the particles themselves, but from the AAVLP concentration buffer used for concentration, 10 μ L of the buffer was added to the NIH-OvCAR3 cells at the end of a running experiment. This amount corresponds approximately to the volume for the highest MOI of the AAV CLDN6_4 particle. A sudden reduction in viability of 20 % was observed during the first hour. After 15 hours, the viability approached that of the mock T cells again (Figure 4.3.8, E). Due to this buffer effect, the exact influence of AAVLPs on CAR T cells above a certain volume can no longer be clearly observed using cell impedance measurements. For this reason, an $INF\gamma$ -ELISA was performed (3.4.4) after this experiment, to determine the level of T cell activation. For this ELISA, the supernatants from the 96 electronic microtitre plate were used undiluted (performed by Alexandra Tuch). The $INF\gamma$ concentration of the samples with AAV CLDN6_3 particles became

lower with increasing MOI but only significant at the highest dose (mean = 2019 pg/ mL). However, all these values are quite close to the untreated CAR T cell concentration (mean = 2410 pg/ mL). The CAR T cells co-cultured with the AAV CLDN6_4 particles showed a strongly reduced $\text{INF}\gamma$ release at 5×10^6 particles per CAR T cell (mean = 719 pg/ mL). The highest dose could no further reduce this low concentration (mean = 729 pg/ mL). These concentrations are closer to the concentration of the mock T cell control (mean = 461 pg/ mL) than to the concentration of the untreated CAR T cells (mean = 2410.67 pg/ mL).

With the help of these experiments, I was able to demonstrate the antagonistic effect of the identified AAVLPs. In different killing assays it was shown that the AAV CLDN6_3 and AAV CLDN6_4 particles were able to slow down the killing of the target cells by the anti-CLDN6-CAR T cells. For the AAV CLDN6_4 particle, a dose of 5×10^6 particles per effector cell is sufficient to significantly reduce the activation of the cells temporarily. Due to the greater reduction in T cell activity, continuation with AAV CLDN6_4 for further experiments is recommended.

5 Discussion

The central aim of this project was to further develop the AAV-based AAViTOP epitope mapping method. In a previous attempt to identify the epitope of the anti-CD19-FMC63 antibody, it was found that some insertions into the capsid were not tolerated and prevented the assembly of the capsids. Hence, the limitations of AAV capsid assembly should be defined more clearly and new strategies developed to overcome these limitations should be implemented into the AAViTOP screening technology.

5.1 Identification of assembly-disturbing motifs

When trying to visualise exon 2 of the CD19 protein as a continuous overlapping peptide library on individual AAVLPs, two things have become evident: the number of particles per insertion varies greatly, and there are regions of the protein that cannot be inserted into the capsid without disturbing the assembly (4.1.1).

I was able to prove that the insertions into the capsid sequence led to viral proteins of the expected sizes with the help of a Western blot (4.1.2). However, treatment of the transfected cells with a proteasome inhibitor did not lead to an improvement in the capsid titer but – on the contrary - resulted in lower capsid numbers even for generally well-producing sequences. Interestingly, β -actin protein levels were not affected. This finding suggests that the addition of the proteasome inhibitor either specifically prevented VP production or lead to degradation of VP proteins. It was observed that the treated cells consumed less cell culture medium (pH change) than the untreated cells (data not shown) indicating that the proteasome inhibitor might had a toxic effect on the cells even though MG132 was added in a variety of concentrations. A closer investigation would be needed to understand exactly what prevented the formation of the proteins. However, due to the observed effect, the treatment was not pursued further as a possible solution to increase the efficiency of capsid assembly.

The fact that some insertions are not tolerated, and no intact particles are produced was observed before, for example, when testing new insertion sites^{12,18,47}. Additionally, it was proven before that the length of the insertion is not a decisive factor in disturbing the capsid formation¹⁰⁰. Functional IgG binding domain (34 aa), the fluorescent protein mCherry (26.7 kDa), and the functional enzyme β -lactamase (29 kDa) were already inserted into the AAV2 capsid^{100–103}. I successfully extended the sequences of the CD19 exon 2 peptide library with the Flag-tag sequenz (DYKDDDDK) to 25 aa without detecting any negative effects (4.1.1). Some capsid structures already rescued by the C-terminal addition of the Flag-tag⁷⁴. This improvement in assembly by the insertion of the C-terminal Flag-tag, is probably due to the charge. The idea to extend the sequence with a negatively charged tag came from the observation that negatively charged insertions interfered less with the assembly of capsids

during CD19 exon 2 screening (4.1.1). The Flag-tag sequence is negatively charged due to the consecutive aspartates, while the region of the AAV2 capsid (VR-VIII loop) into which the sequence fragments are inserted is positively charged. This positive charge is mainly caused by the arginines (R585 and R588) which are present^{8,104}. By adding a negative sequence, the net charge of the complete inserted sequence is changed. I have demonstrated the influence of these two arginines on the tolerance of positively charged insertions when I exchanged the arginines (4.1.5). By exchanging these amino acids, the positively charged insertions CD19_23FL and CD19_33FL could be displayed on more intact AAVLPs. These capsid modifications will be discussed in more detail later. Based on this additional observation, it can be assumed that the increase in assembly is due to the charge of the sequence and not due to the extension of the sequence and the resulting change in the structure of the loop.

I observed that the number of assembled particles varies from sequence to sequence, while the length of the insertions remains constant. Therefore, the change of two amino acids per sequence seems to have greater influence on capsid formation. The composition of random peptide libraries (presented in the capsid behind amino acid 588) has already been studied^{47,100,105}. It was reported that some amino acids are rather underrepresented, such as K, N, F, I, and S and that some amino acids tended to appear in some positions more frequent than in others. For example, leucine (L) was not found at any marginal position¹⁰⁶. In addition, cysteines are said to have negative effects on assembly^{47,100}. The differences in the approaches must also be compared, as I have divided the sequence of a protein into fragments and inserted these into the capsid. These sequences have thus resulted from their function and structure of the protein. In the random peptide library under consideration, sequences were artificially assembled in no functional or structural context¹⁰⁶.

By screening the sequence of CD19 exon 2, I have shown that that many amino acids have no negative effects on the assembly and are well tolerated as insertion into the capsid. In comparison to the studies mentioned above, I observed many sequences in the CD19 exon 2 library where leucine is present at the N-terminal end and which nevertheless lead to intact particles, such as the sequences CD19_7FL, CD19_10FL, CD10_21FL, CD19_35FL, and some more. I also did not observe the negative effect of cysteine in my screening. All sequences from CD19_54FL to CD19_68FL carry one cysteine and these insertions all led to intact particles (4.1.1). Also, when examining the sequences that completely prevented capsid assembly more closely using the alanine scan (4.1.3), I could not detect any intact particles when replacing the N-terminal leucine in CD19_42FL. Interestingly, particles were assembled when the leucine was replaced in the middle of the sequence, which contradicts the observation in the random peptide library. This observation could be related to the fact that leucine has hydrophobic side chains that like to form aggregates for stabilization and are increasingly found inside proteins^{107,108}. In the construct I used, the leucine in the middle of

CD19_42FL would be represented further away from the rest of the protein structure due to the expansion of the loop. The hydrophobic properties of the amino acid could either create bonds or favour folding that would interfere with assembly. The leucine at the N-terminal end of CD19_42FL is closer to the initial structure of the capsid and presumably interferes less with assembly there. The thesis that the hydrophobic side chains of leucine play a role is also supported by the observations in the studies mentioned above, because the other hydrophobic amino acids valine and isoleucine are also hardly represented in random peptide libraries¹⁰⁶. The fact that these hydrophobic amino acids are underrepresented in random peptide libraries and influence assembly in my screening is probably also due to the fact that they are inserted into a loop. Such protein regions usually consist of polar, hydrophilic, and charged amino acids^{108,109}. Which is why the insertion of negatively charged sequences and hydrophilic amino acids was not a challenge.

However, most particles were assembled when the three aromatic amino acids were replaced in the CD19_42FL sequence (W, F, F). Surprisingly, in sequence CD19_51FL, the exchange of two aromatic amino acids was sufficient to ensure the assembly of the particles in higher amounts. Overall, the achieved particle titers of CD19_51FL were higher than those of CD19_42FL after the exchange of aromatic amino acids. This may be due to the position of the critical motif, since in the CD19_51FL sequence it is located at the N-terminal end, which, as mentioned above, directly follows the wildtype capsid sequence. The C-terminal end forms an extension of the loop together with the subsequent Flag-tag. Perhaps, as with leucine, the interactions from this extended loop or the folding of this additional region have more influence on the assembly of the capsid than the amino acids close to the original capsid sequence. In addition, for the CD19_51FL sequence, the alanine scan was only performed on the sequence overlapping with CD19_42FL. The other amino acids were not considered. Furthermore, the effect of this accumulation of aromatic amino acids was not examined in further sequences. The fact that the exchange of the tryptophan has more influence in the combination than the exchange of another phenylalanine can be traced back to the size of the aromatic ring, which takes up more space in the structure of the capsid¹¹⁰. The native structure of the inserted sequences is of course another point to consider. The sequence that interferes with assembly as an insertion (i.e., CD19_42FL) into the capsid is present in the CD19 extracellular domain as part of a β -sheet⁸⁵. In this structure, aromatic amino acids are important components for the stability of the protein¹¹¹. With respect to the application of the assay in epitope identification, one could question the necessity to display such a region of the target protein sequence at all since antibodies usually do not have access to this specific position.

When producing the particles with the inserted peptide library for screening with the anti-CD19 clone 3B10 antibody, there was no accumulation of aromatic amino acids and no particles that could not be produced (4.2.2). Only with the CLDN6 particles did these problems become

apparent again (4.3.1). Claudin-6 also has a β -sheet structure, and the amino acids tryptophan, phenylalanine, and isoleucine again appeared in close proximity in the sequences. In this case, I did not check the individual amino acids regarding their influence but only removed tryptophan with the largest aromatic ring from the sequence, especially since the phenylalanine was described as important for binding⁹⁴. Of note, in regions containing the putative antibody binding epitope, the least sufficient amino acid exchanges should be carried out. Thus, replacing several individual amino acids, especially if it is not known in which region antibody binding takes place should be avoided as this can falsify results.

5.2 Generating a tolerant capsid environment

The further development of the screening method AAViTOP should include a capsid which, ideally, can display insertions of all kinds on the surface ensuring maximal reliability without the need to modify the inserted sequence. To achieve this goal, I pursued two approaches: firstly, insertion at different locations in the capsid and secondly, modification of the capsid by point mutations.

5.2.1 Comparison of different insertion sites

Peptide insertions into the AAV capsid are a common strategy for retargeting the capsids independent of its natural tropism^{47,102}. The variable regions of the capsid, such as the VR-VIII (VR-VIII-aa588) or VR-IV (VR-IV-aa453) loop, were used early on as insertion sites for foreign sequences. Both loops form peaks on the surface^{12,21,112}. But other insertion sites have also been investigated, such as the HI-loop (HI-loop-aa653), which is needed to form the fivefold pore of the capsid¹⁰. I also generated two more insertion sites within the β -sheet structure of the capsid (β B-aa245A/ B), which had not been described before. Insertions in the β -sheet would also be localised around the fivefold pore. The aim was to find out whether a different insertion site would lead to improved titers for epitope screening and whether the aromatic amino acids would be better tolerated at a different site. A comparison to this extent has not been carried out so far.

Insertion into the HI-loop was considered because insertion at this site may affect DNA packaging but should result in intact particles¹⁰. Since empty particles can be used in the screening, this is not an exclusion criterium. However, the observed particle titers with insertions in the HI-loop were very low (4.1.4). Even with changes in the insertion environment by adding parts of the original sequence, only very low titres were achieved. Since this insertion site performed so poorly compared to the others, I decided not to make any further attempts with this region.

Insertions containing aromatic amino acids as clusters were successfully displayed on intact particles when they were inserted into the β -sheet structure. However, this was only possible

in the plasmid variant β B-aa245A, in which the insertion means a larger extension of the sequence and does not completely replace the original sequence. I also saw this effect with the insertions in the HI-loop. This supports the hypothesis that the AAV capsid is tolerant with regard to the expansion of its size, as it was also shown by insertion of whole proteins¹⁰³. At the same time, the original primary sequence is very important, and the secondary structure is very sensitive to changes. As mentioned above in the detailed analysis of this aromatic motif, the cluster of aromatic amino acids in the natural CD19 protein structure is present in a β -sheet and may therefore be better inserted into one. Whether this is really the reason why the aromatic sequences can be successfully inserted here, needs to be shown by further tests in which similar motifs from similar structures could be tried to be displayed, i.e. the CLDN6 sequences that failed to be displayed without changes (4.3.1). Another possibility is that this area forms fewer interactions with other subunits of the capsid and tolerates the insertion of these large amino acids because of less bonds. Except for one further inserted sequence (CD19_6FL), no other sequence could be presented at this position. This is why this position was not an alternative to other insertion sites, although it tolerated aromatic clusters to a limited extent. But it might be an alternative for isolated sequences. However, the accessibility would have to be tested first; since these particles were never used in a binding assay, I cannot say whether an antibody really has access to this position. To test this insertion site for antibody accessibility, it would be possible to try inserting an epitope tag into this β -sheet. Whether the Flag-tag is presentable is uncertain. An alternative might be the HA-tag, as it has more aromatic amino acids in its sequence (YPYDVPDYA)¹¹³. And this tag is less hydrophilic than the Flag tag, which is why it may be more suitable for insertion in this narrow structure of the β -sheet.

Inserting sequences into the VR-IV-loop turned out to be technically more time-consuming. The plasmid (pMT-187-XX2_453mut) already present in the laboratory was opened with the restriction enzymes NheI and SpeI. By using these enzymes, the sequences to be investigated had the chance to be inserted in the wrong orientation. A simple restriction digest was therefore no longer sufficient to verify successful cloning. For larger screenings such as CD19 exon 2 screening, this cloning would take an enormous amount of time and money if plasmids containing sequences in the wrong orientation had to be sorted out during cloning by DNA sequencing. For this reason, I decided to design a new capsid backbone plasmid containing a cleavage site in the VR-IV loop but with the enzymes MfeI and SpeI solving the issue by non-compatible overhangs. I also used the new backbone plasmid later to insert the double insertions (4.2.3). Due to the fact that this plasmid did not exist at that time, I decided to proceed with the insertion site behind amino acid 588, even though the previous quantifications of particles with insertion in the VR-IV loop also looked promising. Due to the different amino acid distributions resulting from the insertion of random peptide libraries into these two loops, the

VR-IV loop insertion site should still be considered¹⁰⁰. A comparison between the titers using the newly designed insertion site should be carried out to be able to make a clear statement about whether this region is more tolerant for insertions. And to find out whether the greater distance from the capsid surface due to the larger peak is an advantage for the presentation and binding of the inserted sequence.

5.2.2 Comparison of different point mutations in the capsid

Another reason why I chose to work with the VR-VIII insertion site behind amino acid 588 is that this insertion site is commonly used and was investigated in many studies before^{20–22,43,102,112,114}. The further development of this region as a carrier of foreign sequences is promising to be useful for further use in gene therapy and the implementation in the design of random peptide libraries.

The tested point mutations in the capsid that I have carried out (4.1.5) represent only a small sample of the possibilities that such modifications open. I have only compared the titers that can be produced and the possibility of inserting different types of sequences. Whether the binding properties of the inserted sequences to antibodies or receptors change or whether new tropisms form as a result of the modifications was not investigated here. Both would be worth to investigate with respect to ensuring safety of modified capsids to ensure.

The inserted point mutations are not randomly chosen changes in the capsid or simple alanine substitutions but are based on the differences in the capsid of AAV-v66 compared to AAV2. The naturally occurring capsid variant AAV-v66 differs from AAV2 in 13 amino acids and is characterised by higher stability and increased production yields⁸¹. A comparison of these individual changes in the AAV2 capsid in relation to the capsid titer with different types of insertions has not yet been carried out. Why some mutations lead to higher capsid titers cannot yet be explained for all mutations. For some amino acids, however, there are explanations based on their function. The amino acids R585 and R588 are very well-characterized positions in the AAV2 capsid. They belong to the heparin-binding site and are therefore important positions for the AAV2 tropism^{115,116}. Furthermore, the two arginines are the main reason for the electrostatic difference between the AAV2 and AAV-v66 capsids and the positively charged surface of the peak⁸¹. Replacing R585 with serine and R588 with threonine destroys the natural tropism of AAV2, which is not needed in the context of epitope screening and is beneficial for the use of the particles as CAR antagonists. Depending on the inserted sequence the tropism is already destroyed by the insertion of the foreign sequences^{47,117}. Furthermore, it was shown that the exchange of the two arginine also enhances the target molecule binding for inserted sequences. By eliminating the positive charge, it is assumed that the electrostatic interactions between capsid residues change, or it even leads to conformational changes and the inserted sequences can be accessed more easily as a result¹⁹. These two positions therefore do not

represent structurally important amino acids but are very important for AAV cell entry. Above all, the changed surface charge of AAVs harbouring R585S and R588T mutations could also be the reason why the positively charged insertions CD19_23FL and CD19_33FL are better tolerated and more capsids can be formed with these insertions, as already briefly mentioned above. Besides the charge, there is another explanation for the improved titers. Both arginines form highly frustrated residue interactions with their surrounding in the multimer structure¹¹⁸. These highly frustrated compounds are often found in protein regions where so-called conformational cracking is found. These connections contradict the principle of evolutionary optimisation of the protein energy landscape, according to which a minimum of frustration is always desired¹¹⁹. With the replacement of the two arginines, the frustrated residue interactions are changed, possibly leading to facilitated assembly. In many AAV serotypes, without HSPG binding motif, S585 and T588 are conserved amino acids and have become evolutionarily established¹¹⁹. I did not investigate the influence of the individual arginine on the assembly of the capsid, as they were only tested in combination.

As mentioned above, the R585 and R588 positions of AAV2 are well investigated, and because of their role in receptor binding and cell entry, it is possible to explain the benefits of the replacement regarding insertion of certain peptide sequences^{115,120-122}. Due to the limited information about this new variant, it is difficult to give individual amino acids a structural significance. Amino acids that are not found in any other serotype, e.g. threonine at position 593 or the methionine at position 457 of AAV-v66, might be required for specific receptor bindings, such as the two arginines in AAV2.

Why some combinations of mutation lead to improved capsid titers, although the individual mutations tended to result in reduced capsid titers is currently not explainable. In order to understand which interactions were interrupted or which new interactions were formed, one would have to go deeper into the structure of the subunits and their connections. An *in-silico* modelling of the modified capsids would be a possibility to show changes in the structure and their influence more precisely. With the help of such models, it would also be possible to take a closer look at the binding partners of the individual amino acids. Probably, improvements can sometimes be explained by originally highly frustrated connections. To understand the consequences of the individual changes on the capsid integrity, experiments observing DNA packaging and/or cell entry would be required. By such experiments, the functional relevance of individual amino acids in the capsid can be explored systematically. However, these experiments were not necessary to further develop the AAViTOP screening method, as the main focus was on the presentation of foreign sequences, and thus out of the scope of my thesis.

However, the performed AAV2 vs. AAV-v66 mutation scan has shown that it is possible to modify the capsid structure in such a way that it leads to more assembled capsids. And some

mutations indeed allow the insertion of sequences that were not tolerated in the original AAV2 environment, e.g. T450A-Q457M-E499D-R585S-R588T-A593T (4.1.5).

The results are, of course, limited to the integration of sequences with the chosen properties and cannot be translated to any sequence. In addition, all sequences were inserted behind amino acid 588, so I cannot draw a conclusion whether the same changes also have a positive effect on the assembly of capsids carrying an insertion in the VR-IV loop. A comparison of the modified capsid backbones in the epitope screening assay could provide information whether the binding properties of the inserted sequences are affected by the modifications and whether the insertions are more (or less) accessible due to altered charge or structure.

5.3 The AAViTOP procedure as a tool for epitope mapping

Knowing the epitope of therapeutic antibodies or CARs is an important feature to improve treatment safety: severe side-effects can be anticipated, prevent and managed more efficiently and identification of suitable patients and putative non-responders will be enabled. In the past, many methods have been developed for the identification of epitopes. A simple and well-known method to identify epitopes is the pepscan, in which an overlapping peptide library is created from the suspected antigen and the binding to these linear peptides is examined. These peptide scans are now available as high-throughput systems^{123,124}. The gold standard for the identification of antibody epitopes is still the co-crystallization of the antibody:antigen complex. However, this is very time-consuming and technically difficult¹²⁵⁻¹²⁷. The aim of this project was to improve the identification of CAR epitopes using the novel AAV-based AAViTOP method and to characterize the identified particles as antagonists of their cognate CARs.

5.3.1 Identifying epitopes in the CD19 protein sequence

5.3.1.1 *Linear epitopes*

In general, there are two forms of epitopes: linear and discontinuous epitopes. In other words, epitopes that consist of a contiguous sequence and epitopes that result from the three-dimensional arrangement of discontinuous primary sequences of a protein¹²⁸. After the first screening attempt for anti-CD19 FMC63 antibody epitopes failed, the AAViTOP screening method was utilised to verify a linear CD19 epitope. Therefore, the published linear epitope of the anti-CD19 antibody clone 3B10 was used as proof of concept (4.2.2). The 3B10 epitope was defined as KLYVWAKDRPEIWEGEPP, and mutation-intolerant amino acids were also determined previously⁸⁸. I successfully reproduced the published results with an overlapping peptide library of 19 sequences and the AAVLPs displaying them on the surface. Based on the screening results, the minimal epitope of antibody clone 3B10 probably consists of the amino acid sequence KDRPEIWE. I observed that binding occurs once this motif is completely

contained in the presented sequence (sequence 8) and no more binding is detected as soon as this motif is no longer entirely presented in the capsid (sequence 16). Particles only displaying the suspected minimal epitope have not yet been tested. However, an experimental approach would be to generate a shrinking peptide library, in which the displayed peptides become shorter and shorter until binding to the antibody is no longer possible. A similar approach has been carried out to verify the minimal epitope of the anti-NYBR1 CAR in WO2019043081⁶⁶.

Besides validating the epitope, I also replaced the amino acids described as completely mutation-intolerant with alanine. In the presumed minimal epitope, these are the lysine (K) at the beginning of the sequence, the tryptophan (W) and the directly following glutamic acid (E) at the end of the epitope⁸⁸. The exchange of amino acids led either to a complete loss of binding or to a reduction, confirming these amino acids to be important for binding of 3B10 (4.3.2). After the replacement of the tryptophan in sequence 15, no antibody binding was detected. However, when the tryptophan in sequence 8 was replaced by an alanine, the binding was only strongly reduced but could still be detected. It seems that there are amino acids in sequence 8 that can compensate for the loss of the tryptophan. The alanine exchange of the lysine and the glutamic acid was only performed in sequence 15. When the glutamic acid was exchanged no binding of the antibody was detected. The exchange of the lysine showed a reduced binding, but the two measurements were very disparate compared to the other sequences. In order to better define the individual amino acids that are crucial for binding, further alanine exchange mutants would have to be screened.

Overall, I was able to verify the published epitope of the anti-CD19 3B10 antibody in multiple runs of the bead assay.

The reason why my results do not completely match the published results may be due to the application of different methods. Klesmith et al. used a modified CD19 extracellular domain to define the epitope. This modified variant was termed CD19.1 and differs from the wild-type protein by 26 mutations. These modifications were necessary to allow the binding of the anti-CD19 FMC63 and 4G7 antibodies to the yeast-displayed protein⁸⁸. It is possible that these mutations affected the binding to the linear epitope and that the influence of individual amino acids was therefore assessed differently. The necessity for these mutations shows how quickly the folding of the CD19 protein and the binding of antibodies can be affected. Other studies have also shown that the deletion of single exons of the protein or single point mutations prevent the binding of the anti-CD19 FMC63 antibody and thus also impair the function of the anti-CD19 CAR which has the identical scFv of FMC63 without eliminating the epitope directly^{76,129,130}. The extracellular domain (ECD) of the CD19 protein tends to misfolding and aggregation, and the expression of this domain is also limited^{131,132}. This phenomenon is probably the reason why the attempt to use a fusion protein of CD19 exon 2 and 3 to look more

closely at the binding of the FMC63 antibody (4.2.1) did not work. While the epitope was detected by 3B10 when displayed on AAVLPs, misfolding could have made the linear epitope inaccessible to the antibody in the fusion protein.

5.3.1.2 *Discontinuous epitopes*

Studies have shown that antibodies generated *in vivo* recognise discontinuous epitopes more frequently than linear ones^{133,134}. Thus, the identification of such epitopes is of great importance and I tried to use the AAV capsid structure to mimic the natural arrangement of the presumed conformational anti-CD19 FMC63 epitope (4.2.3).

Tepljakov et al., determined the epitope of the B43 antibody by co-crystallization of the antibody:CD19 complex: three loops of the CD19 protein built the binding motif. The CD19 FMC63 antibody was shown to compete with the B43 antibody for binding⁸⁵. Therefore, it is possible that these three loops of the protein are also involved in binding to the FMC63 antibody. In the same study that determined the epitope of the anti-CD19 3B10 antibody, Klesmith et al. described possible crucial amino acids for the binding of the FMC63 antibody⁸⁸. These amino acids are located in two of the three B43 binding loops of the CD19 protein. For the attempt to use AAVLPs with double insertions in the capsid, I decided to use those sequences of the third loop of the CD19 protein, that both studies identified as possible binding sites. In addition, I chose the sequence of the CD19 exon 2 screening (CD19_72), that was tested positive for binding of the FMC63 antibody in my master thesis⁷⁴. CD19_72 is part of the B43 epitope, which is why the positive result, although not reproducible in my PhD work, may indeed be part of the FMC63 epitope. The loop with the 3B10 epitope was not investigated. Furthermore, the selected loops were chosen according to the most similar distances between them and the peaks of the AAV2 capsid. However, these measurements were not absolutely accurate because the peaks will lose their natural shape due to the insertion and the shape of the insertion cannot be predicted with precision as well. Besides the drawbacks, the measurements should represent a reference value. The technical feasibility to display two sequences in different positions on the surface of the capsid simultaneously was shown before with different inserted peptides^{19,135}.

The experiments carried out so far showed the strongest binding with PLSWTHVHPKGPKS (3rd_loop_4) in combination with the sequence CD19_72. All tested sequences (3rd_loop_1-3rd_loop_6) contain the amino acids (G and P) reported as crucial for the binding. Since binding was detectable only for one sequence, the position of these amino acids on the capsid could play a role. I tested the double insertion AAVLPs only once for binding of the FMC63 antibody using the bead assay, it is not possible to say for sure whether this result is reproducible. Furthermore, additional controls, such as the respective sequences as single insertions, were missing in order to be able to determine whether the binding really takes place at both sequences or whether the loop sequence alone is sufficient for the binding (CD19_72 alone

was at least not sufficient). In case of a proven reproducibility of these results, AAV display could be a superior alternative to classical peptide scans, given that two peptides can be presented on the capsid at a distance that is close to a natural configuration in the protein. At the same time, the peptides are not denatured but have a loop structure on the AAV capsid.

5.3.2 Identifying epitopes in the CLDN6 sequence

The identification of the epitope of the IMAB027 antibody was not only another example to verify the AAViTOP screening method, but the identified particles should be characterised functionally after screening.

Unlike the production of CD19 3B10 AAVLPs, some CLDN6 constructs failed to produce intact particles as already discussed in section 5.1. I decided to replace the aromatic amino acid tryptophan in the non-producible sequences by alanine to ensure capsid assembly. Because of this process, the first bead assays were only carried out with the capsids that could be produced at that time (4.3.2). The highest binding of the antibody to the AAVLPs was found in the unmodified sequences AAVLPs CLDN6_3 and CLDN6_4. and the functional inhibition experiments with CAR T cells were thus carried out with these particles.

After the modified particles could also be tested for binding of the antibody, the CLDN6_5A particles showed high binding and fewer variation between the individual measurements. However, variations in repeated measurements were evident in the IMAB027 screening for all sequences. These variations may have arisen due to technical differences from the screenings before. The IMAB027 antibody was labelled with PE using the PE / R-Phycoerythrin Conjugation Kit – Lightning-Link®. This process had to be done repeatedly for a certain amount of antibody and can lead to irregularities. Other sensitive components are the beads coupled with anti-A20-biotin and the biotinylated A20 antibody itself that are biotinylated in the lab similar to the PE-labelling of IMAB027.

Furthermore, the replacement of the tryptophan seems to affect the binding of the antibody, although it has not been designated as an important amino acid for antibody binding. However, it can be seen, that binding to the sequence CLDN6_6A was lower than to the sequence CLDN6_6 (4.3.2). The replacement of the tryptophan can influence the binding in different ways. Since I have replaced this large amino acid by a small alanine, the structure may have been changed and thus no longer optimally bind to the antibody. Furthermore, an aromatic side chain was removed, which often plays a role in antibody-antigen interactions¹³⁶. This observation raises the question of whether this effect also occurs with sequence CLDN6_5A and the actual binding to the original sequence would be higher. In addition, this observation underlines the need of an alternative, universal capsid backbone that tolerates the insertion of the original, unmodified sequence. With the help of the systematic point mutations carried out

(4.1.5), it would still be possible to try to display the original sequences of CLDN6 in a different capsid environment, e.g. backbone R447K-E499D-R585S-R588T-A593T.

5.3.3 Opportunities and challenges for the AAViTOP screening method

During this study, I was able to validate the epitope of the anti-CD19 3B10 antibody with the help of AAV display. My results agree to a large extent with the previously published data, but the methods used differ fundamentally. Klesmith et al. used a CD19 ECD mutant, deep mutational scanning, yeast surface display and flow cytometry for their analyses⁸⁸. The AAViTOP method was able to deliver the same results with less resources. The performed epitope screenings (anti-CD19 FMC63/ 3B10, IMAB027) were all limited to a smaller region of the targeted protein. Without the knowledge in which region the binding takes place, larger screenings would have to be carried out. Possibly, one would start with smaller sequence overlaps in the peptide library to narrow down the region first and then perform the assay with larger sequence overlaps. A first step towards the identification of discontinuous epitopes was taken with the help of the double insertions. Although further tests are still open, verification of the hit would encourage, validation of the approach with a further discontinuous epitope.

In order to be used as a robust screening method, the biggest challenge, i.e. capsid assembly, must be solved. In this work, I have demonstrated two approaches, modifying the capsid itself by systematic point mutations in the capsid backbone plasmid (4.1.5) and by replacing amino acids in the primary sequence (4.1.3, 4.3.1). Modifying the inserted sequence can affect the binding of the antibody to the epitope and thus should not be a permanent solution.

However, the greatest potential of the AAViTOP method is not that epitopes can be identified, as I have been able to show here repeatedly, but that the particles used for screening can be used as antagonists for the antibody/ CAR.

5.4 Using AAVLPs as CAR antagonists

Up to 93% of leukaemia or lymphoma patients receiving CAR T cells developed any grade of cytokine release syndrome (CRS)¹³⁷. For the treatment of CRS, symptomatic treatment with tocilizumab (anti-IL-6R) is currently recommended¹³⁸. This treatment does not limit the functionality of the CAR T cells^{139,140}. However, there is an increased risk of infection and treatment with tocilizumab is limited to the treatment of CRS^{138,141}. It has been shown to be ineffective for the treatment or prevention of other side effects of CAR T cell therapy such as neurotoxicity¹⁴¹. Since the first treatment with this living drug, several methods have been developed to better control the toxicity of the engineered cells. The choice of co-stimulatory domains may have an impact on toxicity, e.g., the use of the 4-1BB domain at high tumour burden carries lower risks of toxicity than the use of the CD28 domain¹⁴². Another attempt to gain more control over the induced CAR T cells is the insertion of suicide genes, which cause

the cells to terminate when activated^{143,144}. A method that has a reversible effect on the CAR T cells and thus does not destroy the expensively produced cells is considered more promising: The tyrosine kinase inhibitor dasatinib suppresses T cell activation without destroying the T cells. In the absence of the inhibitor, activation can occur again¹⁴⁵.

In a novel approach identified in our group, AAVLPs are designed to block CAR T cell activation: Through the epitope that is antagonised specifically on the CAR T cells, their activation is inhibited while leaving the unmodified T cells in the patient unaffected. By binding to the CAR, the CAR together with the bound AAVLP is thought to be internalised and not be able to be activated. In the absence of AAVLPs, the CAR returns to the cell surface and can be activated by tumour recognition. This phenomenon was first demonstrated with an anti-NYBR1 CAR and the epitope displaying AAVLPs as antagonists⁶⁶. In this project, I have shown that the phenomenon described is not limited to the NYBR1 as a target antigen. For this purpose, I used the previously identified particles with the integrated sequences CLDN6_3 and CLDN6_4 (4.3.2). The first attempts to reduce anti-CLDN6 CAR expression on transduced Jurkat cells were unsuccessful with MOIs of up to 1×10^6 particles per cell. Only with the use of primary CAR T cells could the reduction be measured (4.3.3). The measured mean of fluorescence intensity of the primary CAR T cells and the CAR-positive cell line differed strongly in the measurements. After performing a PE quantification, I could justify this difference with a four times higher CAR expression on the Jurkat cell line. A similarly large difference in CAR expression is found between the Jurkat NYBR1-CAR cell line and the Jurkat CLDN6-CAR cell line (4.3.3.1). Because of these large differences, one probably also needs at least four times as many particles to detect similar reductions in expression as on primary T cells. The differences between the NYBR1-CAR and CLDN6-CAR results may of course also be due to the different binding properties of the scFv part used. There is no reliable information on binding properties such as affinity for either of the two scFv parts used. However, it may be possible to draw conclusions from the original use of the monoclonal antibodies from which these scFv are derived. The original anti-NYBR1 monoclonal antibody was initially used for immunochemistry testing of tumour tissue for NYBR1 expression¹⁴⁶. For this purpose, it would be sufficient to use an antibody that binds the antigen with a high affinity; how homogeneously this binding takes place in the tissue is of second priority, since the goal of detection is in the focus¹⁴⁷. The antibody IMAB027, which shares the heavy and light chain with the scFv Part of the CLDN6-CAR, was developed for therapeutic applications to treat ovarian cancer¹⁴⁸. Monoclonal antibodies designed to penetrate tumours usually have a lower affinity to allow homogeneous distribution in tumour tissue^{147,149}. Due to the binding site barrier, high affinity is associated with low penetration¹⁵⁰. Based on these considerations, it could be assumed that the affinities of the CAR scFvs differ and that binding to the AAVLPs takes place with different strengths. Another possibility for the less effective inhibition of CAR expression in case of

CLDN6-CAR as compared to the Jurkat NYBR1-CAR cells could be that CLDN6_3 is not the perfect binding partner for the anti-CLDN6-CAR. Although the CAR expression of primary T cells was more reduced by incubation with the AAVLPs CLDN6_3 than CLDN6_4 (4.3.3) and the killing assay curves showed higher viability of the target cells after treatment with the CLDN6_3 particles, it seems CLDN6_4 was the better antagonist (4.3.5). The CLDN6_4 AAVLPs were able to limit the IFN γ release almost to the level of the mock cells starting at an MOI of 5×10^6 (4.3.5). The CLDN6_3 AAVLPs could not achieve this effect even with twice the dose. This larger effect in inhibiting the activation of CAR T cells was not reflected in the viability of the target cells. The AAV concentration buffer contains salts that increased the conductivity of the medium when added to the cells (3.3.3). This change in conductivity made it appear that fewer adherent cells were present. This negative effect of the AAV concentration buffer is more evident in the CLDN6_4 treated cells, as I had to use twice the volume to reach the same MOI as with the CLDN6_3 particles. I could prove this buffer effect by adding the buffer in the same volume without AAVLPs to seeded target cells. In order to only detect the effect of the AAVLPs on the CAR T cell killing activity using the xCelligence device, the AAVLPs must be stored in a buffer that does not interfere with the electrical pulses or the concentration buffer must be present in the same volume in all samples to obtain comparable results. Repetitions of the killing assay should be performed primarily with the CLDN6_4 particles and possibly compared to CLDN6_5A particles due to the results of bead assay (4.3.2). Furthermore, MOIs up to a maximum of 5×10^6 are probably sufficient to slow down the activation of CAR T cells in this setup, because with this number of particles per CAR T cell, IFN γ secretion was reduced to untransduced mock T cell levels (4.3.5). This MOI can be determined more precisely by further titrations.

Another experiment that should be repeated with the CLDN6_4 AAVLPs is co-cultivation of the AAVLPs with the Jurkat Venus reporter cell line. Using the cell line that expresses the reporter gene Venus when the transcription factor NFAT is present at high levels, it could be shown that the AAVLPs do not trigger activation (4.3.4). When the AAVLPs with CLDN6_3 insertion had to compete for binding to the CAR with a CLDN6-positive target cell line, activation could not be prevented. A repetition of this experiment with the more inhibiting CLDN6_4 particle may show greater influence on reporter cell activation, although the high CAR expression might be problematic.

In conclusion, I was able to identify the disturbing motifs of capsid assembly in CD19 exon 2 epitope screening and point out possible solutions. Aromatic amino acids and the β -sheet structure that usually accompanies them seem to prevent the assembly of the capsid from the subunits. As with CD19 exon 2, this was in part also detectable within the CLDN6 sequence. Because there are not many CARs available to date and their scFvs are mostly not commercially available as antibodies, the AAViTOP method was further improved using other

targets. One main focus of assay development is to work on applications that distinguish this screening from others, i.e. the unique selling points of the AAViTOP screen. For example, using the three-dimensional structure of the capsid for the presentation of discontinuous epitopes as shown here for CD19 antibody clone FMC63. A future avenue could possibly be the investigation whether glycosylated epitopes can be displayed which due to the production in a human tumour cell line would be plausible¹⁵¹.

As mentioned above, the development of new CAR antagonists is still limited but with the help of the anti-CLDN6-CAR antagonist identified here, further attempts can be made to understand the mode of action of the AAVLPs by internalisation of the receptor more deeply. Of note, the functionality of the AAVLPs has not yet been tested *in vivo*. To shed light on their inhibitory potential *in vivo*, suitable mouse models that allow the mimicking of an emergency or co-dosage setting of CAR T cells and AAVLPs need to be developed in order to estimate dosage and safety of AAVLPs in a pre-clinical setting.

6 References

1. Atchison, R. W., Casto, B. C. & Hammon, W. McD. Adenovirus-Associated Defective Virus Particles. *Science (1979)* (1965) doi:10.1126/science.149.3685.754.
2. Buller, R. M. L., Janik, J. E., Sebring, E. D. & Rose, J. A. Herpes Simplex Virus Types 1 and 2 Completely Help Adenovirus-Associated Virus Replication. *J Virol* **40**, 241 (1981).
3. David Hoggan, M., Blacklow, N. R. & Rowe, W. P. STUDIES OF SMALL DNA VIRUSES FOUND IN VARIOUS ADENOVIRUS PREPARATIONS: PHYSICAL, BIOLOGICAL, AND IMMUNOLOGICAL CHARACTERISTICS*.
4. Rose, J. A., Berns, K. I., Hoggan, M. D. & Koczot, F. J. EVIDENCE FOR A SINGLE-STRANDED ADENOVIRUS-ASSOCIATED VIRUS GENOME: FORMATION OF A DNA DENSITY HYBRID ON RELEASE OF VIRAL DNA. *Proceedings of the National Academy of Sciences* (1969) doi:10.1073/pnas.64.3.863.
5. Mendelson, E., Trempe, J. P. & Carter, B. J. Identification of the trans-acting Rep proteins of adeno-associated virus by antibodies to a synthetic oligopeptide. *J Virol* **60**, 823–832 (1986).
6. Janik, J. E., Huston, M. M. & Rose, J. A. Adeno-associated virus proteins: origin of the capsid components. *J Virol* (1984).
7. Buller, R. M. & Rose, J. A. Characterization of adenovirus-associated virus-induced polypeptides in KB cells. *J Virol* **25**, 331 (1978).
8. Xie, Q. *et al.* The atomic structure of adeno-associated virus (AAV-2), a vector for human gene therapy. *Proceedings of the National Academy of Sciences* (2002) doi:10.1073/pnas.162250899.
9. Sonntag, F., Schmidt, K. & Kleinschmidt, J. A. A viral assembly factor promotes AAV2 capsid formation in the nucleolus. **107**, (2010).
10. DiPrimio, N., Asokan, A., Govindasamy, L., Agbandje-McKenna, M. & Samulski, R. J. Surface Loop Dynamics in Adeno-Associated Virus Capsid Assembly. *J Virol* **82**, 5178–5189 (2008).
11. Muzyczka, N. Use of adeno-associated virus as a general transduction vector for mammalian cells. *Curr Top Microbiol Immunol* **158**, 97–129 (1992).
12. Wu, P. *et al.* Mutational Analysis of the Adeno-Associated Virus Type 2 (AAV2) Capsid Gene and Construction of AAV2 Vectors with Altered Tropism. *J Virol* **74**, 8635–8647 (2000).
13. Summerford, C. & Samulski, R. J. Membrane-associated heparan sulfate proteoglycan is a receptor for adeno-associated virus type 2 virions. *J Virol* **72**, 1438–45 (1998).
14. Summerford, C., Bartlett, J. S. & Samulski, R. J. $\alpha V\beta 5$ integrin: a co-receptor for adeno-associated virus type 2 infection. *Nature Medicine* 1999 5:1 **5**, 78–82 (1999).
15. Qing, K. *et al.* Human fibroblast growth factor receptor 1 is a co-receptor for infection by adeno-associated virus 2. *Nature Medicine* 1999 5:1 **5**, 71–77 (1999).
16. Bleker, S., Sonntag, F. & Kleinschmidt, J. A. Mutational Analysis of Narrow Pores at the Fivefold Symmetry Axes of Adeno-Associated Virus Type 2 Capsids Reveals a Dual Role in Genome Packaging and Activation of Phospholipase A2 Activity. *J Virol* **79**, 2528 (2005).

17. Grieger, J. C., Johnson, J. S., Gurda-Whitaker, B., Agbandje-Mckenna, M. & Samulski, R. J. Surface-Exposed Adeno-Associated Virus Vp1-NLS Capsid Fusion Protein Rescues Infectivity of Noninfectious Wild-Type Vp2/Vp3 and Vp3-Only Capsids but Not That of Fivefold Pore Mutant Virions. *J Virol* **81**, 7833–7843 (2007).
18. Girod, A. *et al.* Genetic capsid modifications allow efficient re-targeting of adeno-associated virus type 2. *Nat Med* (1999) doi:10.1038/12491.
19. Boucas, J. *et al.* Engineering adeno-associated virus serotype 2-based targeting vectors using a new insertion site-position 453-and single point mutations. *J Gene Med* **11**, 1103–1113 (2009).
20. Work, L. M. *et al.* Development of efficient viral vectors selective for vascular smooth muscle cells. *Molecular Therapy* **9**, 198–208 (2004).
21. Büning, H. & Srivastava, A. Capsid Modifications for Targeting and Improving the Efficacy of AAV Vectors. *Mol Ther Methods Clin Dev* **12**, (2019).
22. Rode, L. *et al.* AAV capsid engineering identified two novel variants with improved in vivo tropism for cardiomyocytes. *Molecular Therapy* **30**, 3601–3618 (2022).
23. Pettersen, E. F. *et al.* UCSF ChimeraX: Structure visualization for researchers, educators, and developers. *Protein Sci* **30**, 70–82 (2021).
24. Samulski, R. J., Berns, K. I., Tan, M. & Muzyczka, N. Cloning of adeno-associated virus into pBR322: rescue of intact virus from the recombinant plasmid in human cells. *Proc Natl Acad Sci U S A* **79**, 2077 (1982).
25. McLaughlin, S. K., Collis, P., Hermonat, P. L. & Muzyczka, N. Adeno-associated virus general transduction vectors: analysis of proviral structures. *J Virol* **62**, 1963–1973 (1988).
26. Xiao, X., Li, J., Samulski, R. J. & Center, G. T. Production of High-Titer Recombinant Adeno-Associated Virus Vectors in the Absence of Helper Adenovirus. *J Virol* **72**, 2224–2232 (1998).
27. Cheung, A. K. M., David Hoggan, M., Hauswirth, W. W. & Berns, K. I. Integration of the adeno-associated virus genome into cellular DNA in latently infected human Detroit 6 cells. *J Virol* **33**, 739–748 (1980).
28. Laughlin, C. A., Cardellicchio, C. B. & Coon, H. C. Latent Infection of KB Cells with Adeno-Associated Virus Type 2. *J Virol* **60**, 515–524 (1986).
29. Kotin, R. M. *et al.* Site-specific integration by adeno-associated virus. *Proc Natl Acad Sci U S A* **87**, 2211 (1990).
30. Giraud, C., Winocour, E. & Bernst, K. I. Site-specific integration by adeno-associated virus is directed by a cellular DNA sequence. *Proc. Nati. Acad. Sci. USA* **91**, 10039–10043 (1994).
31. Penaud-Budloo, M. *et al.* Adeno-Associated Virus Vector Genomes Persist as Episomal Chromatin in Primate Muscle. *J Virol* **82**, 7875 (2008).
32. Daya, S. & Berns, K. I. Gene Therapy Using Adeno-Associated Virus Vectors. *Clin Microbiol Rev* **21**, 583–593 (2008).
33. Li, C. & Samulski, R. J. Engineering adeno-associated virus vectors for gene therapy. *Nature Reviews Genetics* **2020 21:4** **21**, 255–272 (2020).

34. Wu, Z., Asokan, A. & Samulski, R. J. Adeno-associated Virus Serotypes: Vector Toolkit for Human Gene Therapy. *Molecular Therapy* **14**, 316–327 (2006).
35. Issa, S. S., Shaimardanova, A. A., Solovyeva, V. V & Rizvanov, A. A. Various AAV Serotypes and Their Applications in Gene Therapy: An Overview. (2023) doi:10.3390/cells12050785.
36. Nathwani, A. C. *et al.* Adeno-Associated Mediated Gene Transfer for Hemophilia B: 8 Year Follow up and Impact of Removing Empty Viral Particles on Safety and Efficacy of Gene Transfer. *Blood* **132**, 491–491 (2018).
37. Brockstedt, D. G. *et al.* Induction of immunity to antigens expressed by recombinant adeno-associated virus depends on the route of administration. *Clinical Immunology* **92**, 67–75 (1999).
38. Manning, W. C., Zhou, S., Bland, M. P., Escobedo, J. A. & Dwarki, V. Transient immunosuppression allows transgene expression following readministration of adeno-associated viral vectors. *Hum Gene Ther* **9**, 477–485 (1998).
39. Wang, L., Figueredo, J., Calcedo, R., Lin, J. & Wilson, J. M. Cross-Presentation of Adeno-Associated Virus Serotype 2 Capsids Activates Cytotoxic T Cells But Does Not Render Hepatocytes Effective Cytolytic Targets. <https://home.liebertpub.com/hum> **18**, 185–194 (2007).
40. Boutin, S. *et al.* Prevalence of Serum IgG and Neutralizing Factors Against Adeno-Associated Virus (AAV) Types 1, 2, 5, 6, 8, and 9 in the Healthy Population: Implications for Gene Therapy Using AAV Vectors. <https://home.liebertpub.com/hum> **21**, 704–712 (2010).
41. Calcedo, R., Vandenberghe, L. H., Gao, G., Lin, J. & Wilson, J. M. Worldwide epidemiology of neutralizing antibodies to adeno-associated viruses. *J Infect Dis* **199**, 381–390 (2009).
42. Calcedo, R. *et al.* Adeno-Associated Virus Antibody Profiles in Newborns, Children, and Adolescents. *CLINICAL AND VACCINE IMMUNOLOGY* **18**, 1586–1588 (2011).
43. White, S. J. *et al.* Targeted Gene Delivery to Vascular Tissue In Vivo by Tropism-Modified Adeno-Associated Virus Vectors. *Circulation* **109**, 513–519 (2004).
44. Castle, M. J., Turunen, H. T., Vandenberghe, L. H. & Wolfe, J. H. Controlling AAV tropism in the nervous system with natural and engineered capsids. in *Methods in Molecular Biology* vol. 1382 133–149 (Humana Press Inc., 2016).
45. Uhrig, S. *et al.* Successful target cell transduction of capsid-engineered rAAV vectors requires clathrin-dependent endocytosis. *Gene Therapy* **19**, 210–218 (2011).
46. Lochrie, M. A. *et al.* Mutations on the External Surfaces of Adeno-Associated Virus Type 2 Capsids That Affect Transduction and Neutralization. *J Virol* **80**, 821 (2006).
47. Perabo, L. *et al.* Heparan Sulfate Proteoglycan Binding Properties of Adeno-Associated Virus Retargeting Mutants and Consequences for Their In Vivo Tropism. *J Virol* **80**, 7265–7269 (2006).
48. Pasquini, M. C. *et al.* Real-world evidence of tisagenlecleucel for pediatric acute lymphoblastic leukemia and non-Hodgkin lymphoma. *Blood Adv* **4**, 5414 (2020).
49. Schuster, S. J. *et al.* Tisagenlecleucel in Adult Relapsed or Refractory Diffuse Large B-Cell Lymphoma. *New England Journal of Medicine* **380**, 45–56 (2019).

50. Neelapu, S. S. *et al.* Axicabtagene Ciloleucef CAR T-Cell Therapy in Refractory Large B-Cell Lymphoma. *N Engl J Med* **377**, 2531 (2017).
51. Abramson, J. S. *et al.* Lisocabtagene maraleucef for patients with relapsed or refractory large B-cell lymphomas (TRANSCEND NHL 001): a multicentre seamless design study. *Lancet* **396**, 839–852 (2020).
52. Munshi, N. C. *et al.* Idecabtagene Vicleucef in Relapsed and Refractory Multiple Myeloma. *New England Journal of Medicine* **384**, 705–716 (2021).
53. Kumar, S. *et al.* CAR T-Cell Immunotherapy Treating T-ALL: Challenges and Opportunities. (2023) doi:10.3390/vaccines.
54. Mailankody, S. *et al.* GPRC5D-Targeted CAR T Cells for Myeloma. *New England Journal of Medicine* **387**, 1196–1206 (2022).
55. Maher, J., Brentjens, R. J., Gunset, G., Rivière, I. & Sadelain, M. Human T-lymphocyte cytotoxicity and proliferation directed by a single chimeric TCR ζ /CD28 receptor. *Nature Biotechnology* **20**, 70–75 (2002).
56. Anikeeva, N. *et al.* Efficient killing of tumor cells by CAR-T cells requires greater number of engaged CARs than TCRs. *Journal of Biological Chemistry* **297**, 101033 (2021).
57. Labanieh, L. & Mackall, C. L. CAR immune cells: design principles, resistance and the next generation. *Nature* **614**, 635–648 (2023).
58. Shimabukuro-Vornhagen, A. *et al.* Cytokine release syndrome. *J Immunother Cancer* **6**, 1–14 (2018).
59. Choi, G., Shin, G. & Bae, S. J. Price and Prejudice? The Value of Chimeric Antigen Receptor (CAR) T-Cell Therapy. *Int J Environ Res Public Health* **19**, (2022).
60. Oved, J. H., Barrett, D. M. & Teachey, D. T. Cellular therapy: Immune-related complications. doi:10.1111/imr.12768.
61. Frey, N. & Porter, D. Cytokine Release Syndrome with Chimeric Antigen Receptor T Cell Therapy. (2019) doi:10.1016/j.bbmt.2018.12.756.
62. Bonifant, C. L., Jackson, H. J., Brentjens, R. J. & Curran, K. J. Toxicity and management in CAR T-cell therapy. *Mol Ther Oncolytics* **3**, 16011 (2016).
63. Batra, S. A. *et al.* Glypican-3-specific CAR T cells coexpressing IL15 and IL21 have superior expansion and antitumor activity against hepatocellular carcinoma. *Cancer Immunol Res* **8**, 309–320 (2020).
64. Morgan, R. A. *et al.* Case Report of a Serious Adverse Event Following the Administration of T Cells Transduced With a Chimeric Antigen Receptor Recognizing ERBB2. *Molecular Therapy* **18**, 843 (2010).
65. Maalej, K. M. *et al.* CAR-cell therapy in the era of solid tumor treatment: current challenges and emerging therapeutic advances. *Mol Cancer* **22**, 20 (2023).
66. SCHMIDT, P. *et al.* RATIONALLY DESIGNED VIRUS-LIKE PARTICLES FOR MODULATION OF CHIMERIC ANTIGEN RECEPTOR (CAR)-T-CELL THERAPY. (2019).

67. Uhrig-Schmidt, S., Glenz, S., Neukirch, L., Schmidt, P. & Zörnig, I. Epitope mapping by adeno-associated virus capsid display. (2020).
68. Wistuba, A., Kern, A., Weger, S., Grimm, D. & Kleinschmidt, J. A. Subcellular compartmentalization of adeno-associated virus type 2 assembly. *J Virol* **71**, 1341 (1997).
69. bioinformatics.org. <https://www.bioinformatics.org/>.
70. NEBBio Calculator. <https://nebiocalculator.neb.com/#!/ligation>.
71. Dubielzig, R. *et al.* Adeno-Associated Virus Type 2 Protein Interactions: Formation of Pre-Encapsidation Complexes. *J Virol* **73**, 8989–8998 (1999).
72. Grimm, D., Kern, A., Rittner, K. & Kleinschmidt, J. A. Novel Tools for Production and Purification of Recombinant Adenoassociated Virus Vectors. <https://home.liebertpub.com/hum> **9**, 2745–2760 (2008).
73. Wang, Z. *et al.* Rapid and highly efficient transduction by double-stranded adeno-associated virus vectors in vitro and in vivo. *Gene Therapy* **10**, 2105–2111 (2003).
74. Glenz, S. An attempt to map the CD19-CAR epitope using AAVLPs. (Albert-Ludwigs-Universität Freiburg, 2019).
75. Kang, C. H. *et al.* Identification of Potent CD19 scFv for CAR T Cells through scFv Screening with NK/T-Cell Line. *Int J Mol Sci* **21**, 1–12 (2020).
76. Fischer, J. *et al.* CD19 isoforms enabling resistance to CART-19 immunotherapy are expressed in B-ALL patients at initial diagnosis. *Journal of Immunotherapy* (2017) doi:10.1097/CJI.000000000000169.
77. Sotillo, E. *et al.* Convergence of Acquired Mutations and Alternative Splicing of CD19 Enables Resistance to CART-19 Immunotherapy. *Cancer Discov* **5**, 1282 (2015).
78. Palombella, V. J., Rando, O. J., Goldberg, A. L. & Maniatis, T. The ubiquitinproteasome pathway is required for processing the NF- κ B1 precursor protein and the activation of NF- κ B. *Cell* **78**, 773–785 (1994).
79. Dasgupta, S., Castro, L. M., Dulman, R., Yang, C. & Schmidt, M. Proteasome Inhibitors Alter Levels of Intracellular Peptides in HEK293T and SH-SY5Y Cells. *PLoS One* **9**, 103604 (2014).
80. Anjana, R. *et al.* Hypothesis Aromatic-aromatic interactions in structures of proteins and protein-DNA complexes: a study based on orientation and distance. *print) Bioinformatics* **8**, 1220 (2012).
81. Hsu, H. L. *et al.* Structural characterization of a novel human adeno-associated virus capsid with neurotropic properties. *Nat Commun* **11**, 3279 (2020).
82. Neelapu, S. S. *et al.* Axicabtagene Ciloleucef CAR T-Cell Therapy in Refractory Large B-Cell Lymphoma. *New England Journal of Medicine* **377**, 2531–2544 (2017).
83. Schuster, S. J. *et al.* Chimeric Antigen Receptor T Cells in Refractory B-Cell Lymphomas. *New England Journal of Medicine* **377**, 2545–2554 (2017).
84. Wang, K., Wei, G. & Liu, D. CD19: a biomarker for B cell development, lymphoma diagnosis and therapy. *Exp Hematol Oncol* (2012) doi:10.1186/2162-3619-1-36.

85. Teplyakov, A., Obmolova, G., Luo, J. & Gilliland, G. L. Crystal structure of B-cell co-receptor CD19 in complex with antibody B43 reveals an unexpected fold. *Proteins: Structure, Function and Bioinformatics* **86**, 495–500 (2018).
86. Teplyakov, A., Obmolova, G., Luo, J. & Gilliland, G. L. Crystal structure of B-cell co-receptor CD19 in complex with antibody B43 reveals an unexpected fold. *Proteins: Structure, Function, and Bioinformatics* **86**, 495–500 (2018).
87. Klesmith, J. R. *et al.* Retargeting CD19 Chimeric Antigen Receptor T Cells via Engineered CD19-Fusion Proteins. *Mol Pharm* **16**, 3544–3558 (2019).
88. Klesmith, J. R., Wu, L., Lobb, R. R., Rennert, P. D. & Hackel, B. J. Fine Epitope Mapping of the CD19 Extracellular Domain Promotes Design. *Biochemistry* **58**, 4869–4881 (2019).
89. Tsukita, S. & Furuse, M. The structure and function of claudins, cell adhesion molecules at tight junctions. *Ann N Y Acad Sci* **915**, 129–135 (2000).
90. Morita, K., Furuse, M., Fujimoto, K. & Tsukita, S. Claudin multigene family encoding four-transmembrane domain protein components of tight junction strands. *Proc Natl Acad Sci U S A* **96**, 511 (1999).
91. Reinhard, K. *et al.* An RNA vaccine drives expansion and efficacy of claudin-CAR-T cells against solid tumors. *Science (1979)* **367**, 446–453 (2020).
92. Micke, P. *et al.* Aberrantly activated claudin 6 and 18.2 as potential therapy targets in non-small-cell lung cancer. *Int J Cancer* **135**, 2206–2214 (2014).
93. Ushiku, T., Shinozaki-Ushiku, A., Maeda, D., Morita, S. & Fukayama, M. Distinct expression pattern of claudin-6, a primitive phenotypic tight junction molecule, in germ cell tumours and visceral carcinomas. *Histopathology* **61**, 1043–1056 (2012).
94. Screnci, B. *et al.* Antibody specificity against highly conserved membrane protein Claudin 6 driven by single atomic contact point. *iScience* **25**, 105665 (2022).
95. Angelow, S., Ahlstrom, R. & Yu, A. S. L. Biology of claudins. *American Journal of Physiology - Renal Physiology* vol. 295 Preprint at <https://doi.org/10.1152/ajprenal.90264.2008> (2008).
96. Zhang, C. *et al.* Identification of Claudin-6 as a Molecular Biomarker in Pan-Cancer Through Multiple Omics Integrative Analysis. *Front Cell Dev Biol* **9**, 2052 (2021).
97. Encarnação, J. C., Barta, P., Fornstedt, T. & Andersson, K. Impact of assay temperature on antibody binding characteristics in living cells: A case study. *Biomed Rep* **7**, 400 (2017).
98. Karlsson, H. *et al.* Evaluation of Intracellular Signaling Downstream Chimeric Antigen Receptors. (2015) doi:10.1371/journal.pone.0144787.
99. Nagai, T. *et al.* A variant of yellow fluorescent protein with fast and efficient maturation for cell-biological applications. *Nature Biotechnology* **20**, 87–90 (2002).
100. Naumer, M. *et al.* Development and validation of novel AAV2 random libraries displaying peptides of diverse lengths and at diverse capsid positions. *Hum Gene Ther* **23**, 492–507 (2012).
101. Feiner, R. C. *et al.* RAAV engineering for capsid-protein enzyme insertions and mosaicism reveals resilience to mutational, structural and thermal perturbations. *Int J Mol Sci* **20**, (2019).

102. Ried, M. U., Girod, A., Leike, K., Büning, H. & Hallek, M. Adeno-Associated Virus Capsids Displaying Immunoglobulin-Binding Domains Permit Antibody-Mediated Vector Retargeting to Specific Cell Surface Receptors. *J Virol* **76**, 4559 (2002).
103. Judd, J. *et al.* Random Insertion of mCherry Into VP3 Domain of Adeno-associated Virus Yields Fluorescent Capsids With no Loss of Infectivity. *Mol Ther Nucleic Acids* **1**, (2012).
104. Stagg, S. M., Yoshioka, C., Davulcu, O. & Chapman, M. S. Cryo-electron Microscopy of Adeno-associated Virus. *Chem Rev* (2021)
doi:10.1021/ACS.CHEMREV.1C00936/ASSET/IMAGES/LARGE/CR1C00936_0016.JPEG.
105. Müller, O. J. *et al.* Random peptide libraries displayed on adeno-associated virus to select for targeted gene therapy vectors. *Nat Biotechnol* **21**, 1040–1046 (2003).
106. Körbelin, J. *et al.* Optimization of design and production strategies for novel adeno-associated viral display peptide libraries. *Gene Ther* **24**, 470–481 (2017).
107. Nelson, D. & Cox, M. *Lehninger Biochemie*. vol. 4 (Springer Verlag, 2011).
108. Tsai, C. J., Shuo Liang Lin, Wolfson, H. J. & Nussinov, R. Protein-protein interfaces: Architectures and interactions in protein- protein interfaces and in protein cores. Their similarities and differences. *Crit Rev Biochem Mol Biol* **31**, 127–152 (1996).
109. Tsai, C. J., Lin, S. L., Wolfson, H. J. & Nussinov, R. Studies of protein-protein interfaces: a statistical analysis of the hydrophobic effect. *Protein Sci* **6**, 53–64 (1997).
110. Cody, V., Duax, W. L. & Hauptman, H. CONFORMATIONAL ANALYSIS OF AROMATIC AMINO ACIDS BY X-RAY CRYSTALLOGRAPHY. *Int J Pept Protein Res* **5**, 297–308 (1973).
111. Madhusudan Makwana, K. & Mahalakshmi, R. REVIEWS Implications of aromatic-aromatic interactions: From protein structures to peptide models. (2015) doi:10.1002/pro.2814.
112. Girod, A. *et al.* Genetic capsid modifications allow efficient re-targeting of adeno-associated virus type 2. *Nature Medicine* 1999 5:9 **5**, 1052–1056 (1999).
113. Field, J. *et al.* Purification of a RAS-responsive adenylyl cyclase complex from *Saccharomyces cerevisiae* by use of an epitope addition method. *Mol Cell Biol* **8**, 2159 (1988).
114. Büning, H., Huber, A., Zhang, L., Meumann, N. & Hacker, U. Engineering the AAV capsid to optimize vector-host-interactions. *Curr Opin Pharmacol* (2015)
doi:10.1016/j.coph.2015.08.002.
115. Kern, A. *et al.* Identification of a Heparin-Binding Motif on Adeno-Associated Virus Type 2 Capsids. *J Virol* **77**, 11072–11081 (2003).
116. Opie, S. R., Warrington, K. H., Agbandje-McKenna, M., Zolotukhin, S. & Muzyczka, N. Identification of amino acid residues in the capsid proteins of adeno-associated virus type 2 that contribute to heparan sulfate proteoglycan binding. *J Virol* **77**, 6995–7006 (2003).
117. Lochrie, M. A. *et al.* Mutations on the External Surfaces of Adeno-Associated Virus Type 2 Capsids That Affect Transduction and Neutralization. *J Virol* **80**, 821–834 (2006).
118. Thadani, N. N. *et al.* Frustration and Direct Coupling Analyses to Predict Formation and Function of Adeno-Associated Virus. *Biophys J* (2020) doi:10.1016/j.bpj.2020.12.018.

119. Ferreira, D. U., Hegler, J. A., Komives, E. A. & Wolynes, P. G. On the role of frustration in the energy landscapes of allosteric proteins. *Proc Natl Acad Sci U S A* **108**, 3499–3503 (2011).
120. Kern, A. *et al.* Identification of a Heparin-Binding Motif on Adeno-Associated Virus Type 2 Capsids †. *J Virol* **77**, 11072–11081 (2003).
121. Lerch, T. F. & Chapman, M. S. Identification of the heparin binding site on adeno-associated virus serotype 3B (AAV-3B). **423**, 6–13 (2012).
122. Large, E. E., Silveria, M. A., Zane, G. M., Weerakoon, O. & Chapman, M. S. Adeno-associated virus (Aav) gene delivery: Dissecting molecular interactions upon cell entry. *Viruses* **13**, 1336 (2021).
123. Mayers, J., Westcott, D. & Steinbach, F. Identification of Equine Arteritis Virus Immunodominant Epitopes Using a Peptide Microarray. *Viruses* **14**, (2022).
124. Forsström, B. *et al.* Proteome-wide Epitope Mapping of Antibodies Using Ultra-dense Peptide Arrays. *Mol Cell Proteomics* **13**, 1585 (2014).
125. Gershoni, J. M., Roitburd-Berman, A., Siman-Tov, D. D., Freund, N. T. & Weiss, Y. Epitope Mapping: The First Step in Developing Epitope-Based Vaccines. *Biodrugs* **21**, 145 (2007).
126. Nilvebrant, J. & Rockberg, J. An introduction to epitope mapping. *Methods in Molecular Biology* **1785**, 1–10 (2018).
127. Potocnakova, L., Bhide, M. & Pulzova, L. B. An Introduction to B-Cell Epitope Mapping and In Silico Epitope Prediction. *J Immunol Res* **2016**, (2016).
128. Barlow, D. J., Edwards, M. S. & Thornton, J. M. Continuous and discontinuous protein antigenic determinants. *Nature* 1986 322:6081 **322**, 747–748 (1986).
129. Zhang, Z. *et al.* Point mutation in CD19 facilitates immune escape of B cell lymphoma from CAR-T cell therapy. *J Immunother Cancer* **8**, e001150 (2020).
130. De Oliveira, S. N. *et al.* A CD19/Fc fusion protein for detection of anti-CD19 chimeric antigen receptors. *J Transl Med* **11**, 23 (2013).
131. Lobner, E. *et al.* Getting CD19 Into Shape: Expression of Natively Folded “Difficult-to- Express” CD19 for Staining and Stimulation of CAR-T Cells. *Front Bioeng Biotechnol* **8**, (2020).
132. Laurent, E. *et al.* Directed Evolution of Stabilized Monomeric CD19 for Monovalent CAR Interaction Studies and Monitoring of CAR-T Cell Patients. *ACS Synth Biol* **10**, 1184–1198 (2021).
133. Jemmerson, R. Antigenicity and native structure of globular proteins: low frequency of peptide reactive antibodies. *Proc Natl Acad Sci U S A* **84**, 9180 (1987).
134. Van Regenmortel, M. H. V. What is a b-cell epitope? *Methods in Molecular Biology* **524**, 3–20 (2009).
135. Shi, X., Fang, G. & Shi, W. Insertional Mutagenesis at Positions 520 and 584 of Adeno-Associated Virus Type 2 (AAV2) Capsid Gene and Generation of AAV2 Vectors with Eliminated Heparin- Binding Ability and Introduced Novel Tropism. <https://home.liebertpub.com/hum> **17**, 353–361 (2006).

136. Birtalan, S. *et al.* The Intrinsic Contributions of Tyrosine, Serine, Glycine and Arginine to the Affinity and Specificity of Antibodies. *J Mol Biol* **377**, 1518–1528 (2008).
137. Sterner, R. C. & Sterner, R. M. CAR-T cell therapy: current limitations and potential strategies. *Blood Cancer Journal* *2021 11:4* **11**, 1–11 (2021).
138. Si, S. & Teachey, D. T. Spotlight on Tocilizumab in the Treatment of CAR-T-Cell-Induced Cytokine Release Syndrome: Clinical Evidence to Date. (2020) doi:10.2147/TCRM.S223468.
139. Maude, S. L. *et al.* Chimeric Antigen Receptor T Cells for Sustained Remissions in Leukemia. *New England Journal of Medicine* **371**, 1507–1517 (2014).
140. Myers, R. M. *et al.* Humanized CD19-Targeted Chimeric Antigen Receptor (CAR) T Cells in CAR-Naive and CAR-Exposed Children and Young Adults With Relapsed or Refractory Acute Lymphoblastic Leukemia. *Journal of Clinical Oncology* **39**, 3044 (2021).
141. Hunter, B. D. & Jacobson, C. A. CAR T-Cell Associated Neurotoxicity: Mechanisms, Clinicopathologic Correlates, and Future Directions. *JNCI: Journal of the National Cancer Institute* **111**, 646–654 (2019).
142. Salter, A. I. *et al.* Phosphoproteomic analysis of chimeric antigen receptor signaling reveals kinetic and quantitative differences that affect cell function. *Sci Signal* **11**, (2018).
143. Philip, B. *et al.* A highly compact epitope-based marker/suicide gene for easier and safer T-cell therapy. *Blood* **124**, 1277–1287 (2014).
144. Jones, B. S., Lamb, L. S., Goldman, F. & Stasi, A. Di. Improving the safety of cell therapy products by suicide gene transfer. *Front Pharmacol* **5**, (2014).
145. Mestermann, K. *et al.* The tyrosine kinase inhibitor dasatinib acts as a pharmacologic on/off switch for CAR-T cells. doi:10.1126/scitranslmed.aau5907.
146. Jäger, D. *et al.* NY-BR-1 is a differentiation antigen of the mammary gland. *Applied Immunohistochemistry and Molecular Morphology* **15**, 77–83 (2007).
147. Rudnick, S. I. & Adams, G. P. Affinity and Avidity in Antibody-Based Tumor Targeting. *Cancer Biother Radiopharm* **24**, 155 (2009).
148. Jaeger, D., Sahin, U. & Tureci, O. A first-in-human dose escalation and dose-finding phase I/II trial of IMAB027 in patients with recurrent advanced ovarian cancer (GM-IMAB-002-01). https://doi.org/10.1200/jco.2014.32.15_suppl.tps5623 **32**, TPS5623–TPS5623 (2014).
149. Kievit, E., Pinedo, H. M., Schlüper, H. M. M., Haisma, H. J. & Boven, E. Comparison of monoclonal antibodies 17-1A and 323/A3: the influence of the affinity on tumour uptake and efficacy of radioimmunotherapy in human ovarian cancer xenografts. *Br J Cancer* **73**, 457–464 (1996).
150. Fujimori, K., Covell, D. G., Fletcher, J. E. & Weinstein, J. N. A Modeling Analysis of Monoclonal Antibody Percolation Through Tumors: A Binding-Site Barrier. *Journal of Nuclear Medicine* **31**, (1990).
151. Termini, J. M. *et al.* HEK293T cell lines defective for O-linked glycosylation. *PLoS One* **12**, (2017).

7 Supplement

7.1 Row statistics

7.1.1 Alanine Scan CD19_42FL

Sequence	Mean	SD	N
AGIHRPLAIWLFIF	0,0	0,0	2
LAIHRPLAIWLFIF	0,0	0,0	2
LGAHRPLAIWLFIF	0,0	0,0	2
LGIAMRPLAIWLFIF	0,0	0,0	2
LGIHARPLAIWLFIF	0,0	0,0	2
LGIHMAPLAIWLFIF	0,0	0,0	2
LGIHMRALAIWLFIF	0,0	0,0	2
LGIHMRPAAIWLFIF	150138,9	212220,5	2
LGIHMRPLAAWLFIF	16388,9	28386,4	3
LGIHMRPLAIALFIF	0,0	0,0	2
LGIHMRPLAIWAFIF	0,0	0,0	2
LGIHMRPLAIWLAIF	0,0	0,0	2
LGIHMRPLAIWLFIF	0,0	0,0	2
LGIHMRPLAIWLFIA	0,0	0,0	2
LGIHMRPLAIALAIF	137961,9	251376,9	5
LGIHMRPLAIWLAIA	75295,2	95314,1	5
LGIHMRPLAIALFIA	36828,6	49424,4	5
LGIHMRPLAIALAIA	279195,2	333323,9	5
LGIHMRPAAIWLFIA	136061,9	144216,9	5
LGIHMRPAAAWLFIF	0,0	0,0	3
LGIHMRPAAIWLFIF	61333,3	66193,5	3
LGIHMRPAAIWAFIF	31833,3	30807,2	3
LGIHMRPLAIWLAAA	8000,0	13856,4	3

7.1.2 Comparison alternative insertion sites

	β B-aa245A			β B-aa245B		
	Mean	SEM	N	Mean	SEM	N
CD19_6FL	2,90E+05	2,90E+05	2	0	0	2
CD19_23FL	0,00E+00	0,00E+00	1	0	0	2
CD19_33FL	0,00E+00	0,00E+00	1	0	0	2
CD19_42FL	2,37E+05	1,01E+05	3	0	0	3
CD19_51FL	2,88E+05	2,88E+05	2	0	0	2
CD19_55FL	0,00E+00	0,00E+00	2	0	0	2
C2FL	3,77E+04	3,77E+04	3	0	0	3

	VR-IV-aa453*			VR-VIII-aa588		
	Mean	SEM	N	Mean	SEM	N
CD19_6FL				1,46E+06	1,50E+04	2
CD19_23FL	7,77E+05	4,83E+05	3	3,29E+05	1,06E+05	4
CD19_33FL	6,51E+05	2,03E+05	3	7,28E+04	4,75E+04	5
CD19_42FL	7,17E+04	7,17E+04	3	0,00E+00	0,00E+00	5
CD19_51FL	0,00E+00	0,00E+00	3	0,00E+00	0,00E+00	5
CD19_55FL	8,21E+05	4,54E+05	3	4,27E+05	1,59E+05	5
C2FL	6,44E+05	1,79E+05	2	4,18E+05	0,00E+00	1

	HI-loop-aa653		
	Mean	SEM	N
CD19_6FL	0,00E+00	0,00E+00	2
CD19_23FL	0,00E+00	0,00E+00	2
CD19_33FL	0,00E+00	0,00E+00	2
CD19_42FL	2,24E+04	1,39E+04	5
CD19_51FL	3,81E+04	3,81E+04	2
CD19_55FL	4,56E+04	4,56E+04	2
C2FL	0,00E+00	0,00E+00	2

	a)			b)			c)		
	Mean	SEM	N	Mean	SEM	N	Mean	SEM	N
NYBR1 CL2	0	0	5	40760	25608,2	5	0	0	5
NYBR1 CL2 FL	44562,5	31021,2	8	20966,7	15989,1	6	81250	46963,4	4
Flag-tag (FL)	0	0	5	3000	3000	5	34126,7	15452,6	6

7.1.3 Backbone comparison

	VR-VIII-R588			Q457M		
	Mean	SEM	N	Mean	SEM	N
CD19_6FL	1,37E+06	8,21E+04	3	3,58E+05	1,82E+05	3
CD19_23FL	2,35E+05	1,31E+05	4	1,08E+05	4,23E+04	3
CD19_33FL	3,25E+04	3,25E+04	4	6,08E+04	3,85E+04	3
CD19_42FL	0,00E+00	0,00E+00	4	4,77E+03	3,59E+03	3
CD19_51FL	0,00E+00	0,00E+00	4	3,53E+05	2,60E+05	3
CD19_55FL	3,23E+05	8,53E+04	4	4,39E+05	1,72E+05	3
NYBR1_C2FL	8,19E+05	4,01E+05	2	5,75E+05	1,49E+05	3

	T450A			R447K		
	Mean	SEM	N	Mean	SEM	N
CD19_6FL	1,22E+06	2,75E+05	3	1,26E+06	8,50E+04	2
CD19_23FL	1,50E+05	7,83E+04	3	2,46E+05	3,75E+04	2
CD19_33FL	2,88E+04	1,91E+04	3	5,40E+04	5,40E+04	2
CD19_42FL	0,00E+00	0,00E+00	3	0,00E+00	0,00E+00	2
CD19_51FL	0,00E+00	0,00E+00	3	1,25E+04	1,25E+04	2
CD19_55FL	6,13E+05	1,89E+05	3	1,14E+05	9,63E+04	2
NYBR1_C2FL	9,16E+05	7,44E+05	3	5,05E+05	5,05E+05	2

	E548G			E449D		
	Mean	SEM	N	Mean	SEM	N
CD19_6FL	2,93E+06	9,73E+05	3	1,58E+05	0,00E+00	1
CD19_23FL	7,89E+05	4,94E+05	3	8,67E+04	0,00E+00	1
CD19_33FL	2,25E+05	1,19E+05	3	6,34E+04	0,00E+00	1
CD19_42FL	5,83E+03	5,83E+03	3	2,53E+05	0,00E+00	1
CD19_51FL	2,50E+04	2,50E+04	3	1,76E+05	0,00E+00	1
CD19_55FL	1,41E+05	7,13E+04	3	2,96E+05	0,00E+00	1
NYBR1_C2FL	1,65E+06	1,05E+06	3	6,58E+05	0,00E+00	1

	A593T			G546D		
	Mean	SEM	N	Mean	SEM	N
CD19_6FL	3,86E+06	1,00E+05	2	2,22E+06	3,35E+05	2
CD19_23FL	3,07E+06	5,60E+05	2	6,02E+05	6,90E+04	2
CD19_33FL	2,44E+06	4,65E+05	2	3,57E+05	8,40E+04	2
CD19_42FL	1,63E+04	1,63E+04	2	1,77E+05	1,67E+05	2
CD19_51FL	1,50E+04	7,50E+03	2	5,55E+04	5,55E+04	2
CD19_55FL	5,73E+05	2,25E+04	2	4,34E+05	2,11E+05	2
NYBR1_C2FL	1,38E+04	1,38E+04	2	8,99E+05	2,51E+05	2

	K39Q			V151A		
	Mean	SEM	N	Mean	SEM	N
CD19_6FL	8,15E+04	8,15E+04	2	1,38E+05	0,00E+00	1
CD19_23FL	2,24E+05	1,34E+05	2	1,42E+03	0,00E+00	1
CD19_33FL	1,45E+06	1,45E+06	2	0,00E+00	0,00E+00	1
CD19_42FL	1,88E+04	1,88E+04	2	0,00E+00	0,00E+00	1
CD19_51FL	2,13E+04	2,13E+04	2	1,74E+05	0,00E+00	1
CD19_55FL	1,88E+04	1,88E+04	2	1,21E+05	0,00E+00	1
NYBR1_C2FL	2,50E+04	2,50E+04	2	2,11E+05	0,00E+00	1

	S492A			F533Y		
	Mean	SEM	N	Mean	SEM	N
CD19_6FL	2,60E+06	6,75E+05	2	3,48E+06	1,45E+06	2
CD19_23FL	6,67E+05	2,04E+05	2	1,42E+06	6,00E+04	2
CD19_33FL	5,00E+03	5,00E+03	2	3,38E+04	2,38E+04	2
CD19_42FL	4,00E+04	4,00E+04	2	0,00E+00	0,00E+00	2
CD19_51FL	6,25E+03	6,25E+03	2	0,00E+00	0,00E+00	2
CD19_55FL	4,93E+05	3,25E+05	2	8,64E+05	2,16E+05	2
NYBR1_C2FL	4,89E+05	3,91E+05	2	1,22E+06	5,51E+05	2

	R585S-R588T			E449D-Q457M		
	Mean	SEM	N	Mean	SEM	N
CD19_6FL	1,33E+06	3,98E+05	4	4,21E+05	2,11E+05	3
CD19_23FL	9,74E+05	2,57E+05	4	9,55E+05	3,88E+04	3
CD19_33FL	7,08E+05	3,24E+05	4	8,60E+05	2,10E+05	3
CD19_42FL	0,00E+00	0,00E+00	4	0,00E+00	0,00E+00	3
CD19_51FL	0,00E+00	0,00E+00	4	0,00E+00	0,00E+00	3
CD19_55FL	7,95E+05	3,14E+05	4	8,84E+05	3,93E+05	3
NYBR1_C2FL				8,10E+05	0,00E+00	1

	T450A-Q457M			Q457M-R585S-R588T		
	Mean	SEM	N	Mean	SEM	N
CD19_6FL	1,45E+06	4,73E+05	2	2,78E+05	0,00E+00	1
CD19_23FL	6,17E+04	8,35E+03	2	5,77E+05	0,00E+00	1
CD19_33FL	2,50E+03	2,50E+03	2	5,71E+05	0,00E+00	1
CD19_42FL	0,00E+00	0,00E+00	2	0,00E+00	0,00E+00	1
CD19_51FL	0,00E+00	0,00E+00	2	0,00E+00	0,00E+00	1
CD19_55FL	1,61E+05	6,60E+04	2	4,62E+05	0,00E+00	1
NYBR1_C2FL	6,60E+04	6,60E+04	2	6,09E+05	0,00E+00	1

	T450A-R585S-R588T			R447K-R585S-R588T		
	Mean	SEM	N	Mean	SEM	N
CD19_6FL	7,30E+05	1,51E+05	2	5,61E+05	6,25E+04	2
CD19_23FL	4,90E+05	2,03E+05	2	4,94E+05	1,09E+05	2
CD19_33FL	6,73E+05	0,00E+00	1	8,08E+05	1,16E+05	2
CD19_42FL	5,29E+04	1,61E+04	2	0,00E+00	0,00E+00	2
CD19_51FL	0,00E+00	0,00E+00	2	0,00E+00	0,00E+00	2
CD19_55FL	2,32E+05	8,95E+04	2	8,36E+05	3,85E+05	2
NYBR1_C2FL	2,98E+04	5,40E+03	2	4,33E+05	1,57E+05	2

	E548G-R585S-R588T			R585S-R588T-A593T		
	Mean	SEM	N	Mean	SEM	N
CD19_6FL	2,24E+06	3,85E+05	2	8,64E+05	5,40E+04	2
CD19_23FL	3,03E+06	1,88E+06	2	2,85E+05	9,71E+04	3
CD19_33FL	2,74E+06	1,02E+06	2	0,00E+00	0,00E+00	3
CD19_42FL	0,00E+00	0,00E+00	2	0,00E+00	0,00E+00	3
CD19_51FL	0,00E+00	0,00E+00	2	0,00E+00	0,00E+00	3
CD19_55FL	3,54E+06	1,50E+06	2	2,56E+05	9,87E+04	3
NYBR1_C2FL	1,55E+06	4,40E+05	2	2,79E+05	8,70E+04	3

	G546D-R585S-R588T			Q457M-E499D-R585S-R588T		
	Mean	SEM	N	Mean	SEM	N
CD19_6FL	1,38E+06	5,27E+05	2	3,84E+05	2,61E+05	2
CD19_23FL	1,11E+06	2,34E+05	2	4,17E+03	4,17E+03	2
CD19_33FL	1,73E+05	1,73E+05	2	0,00E+00	0,00E+00	2
CD19_42FL	6,65E+03	6,65E+03	2	0,00E+00	0,00E+00	2
CD19_51FL	1,29E+04	1,29E+04	2	0,00E+00	0,00E+00	2
CD19_55FL	3,42E+05	2,90E+04	2	0,00E+00	0,00E+00	2
NYBR1_C2FL	4,04E+04	4,04E+04	2	3,41E+05	3,41E+05	2

	T450A-Q457M-R585S-R588T			T450A-R585S-R588T-A593T		
	Mean	SEM	N	Mean	SEM	N
CD19_6FL	7,08E+05	0,00E+00	1	1,70E+06	7,88E+05	2
CD19_23FL	7,05E+05	0,00E+00	1	1,65E+06	1,05E+05	2
CD19_33FL	7,25E+05	0,00E+00	1	6,74E+05	2,86E+05	2
CD19_42FL	0,00E+00	0,00E+00	1	5,35E+04	5,35E+04	2
CD19_51FL	0,00E+00	0,00E+00	1	5,45E+04	5,45E+04	2
CD19_55FL	7,93E+05	0,00E+00	1	4,46E+04	4,46E+04	2
NYBR1_C2FL	0,00E+00	0,00E+00	1	1,01E+06	7,15E+05	2

	T450A-G546D-R585S-R588T			T450A-E499D-R585S-R588T		
	Mean	SEM	N	Mean	SEM	N
CD19_6FL	1,22E+06	2,58E+05	2	8,81E+05	2,49E+05	2
CD19_23FL	5,03E+05	3,20E+05	2	6,07E+05	3,19E+05	2
CD19_33FL	5,16E+05	2,63E+05	2	6,50E+05	1,98E+05	2
CD19_42FL	0,00E+00	0,00E+00	2	0,00E+00	0,00E+00	2
CD19_51FL	0,00E+00	0,00E+00	2	0,00E+00	0,00E+00	2
CD19_55FL	2,62E+05	2,62E+05	2	7,74E+05	2,26E+05	2
NYBR1_C2FL	0,00E+00	0,00E+00	2	2,89E+05	6,05E+04	2

	R447K-E499D-R585S-R588T			E548G-R585S-R588T-A593T		
	Mean	SEM	N	Mean	SEM	N
CD19_6FL	5,44E+05	2,20E+04	2	1,89E+06	0,00E+00	1
CD19_23FL	5,24E+05	1,15E+04	2	6,10E+05	0,00E+00	1
CD19_33FL	4,54E+05	4,55E+04	2	0,00E+00	0,00E+00	1
CD19_42FL	6,10E+03	6,10E+03	2	1,88E+06	0,00E+00	1
CD19_51FL	2,78E+02	2,78E+02	2	0,00E+00	0,00E+00	1
CD19_55FL	7,21E+05	1,41E+05	2	0,00E+00	0,00E+00	1
NYBR1_C2FL	3,97E+05	7,25E+04	2	2,40E+06	0,00E+00	1

	E499D-R585S-R588T-A593T			T450A-Q457M-E499D-R585S-R588T		
	Mean	SEM	N	Mean	SEM	N
CD19_6FL	8,25E+05	2,06E+05	2	3,48E+06	0,00E+00	1
CD19_23FL	3,49E+05	1,15E+05	3	3,78E+06	0,00E+00	1
CD19_33FL	2,68E+04	2,68E+04	3	4,43E+06	0,00E+00	1
CD19_42FL	0,00E+00	0,00E+00	3	0,00E+00	0,00E+00	1
CD19_51FL	0,00E+00	0,00E+00	3	0,00E+00	0,00E+00	1
CD19_55FL	7,30E+05	2,81E+05	3	1,65E+06	0,00E+00	1
NYBR1_C2FL	5,85E+05	1,88E+05	3	2,35E+06	0,00E+00	1

	R447K-E499D-R585S-R588T-A593T			R447K-Q457M-E499D-R585S-R588T-A593T		
	Mean	SEM	N	Mean	SEM	N
CD19_6FL	2,02E+06	1,04E+06	2	0,00E+00	0,00E+00	1
CD19_23FL	1,80E+06	4,85E+05	2	0,00E+00	0,00E+00	1
CD19_33FL	2,42E+06	0,00E+00	1	0,00E+00	0,00E+00	1
CD19_42FL	5,20E+05	5,20E+05	2	0,00E+00	0,00E+00	1
CD19_51FL	2,17E+05	1,97E+05	2	0,00E+00	0,00E+00	1
CD19_55FL	2,82E+06	1,34E+06	2	0,00E+00	0,00E+00	1
NYBR1_C2FL	2,48E+05	2,48E+05	2	0,00E+00	0,00E+00	1

	R447K-Q457M-E499D-E548G-R585S-R588T-A593T			R447K-Q457M-E499D-G546D-E548G-R585S-R588T-A593T		
	Mean	SEM	N	Mean	SEM	N
CD19_6FL	8,65E+04	8,65E+04	2	0,00E+00	0,00E+00	2
CD19_23FL	8,98E+05	3,83E+05	2	7,00E+04	7,00E+04	2
CD19_33FL	6,15E+05	6,15E+05	2	5,63E+04	3,38E+04	2
CD19_42FL	6,75E+04	4,75E+04	2	0,00E+00	0,00E+00	2
CD19_51FL	1,63E+04	1,63E+04	2	2,50E+04	2,50E+04	2
CD19_55FL	1,99E+06	9,85E+05	2	5,50E+04	5,50E+04	2
NYBR1_C2FL	1,55E+06	3,75E+05	2	5,50E+04	5,50E+04	2

7.2 Abbreviations

aa	amino acid
°C	Degree Celsius
AAP	assembly-activating protein
AAV	adeno-associated virus
AAVLP	adeno-associated virus-like particles
ANOVA	Analysis of variance
APC	allophycocyanin
bp	base pair
BSA	Bovine serum albumin
CAR	chimeric antigen receptor
CLDN6	Claudin-6
CIP	Calf Intestinal Alkaline Phosphatase
cm	centimeter
CMV	Cytomegalovirus
DAPI	4',6-diamidino-2-phenylindole
dNTP	deoxyribonucleotide triphosphate
DMEM	Dulbecco's Modified Eagle's Medium
DMSO	dimethyl sulfoxide
DNA	deoxyribonucleic acid
dsDNA	double-stranded DNA
E. coli	Escherichia coli
ECD	Extracellular domain
EDTA	Ethylenediaminetetraacetic acid
ELISA	enzyme-linked immunosorbent assay
FACS	fluorescence-activated cell sorting
FCS	fetal calf serum
FDA	U.S. Food and Drug Administration
FITC	fluorescein
fwd	forward
g	gravitational force
GFP	green fluorescent protein
h	hour
HEK	human embryonic kidney
HEPES	4-(2-hydroxyethyl)-1-piperazineethanesulfonic acid
HRP	Horseradish peroxidase
HSPG	heparin sulfate proteoglycan
IFN	interferon
IgG	immunoglobulin G
IL	interleukin
ITR	inverted terminal repeat
kb	kilobase
kDa	kilo Dalton
LB medium	lysogeny broth medium
mAb	Monoclonal antibody

MFI	mean fluorescence intensity
min	minute
mg	milligram
MHC	major histocompatibility complex
mL	milliliter
mm	millimeter
NAbs	neutralizing antibodies
nm	nanometer
ORF	Open reading frame
PBMCs	Peripheral blood mononuclear cells
PBS	phosphate-buffered saline
PBS-T	PBS with Tween20
PCR	polymerase chain reaction
PE	phycoerythrin
PEG	polyethylene glycol
PEI	polyethylenimine
Pen/Strep	penicillin + streptavidin
rev	reverse
RPMI	Gibco Roswell Park Memorial Institute 1640 Medium
RPMI	rounds per minute
RT	room temperature
scFv	single chain variable fragment
SDM	site-directed mutagenesis
SEM	standard error of mean
ssDNA	single stranded DNA
T4 PNK	T4 Polynucleotide Kinase
TAE	Tris-acetate EDTA
U	enzyme unit
V	volt
VP	viral protein
wt	wild type
µg	microgram
µL	microliter
µM	micromolar
µm	micrometer

7.3 List of figures

Figure 1.1.1: Genome and capsid structure of AAV2.....	7
Figure 1.2.1: Chimeric antigen receptors for cancer treatment.....	9
Figure 1.3.1: The AAViTOP screening procedure.....	11
Figure 4.1.1: Overlapping sequence library of CD19 exon 2 as basis for further improvements	70
Figure 4.1.2: Inhibiting the proteasome as an attempt to promote capsid assembly.....	72
Figure 4.1.3: Comparison of the impact of the same aromatic amino acids in different positions in short sequence fragments	74
Figure 4.1.4: Comparison of alternative insertion sites in the AAVLP capsid	77
Figure 4.1.5: Sequence changes in the backbone plasmid can improve capsid assembly	79
Figure 4.2.1: An attempt to generate a CD19 fusion protein.....	83
Figure 4.2.2: Using the AAViTOP procedure to verify a linear epitope within the CD19 protein	85
Figure 4.2.3: Recreating discontinuous epitopes on the AAVLP surface	88
Figure 4.3.1: Claudin-6 as a new target for the epitope screening and application beyond the AAViTOP procedure	89
Figure 4.3.2: Generation of assembled AAVLPs with CLDN6 sequence insertion.....	92
Figure 4.3.3: Using the IMAB027 antibody to screen for the epitope of a anti-CLDN6 CAR.....	95
Figure 4.3.4: Low MOI does not lead to down-regulation of CAR expression and CLDN6 presenting AAVLPs do not enter the cells.....	96
Figure 4.3.5: At an MOI of 1×10^6 particles and above, a reduction in CLDN6 CAR expression on primary T cells can be observed.....	98
Figure 4.3.6: Internalisation can be prevented by co-incubation at 4 °C	101
Figure 4.3.7: The presence of epitope-carrying AAVLPs does not lead to activation of Jurkat Venus reporter cell line	106

7.4 List of tables

Table 3.1.1: Transfection mix per 6-well.....	53
Table 3.1.2: Transfection mix for co-transfection of HEK293T cells for lentiviral particle production ..	54
Table 3.2.1: Tris-acetate EDTA (TAE) buffer.....	55
Table 3.2.2: Lysogeny broth (LB) medium.....	55
Table 3.2.3: Restriction sites of the different capsid backbones	57
Table 3.2.4: Annealing of DNA oligonucleotides	57
Table 3.2.5: Linearization of capsid plasmids.....	57
Table 3.2.6: Ligation of annealed DNA oligonucleotides into linearized vector DNA.....	58
Table 3.2.7: Ligation of digested DNA fragments into linearized vector DNA	58
Table 3.2.8: LR- reaction mix.....	58
Table 3.2.9: PCR mix for site-directed mutagenesis	59
Table 3.2.10: PCR cycles for site-directed mutagenesis	59
Table 3.3.1: Cells per well for transfection of HEK293T cells for AAVLP small-scale production.....	60
Table 3.3.2: Transfection mix for AAVLP small-scale transfection in different cell culture plates.....	60

Table 3.3.3: Final volume of crude lysates depending on the transfection plate format	60
Table 3.3.4: Transfection mix for AAVLP large-scale production in 15 cm cell culture dish	61
Table 3.3.5: PEG solution	62
Table 3.3.6: AAVLP lysis buffer	62
Table 3.3.7: Iodixanol solutions	62
Table 3.3.8: AAVLP concentration buffer	63
Table 3.4.1: Coating buffer for IFN γ ELISA.....	65
Table 3.5.1: 8% Polyacrylamide gel	65
Table 3.5.2: 5 % Collection gel	66
Table 3.5.3: 1x Transferbuffer (1 Liter)	66

8 Acknowledgments

At this point I would like to thank some people without whom this project would never have become what it is now.

First of all, I would like to thank Prof. Dr. Dirk Jäger for giving me the opportunity to work in this working group and on this project. I would also like to thank him for his support and scientific input during my TAC meetings. Furthermore, I would like to thank apl. Prof Martin Müller, who always gave me new ideas during the TAC meetings and together with Prof. Dr. Dirk Jäger, Prof. Dr. Nina Papavasiliou and Prof. Dr. Stefan Wöfl, he reviewed this work.

Special thanks go to my project supervisor Dr. Silke Uhrig-Schmidt, as she was always highly motivated and supported me with good advice. I am grateful that we have been able to develop the idea of screening so far together.

Furthermore, I would like to thank Dr. Inka Zörnig and Dr. Patrick Schmidt for their support and scientific advice.

I would also like to thank all the members and former members of the AG Jäger who have accompanied me over the years. Claudia, Annette, Martina, Katharina, Eren, Deva and Jasmin (AG Hassel), every break and every trip with you was a great pleasure. An especially big thank you goes to Alex, because she has experienced all the ups and downs of the project and I could trust that we would manage everything hand in hand.

I am endlessly grateful that my family has supported me all these years. I think the whole lab would also like to thank you for the Christmas cookies.

I am especially grateful that my husband Lars has been by my side all these years, celebrating my results with me and being there for my whims. I would also like to thank my friends, especially Linda, Maren and Angi, every meeting with you was like a holiday.